Mini-symposium M2

NONLINEAR DYNAMICS

Organizer: Katica R. (Stevanović) Hedrih

ON THE DEGREE OF INSTABILITY OF MECHANICAL SYSTEMS

R. M. Bulatović[1], M. Kažić[2]

[1] Faculty of Mechanical Engineering
University of Montenegro, Cetinjski put b.b., 81 000 Podgorica
e-mail: ranislav@ac.me
[2] Faculty of Mechanical Engineering,
University of Montenegro, Cetinjski put b.b., 81 000 Podgorica
e-mail: milak@ac.me

Abstract. Dynamical systems admitting Morse functions that do not increase along trajectories with time are considered. The main relations between the indices of inertia of these functions and the instability degrees of the equilibria are indicated, and these results are supplemented with several new statements. The results are applied to two classes of mechanical systems.

1. Introduction and some general results

Consider the dynamical system

$$\dot{x} = f(x), \ x \in \Re^n,$$ (1)

for which $x = 0$ is an equilibrium point, i. e. $f(0) = 0$. Let the system possess a Morse function $V : \Re^n \to \Re$ with critical point $x = 0$ such that $\dot{V} = (\partial V / \partial x, f) \le 0$ (weak Lyapunov function). In the neighborhood of $x = 0$ the vector field f and the function V may be written as

$$f(x) = Ax + o(|x|), \ A = \left.\frac{\partial f}{\partial x}\right|_{x=0},$$ (2)

and

$$V = V(0) + \frac{1}{2}(Bx, x) + o(|x|^2), \ B = B^*, \ \det B \ne 0,$$ (3)

respectively. Assume that $\det A \ne 0$; in particular, $x = 0$ is an isolated equilibrium point. Obviously, the derivative of the quadratic form in (3) according to the linearized system

$$\dot{x} = Ax$$ (4)

is also non-positive, i.e.

$$BA + A^*B = -S, \ S \ge 0.$$ (5)

The degree of instability, u, of the equilibrium $x = 0$ is defined as the number of eigenvalues of A with positive real part, counting multiplicities. This definition is a natural generalization of the definition of the degree of instability for equilibrium of natural mechanical systems, proposed by Poincare [1,2]. According to classical Lyapunov's instability theorem based on the first approximation, if $u \ge 1$, then the equilibrium $x = 0$ of system (1) is unstable.

The degree of instability u can be related to the negative inertia index, i^-, of the quadratic form (Bx, x).

First, we recall one result of Ostrowski and Schneider [3].

(A) If $S > 0$, then $u = i^-$.

In the more general case $S \geq 0$, the numbers u and i^- do not generally coincide with each other. However, the following important assertions have been formulated

(B) $u \equiv i^- \pmod 2$, Kozlov [2];

(C) $u \leq i^-$, Kozlov [4];

(D) If the matrix A has no eigenvalues on the imaginary axis, then $u = i^-$, Carlson and Schneider [5];

(E) If the pierced cone

$$\{x \in \Re^n : (Sx, x) = 0\} \setminus \{0\} \tag{6}$$

contains no closed trajectories of system (4), then the matrix A has no pure imaginary eigenvalues, and consequently $u = i^-$, Kozlov [4].

The last condition resembles the Barbashin-Krasovski condition in well-known stability theorems.

On the other hand, the absence of pure imaginary eigenvalues of A can be established by means of the controllability matrix of A^* and S. The controllability matrix $C(A^*, S)$ of A^* and S is defined as the $n \times n^2$ matrix

$$C(A^*, S) = (S, A^*S, ..., A^{*n-1}S). \tag{7}$$

Let be $rankC(A^*, S) = r$. It is clear that if $rankS = n$, then $r = n$. The converse is, however, generally not true. If $r = n$, the pair (A^*, S) is said to be controllable in the control theory [6].

The following assertion is due to Chen [7] (see, also, Wimmer [8]).

(F) If the pair (A^*, S) is controllable, then A has no pure imaginary eigenvalues, and, according to result (D), $u = i^-$.

It is natural to ask what happens if the pair (A^*, S) is not controllable. Several partial answers on this question we give in the next section.

2. The instability degree in the case $rankC(A^*, S) < n$

Let $rankC(A^*, S) = r < n$, and let $\hat{A}$ denotes the restriction of A to $KerC^*(A^*, S)$ - the kernel of $C^*(A^*, S)$. Note that the subspace $KerC^*(A^*, S)$ is A-invariant and $\dim(KerC^*(A^*, S)) = n - r$.

Lemma 1. *The purely imaginary eigenvalues of the operator A coincide with the purely imaginary eigenvalues of the restriction $\hat{A}$.*

Proof. Let $\lambda = i\omega$ be a purely imaginary eigenvalue of A with corresponding eigenvector X. By the definition of $C^*(A^*, S)$, it follows that

$$C^*(A^*,S)X = \begin{pmatrix} SX \\ SAX \\ . \\ . \\ . \\ SA^{n-1}X \end{pmatrix} = \begin{pmatrix} SX \\ \lambda SX \\ . \\ . \\ . \\ \lambda^{n-1}SX \end{pmatrix}. \tag{8}$$

On the other hand, from (5) we have

$$-(SX, X) = ((BA + A^*B)X, X) = i\omega(BX, X) - i\omega(BX, X) \equiv 0, \tag{9}$$

which yields $SX = 0$ because S is semi-definite. Now (8) implies $X \in KerC^*(A^*,S)$. □
The following theorem is an immediate consequence of the result (D) and Lemma 1.

Theorem 1. *If the restriction $\hat{A}$ has no pure imaginary eigenvalues, then $u = i^-$.*

Corollary 1. *If $r = n-1$, then $u = i^-$.*

It is follows from the fact that $\hat{A}$ is a real matrix.

Example 1. Let

$$A = \begin{pmatrix} 1 & 2 \\ 0 & -1 \end{pmatrix} \text{ and } B = \begin{pmatrix} -1 & 0 \\ 0 & 1 \end{pmatrix}. \tag{10}$$

Obviously, the eigenvalues of A are 1 and -1, i. e., $u = 1$. On the other hand, we have

$$S = -(BA + A^*B) = \begin{pmatrix} 2 & 2 \\ 2 & 2 \end{pmatrix} \geq 0, \tag{11}$$

and

$$C(A^*,S) = \begin{pmatrix} 2 & 2 & 2 & 2 \\ 2 & 2 & 2 & 2 \end{pmatrix}. \tag{12}$$

Since $r = rankC(A^*,S) = 1$, $n = 2$, and $i^- = 1$, according Corollary 1, we conclude that $u = 1$.
Let T denotes the $n \times n$ matrix whose columns are an orthonormal basis so that the first $n - r$ columns of T are a basis of the subspace $KerC^*(A^*,S)$ and its last r columns are a basis of $KerC^*(A^*,S)^\perp$. Since $KerC^*(A^*,S)$ is A-invariant,

$$T^*AT = \begin{pmatrix} A_{11} & A_{12} \\ 0 & A_{22} \end{pmatrix}, \tag{13}$$

where the $(n-r) \times (n-r)$ matrix A_{11} is the representation of the restriction $\hat{A}$ relative to the basis of $KerC^*(A^*,S)$. Also we have

$$T^* ST = \begin{pmatrix} 0 & 0 \\ 0 & S_{22} \end{pmatrix} \text{ and } T^* BT = \begin{pmatrix} B_{11} & B_{12} \\ B_{12}^T & B_{22} \end{pmatrix}, \tag{14}$$

where S_{22} and B_{22} are $r \times r$ matrices. It is easy to see that $rankC(A^*, S) = rankC(A_{22}^*, S_{22}) = r$, i. e., the pair (A_{22}^*, S_{22}) is controllable.

Let v and (i_v^+, i_v^-) denote the restriction of the form (Bx, x) to the subspace $KerC^*(A^*, S)$ and its signature, respectively.

Theorem 2. *Let the quadratic form v be non-degenerate. Then, the following is true:*

(i) $(n - r)$ is even and $\max(0, i^- + r - n) \le u \le i^-$;

(ii) if v is positive definite, then $u = i^-$;

(iii) if v is negative definite, then $u = i^- + r - n$;

(iv) if i_v^- (i_v^+) is equal to unity, then $u = i^-$ ($u = i^- + r - n + 2$).

Proof. Without loss of generality we can assume that A, S and B have the forms (13) and (14). Note that B_{11} is the representation of the matrix associated with the quadratic form v relative to the basis determined by columns of T, and non-degeneracy of v implies $\det B_{11} \ne 0$. The matrix

$$R = \begin{pmatrix} I & -B_{11}^{-1}B_{12} \\ 0 & I \end{pmatrix} \tag{15}$$

transforms B into block-diagonal form

$$R^* BR = \begin{pmatrix} B_{11} & 0 \\ 0 & \widetilde{B}_{22} \end{pmatrix}, \tag{16}$$

where $\widetilde{B}_{22} = B_{22} - B_{12}^* B_{11}^{-1} B_{12}$. Also we have

$$R^* SR = \begin{pmatrix} 0 & 0 \\ 0 & S_{22} \end{pmatrix}, \tag{17}$$

and

$$R^{-1} AR = \begin{pmatrix} A_{11} & \widetilde{A}_{12} \\ 0 & A_{22} \end{pmatrix}. \tag{18}$$

From (5) we have

$$R^*(BA + A^*B)R = (R^*BR)(R^{-1}AR) + (R^{-1}AR)^*(R^*BR) = -R^*SR, \tag{19}$$

which yields

$$B_{11}A_{11} + A_{11}^*B_{11} = 0, \tag{20}$$

$$\widetilde{B}_{22}A_{22} + A_{22}^*\widetilde{B}_{22} = -S_{22}, \ S_{22} \ge 0. \tag{21}$$

Equation (20) implies that $B_{11}A_{11}$ is a skew-symmetric matrix. Since $\det(B_{11}A_{11}) \ne 0$, it follows that $n - r$ is even. In (21) the condition of result (F) is satisfied, therefore $u(A_{22}) = i^-(\widetilde{B}_{22})$. Obviously, $\max(0, i^- + r - n) \le i^-(\widetilde{B}_{22}) \le u$. Also, according to the estimation (C), $u \le i^-$, which finishes the proof of part (i).

In (20) the definiteness of v implies A_{11} is similar to a skew-symmetric matrix, hence all eigenvalues of A_{11} are purely imaginary, and, consequently, $u = u(A_{22}) = i^-(\widetilde{B}_{22})$. If v is positive (negative) definite, then $i^-(\widetilde{B}_{22}) = i^-$ ($i^-(\widetilde{B}_{22}) = i^- + r - n$).We have thus proved parts (*ii*) and (*iii*).

Under the condition of the part (*iv*) it follows from the congruence (*B*) that $u(A_{11}) = 1$. On the other hand, $u(A_{22}) = i^-(\widetilde{B}_{22})$, $i^-(\widetilde{B}_{22}) = i^- - 1$ if $i_v^- = 1$, and $i^-(\widetilde{B}_{22}) = i^- - n + r + 1$ if $i_v^+ = 1$, which proves part (*iv*). □

Example 2. Let
$$A = \begin{pmatrix} -1 & 1 & 1 & 1 \\ 1 & -1 & 1 & 1 \\ -1 & -1 & 1 & -1 \\ -1 & -1 & -1 & 1 \end{pmatrix}. \tag{22}$$

If we choose
$$2V = -2x_1 x_2 - x_3^2 - x_4^2, \tag{23}$$
then the derivative of this function, by virtue of system (4), (22), is
$$\dot{V} = -(x_2 - x_1)^2 - (x_4 - x_3)^2 \le 0. \tag{24}$$
The matrix S associated with quadratic form (24) is
$$S = \begin{pmatrix} 1 & -1 & 0 & 0 \\ 1 & 1 & 0 & 0 \\ 0 & 0 & 1 & -1 \\ 0 & 0 & -1 & 1 \end{pmatrix}, \tag{25}$$
and the controllability matrix $C(A^*, S)$ can be written in the partitioned form
$$C(A^*, S) = \begin{pmatrix} 0 & F & 0 & 2F & 0 & 4F & 0 & 8F \\ F & 0 & -2F & 0 & 4F & 0 & -8F & 0 \end{pmatrix}, \tag{26}$$
where
$$F = \begin{pmatrix} 1 & -1 \\ -1 & 1 \end{pmatrix}. \tag{27}$$
Obviously $r = rank C(A^*, S) = 2$. Also, it is easy to see that $i^- = 3$, and
$$KerC^*(A^*, S) = \{x \in \Re^4 : x_2 = x_1, x_4 = x_3\}. \tag{28}$$
The restriction $v = -x_1^2 - x_3^2$ is negative definite and, according to part (*iii*) of Theorem 2, $u = 1$.

By a review of the proof of result (*C*) given in [4], we see that $i^- \ge u \ge \max\{0, i^- - s\}$ where s is the number of purely imaginary eigenvalues of A. If those eiganvalues are simple, then $s \le n - r$, since the subspace spanned by their eigenvectors, according to proof of Lemma 1, belongs to $KerC^*(A^*, S)$. Consequently , $u \ge \max\{0, i^- + r - n\}$. Further, this inequality is also valid in the general case of multiple eigenvalues of A, as follows from a generalization of the inertia theorem [9]. Now we can formulate the following assertion.

Theorem 3.

$$\max(0, i^- + r - n) \le u \le i^- . \tag{29}$$

Remark 1. If we drop the assumptions $\det A \ne 0$ and $\det B \ne 0$, the left inequality in (29) remains true. It follows from [9].

3. The instability degree of mechanical systems

In this section the above results will be applied to two classes of mechanical systems with finite numbers of degrees of freedom.

3.1 Non-conservative systems

The equations of motion of a mechanical system with m degrees of freedom subjected to potential and non-conservative positional (circulatory) forces may be reduced in a neighborhood of the equilibrium position $q = 0$ to the form

$$\ddot{q} + Kq + Pq = N(q, \dot{q}), q \in \mathfrak{R}^m , \tag{30}$$

where $K = K^*$ and $P = -P^*$, and $N(q, \dot{q})$ is a collection of terms of no lower than second order in $q, \dot{q}$ [10]. The real matrices K and P are related to potential and circulatory forces, respectively.

Equation (30) is equivalent to the first order equation (1), (2) with $x \in \mathfrak{R}^m \{q\} \times \mathfrak{R}^m \{\dot{q}\}$ and

$$A = \begin{pmatrix} 0 & I \\ -(K+P) & 0 \end{pmatrix}, \tag{31}$$

where I is the identity matrix of order m. The eigenvalues of A are the roots of the polynomial

$$\Delta(\lambda) = \det(\lambda^2 I + K + P) . \tag{32}$$

It is clear that $0 \le u \le m$, since $\Delta(\lambda) = \Delta(-\lambda)$.

We put $V = -2(P\dot{q}, q)$, i. e.,

$$B = \begin{pmatrix} 0 & P \\ -P & 0 \end{pmatrix}. \tag{33}$$

Then $i^- = rankP$ and

$$BA + A^* B = -S \tag{34}$$

with

$$S = \begin{pmatrix} D & 0 \\ 0 & 0 \end{pmatrix}, D = KP - PK - 2P^2 . \tag{35}$$

Note that $P^2 \le 0$, since P is a skew-symmetric matrix. On the other hand, it is easy to see that $rankC(A^*, S) = 2rankC(K - P, D)$. Applying Theorem 3 to (34) we obtain the following result.

Theorem 4. *If the matrix*
$$D = KP - PK - 2P^2 \tag{36}$$
is positive semi-definite, then
$$u \geq \max\{0, \; 2rankC(K - P, D) + rankP - 2m\} . \tag{37}$$

Corollary 1. *If* $D > 0$, *then* $u = m$, *i. e. the equilibrium state* $q = \dot{q} = 0$ *is completely unstable.*

Proof. $D > 0$ requires $\det P \neq 0$. Also, in this case $rankC(K - P, D) = m$. □

Theorem 5. *Suppose that* $K \leq 0$. *Then*
$$m \geq u \geq \max\{rankC(P, K), rank(K + P)\} . \tag{38}$$

Proof. We assume that $V = -(q, \dot{q})$. Then $i^- = m$ and $\dot{V} = (Kq, q) - (\dot{q}, \dot{q})$, i. e.
$$S = \begin{pmatrix} -K & 0 \\ 0 & I \end{pmatrix} \geq 0 . \tag{39}$$
Further we have $r = rank(A^*, S) \geq m + \max\{rankC(P, K), rank(K + P)\}$, because of the given block structure of matrices (31) and (39). Hence, (38) follows from Theorem 3. □

Corollary 2. *If* $K < 0$, *then* $u = m$.

Theorem 6. *Suppose that* $\det(K + P) \neq 0$ *and* $K \geq 0$. *If the matrix*
$$F = K^2 + P^2 \tag{40}$$
is negative semi-definite, then
$$m \geq u \geq rankF + \max\{rankK, rankF\} - m . \tag{41}$$

Proof. Assume that $V = -((K + P)\dot{q}, q)$. Then $i^- = m$, since $\det(K + P) \neq 0$. The derivative of V according to the linearized system of (30) is $\dot{V} = (Fq, q) - (K\dot{q}, \dot{q})$, because $KP + PK$ is skew-symmetric. Consequently, the matrix S has the block diagonal form
$$S = \begin{pmatrix} -F & 0 \\ 0 & K \end{pmatrix} \tag{42}$$
and, by assumptions $K \geq 0$ and $F \leq 0$, its is positive semi definite. It is easy to see that $r = rankC(A^*, S) \geq rankF + \max\{rankF, rankK\}$. It remains to use inequality (29). □
The following corollary supplements one instability result in [11].

Corollary 3. *If matrix (40) is negative definite, then* $u = m$.

3.2 Conservative gyroscopic systems

The equations of motion of a system with gyroscopic and potential forces linearized in a neighborhood of the equilibrium position may be reduced to the form

$$\ddot{q} + G\dot{q} + Kq = 0 \,, q \in \Re^m \,, \tag{43}$$

where $G = -G^*$ and $K = K^*$. The skew-symmetric matrix G is related to gyroscopic forces.

The equations of motion have a first integral, namely, the energy integral $2V = (\dot{q}, \dot{q}) + (Kq, q)$. If $\det K \neq 0$, then V is non-degenerate quadratic form and $q = 0$ is an isolated equilibrium position of the system. The instability degree of Poincare, i_K^-, is negative inertia index of quadratic form (Kq, q), and, obviously, it is identical with the inertia index of V. It follows from congruence (B) that if i_K^- is odd, then gyroscopic stabilization is impossible (Kelvin's theorem, [1]).

Theorem 7. *If the matrix*

$$H = G^2 - 4K \tag{44}$$

is positive semi-definite, then

$$u \geq rankC(G, H) \,. \tag{45}$$

Proof. Equation (43) is equivalent to the first order equation (4) with

$$A = \begin{pmatrix} -G & -K \\ I & 0 \end{pmatrix} . \tag{46}$$

The substitution $x = Ry$, with

$$R = \begin{pmatrix} I & -G/2 \\ 0 & I \end{pmatrix} , \tag{47}$$

transform equation (4), (46) to the form $\dot{y} = \widetilde{A}y$, where

$$\widetilde{A} = R^{-1}AR = \begin{pmatrix} -G/2 & G^2/4 - K \\ I & -G/2 \end{pmatrix} . \tag{48}$$

Now we put

$$B = \frac{1}{2}\begin{pmatrix} 0 & -I \\ -I & 0 \end{pmatrix} . \tag{49}$$

Then $i^- = m$ and

$$S = -(B\widetilde{A} + \widetilde{A}^*B) = \begin{pmatrix} I & 0 \\ 0 & G^2/4 - K \end{pmatrix} \geq 0 \,. \tag{50}$$

One can readily see that $r = rankC(\widetilde{A}^*, S) = m + rankC(G, G^2 - 4K)$. It remains to use inequality (29). □

The following corollary supplements the well-known instability condition of Hagedorn [12].

Corollary 4. *If matrix (44) is positive definite, then* $u = m$.

References

[1] Chetayev N G (1955) *Stability of Motion*, Gostekhizdat, Moscow.

[2] Kozlov V V (1993) On the degree of instability, *Prikl. Mat. Mekh.,* 57(5), pp. 14-19.

[3] Ostrowski A and Schneider H (1962) Some theorems on the inertia of general matrices, *J. Math. Anal. Appl.*, 4, pp. 72-84.

[4] Kozlov V V (2010) Remarks on the degree of instability, *Prikl. Mat. Mekh.,* 74(1), pp. 18-21.

[5] Carlson D and Schneider H (1963) Inertia theorems: the semidefinite case, *J. Math. Anal. Appl.*, 6, pp. 430-446.

[6] Lee E B and Markus L (1967) *Foundations of Optimal Control Theory,* Wiley, New York.

[7] Chen C (1973) A generalization of the inertia theorem, *SIAM J. Appl. Math.*, 25(2), pp. 158-161.

[8] Wimmer H K (1974) Inertia Theorems for Matrices, Controllability, and Linear Vibrations, *Linear Algebra and its applications*, 8, pp. 337-343.

[9] Loewy R (1997) An Inertia Theorem for Lyapunov's Equation and the Dimension of a Controllability Space, *Linear Algebra and its applications*, 260, pp. 1-7.

[10] Merkin D R (1997) *Introduction to the Theory of Stability*, Springer-Verlag, NY.

[11] Bulatovic R M (1999) On the stability of linear circulatory systems, *Z. Angew. Math. Phys.,* 50, pp. 669-674.

[12] Hagedorn P (1975) Uber die Inatabilitat Konservativer Systeme mit Gyroskopishen Kraften, *Arch. Rat. Mech. Anal.,* 58, pp. 1-9.

REVIEW ON MECHANICAL MODELING OF THE HUMAN VOICE PRODUCTION SYSTEMS

L. Cveticanin[1]

[1] Faculty of Technical Scineces,
The University of Novi Sad, Trg D. Obradovica 6, 21000 Novi Sad
e-mail: cveticanin@uns.ac.rs

Abstract. In this paper a review on mechanical modeling of the human voice production systems is given. The basic model of the vocal cords/vocal tracts and vocal folds is a two-mass non-linear oscillator system which is assumed to be the basic one for mechanical description in voice production [1]. The corresponding mathematical model is a system of two coupled second order non-linear differential equations. Usually, this system of equations does not have an exact closed form solution and various analytical and numerical solving methods are applied. The solutions describe the self-excited vibrations of the mechanical elements of voice production. The influence of air flow in glottis is additionally modeled and included into the previously developed mechanical system. Analyzing the corresponding mathematical models it is evident that beside the self-excited oscillations of vocal cords some additional vibrations appear. The vibrations may be regular but also irregular like bifurcation and chaos. The numerical simulation gives the parameter values for proper and improper voice production. Based on the results given in review the objectives for future investigation in the matter are given.

1. Introduction

For a long time the researchers are trying to simulate the human voice production. Various mechanical and mathematical models are developed for describing of the human organs which are connected with voice production but also of the process of phonation. In essence, voice is generated by movement of two lateral opposing vocal folds located in the larynx. Vibration of the vocal folds is produced by air flow through the trachea, generated by lung. Vocal folds vibrate, modulating the flow of air being expelled from the lungs during phonation. Sound is generated in the larynx by chopping up a steady flow of air into little puffs of sound waves.

Complexity of vocal folds, their histology, shape, position, etc., give us a possibility to treat the problem in quite different manner. Same ability is evident for modeling of the process of phonation. It is the reason that a numerous aspects of the problem are investigated and a great number of results are published (more than 1000).

For mechanical view of the human voice producing it is necessary to connect the dynamics of vocal folds and the aerodynamics of the vocal tract. Coupling between vocal fold dynamics and vocal tract acoustics attracts the interest in examining the voice quality of various kinds of vocalization and detecting of pathology of voice production system when there is no visual evidence for morphological laryngeal abnormalities. The studies of vocal fold biomechanics give an insight into voice production and also provide important information about laryngeal pathology development. In this paper some of the essential investigation will be shown.

2 Basic two-mass model of the vocal fold

Two-mass model, developed and analyzed by Ishizaka and Flanagan [1], evolved to a standard for exploring the voice producing system through the years. The basic principle of modeling is intimately related to the observed phase difference between the lower and the upper edge of the vocal fold. This effect can be modeled by representing each fold by two coupled oscillators (Fig.1). For normal voice, the oscillators are bilaterally symmetric.
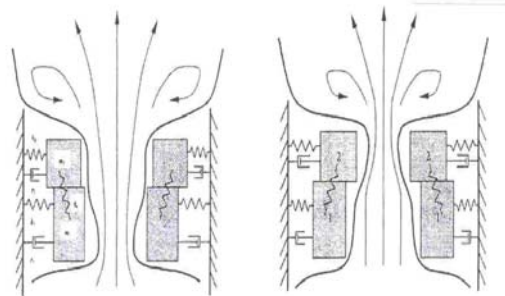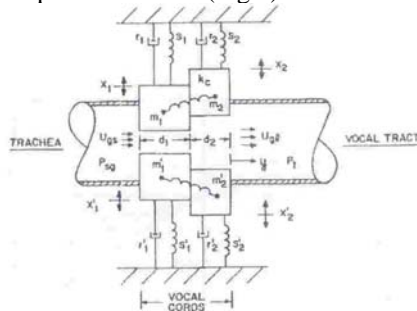
Fig.1 Two-mass model of voice folds [1]   **Fig.2** Air flow through glottis [2]

The displacing tissue of each cord is considered to be approximated by two stiffness-coupled masses. The masses are permitted displacement in both the lateral (x) direction and the longitudinal (y) direction. Motion in both directions is opposed by nonlinear restoring stiffness s and viscous damping r, shown explicitly only for the x direction. The x and y motions are assumed independent and uncoupled and represent the generalized coordinates for the two-degree-of-freedom system. Lateral displacement of masses m_1 and m_2 is conditioned by the internal coupling stiffness k_c which permits realistic phase differences in the lateral displacements. For motion in the longitudinal direction, masses m_1 and m_2 are assumed to be locked together and move cophasically. The characteristics of all mechanical elements are based upon dates obtained by clinical observations (see [2]-[4]) and measuring [5],[6].

The main goal of the model was to synthesize voice by a self-oscillating mechanism. The oscillations are driven by the lung pressure. The driving Bernoulli force which is influenced by the subglottal pressure and the time-varying glottal geometry induces self-sustained oscillations. The induced phase difference of the upper and the lower mass enables the energy transfer from the airstreams to the vocal folds. For a sufficiently large subglottal pressure the dissipative losses can be compensated and phonation sets in.

Gunter [7] believes that the oscillating vocal folds maintain their motion by deriving energy from the flow of air through the glottis. To oscillate, the vocal folds are brought near enough together such that air pressure builds up beneath the larynx (Fig.2). The folds are pushed apart by this increased subglottal pressure, with the inferior part of each fold leading the superior part. Under the correct conditions, this oscillation pattern will sustain itself. Maximum area declination rate affects the maximum air flow declination [8]. Varying of the area the vocal folds vibrate and generate a sound rich in harmonics [9]. The harmonics are produced by collisions of the vocal folds with themselves, by recirculation of some of the air back through the trachea, or both.

Finally, it is important to be said that the air flow – mechanical structure model of the human voice producing has an important role in acoustic integration [10],[11].

REMARK: Suggested mechanical model is convenient not only for voice folds vibration but also for their posturing. Namely, vocal fold dynamics for phonation can be treated in two parts [12]:

1. large and relatively slow deformation occurring when the vocal folds are positioned for voicing, coughing and breathing by moving laryngeal cartilages with muscle forces – this part is referred as vocal fold posturing which is subdivided into:
    a) adducting or abducting the medial surfaces of the vocal folds and
    b) elongating or shortening of the vocal folds;
2. small and relatively fast deformations occurring when the tissue is driven into self-sustained oscillation by aerodynamic and acoustic pressures – this part is referred as fold vibration.

The posturing occurs in a nonperiodic but ultimately always cyclic fashion at frequencies 1-10 Hz, but the vocal fold vibration occurs at 100-1000 Hz. Although vocal fold posturing and vocal fold vibration is often thought to be separate mechanical processes, many parameters of vibration (for example, fundamental frequency, amplitude of vibration and voice onset time) are dependent on posturing. Analyzing the model simulating the adduction of the medial surface of the vocal cord during posturation it is concluded that it affects the intensity of vocal folds vibration and involves into fundamental frequency regulation [13]. This result is previously obtained by clinical observation [14], too.

During last forty years, the two mass-model of Ishizaka & Flanagan [1] was the basic one for the most of investigations in physical properties of human voice production. Due to its simplicity the model was convenient for application: the authors applied it for investigation of excitation in vocal-cord/vocal-tract speech synthesizer [15], to obtain effect of air volume displace by the vibrating vocal cords [16], and also for analyzing of the influence of the oral airflow in men and woman on vocal folds dynamics [17], for example. Nowadays, the model is used for clarifying of the phenomena in voice production due to nonlinear properties of the system but also to explain and detect the anomalies and diseases which are not visible with apparatus for clinical observation. It requires another types of mechanical models to be developed.

3. From one- to finite-element vocal fold models

3.1 One-mass one-degree-of-freedom model of the vocal cord

Fulcher et al. [18] assumed another type of energization of the vocal folds than the previously mentioned one (see Sec.2). Namely, they stated that the action of the aerodynamic forces on the vocal folds is captured by negative Coulomb damping which causes the vibration of the vocal cords (Fig.3). Effective one-mass model with negative Coulomb damping force is introduced. This force adds energy to the oscillator instead of removing it. Adding a viscous damping term makes steady state motion possible. In the long-time limit the analytical solutions approach a limit cycle and the amplitude and velocity lose their dependence on the history of the motion. An elevated lung pressure gives rise to a flow of air through the glottis and produces a series of alternating converging and diverging shapes of the vertical dimensions of the vocal folds. The pressure distributions in the glottis resulting from the series of shapes are alternately higher and lower than the pressures in the vocal tract. These pressure variations are in phase with the motion of the

vocal folds and add energy to the oscillator in the same way as negative Coulomb damping does. Limit cycle of the oscillator with negative Coulomb damping provides a natural explanation of the self-oscillation property of the model.
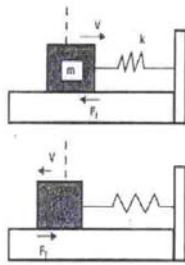
Fig.3 Model with Coulomb damping [18]   **Fig.4** One-mass with two-degrees-of-freedom model of the vocal cord [20]
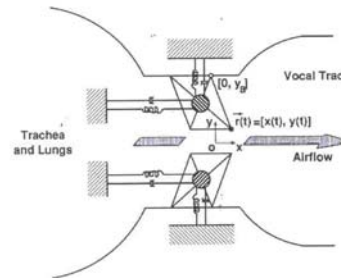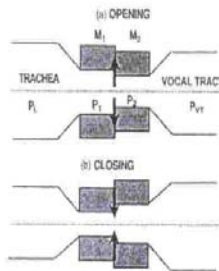
Simple, one-degree-of-freedom vocal fold model was developed to investigate whether kinematic features of vocal fold movement confirm increased muscle stiffness [19]. Model simulations verified that increases in stiffness were associated with changes in kinematic parameters, suggesting that increases in gesture rate would affect kinematic features during phonation. This conclusion was proved experimentally in individuals with trans-nasal endoscopy during a simple vocal fold abductory-adductory task.

3.2 One-mass vocal cord model with two-degrees-of-freedom
An acoustic tube generally yields an inductive load in the fundamental frequency bellow a resonance peak, while the load turns out to be capacitive in the formant frequency above the peak. The two-mass model can simulate self-excited oscillation with a capacitive acoustic load because it can represent the phase difference between the upper and lower parts of the vocal fold. Unfortunately, the model is not correct for the case when the frequencies meet. Then the low frequency suddenly jumps to a value much larger than resonance peak. Adachi and Yu [20] show that the one-mass model with two-degrees-of-freedom (parallel and perpendicular to the airflow) can eliminate this lack. Due to the two-dimensional motion of the vocal folds the model can successfully simulate self-excited oscillation in a wide frequency range with no discontinuity of vibration. The model yields a smooth transition between oscillations with an inductive load and a capacitive load of the vocal tract with no sudden jumps in the vibration frequency. Self-excitation is possible both below and above the first formant frequency of the vocal tract. By taking advantage of the wider continuous frequency range, the model can successfully be applied to the sound synthesis of a high pitched soprano singing, where the fundamental frequency sometimes exceeds the first formant frequency. Geometry of the vocal fold is represented by a parallelogram (Fig.4). As the mass moves the parallelogram is deformed and the vocal fold simultaneous executes both swinging and elastic motions. The motions are coupled and mathematically described with a complex function. Comparing the suggested model with the usual two-mass model among other similar features, the similarities in the amplitudes of the glottal area and the glottal volume flow velocity, the variation in the volume flow waveform with the vocal tract shape and the dependence of the oscillation amplitude upon the averaging opening area of the glottis, are found.

3.3. Three-degree-of-freedom vocal cord models

Story and Titze [21] extended the previous two-mass model of the vocal fold by introducing of the cover-body model as a three-degree-of-freedom system. Cover-body model represents the three mass version: cover is modelled with two masses and three springs and the body connected to the thyroid cartilage is modelled as one mass with compressible spring. In the paper of Titze and Story [22] the modification of the cover-body model is done: the cover is modelled with a rotating plate which substitutes the two mass system, while the body remains as previously included mass a compressible spring (Fig.5).
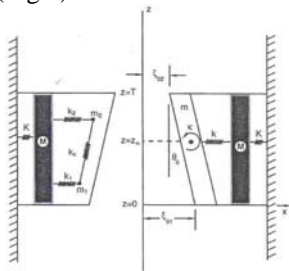
Fig.5 Three-degree-of-freedom model [22]   **Fig.6** Three-dimensional model [23]
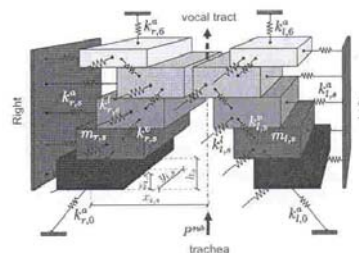
The following assumptions throughout the body-cover derivations are made:
1. The two vocal folds move symmetrically with respect to the glottal midplane.
2. There is no vertical displacement of tissue.
3. The glottal area varies linearly from the bottom to top of the vocal folds.
4. For glottal aerodynamics it is assumed the Bernoulli flow from the lungs to the point of flow separation, at which point jet flow continues and the pressure remains constant in the jet from flow detachment to glottal exit.

Motion of the cover – body system is described with three coupled differential equations. The case when the aerodynamic torques and forces act and also when they are omitted are considered. For the first case the model is focused on vocal fold tissue characteristics. When the driving forces are not zero the equations of motion are coupled by the fact that both the driving torque and the driving force on the cover are dependent on a common glottal flow. The oscillation regions are affected by acoustic loading of the vocal tract both subglottal and supraglottal. The results obtained by using of the bar-plate model are compared with three-mass lumped model.

Recently, Yang et al. [23] extended the two-dimensional model of the vocal fold into a three-dimensional one by including the vertical vibration (in the two-dimensional model only the lateral and longitudinal displacements of the vocal cord were discussed). Vocal fold is assumed to consist of five horizontal layers (planes) arranged from inferior to superior (Fig.6). The anchor forces, which connect the masses to fixed body, and the vertical and longitudinal coupling internal forces between masses are supposed to be nonlinear deflection functions. The collision impact force is included into the model, too. The influence of the aerodynamic force, which causes the three-dimensional mass elements of vocal fold to oscillate, is investigated. The driving force is of Bernoulli type produced by the glottal flow originating from the lung and acting on the vocal folds from inferior to superior through the whole larynx. The driving force depends not only on the subglottal pressure but also the geometric dimensions (thickness and length of the vocal folds and on

the rest positions). The resulting model enables visualization of the three-dimensional dynamics of the human vocal folds during phonation for both symmetric and asymmetric vibrations.

3.4 Finite-element model
Finite-element model of vocal fold vibration was introduced by Alipour-Haghighi et al. [24]. Suggested model is modified into a self-oscillating finite-element one capable of simulating vocal fold vibration and airflow [25]. Model is suitable for investigation of the vocal fold impact. The calculated airflow pressure is applied on the vocal fold as the driving force. The interaction between airflow and the vocal folds produces a self-oscillating solution. Lung pressures between 0.2 and 2.5 kPa were used to drive the self-excited model. Tissue collision during phonation produces a very large impact pressure which correlates with the lung pressure and glottal width. Larger lung pressure and a narrower glottal width increase the impact pressure. In the inferior-superior direction the maximum impact pressure is related to the narrowest glottis. In the anterior-posterior direction the greatest impact pressure appears at the midpoint of the vocal folds.

7. Conclusions and directions to future investigation

Based on the published results it is concluded that mathematical models, based on the physical model of human voice production, give very good qualitative description of the phenomena, but in spite of the fact that the clinically observed and measured parameters are used for modeling, the obtained results quantitatively differ from real one. It requires the improvement of the accuracy of models. The following is suggested:
1. Although simulation of vocal fold vibration is clearly more realistic with a model having a large degree of freedom, a model with a small degree of freedom still has its merits. Namely, more than ten coupled ordinary differential equations with many parameters are necessary to solve the mechanical and the aerodynamical problem. In comparison with more realistic models, such as those based on partial differential equations simulations, or systems of more than two coupled oscillators, the two-mass model appears to be quite simple. Such a minimal model highlights the self-excitation mechanism by abstracting the essence from the actual complex vocal fold vibration. The two-mass model has actually been devised as such a minimal model to simulate self-sustained oscillation with a capacitive acoustic load of the vocal tract, which cannot be replicated with the one-mass model. We suggest to apply the two-mass model as a basic one, but to include the nonlinear properties of the system. Analytical solving procedures used for analysing two mass systems and corresponding system of two second order nonlinear differential equations have to be applied.
2. One of the most severe restrictions of low-dimensional models is the exclusion of vertical movement of the tissue. Much more variability in the medial shaping of the glottis e.g., more convergence and divergence is possible if the tissue is simultaneously driven upward and outward, forming elliptic trajectories. But this would double the degrees of freedom and would minimize the interpretive power that nonlinear dynamics can offer. To investigate many aspects of vocal quality and for modelling pathology higher dimensional models and fewer rules are necessary.
3. In the three-mass model the vocal tract simulation is not included. Vocal fold vibration can be profoundly affected by the acoustic load of the vocal tract, but this have to be investigated in future.

4. Further improvement is possible by analyzing of the vocal fold as a two-mass system where each mass has two-degrees-of-freedom. The inclusion of the degree of freedom along the length of the vocal fold (in vertical direction) will help in more accurate simulation of the phase difference between the upper and lower parts of the vocal folds which is observed in actual vocal fold vibration. Vibration of a mass with two-degree-of-freedom would be described with the complex deflection function.

5. Results obtained by modeling the vocal ligament as a beam with linear longitudinal tension and bending stiffness (without shear) are qualitatively correct, but quantitatively differ from real one. Existing model has to be modified by introducing the nonlinear properties of the system and of the shear effect. Obtained partial differential equation with nonlinearity has to be solved and discussed.

6. In the model of vocal cord the negative Coulomb damping is assumed to be a linear one. To improve the model we suggest introducing the nonlinear damping of the integer or noninteger order which is obtained empirically by clinical measuring. We believe that such models would give more accurate.

7. Non-stationary vocal-fold oscillations are typical for many voice disorders. Inclusion of the time variable parameters and the reactive force, which acts due to parameter variation in time, gives an additional influence on the vibration of the fold. Dynamics of the system with time-variable parameters is widely developed and we suggest its application. Besides, the stability of non-stationary vocal folds vibration has to be more intensively analyzed. Known stability analysis of time-variable systems may be applied.

8. Simplified asymmetric two-mass model encompasses the minimum number of degrees of freedom and of parameters. However, Mergel and Titze (2000) show that it allows the reconstruction of very complex laryngeal mechanisms with high accuracy. Vocal fold oscillations are representative for the class of pathologies characterized by:
- laryngeal asymmetry without morphological changes i.e. asymmetric vocal fold tension
- increased glottal rest area
- abnormally increased subglottal pressure which are the characteristics of many forms of laryngeal paralyses.

These diseases are accompanied by instabilities and irregular motion of the vocal folds, as it is obtained analyzing the corresponding voice cord model. New results would be expected by investigating of the chaotic motion and bifurcation in the model which is closer to the real system (one-mass model with two-degrees-of-freedom).

References

[1] Ishizaka K, Flanagan JL (1972) Synthesis of Voiced Sounds from a Two-Mass Model of the Vocal Cords, *Bell Sys Tech J* **50**: 1233-1268.
[2] Titze IR (1984) Parameterization of the glottal area, glottal flow, and vocal fold contact area. *J Acoust Soc Am* 75:570-580
[3] Dollinger M, Hoppe U, Hettlich F, Lohscheller J, Schubert S, Eysholdt U (2002) Vibration parameter extraction from endoscopic image series of the vocal fold. *IEEE Trans Biomed Eng* **49**:773-781

[4]   Dollinger M, Braunschweig T, Lohscheller J, Eysholdt U, Hoppe U (2003) Normal voice production: Computation of driving parameters from endoscopic digital high speed images. *Methods Inf Med* **42**:271-276

[5]   Spencer M, Siegmund T, Mongeau L (2008) Determination of superior surface strains and stresses, and vocal fold contact pressure in a synthetic larynx model using digital image correlation. *J Acoust Soc Am* **123**:1089-1103

[6]   Schwarz R, Dollinger M, Wurzbacher T, Eysholdt U, Lohscheller J (2008) Spatiotemporal quantification of vocal fold vibrations using high-speed videonedoscopy and a biomechanical model. *J Acous Soc Am* **123**:2717-2732

[7]   Gunter HE (2003) A mechanical model of vocal-fold collision with high spatial and temporal resolution. *J Acoust Soc Am* **113** (2):994-1000

[8]   Titze IR (2006) Theoretical analysis of maximum flow declination rate versus maximum area declination rate in phonation. *J Speech Lang Hear Res* **49**:439-447.

[9]   Zhang Z, Neubauer J, Berry DA (2006) Aerodynamically and acoustically driven modes of vibration in a physical model of the vocal folds. *J Acoust Soc Am* **120**:2841-2849

[10] Becker S, Kniesburges S, Muller S, Delgado A, Link G, Kaltenbacher M, Dollinger M (2009) Flow-structure-acoustic integration in a human voice model. *J Acoust Soc Am* **125**:1351-1361

[11] Bailly L, Henrich N, Pelorson X (2010) Physiological description and aerodynamic modeling. *J Acoust Soc Am* **127** (5):3212-3222

[12] Titze IR, Hunter EJ (2007)A two dimensional biomechanical model of vocal fold posturing. J Acoust Soc Am 121 (4):2254-2260

[13] Dollinger M, Berry DA (2006) Visualization and quantification of the medial surface dynamics of an excised human vocal fold during phonation. *J Voice* 20:401-413

[14] Berry DA, Montequin DW, Tayama N (2001) High-speed digital imagining of the medial surface of the vocal folds. *J Acoust Soc Am* **110**:2539-2547

[15] Flanagan JL, Ishizaka K (1976) Automatic generation of voiceless excitation in a vocal-cord/vocal-tract speech synthesizer. *IEEE Trans Acoust Speech Sig Proc* **24**:163-170

[16] Flanagan JL, Ishizaka K (1978) Computer model to characterize the air volume displaced by the vibrating vocal cords. *J Acoust Soc Am* **63** (5):1559-1565

[17] Lucero JC, Koenig LL (2005) Simulations of temporal patters of oral airflow in men and women usding a two-mass model of the vocal folds under dynamic control. *J Acoust Soc Am* **117**:1362-1372

[18] Fulcher LP, Scherer RC, Melynikov A, Gateva V, Limes ME (2006) Negative Coulomb damping, limit cycles, and self-oscillation of the vocal folds. *Am J Phys* **74** (5):386-393

[19] Stepp CE, Hillman RE, Heaton JT (2010) A virtual trajectory model predicts differences in vocal fold kinematics in individuals with vocal hyperfunction. *J Acoust Soc Am* **127** (5):3166-3176

[20] Adachi S, Yu J (2005) Two-dimensional model of vocal fold vibration for sound synthesis of voice and soprano singing. *J Acoust Soc Am* 117 (5):3213-3224

[21] Story BH, Titze IR (1995) Voice simulation with a body cover model of the vocal folds. *J Acoust Soc Am* **97**:1249-1260.

[22] Titze IR, Story BH (2002) Rules for controlling low-dimensional vocal fold models with muscle activation. *J Acoust Soc Am* **112** (3):1064-1076

[23] Yang A, Loscheller J, Berry DA, Becker S, Eysholdt U, Voigt D, Dollinger M (2010) Biomechnical modeling of the three-dimensional aspects of human vocal fold dynamics. *J Acoust Soc Am* **127** (2):1014-1031

[24] Alipour-Haghighi F, Berry DA, Titze IR (2000) A finite-element model of vocal fold vibration. *J Acoust Soc Am* 108:3003-3012

[25] Tao C, Jiang JJ, Zhang Y (2006) Simulation of vocal fold impact pressures with a self-oscillating finite-element model. *J Acoust Soc Am* 119 (6):3987-3994

GEOMETRIC ASPECTS OF NONHOLONOMIC MECHANICAL SYSTEMS

C. Frigioiu

Faculty of Sciences, Dunărea de Jos University, 47 Domneasca, 800008-Galaţi, România

e-mail: cfrigioiu@ugal.ro

Abstract. In this paper we present the nonholonomic mechanical systems studied from a geometric point of view using the Lagrange Geometry. One gives a geometrization of nonholonomic mechanical systems using the geometry of tangent bundle and one obtains the Lagrange equations.

Keywords: Euler-Lagrange equations, Lagrange multipliers, nonholonomic Lagrange space, non-linear connection, semispray.

1. Introduction

In classical mechanics one naturally encounters different kinds of constraints on the motion, mostly holonomic and linear nonholonomic constraints (integrable or non-integrable). Nonholonomic constrained systems have a long subject of research since the first times of Mechanics and they have received a lot of attention in recent years especially, from the geometrical point of view.Surveys of nonholonomic systems can be found in [1], [9], and [7]. A major thrust of present research is to give a complete description of the Hamiltonian [8], [10], [11] and Lagrangian [2], [3] geometry of nonholonomic systems.

This work develops the geometry and dynamics of mechanical systems with nonholonomic constraints from the perspective of Lagrangian geometry. The main idea is to determine the canonical semispray S, whose integral curves give the evolution curves. The geometry of the canonical semispray will determine on the phase space the geometry of the dynamical system associated to the mechanical system.

The part 2 of this article is an overview of the geometry of the tangent bundle TM (phase space), who furnishes the basic tools that have an important role: the Liouville vector field C, the almost tangent structure J, the concept of semispray and the concept of non-linear connection. The theory presented in this section has good applications for a geometric study of the dynamical system determined by a nonholonomic mechanical Lagrangian system.

In part 3, one gives a geometrization of the non-holonomic mechanical systems using the geometry of tangent bundle TM and one obtains the Lagrange equations. The canonical semispray S^*, the non-linear connection N^* generated by the mechanical system and the N^*-linear connection for a nonholonomic mechanical system are studied in this section.

2. Geometric structures on tangent bundle

In this section we introduce the geometric structure that live on the total space of tangent bundle: Liouville vector field, semispray, non-linear connection.

Let M be a smooth C^∞ manifold of finite dimension n. One denotes by (TM, π, M) its tangent bundle. The total space TM of the tangent bundle is a $2n-$dimensional, real manifold, and will be the phase space of the coordinate velocities of the mechanical system.

In a domain of a local chart $U \subset E$, the points $(x, y) \in TM$ have the local coordinates (x^i, y^i). A change of local coordinates on TM has the following form:

$$\tilde{x}^i = \tilde{x}^i(x^1, x^2, ..., x^n), \quad det\left(\frac{\partial \tilde{x}^i}{\partial x^j}\right) \neq 0 \tag{1}$$

$$\tilde{y}^i = \frac{\partial \tilde{x}^i}{\partial x^j} y^j.$$

The canonical projection $\pi : TM \to M$ is defined by:

$$\pi(x, y) = x, \quad \forall (x, y) \in TM. \tag{2}$$

The linear map $\pi_{*,u} : T_u TM \to T_{\pi(u)} M$ induced by the canonical submersion π is an epimorphism of linear spaces for each $u \in TM$. Therefore, its kernel determines a regular, $n-$dimensional, integrable distribution

$$V : u \in TM \to V_u TM := Ker\pi_{*,u} \in T_u TM$$

which is called *the vertical distribution*.

For every $u \in TM$, $\left(\dfrac{\partial}{\partial y^1}, \dfrac{\partial}{\partial y^2}, ..., \dfrac{\partial}{\partial y^n}\right)$ is a basis of $V_u TM$.

The natural basis of tangent space $T_u(TM)$ at the point $u = (x, y) \in U \subset TM$ is given by

$$\left(\frac{\partial}{\partial x^i}, \frac{\partial}{\partial y^i}\right)_{|u}. \tag{3}$$

The coordinates transformation (1) determines the transformations of the natural basis as follows

$$\frac{\partial}{\partial x^i} = \frac{\partial \tilde{x}^j}{\partial x^i} \frac{\partial}{\partial \tilde{x}^j} + \frac{\partial \tilde{y}^j}{\partial x^i} \frac{\partial}{\partial \tilde{y}^j}; \quad \frac{\partial}{\partial y^i} = \frac{\partial \tilde{y}^j}{\partial y^i} \frac{\partial}{\partial \tilde{y}^j}, \tag{4}$$

where

$$\frac{\partial \tilde{y}^j}{\partial y^i} = \frac{\partial \tilde{x}^j}{\partial x^i}; \quad \frac{\partial \tilde{y}^j}{\partial x^i} = \frac{\partial^2 \tilde{x}^j}{\partial x^i \partial x^h} y^h.$$

Denote by $\mathscr{F}(TM)$ the ring of real-valued functions over TM and by $\chi(TM)$ the $\mathscr{F}(TM)$-module of vector fields on TM.

We also consider $\chi^v(TM)$ the $\mathscr{F}(TM)$-module of vertical vector fields on TM. An important vector field is

$$C = y^i \frac{\partial}{\partial y^i}$$

which is called the *Liouville vector field*.

The mapping $J : \chi(TM) \to \chi(TM)$, given by:

$$J\left(\frac{\partial}{\partial x^i}\right) = \frac{\partial}{\partial y^i}; \quad J\left(\frac{\partial}{\partial y^i}\right) = 0, \quad i = 1, 2, ..., n \tag{5}$$

2

is called the tangent structure and it has the following properties:

$$KerJ = ImJ = \chi^v(TM);$$

$$rankJ = n, \quad J^2 = 0.$$

A vector field $S \in \chi(TM)$ is called a semispray, or a second-order vector field, if

$$JS = C.$$

In local coordinates a semispray can be represented as:

$$S = y^i \frac{\partial}{\partial x^i} - 2G^i(x,y) \frac{\partial}{\partial y^i}.$$

A non-linear connection in TM is an $n-$dimensional distribution:

$$N : u \in TM \rightarrow N_u \subset T_u TM, \tag{6}$$

which is supplementary to the vertical distribution V:

$$T_u TM = N_u TM \oplus V_u TM, \quad \forall u = (x,y) \in TM. \tag{7}$$

The local basis adapted to the decomposition (7) is $\left(\dfrac{\delta}{\delta x^i}, \dfrac{\partial}{\partial y^i} \right)$, where

$$\frac{\delta}{\delta x^i} = \frac{\partial}{\partial x^i} - N_i^j(x,y) \frac{\partial}{\partial y^j}. \tag{8}$$

The real functions $N_i^j(x,y)$ are locally defined on TM and subject to the following transformation rule under (1):

$$\tilde{N}_m^j \frac{\partial \tilde{x}^m}{\partial x^i} = \frac{\partial \tilde{x}^j}{\partial x^m} N_i^m - \frac{\partial \tilde{y}^j}{\partial x^i}. \tag{9}$$

The coordinate transformation (1) determines the transformation of the local basis adapted to the decomposition (7) as follows:

$$\frac{\delta}{\delta x^i} = \frac{\partial \tilde{x}^j}{\partial x^i} \frac{\delta}{\delta \tilde{x}^j}; \quad \frac{\partial}{\partial y^i} = \frac{\partial \tilde{x}^j}{\partial x^i} \frac{\partial}{\partial \tilde{y}^j}. \tag{10}$$

3. Nonholonomic Mechanical Systems

The term *nonholonomic system* was introduced in mechanics by H.Hertz [6]. It means that a material system is subjected to such kind of constraints that restrict the velocities of particles composed the system, but not their position (configuration of the system).

A sclerhonomic nonholonomic mechanical system is a quadruple

$$\Sigma = (M, g, F, Q_\sigma),$$

with M the configuration space, a real $n-$dimensional manifold, (M,g) is a Riemannian space, $F = (F_i)$ is the external forces vector field on M and $Q_\sigma \equiv (a_{\sigma i})$, $\sigma = p+1,...n$ are supplementary forces determined by the nonholonomic constraints given by the relations

$$Q_\sigma(x)dx = a_{\sigma i}(x)dx^i = 0. \tag{11}$$

3

The vector field of the forces is given by $F + \lambda^\sigma Q_\sigma$, where $\lambda^\sigma : R \to R, \sigma = p+1,...,n$ are *Lagrange multipliers* and $\lambda^\sigma Q_\sigma$ are the components of the so-called nonholonomic constraint force .

Let consider the Riemannian manifold (M, g) and ∇ its Levi-Civita connection.

A trajectory of nonholonomic mechanical system Σ is a differentiable curve c in M, $c : t \in I \to (x^i(t)) \in V \subset M$ ($I \subset R$, V is a domain of a local chart of M), who verify the following Lagrange equations:

$$\nabla_{\dot{c}}\dot{c} = F \circ c + \lambda^\sigma Q_\sigma \circ c. \tag{12}$$

Using the local coordinates on M, the equations (12) may be written

$$\frac{d^2 x^k}{dt^2} + \Gamma_{ij}^k(x)\frac{dx^i}{dt}\frac{dx^j}{dt} = F^k(x) + \lambda^\sigma a_\sigma^i(x), \tag{13}$$

with $\{\Gamma_{ij}^k\}$ the Christoffel symbols of the connection ∇ of the Riemannian metric tensor g, $F^k(x) = g^{ki}(x)F_i(x), a_\sigma^i(x) = g^{ij}a_{\sigma j}(x)$, and

$$Q_\sigma(x)dx \equiv a_{\sigma i}(x)dx^i = 0, (\sigma = p+1,...,n).$$

For the nonholonomic mechanical system Σ one studies the Lagrange space $L^{*n} = (M, L^*(x, y))$, with the fundamental function

$$L^*(x, y) = L(x, y) + \lambda^\sigma a_{\sigma i}(x)y^i, \tag{14}$$

where $L(x, y)$ is the regular Lagrangian, given by kinetic energy:

$$L(x, y) = g_{ij}\frac{dx^i}{dt}\frac{dx^j}{dt}.$$

In order to determine the multipliers λ^σ (which, in general depend on the material points x^i) we adopt the following postulate:

The Lagrangians $L(x, y)$ and $L^*(x, y)$ are equivalent.

So, the Lagrangians $L(x, y)$ and $L^*(x, y)$ satisfy the Euler-Lagrange equations:

$$\frac{d}{dt}\frac{\partial L^*}{\partial y^i} - \frac{\partial L^*}{\partial x^i} = \frac{d}{dt}\frac{\partial L}{\partial y^i} - \frac{\partial L}{\partial x^i} = 0. \tag{15}$$

Using eqs. (15), one obtains:

$$\left(\frac{\partial \lambda^\sigma}{\partial x^i}a_{\sigma j} - \frac{\partial \lambda^\sigma}{\partial x^j}a_{\sigma i} + \lambda^\sigma\left(\frac{\partial a_{\sigma i}}{\partial x^j} - \frac{\partial a_{\sigma j}}{\partial x^i}\right)\right)y^j = 0,$$

and deriving with respect to y^j we obtain:

$$\frac{\partial \lambda^\sigma}{\partial x^i}a_{\sigma j} - \frac{\partial \lambda^\sigma}{\partial x^j}a_{\sigma i} + \lambda^\sigma\left(\frac{\partial a_{\sigma i}}{\partial x^j} - \frac{\partial a_{\sigma j}}{\partial x^i}\right) = 0. \tag{16}$$

Let consider the $1-$form, [4]

$$\lambda^\sigma(x)Q_\sigma(x)dx = \lambda^\sigma(x)a_{\sigma i}(x)dx^i. \tag{17}$$

This $1-$form is clossed if and only if the equations (16) hold.

Indeed, it is not difficult to see that the equations (16) are equivalent to the exterior equations

$$d[\lambda^\sigma(x)Q(x)dx] = 0. \tag{18}$$

4

The Lagrange equations of the nonholonomic mechanical system Σ are:

$$\frac{d^2 x^k}{dt^2} + \Gamma^k_{ij}(x)\frac{dx^i}{dt}\frac{dx^j}{dt} = F^k(x) + \lambda^\sigma(x)a^k_\sigma(x); \tag{19}$$

$$\lambda^\sigma(x)a_{\sigma i}(x)dx^i = 0; \quad d\left[\lambda^\sigma(x)a_{\sigma i}(x) \wedge dx^i\right] = 0.$$

3.1. Canonical semispray and canonical non-linear connection of Σ

The Lagrange space $L^n = (M, L(x,y))$ has a canonical semispray

$$S = y^i\frac{\partial}{\partial x^i} - 2G^i(x,y)\frac{\partial}{\partial y^i},$$

where

$$2G^k(x,y) = \Gamma^k_{ij}(x)y^i y^j.$$

Looking at the Lagrange equations (19) we remark that the system of functions

$$G^{*i}(x,y) = G^i(x,y) - \frac{1}{2}\left(F^i(x) + \lambda^\sigma(x)a^i_\sigma(x)\right)$$

determines the coefficients of a semispray on the phase space TM.

The semispray S^* on the phase space TM, [11]

$$S^* = y^i\frac{\partial}{\partial x^i} - 2G^{*i}(x,y)\frac{\partial}{\partial y^i} \tag{20}$$

with the coefficients given by

$$2G^{*k}(x,y) = \Gamma^k_{ij}y^i y^j - \left(F^k(x) + \lambda^\sigma(x)a^k_\sigma(x)\right) \tag{21}$$

and the multipliers $\lambda^\sigma(x)$ satisfying the equations

$$d\left(\lambda^\sigma(x)a^i_\sigma(x)\right) \wedge dx^i = 0$$

is called the canonical semispray of the mechanical system Σ.

The semispray S^* depend only on the nonholonomic mechanical system Σ.

Therefore: The geometrical theory on nonholonomic mechanical system is the Lagrange geometry of the triple

$$(TM, S^*, d\left(\lambda^\sigma a^i_\sigma\right) \wedge dx^i = 0).$$

The integral curves of the canonical semispray S^* are given by the Lagrange equations of the mechanical system Σ, eqs. (19).

So, the non-linear connection N^* determined by the canonical semispray S^*, called canonical non-linear connection of Σ, has the coefficients

$$N^{*i}_j = \frac{\partial G^{*i}}{\partial y^j} = \Gamma^i_{jk}(x)y^k. \tag{22}$$

The canonical non-linear connection N^* of nonholonomic mechanical system Σ does not depend on the forces F_i and Q_σ.

A linear connection D on TM is called an N^*-linear connection if:

5

1.D preserves by parallelism the horizontal distribution N^*;

2.J is absolute parallel with respect to D, that is $D_X J = 0, \forall X \in \chi(E)$.

In the local basis $\left(\dfrac{\delta}{\delta x^i}, \dfrac{\partial}{\partial y^i} \right)$ adapted to the decomposition (7), an N^*-linear connection can be uniquely written in the form:

$$D_{\frac{\delta}{\delta x^k}} \frac{\delta}{\delta x^j} = L^i_{jk}(x,y)\frac{\delta}{\delta x^i}; \quad D_{\frac{\delta}{\delta x^k}} \frac{\partial}{\partial y^j} = L^i_{jk}(x,y)\frac{\partial}{\partial y^i} \tag{23}$$

$$D_{\frac{\partial}{\partial y^k}} \frac{\delta}{\delta x^j} = C^i_{jk}(x,y)\frac{\delta}{\delta x^i}; \quad D_{\frac{\partial}{\partial y^k}} \frac{\partial}{\partial y^j} = C^i_{jk}(x,y)\frac{\partial}{\partial y^i}. \tag{24}$$

The system of functions $L^k_{ij}(x,y), C^k_{ij}(x,y)$ are called the coefficients of the N^*-linear connection D. It is important to remark that $C^k_{ij}(x,y)$ are the coordinates of a $d-$tensor field of type $(1,2)$.

In our case, $G^{*i}(x,y)$ are the coefficients of the semispray S^*, eq. (20), it is easily to see that $\left(\dfrac{\partial^2 G^{*i}}{\partial y^i \partial y^j}, 0 \right)$ are the coefficients of an N^*-linear connection on TM, N^* having the coefficients $N^{*i}_j = \dfrac{\partial G^{*i}}{\partial y^j}$.

There exists a unique N^*-linear connection D on $\tilde{T}M$ verifying the axioms

$$\begin{aligned} g_{ij|k} = 0; \quad g_{ij}|_k = 0 \\ T^k_{ij} = 0; \quad S^k_{ij} = 0, \end{aligned} \tag{25}$$

where "$|$" and "$|$" are the $h-$covariant derivation and $v-$ covariant derivative and

$$T^k_{ij} = L^k_{ij} - L^k_{ji}, \quad S^k_{ij} = C^k_{ij} - C^k_{ji}.$$

This connection has the coefficients

$$\begin{aligned} L^i_{jk} &= \frac{1}{2}g^{im}\left(\frac{\delta g_{mk}}{\delta x^j} + \frac{\delta g_{mj}}{\delta x^k} - \frac{\delta g_{jk}}{\delta x^m} \right) \\ C^i_{jk} &= \frac{1}{2}g^{im}\left(\frac{\partial g_{mk}}{\partial y^j} + \frac{\partial g_{mj}}{\partial y^k} - \frac{\partial g_{jk}}{\partial y^m} \right). \end{aligned} \tag{26}$$

The previous connection depend only on the fundamental function $L^*(x,y)$ of the Lagrange space and will be called *canonical metrical connection* on the space L^{*n}.

Now, we consider, more general the case when the equations of movement for the nonholonomic, sclerhonomic system are given by

$$\frac{\partial L}{\partial x^i} - \frac{d}{dt}\frac{\partial L}{\partial y^i} + \left(\frac{\partial \lambda^\sigma}{\partial x^i}a_{\sigma j} - \frac{\partial \lambda^\sigma}{\partial x^j}a_{\sigma i} + \lambda^\sigma\left(\frac{\partial a_{\sigma i}}{\partial x^j} - \frac{\partial a_{\sigma j}}{\partial x^i} \right) \right)y^j = F_i(x,y)$$

$$y^i = \frac{dx^i}{dt} \tag{27}$$

and the multipliers λ^σ verify eqs. (18) , where $F_i(x,y)$ is a $d-$tensorial field on TM.

6

The equations (27) may be written in equivalent form

$$\frac{d^2 x^k}{dt^2} + \Gamma_{ij}^k(x)\frac{dx^i}{dt}\frac{dx^j}{dt} = \frac{1}{2}g^{kj}(x)F_j(x,y) + \lambda^\sigma(x)a_\sigma^k(x)$$
$$y^i = \frac{dx^i}{dt}.$$

(28)

One denotes

$$2\check{G}^k(x,y) = \Gamma_{ij}^k y^i y^j - \frac{1}{2}g^{kj}(x)F_j(x,y)$$

(29)

and the equation (28) give us the integral curves of the semispray

$$\check{S} = y^i \frac{\partial}{\partial x^i} - 2\check{G}^i(x,y)\frac{\partial}{\partial y^i}.$$

(30)

This semispray $\check{S}$ determine the non-linear connection $\check{N}$ with the coefficients

$$\check{N}_j^i = \frac{\partial \check{G}^i}{\partial y^j} = \frac{\partial G^i}{\partial y^j} - \frac{1}{4}\frac{\partial F^i}{\partial y^j},$$

(31)

where $F^i(x,y) = g^{ij}(x)F_j(x,y)$ and $2G^k(x,y) = \Gamma_{ij}^k(x)y^i y^j$.

The study of the nonholonomic, sclerhonomic mechanical system will be made in Lagrange space $L^{*n} = (M, L^*(x,y))$, with the fundamental function $L^*(x,y)$ from eq. (14) and the non-linear connection $\check{N}$ with the coefficients given by eqs. (31) .

Using the non-linear connection $\check{N}$, we can consider the adapted basis $\left(\dfrac{\delta}{\delta \check{x}^i}, \dfrac{\partial}{\partial y^i}\right)$ to the decomposition

$$T_u(TM) = \check{N}_u \oplus V_u, \quad \forall u = (x,y) \in TM,$$

with

$$\frac{\delta}{\delta \check{x}^i} = \frac{\partial}{\partial x^i} - \check{N}_i^j(x,y)\frac{\partial}{\partial y^j}.$$

(32)

We may construct the $\check{N}-$linear connection D, which preserves by parallelism the horizontal distribution $\check{N}$ and the tangent structure J is absolute parallel with respect connection D.

If $D\Gamma(\check{N}) = (\check{L}_{jk}^i(x,y), \check{C}_{jk}^i(x,y))$ are the coefficients of D in the adapted basis, denoting by $g_{ij|h}$ and $g_{ij}|_h$ the $h-$ and $v-$ covariant derivatives, then we have:

$$g_{ij|h} = \frac{\delta g_{ij}}{\delta x^h} - \check{L}_{ih}^m g_{mj} - \check{L}_{jh}^m g_{im};$$
$$g_{ij}|_h = \frac{\partial g_{ij}}{\partial y^h} - \check{C}_{ih}^m g_{mj} - \check{C}_{jh}^m g_{im}.$$

(33)

In a nonholonomic Lagrange space $L^{*n} = (M, L^*(x,y))$ the following properties hold:
a) There exists a unique $\check{N}$-linear connection D on TM satisfying the axioms:

$$g_{ij|h} = 0; \quad g_{ij}|_h = 0;$$

(34)

and

$$T_{jk}^i = 0, \quad S_{jk}^i = 0.$$

(3.34')

b)The coefficients $(\check{L}^i_{jk}(x,y), \check{C}^i_{jk}(x,y))$ of this connection are:

$$\check{L}^i_{kj} = \frac{1}{2}g^{ih}\left(\frac{\delta g_{hk}}{\delta x^j} + \frac{\delta g_{hj}}{\delta x^k} - \frac{\delta g_{kj}}{\delta x^h}\right) = L^i_{kj} - \frac{1}{4}C^i_{kr}\frac{\partial F^r}{\partial y^j}$$

$$\check{C}^i_{kj} = \frac{1}{2}g^{ih}\left(\frac{\partial g_{hk}}{\partial y^j} + \frac{\partial g_{hj}}{\partial y^k} - \frac{\partial g_{kj}}{\partial y^h}\right) = C^i_{kj} \tag{35}$$

where $(L^i_{jk}(x,y), C^i_{jk}(x,y))$ are the coefficients of the metrical connection N, from eqs. (26).

In conclusion: The Lagrange space L^{*n} endowed with the non-linear connection $\check{N}$ gives us a geometrical model for the nonholonomic mechanical system Σ.

4. References

[1] Bloch A M (2003) *Nonholonomic Mechanics and Control*, Springer-Verlag, New York.

[2] Bloch A M, Krishnaprasad P S, Marsden J E, Murray R (2009) Nonholonomic mechanical systems with symmetry, *Arch. Ratl. Mech. Anal.* **136**, no.1, pp 245-273.

[3] Cendra H, Marsden J E, Ratiu T S (2001), Geometric mechanics, Lagrangian reduction,and nonholonomic systems. *Mathematics Unlimited-2001 and Beyond*, pp.221-273, Springer,Berlin.

[4] Frigioiu C (2005), On the geometrization of non-holonomic mechanical systems, *Proceedings of the Romanian Academy, A*, **6**, nr.2, pp.121-128.

[5] Frigioiu C, Hedrih (Stevanovic) K, Birsan I G (2011), Lagrangian geometrical model of the rheonomic mechanical systems, *Proceedings of World Academy of Science, Engineering and Technology*, **73**, pp.1178-1184.

[6] Hertz H (1894), *Die Prinzipien der Mechanik in neuem Zusammenhange dargestellt*, Lepzig.

[7] De Leon M, Rodriguez P R (1989), *Methods of Differential Geometry in Analytical Mechanics*, North-Holland.

[8] Marle C M(1998), Various approaches to conservative and nonconservative nonholonomic systems, Pacific Institute of Mathematical Sciences Workshop on Nonholonomic Constraints in Dynamics (Calgary, AB, 1997), *Rep. Math. Phys.* **42**, pp.211-229.

[9] Mestdag T, Bloch A M, Fernandez O E (2009), Hamiltonization and geometric integration of nonholonomic mechanical systems, *Proceedings 8th National Congress on Theoretical and Applied Mechanics*, Brussels (Belgium), pp. 230-236.

[10] Miron R (2006), Dynamical Systems of Lagrangian and Hamiltonian Mechanical Systems, *Advanced Studies in Pure Math.*,**24**, pp.165-199.

[11] Miron R, Anastasiei M, Bucataru I (2003), The Geometry of Lagrange Spaces, *Handbook of Finsler Geometry*, P.L.Antonelli (Ed.), Kluwer Acad. Publ.FTPH, pp. 969-1124.

MODELING DOUBLE DNA HELIX MAIN CHAINS FORCED VIBRATIONS

Andjelka N. Hedrih[1], Katica R. (Stevanović) Hedrih[2]

[1] Department for bio- medical science, State University of Novi Pazar, Novi Pazar, Serbia, 18 000 – Niš, ul. Trg učitelj Tase br. 3/9, Serbia
e-mail: andjelka@hm.co.rs
[2]Mathematical Institute SANU Belgrade, Department for Mechanics
11 000-Belgrade, ul. Knez Mihailova 36/III, and Faculty of Mechanical Engineering, University of Niš. Priv. address: 18000-Niš, ul Vojvode Tankosića 3/22, Serbia, e-mail: khedrih@eunet.rs

ABSTRACT.

   DNA transcription process is well described at biochemical level. During transcription double DNA interacts with transcription proteins; part of double DNA is unzipped, and only one chain helix is used as a matrix for transcription.

   For better understanding the DNA transcription process and its behavior through biomechanical point of view, we consider double DNA (dDNA) as an oscillatory system that oscillates in forced regimes. In this paper analytical expressions of the forced oscillations of the dDNA helix chains are presented for both introduced models, ideally elastic as well as fractional order model. On the basis of previous results (DNA mathematical models published by N. Kovaleva, L. Manevich in 2005 and 2007, and multipendulum models by Hedrih (Stevanović) and Hedrih) where we obtain main chain subsystems of the double DNA helix, new results analysis of the forced vibrations is done. There are different cases of the resonant state in one of the main chains, and there are no interactions between main chains.

   The possibilities of appearance of resonant regimes only in one of the two main chains is proved, as well as dynamical absorption under external one frequency forced excitations is considered.

   Keywords: *Double DNA helix chain, forced vibrations, eigen main chains, resonant state, dynamical absorption, fractional order model.*

1 Introduction - DNA-structure and function

   DNA is a biological polymer which can exist in different forms (A, B, Z, E …) but only B form can be funded in live organisms. Chemically, DNA consists of two long polymers of simple units called nucleotides, with backbones made of sugars and phosphate groups joined by ester bonds. To each sugar is attached one of four types of molecules called bases. (Adenine-A, thymine-T guanine-G and cytosine-C). Two bases on opposite strands are linked via hydrogen bonds holding the two

strands of DNA together. It is the sequence of these four bases along the backbone that encodes information.

The basic function of DNA in the cell is to encode the genetic material. For using that information to make proteins, DNA molecule has to interact with other molecules in the cell. DNA molecule is moving, changing its position and shape during the interactions. DNA molecules can be considered to be a mechanical structure on the nanolevel.

The mechanical properties of DNA are closely related to its molecular structure and sequence, particularly the weakness of hydrogen bonds and electronic interactions that hold strands of DNA together compared to the strength of bonds within each strand. Every process which binds or reads DNA is able to use or modify the mechanical properties of DNA for purposes of recognition, packaging and modification. It is important to note the DNA found in many cells can be macroscopic in length - a few centimeters long for each human chromosome. Consequently, cells must compact or "package" DNA to carry it within them (Bryant et al, 2003).

Single-molecule biomechanics of DNA extension, bending and twisting; protein domain motion, deformation and unfolding; and the generation of mechanical forces and motions by bimolecular motors is another approach to explain the biological function of DNA in the cell (Bao, 2002). Knowledge of the elastic properties of DNA is required to understand the structural dynamics of cellular processes such as replication and transcription.
There are different approaches to studding the mechanical properties of the DNA molecule (experimental, theoretical modeling).

2 Mechanical properties of DNA achieved experimentally.

Experimental evidence suggests DNA mechanical properties, in particular intrinsic curvature and flexibility, have a role in many relevant biological processes.
For small distortions, DNA overwinds under tension (see Ref. [13] by Jeff Gore, Zev Bryant, Marcelo (2006)). Lowering of the temperature does increase the DNA curvature. The DNA double helix is much more resistant to twisting deformations than bending deformations; almost all of the supercoiling pressure is normally relieved by writhing (see Ref. [1] by Javier Arsuaga, Robert K.-Z. Tan , Mariel Vazquez , De Witt Sumners , Stephen C. Harvey (2002)). The twist angle of the helix has been shown to depend on sequence when the molecule is in solution, both by the effects on supercoiling parameters when short segments of known sequence are inserted into closed circular DNA (see Refs. [28] by Peck, L.J. and Wang, J.C. (1981) and [31] by Chang-Shung Tung1 and Stephen C.Harvey (1984).

Under low tension, DNA behaves like an isotropic flexible rod. At higher tensions, the behavior of over- and underwound molecules is different. In each case, DNA undergoes a structural change before the twist density necessary for buckling is reached (see Refs. [5] by Zev Bryant, Michael D. Stone, Jeff Gore, Steven B. Smith and Nicholas R. Cozzarelli (2003)).
Mg2+ can induce or enhance curvature in DNA fragments and helps stabilize several types of DNA structures (see Ref. [4] by Brukner, S. Susic, M. Dlakic, A. Savic, S. Pongor (1994)). DNA length varied in solution with different ionic force. It is significantly longer

in solution with lower ionic force (see Ref. [10] by C. Frontali, E. Dore, A. Ferrauto, E. Gratton, A. Bettini, M.R. Pozzan, E. Valdevit (1979)).

3. Mechanical models of the DNA

A number of mechanical models of the DNA double helix have been proposed till today. Different models are focusing on different aspects of the DNA molecule (biological, physical and chemical processes in which DNA is involved). A number of models have been constructed to describe different kinds of movements in a DNA molecule: asymmetric and symmetric motion; movements of long and short segments; twisting and stretching of dsDNA, twist-opening conditions. We are going to mention some of the models that may explain twist-opening conditions.

Bryant et al (see Ref. [5] by Bryant et al, 2003) have shown that an over- or underwound DNA molecule behaves as a constant-torque wind-up motor capable of repeatedly producing thousands of rotations, and that an overstretched molecule acts as a force–torque converter. The production of continuous directed rotation by molecular devices has potential applications in the construction of nanomechanical systems (see Ref. [2] by Bao, 2002). Polymer models are used to interpret single-molecule force-extension experiments on ssDNA and dsDNA. They show how combining the elasticity of two single nucleic acid strands with a description of the base-pairing interactions between them explains much of the phenomenology and kinetics of RNA and DNA 'unzipping' experiments" (see Refs. [7] by Cocco et al,2002; and [33] by Zhou and Lai, 2001). **Eslami-Mossallam** and **Ejtehadi, (**see Ref. [9] by **Eslami-Mossallam** and **Ejtehadi, 2009)** proposed the asymmetric elastic rod model for DNA. Their model accounts for the difference between the bending energies of positive and negative rolls, which comes from the asymmetric structure of the DNA molecule. The model can explain the high flexibility of DNA at small length scales, as well as kink formation at high deformation limit. Specially type of DNA models are s**oliton - existence supporting models.** One of the first of this kind was Yakushevich model of DNA and models based on it (see Ref. [11] by Gaeta, 1992). Dynamics of topological solitons describing open states in the DNA double helix are studied in the framework of a model that takes into account asymmetry of the helix. Yakushevich, et al (see Ref. [32] by Yakushevich, et al, 2002) investigated interaction between the solitons, their interactions with the chain inhomogeneities, and stability of the solitons with respect to thermal oscillations and have shown that three types of topological solitons can occur in the DNA double chain. González and Martín-Landrove (see Ref. [12] by González and Martín-Landrove, 1994) gave the complete qualitative analysis of soliton interaction in DNA torsional equations. The model emphasizes the importance of the solitons for opening of the double DNA helix. Thee region of the chain where there is a maximum opening is larger for the general case, since the asymptotical behavior for the kink type solitons is smoother than the one corresponding to the solutions in the particular case. There is possibility that an enzyme take charge for the opening of the chain. The supersonic solutions, since they represent states that are totally open, could contribute significantly to the fusion of the DNA chain to the enzymatic activity. The presence of a propagating soliton along the chain could contribute to its opening through the interaction among different types of open states. **The composite model for DNA** is also based on Yakushevich model (Y model). The mechanism for selecting the speed of solitons by tuning the physical parameters of the non-linear medium and the hierarchal separation of the relevant degrees of freedom are decribed in this model (see Refs. [8] by De Leo and Demelio, 2008; [6] by Cadoni et al, 2008). **In**

the symmetric twist-opening model of DNA the small amplitude dynamics of the model is shown to be governed by a solution of a set of coupled nonlinear Schrödinger equations. Conditions for modulation instability occurrence are presented and attention is paid to the impact of the backbone elastic constant K. It is shown that high values of K extend the instability region. This model can be reduced to a set of coupled discrete nonlinear system equations. The growth rate of instability has been evaluated and increases with the coupling constant K. The kink-bubble soliton, made of two part of different size, has been shown to be mobile. Authors supposed that the kink-bubble solution can be used the describe the internal dynamics which usually consists of long-range collective bending and twisting modes of the bases, short-range oscillations of individual bases, and the reorientation of the spin label (see Ref. [30] by Tabi et al, 2009).

Binding of proteins and other ligands on DNA, induces a strong deformation of the DNA structure.

The aim of our work was to model the DNA dynamics (vibrations of DNA chains) as a biological system in a specific boundary condition that are possible to occur in a life system during regular function of DNA molecule. We consider double DNA (dDNA) as an oscillatory system that oscillates in forced regimes during the DNA transcription process.

For mathematical descriptions we use References by Kovaleva and Manevich (see Refs. [26-27]), Hedrih (see Refs. [14-22]), Bačlić and Atanacković (see Ref. [3]), Hedrih and Filipobski (see Ref. [23]), Hedrih and Hedrih (see Refs. [24-25]) and Rašković P. Danilo see Ref. [29]).

4 DNA models by N. Kovaleva and L. Manevich

To model oscillation of dDNA in forced regimes we use as a basic approach model of dDNA proposed by N.Kovaleva, L.Manevich, V.Smirnov (see Ref [26]). They show that in a double DNA helix localized excitation (breather) can exist which corresponds to predominant rotation of one chain and small perturbation of second chain using coarse-grained model of DNA double helix.

| Figure 1. a* | Figure 1. b* | Figure 1. c* |
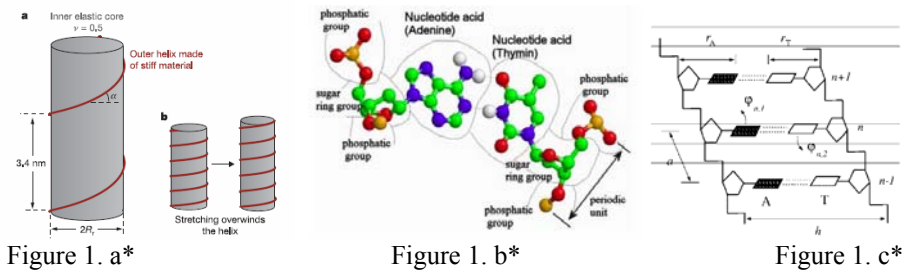
Figure 1. a* "Toy mechanical" model of DNA. a, DNA is modeled as an elastic rod (grey) wrapped helically by a stiff wire (red). see Ref. [9] by Jeff Gore, Zev Bryant, Marcelo (2006)
Figure1. b* The model scheme of a double helix on six coarse-grained particles [10].
Figure 1.c* Fragment of the DNA double chain consisting of three AT base pairs.

Longitudinal pitch of the helix $a = 3.4 \overset{\circ}{\text{A}}$; transverse pitch $h = 16.15 \overset{\circ}{\text{A}}$ [11].

Reference [26] by N.Kovaleva, L.Manevich, V.Smirnov presented 8th conference on DSTA 2007, point out that solitons and breathers play a functional role in DNA chains. In a model, the DNA backbone is reduced to the polymeric structure and the base is covalently linked to the center of sugar ring group, thus a DNA molecule with N nucleotides corresponds to 3N interaction centers. Starting from a coarse-grained off-lattice model of DNA and using cylindrical coordinates, authors derive simplified continuum equations corresponding to vicinities of gap frequencies in the spectrum of linearized equations of motion. It is shown that obtained nonlinear continuum equations describing modulations of normal modes, admit spatially localized solitons, which can be identified with breathers. Authors formulated conditions of the breathers existence and estimate their characteristic parameters. The relationship between derived model and more simple and widely used models is discussed. The analytical results are compared with the data of numerical study of discrete equations of motion. See Figure 1.b*.

Ref. [27] by N.Kovaleva, L.Manevich (2005)) presented at the 8th conference on Dinamical systems theory and applications, presented a simplest model describing opening of DNA double helix. Corresponding differential equations are solved analytically using multiple-scale expansions after transition to complex variables. Obtained solution corresponds to localized torsional nonlinear excitation – breather. Stability of breather is also investigated.

In this Reference [27] N.Kovaleva, L.Manevich (2005)) consider B form of the DNA molecule, the fragment of which is presented in Fig.1. b*. The lines in the figure correspond to skeleton of the double helix, black and gray rectangles show the bases in pairs (AT and GC). Let us focus our attention on the rotational motions of bases around the sugarphosphate chains in the plane perpendicular to the helix axis. See Figure 1.c*

Authors deal with the planar DNA model in which the chains of the macromolecule form two parallel straight lines placed at a distance h from each other, and the bases can make only rotation motions around their own chain, being all the time perpendicular to it. Authors accepted as generalized (independent) coordinates $\varphi_{k,1}$ that are the angular displacement of the k-th base of the first chain, and as generalized (independent) coordinates $\varphi_{k,2}$ is the angular displacement of the k-th base of the second chain. Then, by using accepted generalized coordinates $\varphi_{k,1}$ and $\varphi_{k,2}$ for k-th bases of both chains in the DNA model, authors derived a system of differential equations describing DNA model vibrations in the following forms:

$$\mathbf{J_{k,1}}\ddot{\varphi}_{\mathbf{k,1}} - \frac{K_{\mathbf{k,1}}}{2}\left[\sin\left(\varphi_{\mathbf{k+1,1}} - \varphi_{\mathbf{k,1}}\right) - \sin\left(\varphi_{\mathbf{k,1}} - \varphi_{\mathbf{k-1,1}}\right)\right] + K_{\alpha\beta}r_\alpha\left(r_\alpha - r_\beta\right)\sin\varphi_{\mathbf{k,1}} -$$

$$- K_{\alpha\beta}\frac{1}{4}\left(1 - \frac{\omega_{\alpha\beta2}}{\omega_{\alpha\beta1}}\right)\left(r_\alpha - r_\beta\right)^2\sin\left(\varphi_{\mathbf{k,1}} - \varphi_{\mathbf{k,2}}\right) = 0$$

$$\mathbf{J_{k,2}}\ddot{\varphi}_{\mathbf{k,2}} - \frac{K_{\mathbf{k,2}}}{2}\left[\sin\left(\varphi_{\mathbf{k+1,2}} - \varphi_{\mathbf{k,2}}\right) - \sin\left(\varphi_{\mathbf{k,2}} - \varphi_{\mathbf{k-1,2}}\right)\right] + K_{\alpha\beta}r_\alpha\left(r_\alpha - r_\beta\right)\sin\varphi_{\mathbf{k,2}} +$$

$$+ K_{\alpha\beta}\frac{1}{4}\left(1 - \frac{\omega_{\alpha\beta2}}{\omega_{\alpha\beta1}}\right)\left(r_\alpha - r_\beta\right)^2\sin\left(\varphi_{\mathbf{k,1}} - \varphi_{\mathbf{k,2}}\right) = 0$$

(1)

Here $\mathbf{J_{k,1}}$ is the axial moment of mass inertia of the k-th base of the first chain; $\mathbf{J_{k,2}}$ is the axial moment of mass inertia of the k-th base of the second chain, and the point denotes differentiation in time t. For the base pair the axial moments of mass inertia are equal to $\mathbf{J_{k,1}} = m_\alpha r_\alpha^2$, $\mathbf{J_{k,12}} = m_\beta r_\beta^2$. The value of the base mass m_α, the length r_α, and the corresponding axial moment of mass inertia $\mathbf{J_{k,1}} = m_\alpha r_\alpha^2$ for all possible base pair authors accepted as in the Reference [19]. The fourth terms in previous system equations describe interaction of the neighboring bases along each of the macromolecule chains. Parameter $K_{k,i}$, $i = 1,2$ characterizes the energy of interaction of the k-th base with the $(k+1)$-th one along the i-th chain $i = 1,2$. There are different estimations of rigidity. For the calculation that the most appropriate value is close $K_{k,i} = K = 6 \times 10^3 [kJ/mol]$.

5 Consideration of the basic DNA model - linearized Kovaleva-Manevich's DNA model

Let us investigate an oscillatory model of DNA, considered in the Reference [27] by N.Kovaleva, L. Manevich, (2005) and presented in the previous chapter III, by a system of differential equations (1) expressed by generalized (independent) coordinates $\varphi_{k,1}$ and $\varphi_{k,2}$ for k-th bases of both chains in the DNA model.

For the beginning, it is necessary to consider a corresponding linearized system of the previous system of the differential equations in the following form:

$$\mathbf{J_{k,1}}\ddot{\varphi}_{\mathbf{k,1}} - \frac{K_{\mathbf{k,1}}}{2}\left[\left(\varphi_{\mathbf{k+1,1}} - \varphi_{\mathbf{k,1}}\right) - \left(\varphi_{\mathbf{k,1}} - \varphi_{\mathbf{k-1,1}}\right)\right] + K_{\alpha\beta}r_\alpha\left(r_\alpha - r_\beta\right)\varphi_{\mathbf{k,1}} - \tag{2}$$

$$- K_{\alpha\beta}\frac{1}{4}\left(1 - \frac{\omega_{\alpha\beta 2}}{\omega_{\alpha\beta 1}}\right)\left(r_\alpha - r_\beta\right)^2\left(\varphi_{\mathbf{k,1}} - \varphi_{\mathbf{k,2}}\right) = \mathsf{M}_{0,k,1}\cos\Omega_{,k,1}t$$

$$\mathbf{J_{k,2}}\ddot{\varphi}_{\mathbf{k,2}} - \frac{K_{\mathbf{k,2}}}{2}\left[\left(\varphi_{\mathbf{k+1,2}} - \varphi_{\mathbf{k,2}}\right) - \left(\varphi_{\mathbf{k,2}} - \varphi_{\mathbf{k-1,2}}\right)\right] + K_{\alpha\beta}r_\alpha\left(r_\alpha - r_\beta\right)\varphi_{\mathbf{k,2}} + \tag{3}$$

$$+ K_{\alpha\beta}\frac{1}{4}\left(1 - \frac{\omega_{\alpha\beta 2}}{\omega_{\alpha\beta 1}}\right)\left(r_\alpha - r_\beta\right)^2\left(\varphi_{\mathbf{k,1}} - \varphi_{\mathbf{k,2}}\right) = \mathsf{M}_{0,k,2}\cos\Omega_{k,2}t$$

or in the following form:

$$\frac{2\mathbf{J_{k,1}}}{K_{\mathbf{k,1}}}\ddot{\varphi}_{\mathbf{k,1}} - \left[\left(\varphi_{\mathbf{k+1,1}} - \varphi_{\mathbf{k,1}}\right) - \left(\varphi_{\mathbf{k,1}} - \varphi_{\mathbf{k-1,1}}\right)\right] + \frac{2K_{\alpha\beta}r_\alpha\left(r_\alpha - r_\beta\right)}{K_{\mathbf{k,1}}}\varphi_{\mathbf{k,1}} - \tag{2*}$$

$$- \frac{K_{\alpha\beta}}{2K_{\mathbf{k,1}}}\left(1 - \frac{\omega_{\alpha\beta 2}}{\omega_{\alpha\beta 1}}\right)\left(r_\alpha - r_\beta\right)^2\left(\varphi_{\mathbf{k,1}} - \varphi_{\mathbf{k,2}}\right) = \frac{\mathsf{M}_{0,k,1}}{K_{\mathbf{k,1}}}\cos\Omega_{k,1}t$$

$$\frac{2\mathbf{J}_{k,2}}{K_{k,2}}\ddot{\varphi}_{k,2} - [(\varphi_{k+1,2} - \varphi_{k,2}) - (\varphi_{k,2} - \varphi_{k-1,2})] + \frac{2K_{\alpha\beta}r_\alpha(r_\alpha - r_\beta)}{K_{k,2}}\varphi_{k,2} +$$

$$+ \frac{K_{\alpha\beta}}{2K_{k,2}}\left(1 - \frac{\omega_{\alpha\beta2}}{\omega_{\alpha\beta1}}\right)(r_\alpha - r_\beta)^2(\varphi_{k,1} - \varphi_{k,2}) = \frac{M_{0,k,2}}{K_{k,2}}\cos\Omega_{k,2}t \qquad (3*)$$

For the case of homogeneous systems we can take into consideration that are $\mathbf{J}_{k,1} = \mathbf{J}_{k,2} = \mathbf{J}$ and $K_{k,1} = K_{k,2} = K$.

By using change of the generalized coordinates $\varphi_{k,1}$ and $\varphi_{k,2}$ for k-th bases of both chains in the DNA model into following new ξ_k and η_k by the following dependence (see Hedrih and Hedrih [17, 24, 25]):

$$\xi_k = \varphi_{k,1} - \varphi_{k,2} \quad \text{and} \quad \eta_k = \varphi_{k,1} + \varphi_{k,2} \qquad (4)$$

Previous system of differential equations (3) obtains the following form:

$$\frac{2\mathbf{J}}{K}\ddot{\xi}_k - \xi_{k+1} + 2\xi_k\left[1 + \frac{K_{\alpha\beta}r_\alpha(r_\alpha - r_\beta)}{K} - \frac{K_{\alpha\beta}}{2K}\left(1 - \frac{\omega_{\alpha\beta2}}{\omega_{\alpha\beta1}}\right)(r_\alpha - r_\beta)^2\right] - \xi_{k-1} = \frac{M_{0,k,1}}{K}\cos\Omega_{0.k.1}t - \frac{M_{0,k,2}}{K}\cos\Omega_{0.k.2}t$$

$$(5)$$

$$\frac{2\mathbf{J}}{K}\ddot{\eta}_k - \eta_{k+1} + 2\eta_k\left(1 + \frac{K_{\alpha\beta}r_\alpha(r_\alpha - r_\beta)}{K}\right) - \eta_{k-1} = \frac{M_{0,k,1}}{K}\cos\Omega_{0.k.1}t + \frac{M_{0,k,2}}{K}\cos\Omega_{0.k.2}t ,$$

$$k = 1,2,3,.....,n \qquad (6)$$

First series of the previous system equations are decoupled and independent with relations of the second series of the equations. *Then we can conclude that new coordinates of ξ_k and η_k are main coordinates of DNA chains and that we obtain two fictive decoupled eigen single chains of the DNA liner model. This is the first fundamental conclusion as an important property of the linear model of vibrations in a* double DNA helix.

Systems of differential equations (5)-(6) contain two separate subsystems of no autonomous differential equations expressed by *coordinates of ξ_k and η_k* which are main *coordinates of a double DNA chain helix system and separate linear DNA model of forced vibrations into two independent chains.*

6. Consideration of the forced vibrations of a basic DNA model - linearized Kovaleva-Manevich's DNA model

For obtaining general solutions of the both systems (5)-(6) of no autonomous differential equations which correspond to forced regimes of the main chains vibrations, for beginning it is necessary to find particular solutions of this system. Taking into account denotation

$$\mu - \kappa = \frac{K_{\alpha\beta}r_\alpha(r_\alpha - r_\beta)}{K} - \frac{K_{\alpha\beta}}{2K}\left(1 - \frac{\omega_{\alpha\beta2}}{\omega_{\alpha\beta1}}\right)(r_\alpha - r_\beta)^2 \qquad (7)$$

$$\kappa = \frac{K_{\alpha\beta}}{2K}\left(1 - \frac{\omega_{\alpha\beta 2}}{\omega_{\alpha\beta 1}}\right)(r_\alpha - r_\beta)^2 \cdot \qquad \mu = \frac{K_{\alpha\beta} r_\alpha (r_\alpha - r_\beta)}{K} \qquad (8)$$

$$u = \frac{\mathbf{J}}{K}\omega^2 \qquad (9)$$

previous systems (5)-(6) of no autonomous differential equations is possible to express in the form:

$$\frac{2\mathbf{J}}{K}\ddot{\xi}_{\mathbf{k}} - \xi_{\mathbf{k+1}} + 2\xi_{\mathbf{k}}[1 + \mu - \kappa] - \xi_{\mathbf{k-1}} = h_{0,k,1}\cos\Omega_{k.1}t - h_{0,k,2}\cos\Omega_{k.2}t$$
$$k = 1,2,3,.....,n \qquad (10)$$

$$\frac{2\mathbf{J}}{K}\ddot{\eta}_{\mathbf{k}} - \eta_{\mathbf{k+1}} + 2\eta_{\mathbf{k}}(1+\mu) - \eta_{\mathbf{k-1}} = h_{0,k,1}\cos\Omega_{k.1}t + h_{0,k,2}\cos\Omega_{k.2}t,$$
$$k = 1,2,3,.....,n \qquad (11)$$

where $h_{0,k,1} = \dfrac{\mathsf{M}_{0,k,.1}}{K} \qquad h_{0,k,2} = \dfrac{\mathsf{M}_{0,k,.2}}{K}$, $k = 1,2,3,.....,n$, educed amplitude od external excitations..

Next, taking into account that this system is linear, for simplifications of the calculation procedure, without loosing generality, we can solve system of no autonomous differential equations describing main chains forced vibrations of double DNA helix chain system under one frequency external excitation, with frequency $\Omega_{1,1}$ and reduces amplitude

applied $h_{0,k,1} = \dfrac{\mathsf{M}_{0,k,.1}}{K}$ applied to one mass particle to the first real chain from he coupled chains. For that reason we take for find particular solutions which correspond to forced vibrations with frequency $\Omega_{1,1}$ in the following form (see Figure 2):

$$\frac{2\mathbf{J}}{K}\ddot{\xi}_{\mathbf{k}} - \xi_{\mathbf{k+1}} + 2\xi_{\mathbf{k}}[1+\mu-\kappa] - \xi_{\mathbf{k-1}} = \begin{cases} h_{0,1,1}\cos\Omega_{1.1}t & k=1 \\ 0 & k\neq 1 \end{cases}, k = 1,2,3,.....,n$$

$$(12)$$

$$\frac{2\mathbf{J}}{K}\ddot{\eta}_{\mathbf{k}} - \eta_{\mathbf{k+1}} + 2\eta_{\mathbf{k}}(1+\mu) - \eta_{\mathbf{k-1}} = \begin{cases} h_{0,1,1}\cos\Omega_{1.1}t & k=1 \\ 0 & k\neq 1 \end{cases},$$
$$k = 1,2,3,.....,n \qquad (13)$$

Particular solutions for first and second system (12)-(13), we propose in the forms:

$$\xi_{port,k} = N_k \cos\Omega_{1,1}t \qquad k = 1,2,3,.....,n \qquad (14)$$

$$\eta_{port,k} = \widetilde{N}_k \cos\Omega_{1,1}t \qquad k = 1,2,3,.....,n \qquad (15)$$

and introducing following denotations:

$$u = \frac{\mathbf{J}}{K}\omega^2 \qquad v_{k,1} = \frac{\mathbf{J}}{K}\Omega_{k,1}^2 \qquad v_{k,2} = \frac{\mathbf{J}}{K}\Omega_{k,12}^2 \qquad (16)$$

and introducing proposed particular solutions (14)-(16) into system (12)-(13), we obtain the following system of algebra no homogeneous system::

$$-N_{k+1} + 2N_k\left(1 + \mu - \kappa - v_{1,1}\right) - N_{k-1} = \begin{cases} h_{0,1,1} & k = 1 \\ 0 & k \neq 1 \end{cases} \quad k = 1,2,3,\ldots,n$$

(17)

$$-\widetilde{N}_{k+1} + 2\widetilde{N}_k\left(1 + \mu - \widetilde{v}_{1,1}\right) - \widetilde{N}_{k-1} = \begin{cases} h_{0,1,1} & k = 1 \\ 0 & k \neq 1 \end{cases} \quad k = 1,2,3,\ldots,n$$

(18)

where $\quad v_{1,1} = \widetilde{v}_{1,1} = \dfrac{\mathbf{J}}{K}\Omega_{1,1}^2$.

Using Cramer low, for the amplitudes of the particular solutions we obtain the following:

$$N_k\left(v_{1,1}\right) = \frac{\Delta_k\left(v_{1,1}\right)}{\Delta\left(v_{1,1}\right)} \qquad\qquad k = 1,2,3,\ldots,n \qquad\qquad (19)$$

$$\widetilde{N}_k\left(\widetilde{v}_{1,1}\right) = \frac{\widetilde{\Delta}_k\left(\widetilde{v}_{1,1}\right)}{\widetilde{\Delta}\left(\widetilde{v}_{1,1}\right)} \qquad\qquad k = 1,2,3,\ldots,n \qquad\qquad (20)$$

where, for example, two system determinates, $\Delta\left(v_{1,1}\right)$ and $\widetilde{\Delta}\left(\widetilde{v}_{1,1}\right)$ are in the following forms(for the coupled chains each with four degree of freedom):

$$\Delta\left(v_{1,1}\right) = \begin{vmatrix} 2\left(1 + \mu - \kappa - v_{1,1}\right) & -1 & & \\ -1 & 2\left(1 + \mu - \kappa - v_{1,1}\right) & -1 & \\ & -1 & 2\left(1 + \mu - \kappa - v_{1,1}\right) & -1 \\ & & -1 & 2\left(1 + \mu - \kappa - v_{1,1}\right) \end{vmatrix} \neq 0$$

(21)

$$\widetilde{\Delta}\left(\widetilde{v}_{1,1}\right) = \begin{vmatrix} 2\left(1 + \mu - \widetilde{v}_{1,1}\right) & -1 & & \\ -1 & 2\left(1 + \mu - \widetilde{v}_{1,1}\right) & -1 & \\ & -1 & 2\left(1 + \mu - \widetilde{v}_{1,1}\right) & -1 \\ & & -1 & 2\left(1 + \mu - \widetilde{v}_{1,1}\right) \end{vmatrix} \neq 0$$

(22)

For same example other determinants $\Delta_k\left(v_{1,1}\right)$ and $\widetilde{\Delta}_k\left(\widetilde{v}_{1,1}\right)$, $k = 1,2,3,\ldots,n$, we obtain from corresponding two system determinates, $\Delta\left(v_{1,1}\right)$ and introducing into corresponding column, column with free members from right sides of the no homogeneous algebra equations (17)-(18):

$$\Delta_1\left(v_{1,1}\right) = \begin{vmatrix} h_{0,1,1} & -1 & & \\ -1 & 2\left(1 + \mu - \kappa - v_{1,1}\right) & -1 & \\ & -1 & 2\left(1 + \mu - \kappa - v_{1,1}\right) & -1 \\ & & -1 & 2\left(1 + \mu - \kappa - v_{1,1}\right) \end{vmatrix} = h_{0,1,1}2^{4-1}\prod_{s=1}^{s=3}\left(v_{1,1} - u_s^{(n=3)}\right)$$

(23)

$$\widetilde{\Delta}_1\left(\widetilde{v}_{1,1}\right)=\begin{vmatrix} h_{0,1,1} & -1 & & \\ -1 & 2\left(1+\mu-\widetilde{v}_{1,1}\right) & -1 & \\ & -1 & 2\left(1+\mu-\widetilde{v}_{1,1}\right) & -1 \\ & & -1 & 2\left(1+\mu-\widetilde{v}_{1,1}\right) \end{vmatrix}=h_{0,1,1}2^{4-1}\prod_{r=1}^{r=3}\left(\widetilde{v}_{1,1}-\widetilde{u}_r^{(n=3)}\right)$$

(24)

$$\Delta_2\left(v_{1,1}\right)=\begin{vmatrix} 2\left(1+\mu-\kappa-v_{1,1}\right) & h_{0,1,1} & & \\ -1 & & -1 & \\ & & 2\left(1+\mu-\kappa-v_{1,1}\right) & -1 \\ & & -1 & 2\left(1+\mu-\kappa-v_{1,1}\right) \end{vmatrix}=h_{0,1,1}2^{4-2}\prod_{s=1}^{s=2}\left(v_{1,1}-u_s^{(n=2)}\right)$$

(25)

$$\widetilde{\Delta}_2\left(\widetilde{v}_{1,1}\right)=\begin{vmatrix} 2\left(1+\mu-\widetilde{v}_{1,1}\right) & h_{0,1,1} & & \\ -1 & & -1 & \\ & & 2\left(1+\mu-\widetilde{v}_{1,1}\right) & -1 \\ & & -1 & 2\left(1+\mu-\widetilde{v}_{1,1}\right) \end{vmatrix}=h_{0,1,1}2^{4-2}\prod_{r=1}^{r=2}\left(\widetilde{v}_{1,1}-\widetilde{u}_r^{(n=2)}\right)$$

(26)

$$\Delta_3\left(v_{1,1}\right)=\begin{vmatrix} 2\left(1+\mu-\kappa-v_{1,1}\right) & -1 & h_{0,1,1} & \\ -1 & 2\left(1+\mu-\kappa-v_{1,1}\right) & & \\ & -1 & & -1 \\ & & & 2\left(1+\mu-\kappa-v_{1,1}\right) \end{vmatrix}=h_{0,1,1}2\left(\widetilde{v}_{1,1}-\widetilde{u}_r^{(n=1)}\right)$$

(27)

$$\widetilde{\Delta}_3\left(\widetilde{v}_{1,1}\right)=\begin{vmatrix} 2\left(1+\mu-\widetilde{v}_{1,1}\right) & -1 & h_{0,1,1} & \\ -1 & 2\left(1+\mu-\widetilde{v}_{1,1}\right) & & \\ & -1 & & -1 \\ & & & 2\left(1+\mu-\widetilde{v}_{1,1}\right) \end{vmatrix}=h_{0,1,1}2\left(\widetilde{v}_{1,1}-\widetilde{u}_r^{(n=1)}\right)$$

(28)

$$\Delta_4\left(v_{1,1}\right)=\begin{vmatrix} 2\left(1+\mu-\kappa-v_{1,1}\right) & -1 & & h_{0,1,1} \\ -1 & 2\left(1+\mu-\kappa-v_{1,1}\right) & -1 & \\ & -1 & 2\left(1+\mu-\kappa-v_{1,1}\right) & \\ & & -1 & \end{vmatrix}=h_{0,1,1}$$

(29)

$$\widetilde{\Delta}_4\left(\widetilde{v}_{1,1}\right) = \begin{vmatrix} 2\left(1+\mu-\widetilde{v}_{1,1}\right) & -1 & & h_{0,1,1} \\ -1 & 2\left(1+\mu-\widetilde{v}_{1,1}\right) & -1 & \\ & -1 & 2\left(1+\mu-\widetilde{v}_{1,1}\right) & \\ & & -1 & \end{vmatrix} = h_{0,1,1} \qquad (30)$$
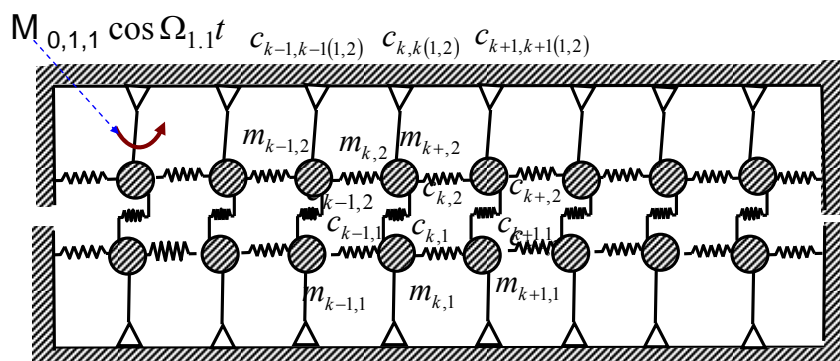
Figure 2. Double DNK Chain helix d model in the form of multipendulum system with fixed ends

Particular solutions of the considered examples with eight degree of freedom double DNA helix chain system containing two coupled chains each with four degree of freedom and excited bey one frequency external excitation are in the following forms:

$$\xi_{port,1} = N_1 \cos\Omega_{1,1}t = \frac{h_{0,1,1}\prod\limits_{s=1}^{s=3}\left(v_{1,1}-u_s^{(n=3)}\right)}{2\prod\limits_{s=1}^{s=4}\left(v_{1,1}-u_s^{(4)}\right)}\cos\Omega_{1,1}t \qquad (31)$$

$$\eta_{port,1} = \widetilde{N}_1 \cos\Omega_{1,1}t = \frac{h_{0,1,1}\prod\limits_{r=1}^{r=3}\left(\widetilde{v}_{1,1}-\widetilde{u}_r^{(n=3)}\right)}{2\prod\limits_{r=1}^{r=4}\left(\widetilde{v}_{1,1}-\widetilde{u}_r^{(4)}\right)}\cos\Omega_{1,1}t \qquad (32)$$

$$\xi_{port,2} = N_2 \cos\Omega_{1,1}t = \frac{h_{0,1,1}\prod\limits_{s=1}^{s=2}\left(v_{1,1}-u_s^{(n=2)}\right)}{4\prod\limits_{s=1}^{s=4}\left(v_{1,1}-u_s^{(4)}\right)}\cos\Omega_{1,1}t \qquad (33)$$

$$\eta_{port,2} = \widetilde{N}_2 \cos\Omega_{1,1}t = \frac{h_{0,1,1}\prod\limits_{r=1}^{r=2}\left(\widetilde{v}_{1,1}-\widetilde{u}_r^{(n=2)}\right)}{4\prod\limits_{4r=1}^{r=4}\left(\widetilde{v}_{1,1}-\widetilde{u}_r^{(4)}\right)}\cos\Omega_{1,1}t \qquad (34)$$

$$\xi_{port,3} = N_3 \cos\Omega_{1,1}t = \frac{h_{0,1,1}\left(v_{1,1} - u_s^{(n=1)}\right)}{8\prod\limits_{s=1}^{s=4}\left(v_{1,1} - u_s^{(n)}\right)}\cos\Omega_{1,1}t \tag{35}$$

$$\eta_{port21} = \widetilde{N}_2 \cos\Omega_{1,1}t = \frac{h_{0,1,1}\left(\widetilde{v}_{1,1} - \widetilde{u}_r^{(n=1)}\right)}{8\prod\limits_{r=1}^{r=4}\left(\widetilde{v}_{1,1} - \widetilde{u}_r^{(n)}\right)}\cos\Omega_{1,1}t \tag{36}$$

$$\xi_{port,4} = N_4 \cos\Omega_{1,1}t = \frac{h_{0,1,1}}{16\prod\limits_{s=1}^{s=4}\left(v_{1,1} - u_s^{(4)}\right)}\cos\Omega_{1,1}t \tag{37}$$

$$\eta_{port,4} = \widetilde{N}_4 \cos\Omega_{1,1}t = \frac{h_{0,1,1}}{16\prod\limits_{r=1}^{r=4}\left(\widetilde{v}_{1,1} - \widetilde{u}_r^{(4)}\right)}\cos\Omega_{1,1}t \tag{38}$$

Solutions of the homogeneous system for considered example are:

$$\xi_{free,k} = \sum_{s=1}^{s=4} C_s \sin k\varphi_s \cos(\omega_s t + \alpha_s), \ k = 1,2,3,4 \tag{39}$$

$$\eta_{free,k} = \sum_{r=1}^{r=4} D_r \sin k\vartheta_r \cos(\widetilde{\omega}_r t + \beta_r), \ k = 1,2,3,4 \tag{40}$$

General solutions are:

$$\xi_k = \xi_{free,k} + \xi_{part,k} = \sum_{s=1}^{s=4} C_s \sin k\varphi_s \cos(\omega_s t + \alpha_s) + \xi_{part,k}, k = 1,2,3,4 \tag{41}$$

$$\eta_k = \eta_{free,k} + \eta_{part,k} = \sum_{r=1}^{r=4} D_r \sin k\vartheta_r \cos(\widetilde{\omega}_r t + \beta_r) + \eta_{part,k}, k = 1,2,3,4$$

$$\tag{42}$$

or in the form

$$\xi_k = \xi_{free,k} + \xi_{part,k} = \sum_{s=1}^{s=4} C_s \sin k\varphi_s \cos(\omega_s t + \alpha_s) + N_k(v_{1,1})\cos\Omega_{1,1}t, k = 1,2,3,4$$

$$\tag{43}$$

$$\eta_k = \eta_{free,k} + \eta_{part,k} = \sum_{r=1}^{r=4} D_r \sin k\vartheta_r \cos(\widetilde{\omega}_r t + \beta_r) + \widetilde{N}_k(\widetilde{v}_{1,1})\cos\Omega_{1,1}t, k = 1,2,3,4$$

$$\tag{44}$$

For the system of double DNA helix chain system with $2n$ degrees of freedom previous two system determinates $\Delta(v_{1,1})$ and $\widetilde{\Delta}(\widetilde{v}_{1,1})$ are not difficult to express in the similar forms.

Then taking into account that determinates $\Delta(v_{1,1})$ and $\widetilde{\Delta}(\widetilde{v}_{1,1})$ are analogous as determinates, which describe frequency equations of the free vibrations of the double DNA

helix chain system, which is possible express in the following forms $\Delta(u) = 0$ and $\widetilde{\Delta}(u) = 0$, and that we have roots of these frequency equations in the forms (21)-(22) then we have roots of the two system determinates, $\Delta(v_{1,1})$ and $\widetilde{\Delta}(\widetilde{v}_{1,1})$ in the forms:

$$v_{1,1}^{(s)} = \frac{J}{K}\Omega_{1,1}^{(s)} = u_s^{(n)} = \frac{J}{K}\omega_s^2 = 2\sin^2\frac{\varphi_s}{2} + (\mu - \kappa), \qquad s = 1,2,3,.....,n$$

(45)

$$\widetilde{v}_{1,1}^{(r)} = \frac{J}{K}\widetilde{\Omega}_{1,1}^{(r)} = \widetilde{u}_r^{(n)} = \frac{J}{K}\widetilde{\omega}_r^2 = 2\sin^2\frac{\vartheta_r}{2} + \mu \quad . \qquad r = 1,2,3,.....,n$$

(46)

By use previous characteristic numbers of the previous two system determinates, these determinants $\Delta_k(v_{1,1})$ and $\widetilde{\Delta}_k(\widetilde{v}_{1,1})$ are possible express in the forms of products:

$$\Delta(v_{1,1}) = 2^n \prod_{s=1}^{s=n}\left(v_{1,1} - u_s^{(n)}\right)$$

(47)

$$\widetilde{\Delta}(\widetilde{v}_{1,1}) = 2^n \prod_{r=1}^{r=n}\left(\widetilde{v}_{1,1} - \widetilde{u}_r^{(n)}\right)$$

(48)

By same way, it is possible to fined expressions for amplitude of the particular solutions depending of the number of degree of freedom $2n$. For example it is visible without calculations that amplitude N_1, $\widetilde{N}_1$ and N_2, $\widetilde{N}_2$ of the particular solutions of the first and second normal coordinates, $\xi_{part,1}$, $\eta_{part,1}$ and $\xi_{part,2}$, $\eta_{part,2}$ of the both main chains are in the following forms:

$$N_1 = \frac{h_{0,1,1}\prod_{s=1}^{s=n-1}\left(v_{1,1} - u_s^{(n-1)}\right)}{2\prod_{s=1}^{s=n}\left(v_{1,1} - u_s^{(n)}\right)} \qquad \text{and} \qquad \widetilde{N}_1 = \frac{h_{0,1,1}\prod_{r=1}^{r=n-1}\left(\widetilde{v}_{1,1} - \widetilde{u}_r^{(n-1)}\right)}{2\prod_{r=1}^{r=n}\left(\widetilde{v}_{1,1} - \widetilde{u}_r^{(n)}\right)}$$

(49)

$$N_2 = \frac{h_{0,1,1}\prod_{s=1}^{s=n-2}\left(v_{1,1} - u_s^{(n-2)}\right)}{2^2\prod_{s=1}^{s=n}\left(v_{1,1} - u_s^{(n)}\right)} \qquad \text{and} \qquad \widetilde{N}_2 = \frac{h_{0,1,1}\prod_{r=1}^{r=n-1}\left(\widetilde{v}_{1,1} - \widetilde{u}_r^{(n-2)}\right)}{2^2\prod_{r=1}^{r=n}\left(\widetilde{v}_{1,1} - \widetilde{u}_r^{(n)}\right)}$$

(50)

Then general solutions are in the following forms:

$$\xi_k = \xi_{free,k} + \xi_{part,k} = \sum_{s=1}^{s=n} C_s \sin k\varphi_s \cos(\omega_s t + \alpha_s) + \xi_{part,k}, \quad k = 1,2,3,.....,n$$

(51)

$$\eta_k = \eta_{free,k} + \eta_{part,k} = \sum_{r=1}^{r=n} D_r \sin k\vartheta_r \cos(\widetilde{\omega}_r t + \beta_r) + \eta_{part,k}, \; k = 1,2,3,\ldots,n$$

(52)

or in the form

$$\xi_k = \xi_{free,k} + \xi_{part,k} = \sum_{s=1}^{s=n} C_s \sin k\varphi_s \cos(\omega_s t + \alpha_s) + N_k(v_{1,1})\cos\Omega_{1,1}t, \; k = 1,2,3,\ldots,n$$

(53)

$$\eta_k = \eta_{free,k} + \eta_{part,k} = \sum_{r=1}^{r=n} D_r \sin k\vartheta_r \cos(\widetilde{\omega}_r t + \beta_r) + \widetilde{N}_k(\widetilde{v}_{1,1})\cos\Omega_{1,1}t, \; k = 1,2,3,\ldots,n$$

(54)

For the case that one frequency external excitation, with reduced amplitude $h_{0,2,1} = \dfrac{\mathsf{M}_{0,1,.2}}{K}$ is with frequency $\Omega_{2,1}$, applied to the other first material particle n the other of the coupled real chains, then two subsystems of the main eigen chains are described by following subsystems of differential equations:

$$\frac{2\mathbf{J}}{K}\ddot{\xi}_{\mathbf{k}} - \xi_{\mathbf{k+1}} + 2\xi_{\mathbf{k}}[1 + \mu - \kappa] - \xi_{\mathbf{k-1}} = \begin{cases} -h_{0,2,1}\cos\Omega_{2,1}t & k = 1 \\ 0 & k \neq 1 \end{cases}$$

(55)

$$\frac{2\mathbf{J}}{K}\ddot{\eta}_{\mathbf{k}} - \eta_{\mathbf{k+1}} + 2\eta_{\mathbf{k}}(1 + \mu) - \eta_{\mathbf{k-1}} == \begin{cases} h_{0,2,1}\cos\Omega_{2,1}t & k = 1 \\ 0 & k \neq 1 \end{cases},$$

(56)

Particular and general solutions of these previous equations is not difficult to obtain analogous by previous procedure and changing corresponding indices of the kinetic parameters of the main chains.

7. Consideration of the forced vibration regimes of a basic DNA model - linearized Kovaleva-Manevich's DNA model

From expressions (21) and (22) is possible to consider possibilities of appearance resonant regimes in eigen main chains.

For the case that determinants (21) and (22), $\Delta(v_{1,1}) = 2^n \prod_{s=1}^{s=n}(v_{1,1} - u_s^{(n)}) = 0$ and

$\widetilde{\Delta}(\widetilde{v}_{1,1}) = 2^n \prod_{r=1}^{r=n}(\widetilde{v}_{1,1} - \widetilde{u}_r^{(n)}) = 0$ are equal to zero, then we obtain two sets of external excitation

frequencies for which in the system appear resonant regime. But taking into account that eigen main chains have different sets of eigen circular frequencies as well as different sets of the resonant circular frequencies of external excitation, then we can conclude that if in one eigen main chain appear resonant regime in other no resonant regime. This is important fact to consider in the light of the real double DNA helix chain system.

Also by use expressions for amplitudes of the particular forced solutions is possible appearance of dynamical absorptions at corresponding main coordinate of main

eigen chain. To obtain external excitation frequencies at which appear dynamical absorption at first or second main coordinate of the main chains are equal to zero:

$$N_1 = \frac{h_{0,1,1} \prod_{s=1}^{s=n-1}\left(v_{1,1} - u_s^{(n-1)}\right)}{2\prod_{s=1}^{s=n}\left(v_{1,1} - u_s^{(n)}\right)} = 0 \quad \text{or} \quad \widetilde{N}_1 = \frac{h_{0,1,1} \prod_{r=1}^{r=n-1}\left(\widetilde{v}_{1,1} - \widetilde{u}_r^{(n-1)}\right)}{2\prod_{r=1}^{r=n}\left(\widetilde{v}_{1,1} - \widetilde{u}_r^{(n)}\right)} = 0$$

(57)

$$N_2 = \frac{h_{0,1,1} \prod_{s=1}^{s=n-2}\left(v_{1,1} - u_s^{(n-2)}\right)}{2^2\prod_{s=1}^{s=n}\left(v_{1,1} - u_s^{(n)}\right)} = 0 \quad \text{or} \quad \widetilde{N}_2 = \frac{h_{0,1,1} \prod_{r=1}^{r=n-1}\left(\widetilde{v}_{1,1} - \widetilde{u}_r^{(n-2)}\right)}{2^2\prod_{r=1}^{r=n}\left(\widetilde{v}_{1,1} - \widetilde{u}_r^{(n)}\right)} = 0$$

(58)

and next.

$$\prod_{s=1}^{s=n-1}\left(v_{1,1} - u_s^{(n-1)}\right) = 0 \quad \text{or} \quad \prod_{r=1}^{r=n-1}\left(\widetilde{v}_{1,1} - \widetilde{u}_r^{(n-1)}\right) = 0$$

(59)

$$\prod_{s=1}^{s=n-2}\left(v_{1,1} - u_s^{(n-2)}\right) = 0 \quad \text{or} \quad \prod_{s=1}^{s=n-2}\left(v_{1,1} - u_s^{(n-2)}\right) = 0$$

(60)

From the last conditions (59) and (60), we can conclude that:

* Dynamical absorption on the first pair of the main coordinates of the main chains appear on the resonate circular frequencies of the set of the double DNA helix chain system with one less pair of the material particles in comparison with the considered real system.*

* Dynamical absorption on the second pair of the main coordinates of the main chains appear on the resonate circular frequencies of the set of the double DNA helix chain system with two less pairs of the material particles in comparison with considered system.*

* This mathematical fact is important to considered in the light of the interruption or break of the double DNA helix chain system into finite parts.*

8. The double DNA fractional order chain model on the basis of the linearized Kovaleva-Manevich's DNA models for free and forced vibrations

8.1. Constitutive relation of the standard light fractional order creep element.

Basic elements of multi mathematical pendulum system or multi coupled chain system are:

1* Material particles with mass m_k, with each particle having one degree of motion

freedom, defined by following coordinate φ_k, when k changes by $k = 1,2,3,4,....,N$.

2* Standard light fractional order coupling element of negligible mass in the form of axially stressed rod without bending, and which has the ability to resist deformation under static and dynamic conditions. *Standard light creep constraint element* for which the stress-strain relation for the restitution force as the function of element elongation is given by fractional order derivatives in the form

$$P(t) = -\left\{ c_0 x(t) + c_\alpha \mathsf{D}_t^\alpha [x(t)] \right\} \tag{61}$$

where $\mathsf{D}_t^\alpha [\bullet]$ is operator of the αth derivative with respect to time t in the following form:

$$\mathsf{D}_t^\alpha [x(t)] = \frac{d^\alpha x(t)}{dt^\alpha} = x^{(\alpha)}(t) = \frac{1}{\Gamma(1-\alpha)} \frac{d}{dt} \int_0^t \frac{x(\tau)}{(t-\tau)^\alpha} d\tau \tag{62}$$

where c, c_α are rigidity coefficients–momentary and prolonged one, and α a rational number between 0 and 1, $0 < \alpha < 1$.
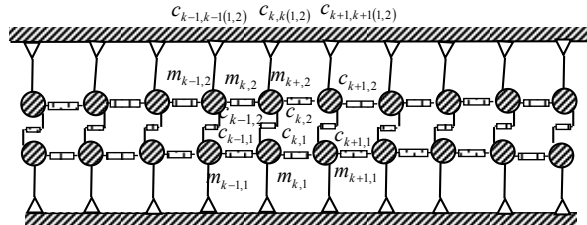
Figure 3. Double DNK fractional order chain helix in the form of multipendulum model with free ends
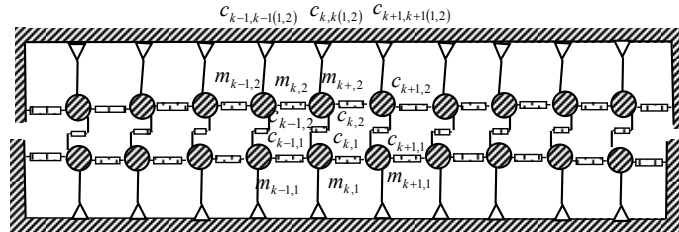
Figure 4. Double DNK fractional order chain helix d model in the form of multipendulum system with fixed ends

8.2. The double DNA fractional order chain forced vibration model on the basis of the linearized Kovaleva-Manevich's DNA model

For the fractional order forced vibrations of a fractional order double DNA chain model on the basis of the linearized Kovaleva-Manevich's DNA model, we accept a two chains as it is presented in Figure 3 or 4, in the form of the double chain fractional order system containing two coupled multi pendulum subsystem, in which corresponding material particles of the corresponding multi-pendulum chains are coupled by series of the same standard light fractional order elements.

Let's suppose that both coupled chains from system of the fractional order DNA model are excited by the system of external excitation containing two series of the one frequency excitations in the forms $\mathsf{M}_{0,k,.1}\cos\Omega_{k.1}t$ and $\mathsf{M}_{0,k,.2}\cos\Omega_{k.2}t$, $k = 1,2,3,.....,n$, where $\mathsf{M}_{0,k,.1}$ and $\mathsf{M}_{0,k,.2}$ are amplitudes, $\Omega_{k.1}$ and $\Omega_{k.2}$ frequencies of the external forced couples each applied to one of the mass particles of the double DNA model coupled chains. Then, corresponding system of the nonlinear forced vibrations of the double DNA model coupled chains are in the following forms:

Then, we can use system of the coupled fractional order coupled differential equations extended by terms containing external excitation forces or couples. Then, we can write corresponding system of the fractional order differential coupled equations in the form:

$$\mathbf{J}_{\mathbf{k,1}}\ddot{\varphi}_{\mathbf{k,1}} - \frac{K_{\mathbf{k,1}}}{2}\big[(\varphi_{\mathbf{k+1,1}} - \varphi_{\mathbf{k,1}}) - (\varphi_{\mathbf{k,1}} - \varphi_{\mathbf{k-1,1}})\big] - \frac{K_{\mathbf{k,1},\sigma}}{2}\mathsf{D}_t^{\sigma}\big[(\varphi_{\mathbf{k+1,1}} - \varphi_{\mathbf{k,1}}) - (\varphi_{\mathbf{k,1}} - \varphi_{\mathbf{k-1,1}})\big] +$$

$$+ K_{\alpha\beta}r_\alpha(r_\alpha - r_\beta)\varphi_{\mathbf{k,1}} - - K_{\alpha\beta} - \frac{1}{4}\bigg(1 - \frac{\omega_{\alpha\beta2}}{\omega_{\alpha\beta1}}\bigg)(r_\alpha - r_\beta)^2(\varphi_{\mathbf{k,1}} - \varphi_{\mathbf{k,2}}) -$$

$$- K_{\alpha\beta,\sigma}\frac{1}{4}\bigg(1 - \frac{\omega_{\alpha\beta2}}{\omega_{\alpha\beta1}}\bigg)(r_\alpha - r_\beta)^2\mathsf{D}_t^{\sigma}\big[(\varphi_{\mathbf{k,1}} - \varphi_{\mathbf{k,2}})\big] = \mathsf{M}_{0,k,.1}\cos\Omega_{k,1}t$$

$$\mathbf{J}_{\mathbf{k,2}}\ddot{\varphi}_{\mathbf{k,2}} - \frac{K_{\mathbf{k,2}}}{2}\big[(\varphi_{\mathbf{k+1,2}} - \varphi_{\mathbf{k,2}}) - (\varphi_{\mathbf{k,2}} - \varphi_{\mathbf{k-1,2}})\big] - \frac{K_{\mathbf{k,2},\sigma}}{2}\mathsf{D}_t^{\sigma}\big[(\varphi_{\mathbf{k+1,2}} - \varphi_{\mathbf{k,2}}) - (\varphi_{\mathbf{k,2}} - \varphi_{\mathbf{k-1,2}})\big] +$$

$$+ K_{\alpha\beta}r_\alpha(r_\alpha - r_\beta)\varphi_{\mathbf{k,2}} + + K_{\alpha\beta}\frac{1}{4}\bigg(1 - \frac{\omega_{\alpha\beta2}}{\omega_{\alpha\beta1}}\bigg)(r_\alpha - r_\beta)^2(\varphi_{\mathbf{k,1}} - \varphi_{\mathbf{k,2}}) +$$

$$+ K_{\alpha\beta,\sigma}\frac{1}{4}\bigg(1 - \frac{\omega_{\alpha\beta2}}{\omega_{\alpha\beta1}}\bigg)(r_\alpha - r_\beta)^2\mathsf{D}_t^{\sigma}\big[(\varphi_{\mathbf{k,1}} - \varphi_{\mathbf{k,2}})\big] = \mathsf{M}_{0,k,.2}\cos\Omega_{k,2}t$$

$$(63)$$

Previous system is possible to rewrite in the following form:

$$\frac{2\mathbf{J}_{\mathbf{k,1}}}{K_{\mathbf{k,1}}}\ddot{\varphi}_{\mathbf{k,1}} - \big[(\varphi_{\mathbf{k+1,1}} - \varphi_{\mathbf{k,1}}) - (\varphi_{\mathbf{k,1}} - \varphi_{\mathbf{k-1,1}})\big] + - \frac{K_{\mathbf{k,1},\sigma}}{K_{\mathbf{k,1}}}\mathsf{D}_t^{\sigma}\big[(\varphi_{\mathbf{k+1,1}} - \varphi_{\mathbf{k,1}}) - (\varphi_{\mathbf{k,1}} - \varphi_{\mathbf{k-1,1}})\big] +$$

$$+ \frac{2K_{\alpha\beta}r_\alpha(r_\alpha - r_\beta)}{K_{\mathbf{k,1}}}\varphi_{\mathbf{k,1}} - - \frac{K_{\alpha\beta}}{2K_{\mathbf{k,1}}}\bigg(1 - \frac{\omega_{\alpha\beta2}}{\omega_{\alpha\beta1}}\bigg)(r_\alpha - r_\beta)^2(\varphi_{\mathbf{k,1}} - \varphi_{\mathbf{k,2}}) -$$

$$- \frac{K_{\alpha\beta,\sigma}}{2K_{\mathbf{k,1}}}\bigg(1 - \frac{\omega_{\alpha\beta2}}{\omega_{\alpha\beta1}}\bigg)(r_\alpha - r_\beta)^2\mathsf{D}_t^{\sigma}\big[(\varphi_{\mathbf{k,1}} - \varphi_{\mathbf{k,2}})\big] = \frac{\mathsf{M}_{0,k,.1}}{K_{\mathbf{k,1}}}\cos\Omega_{k,1}t$$

$$\frac{2\mathbf{J}_{\mathbf{k},2}}{K_{\mathbf{k},2}}\ddot{\varphi}_{\mathbf{k},2} - \left[\left(\varphi_{\mathbf{k}+1,2} - \varphi_{\mathbf{k},2}\right) - \left(\varphi_{\mathbf{k},2} - \varphi_{\mathbf{k}-1,2}\right)\right] - \frac{K_{\mathbf{k},2,\sigma}}{K_{\mathbf{k},2}}\mathsf{D}_t^{\sigma}\left[\left(\varphi_{\mathbf{k}+1,2} - \varphi_{\mathbf{k},2}\right) - \left(\varphi_{\mathbf{k},2} - \varphi_{\mathbf{k}-1,2}\right)\right] +$$

$$+ \frac{2K_{\alpha\beta}r_{\alpha}\left(r_{\alpha} - r_{\beta}\right)}{K_{\mathbf{k},2}}\varphi_{\mathbf{k},2} + + \frac{K_{\alpha\beta}}{2K_{\mathbf{k},2}}\left(1 - \frac{\omega_{\alpha\beta2}}{\omega_{\alpha\beta1}}\right)\left(r_{\alpha} - r_{\beta}\right)^2\left(\varphi_{\mathbf{k},1} - \varphi_{\mathbf{k},2}\right) +$$

$$+ \frac{K_{\alpha\beta,\sigma}}{2K_{\mathbf{k},2}}\left(1 - \frac{\omega_{\alpha\beta2}}{\omega_{\alpha\beta1}}\right)\left(r_{\alpha} - r_{\beta}\right)^2\mathsf{D}_t^{\sigma}\left[\left(\varphi_{\mathbf{k},1} - \varphi_{\mathbf{k},2}\right)\right] = \frac{\mathsf{M}_{0,k,2}}{K_{\mathbf{k},2}}\cos\Omega_{k,2}t$$

(64)

As our intention is to use previous double DNA fractional order chain model for the case of the homogeneous system parameters, we take into account that: $K_{\mathbf{k},1,\sigma} = K_{\mathbf{k},2,\sigma} = K$. and $K_{\alpha\beta,\sigma} = K_{\alpha\beta,\sigma}$ and taking into account that, we introduce notation (7) and (8) then the precious system of coupled fractional order differential equations is possible write in the following form:

$$\frac{2\mathbf{J}}{K}\ddot{\varphi}_{\mathbf{k},1} - \left[\left(\varphi_{\mathbf{k}+1,1} - \varphi_{\mathbf{k},1}\right) - \left(\varphi_{\mathbf{k},1} - \varphi_{\mathbf{k}-1,1}\right)\right] - \kappa_{\sigma}\mathsf{D}_t^{\sigma}\left[\left(\varphi_{\mathbf{k}+1,1} - \varphi_{\mathbf{k},1}\right) - \left(\varphi_{\mathbf{k},1} - \varphi_{\mathbf{k}-1,1}\right)\right] +$$

$$+ 2\mu\varphi_{\mathbf{k},1} - \kappa\left(\varphi_{\mathbf{k},1} - \varphi_{\mathbf{k},2}\right) - \kappa\kappa_{\sigma}\mathsf{D}_t^{\sigma}\left[\left(\varphi_{\mathbf{k},1} - \varphi_{\mathbf{k},2}\right)\right] = \frac{\mathsf{M}_{0,k,1}}{K}\cos\Omega_{k,1}t$$

$$\frac{2\mathbf{J}_{\mathbf{k},2}}{K}\ddot{\varphi}_{\mathbf{k},2} - \left[\left(\varphi_{\mathbf{k}+1,2} - \varphi_{\mathbf{k},2}\right) - \left(\varphi_{\mathbf{k},2} - \varphi_{\mathbf{k}-1,2}\right)\right] - \kappa_{\sigma}\mathsf{D}_t^{\sigma}\left[\left(\varphi_{\mathbf{k}+1,2} - \varphi_{\mathbf{k},2}\right) - \left(\varphi_{\mathbf{k},2} - \varphi_{\mathbf{k}-1,2}\right)\right] +$$

$$+ 2\mu\varphi_{\mathbf{k},2} + \kappa\left(\varphi_{\mathbf{k},1} - \varphi_{\mathbf{k},2}\right) + \kappa\kappa_{\sigma}\mathsf{D}_t^{\sigma}\left[\left(\varphi_{\mathbf{k},1} - \varphi_{\mathbf{k},2}\right)\right] = \frac{\mathsf{M}_{0,k,2}}{K}\cos\Omega_{k,2}t$$

(65)

where $\kappa_{\sigma} = \dfrac{K_{\alpha\beta,\sigma}}{K}$.

By using change of the generalized coordinates $\varphi_{k,1}$ and $\varphi_{k,2}$ for k-th bases of both chains in the DNA model into following new ξ_k and η_k by the following dependence: $\xi_k = \varphi_{k,1} - \varphi_{k,2}$ and $\eta_k = \varphi_{k,1} + \varphi_{k,2}$, previous system of differential equations (65) obtains the following form:

$$\frac{2\mathbf{J}}{K}\ddot{\xi}_{\mathbf{k}} - \xi_{k-1} + 2\xi_k - \xi_{k+1} + \kappa_{\sigma}\mathsf{D}_t^{\sigma}\left[-\xi_{k-1,} + 2\xi_k - \xi_{k+1}\right] + 2\mu\xi_{\mathbf{k}} - 2\kappa\xi_{\mathbf{k}} - 2\kappa\kappa_{\sigma}\mathsf{D}_t^{\sigma}\left[\xi_{\mathbf{k}}\right] =$$

$$= \frac{\mathsf{M}_{0,k,1}}{K}\cos\Omega_{k,1}t - \frac{\mathsf{M}_{0,k,2}}{K}\cos\Omega_{k,2}t$$

(66)

$$\frac{2\mathbf{J}}{K}\ddot{\eta}_{\mathbf{k}} - \eta_{k-1,} + 2\eta_k - \eta_{k+1} + \kappa_{\sigma}\mathsf{D}_t^{\sigma}\left[-\eta_{k-1,} + 2\eta_k - \eta_{k+1}\right] + 2\mu\eta_{\mathbf{k}} = \quad , \; k = 1,2,3,\ldots,n$$

$$= \frac{\mathsf{M}_{0,k,1}}{K}\cos\Omega_{k,1}t + \frac{\mathsf{M}_{0,k,2}}{K}\cos\Omega_{k,2}t$$

(67)

First series (66) and second series (67) of the previous system (64)-(65) of the fractional order differential equations are decoupled and independent. *Then, we can conclude that new coordinates ξ_k and η_k are main coordinates of fractional order double*

DNA helix chain model system for forced vibration regimes and that we obtain two fictive decoupled eigen single fractional order chains of the double DNA fractional order model. This is also one of the fundamental conclusion as an important property of the fractional order homogeneous model of forced vibrations in a fractional order double DNA homogeneous helix.

Systems of fractional order differential equations (66)-(67) contains two separate subsystems of fractional order differential equations expressed by *coordinates of* ξ_k *and* η_k which are main *coordinates of a fractional order double DNA chain helix forced vibration model and separate DNA fractional order model into two independent fractional order chains.*

8.3. Analytical solutions of the subsystems of the main chains fractional order differential equations for forced regime oscillations

We solve previous subsystems (66) and (67) through the use of Laplace transformations. After conducting Laplace transformations of the previous systems (66) and (67) of differential equations with fractional order derivative and having in account that we introduced notations $\mathsf{L}\{\xi_k(t)\}$ and $\mathsf{L}\{\eta_k(t)\}$ for Laplace transformations, as well as having in mind, that we accepted the hypothesis that the initial conditions of fractional order derivatives of the system are given through the use of: $\left.\dfrac{d^{\sigma-1}\xi_k(t)}{dt^{\sigma-1}}\right|_{t=0}=0$ and $\left.\dfrac{d^{\sigma-1}\eta_k(t)}{dt^{\sigma-1}}\right|_{t=0}=0$, as well that is

$$\mathsf{L}\left\{\frac{\mathsf{M}_{0,k,1}}{K}\cos\Omega_{k,1}t \mp \frac{\mathsf{M}_{0,k,2}}{K}\cos\Omega_{k,2}t\right\} = \frac{\mathsf{M}_{0,k,1}}{K}\frac{p}{p^2+\Omega_{k,1}^2} \mp \frac{\mathsf{M}_{0,k,2}}{K}\frac{p}{p^2+\Omega_{k,2}^2}$$

(68)

where ξ_{0k} and $\dot{\xi}_{0k}$ as well as η_{0k} and $\dot{\eta}_{0k}$ are initial angular positions and angular velocities defined by initial conditions of system material particles dynamics in the chains at initial moment, we can write the following system of the equations with unknown Laplace transforms:

$$\mathsf{L}\left\{\frac{2\mathbf{J}}{K}\ddot{\xi}_\mathbf{k}\right\} - \mathsf{L}\{\xi_{k-1}\} + 2\mathsf{L}\{\xi_k\} - \mathsf{L}\{\xi_{k+1}\} + \kappa_\sigma\mathsf{L}\left\{\mathsf{D}_t^\sigma\left[-\xi_{k-1,}+2\xi_k-\xi_{k+1}\right]\right\} + 2\mu\mathsf{L}\{\xi_\mathbf{k}\} - 2\kappa\mathsf{L}\{\xi_k\} - 2\kappa\kappa_\sigma\mathsf{L}\left\{\mathsf{D}_t^\sigma[\xi_\mathbf{k}]\right\} =$$

$$= +h_{0,k,1}\frac{p}{p^2+\Omega_{k,1}^2} - h_{0,k,2}\frac{p}{p^2+\Omega_{k,2}^2}$$

(69)

$$\frac{2\mathbf{J}}{K}\mathsf{L}\{\ddot{\eta}_\mathbf{k}\} - \mathsf{L}\{\eta_{k-1,}\} + 2\mathsf{L}\{\eta_k\} - \mathsf{L}\{\eta_{k+1}\} + \kappa_\sigma\mathsf{L}\left\{\mathsf{D}_t^\sigma\left[-\eta_{k-1,}+2\eta_k-\eta_{k+1}\right]\right\} + 2\mu\mathsf{L}\{\eta_\mathbf{k}\} = ,$$

$$= +h_{0,k,1}\frac{p}{p^2+\Omega_{k,1}^2} + h_{0,k,2}\frac{p}{p^2+\Omega_{k,2}^2}$$

$$k = 1,2,3,.....,n$$

(79)

Previous system is possible to rewrite in the following form:

$$\frac{\left[\frac{2\mathbf{J}}{K}p^2 + 2\mu - 2\kappa\left(1 + \kappa_\sigma p^\sigma\right)\right]}{\left(1 + \kappa_\sigma p^\sigma\right)}\mathsf{L}\{\xi_k(t)\} - \mathsf{L}\{\xi_{k-1}\} + 2\mathsf{L}\{\xi_k(t)\} - \mathsf{L}\{\xi_{k+1}\} = \frac{2\mathbf{J}}{K}\frac{\left[p\xi_{0k} + \dot\xi_{0k}\right]}{\left(1 + \kappa_\sigma p^\sigma\right)} +$$

$$+ h_{0,k,1}\frac{p}{\left(p^2 + \Omega_{k,1}^2\right)\left(1 + \kappa_\sigma p^\sigma\right)} - h_{0,k,2}\frac{p}{\left(p^2 + \Omega_{k,2}^2\right)\left(1 + \kappa_\sigma p^\sigma\right)}$$

(80)

$$\frac{\left(p^2\frac{2\mathbf{J}}{K} + 2\mu\right)}{\left(1 + \kappa_\sigma p^\sigma\right)}\mathsf{L}\{\eta_\mathbf{k}\} - \mathsf{L}\{\eta_{k-1,}\} + 2\mathsf{L}\{\eta_k\} - \mathsf{L}\{\eta_{k+1}\} = \frac{2\mathbf{J}}{K}\frac{\left[p\eta_{0k} + \dot\eta_{0k}\right]}{\left(1 + \kappa_\sigma p^\sigma\right)} +$$

$$+ h_{0,k,1}\frac{p}{\left(p^2 + \Omega_{k,1}^2\right)\left(1 + \kappa_\sigma p^\sigma\right)} + h_{0,k,2}\frac{p}{\left(p^2 + \Omega_{k,2}^2\right)\left(1 + \kappa_\sigma p^\sigma\right)}$$

(81)

Now, we have two separate, uncoupled non homogeneous subsystems of the algebraic equations in the following forms:

$$- \mathsf{L}\{\xi_{k-1}\} + (2+v)\mathsf{L}\{\xi_k(t)\} - \mathsf{L}\{\xi_{k+1}\} = \frac{\left[p\xi_{0k} + \dot\xi_{0k}\right]}{\omega_0^2\left[1 + \kappa_\sigma p^\sigma\right]} + h_{0,k,1}\frac{p}{\left(p^2 + \Omega_{k,1}^2\right)\left(1 + \kappa_\sigma p^\sigma\right)} -$$

$$- h_{0,k,2}\frac{p}{\left(p^2 + \Omega_{k,2}^2\right)\left(1 + \kappa_\sigma p^\sigma\right)}$$

(82)

$$- \mathsf{L}\{\eta_{k-1,}\} + (2+u)\mathsf{L}\{\eta_k\} - \mathsf{L}\{\eta_{k+1}\} = \frac{\left[p\eta_{0k} + \dot\eta_{0k}\right]}{\omega_0^2\left(1 + \kappa_\sigma p^\sigma\right)} + h_{0,k,1}\frac{p}{\left(p^2 + \Omega_{k,1}^2\right)\left(1 + \kappa_\sigma p^\sigma\right)} +$$

$$+ h_{0,k,2}\frac{p}{\left(p^2 + \Omega_{k,2}^2\right)\left(1 + \kappa_\sigma p^\sigma\right)}$$

(83)

or in the following forms:

$$- \mathsf{L}\{\xi_{k-1}\} + (2+v)\mathsf{L}\{\xi_k(t)\} - \mathsf{L}\{\xi_{k+1}\} = h_{\xi hk}\left(p,\xi_{0k},\dot\xi_{0k}\right) + h_{\xi pk}\left(p,\Omega_{k,1}^2,\Omega_{k,2}^2,h_{0k,1},h_{0k,2}\right)$$

(84)

$$- \mathsf{L}\{\eta_{k-1,}\} + (2+u)\mathsf{L}\{\eta_k\} - \mathsf{L}\{\eta_{k+1}\} = h_{\eta hk}\left(p,\eta_{0k},\eta_{0k}\right) + h_{\eta pk}\left(p,\Omega_{k,1}^2,\Omega_{k,2}^2,h_{0k,1},h_{0k,2}\right)$$

(85)

where

$$v = \frac{\left[p^2 + 2\mu\omega_0^2\right]}{\omega_0^2\left[1 + \kappa_\sigma p^\sigma\right]} - 2\kappa, \qquad u = \frac{\left[p^2 + 2\mu\omega_0^2\right]}{\omega_0^2\left[1 + \kappa_\sigma p^\sigma\right]}, \quad \omega_0^2 = \frac{K}{2\mathbf{J}}$$

(86)

$$h_{\xi hk}\left(p,\xi_{0k},\dot\xi_{0k}\right) = \frac{\left[p\xi_{0k} + \dot\xi_{0k}\right]}{\omega_0^2\left[1 + \kappa_\sigma p^\sigma\right]}, \quad h_{\eta hk}\left(p,\eta_{0k},\eta_{0k}\right) = \frac{\left[p\eta_{0k} + \dot\eta_{0k}\right]}{\omega_0^2\left(1 + \kappa_\sigma p^\sigma\right)}$$

(87)

$$h_{\xi pk}\left(p,\Omega_{k,1}^2,\Omega_{k,2}^2,h_{0k,1},h_{0k,2}\right) = h_{0,k,1}\frac{p}{\left(p^2 + \Omega_{k,1}^2\right)\left(1 + \kappa_\sigma p^\sigma\right)} - h_{0,k,2}\frac{p}{\left(p^2 + \Omega_{k,2}^2\right)\left(1 + \kappa_\sigma p^\sigma\right)}$$

(88)

$$h_{\xi pk}\left(p,\Omega_{k,1}^2,\Omega_{k,2}^2,h_{0k,1},h_{0k,2}\right)=h_{0,k,1}\frac{p}{\left(p^2+\Omega_{k,1}^2\right)\left(1+\kappa_\sigma p^\sigma\right)}+h_{0,k,2}\frac{p}{\left(p^2+\Omega_{k,2}^2\right)\left(1+\kappa_\sigma p^\sigma\right)}$$

(89)

Both subsystems are same form and it is necessary to solve one of the subsystems and by use analogy is easy to solve other of the subsystem equations. For that reason we can use method proposed in the papers [14] amd [20]. Determinate of the previous subsystem (84) as well (85) are in following form (21) as well as (22) by similar way as for the subsystems of algebra equations in paragraph 5..

Determinates of the previous algebra subsystem (84) as well as (85) are in the same form as it is presented in (21)-(22).

Next consideration we focus to the case:

$$-\mathsf{L}\{\xi_{k-1}\}+(2+v)\mathsf{L}\{\xi_k(t)\}-\mathsf{L}\{\xi_{k+1}\}=\begin{cases}h_{\xi h1}\left(p,\xi_{01},\dot{\xi}_{01}\right)+h_{\xi p1}\left(p,\Omega_{1,1}^2,\Omega_{1,2}^2,h_{01,1},h_{01,2},\right) & k=1\\ 0 & k\neq 1\end{cases}$$

(90)

$$-\mathsf{L}\{\eta_{k-1,}\}+(2+u)\mathsf{L}\{\eta_k\}-\mathsf{L}\{\eta_{k+1}\}=\begin{cases}h_{\eta h1}\left(p,\eta_{01},\dot{\eta}_{01}\right)+h_{\eta p1}\left(p,\Omega_{1,1}^2,\Omega_{1,2}^2,h_{01,1},h_{01,2}\right) & k=1\\ 0 & k\neq 1\end{cases}$$

(91)

By introduce the notation $h_{\xi h1}\left(p,\xi_{01},\dot{\xi}_{01}\right)+h_{\xi}\left(p,\Omega_{1,1}^2,\Omega_{1,2}^2,h_{0k,1},h_{0k,2}\right)$ and $h_{\eta h1}\left(p,\eta_{01},\eta_{01}\right)+h_{\eta p1}\left(p,\Omega_{1,1}^2,\Omega_{1,2}^2,h_{01,1},h_{01,2}\right)$ defined by (86)-(87), for the determinants $\widetilde{\Delta}_{(k)}\left(v,h_\xi\right)$, we can write similar expressions as defined by (21)-(22) changing expressions $h_\xi\left(p,\xi_{01},\dot{\xi}_{01}\right)$ by expressions $h_{\xi h1}\left(p,\xi_{01},\dot{\xi}_{01}\right)+h_\xi\left(p,\Omega_{1,1}^2,\Omega_{1,2}^2,h_{0k,1},h_{0k,2}\right)$ as well as by $h_{\eta h1}\left(p,\eta_{01},\eta_{01}\right)+h_{\eta p1}\left(p,\Omega_{1,1}^2,\Omega_{1,2}^2,h_{01,1},h_{01,2}\right)$.

For solving the system of the algebraic no homogeneous equations (90) or (91) with respect to unknown Lapalce transforms $\mathsf{L}\{\xi_k(t)\}$ or $\mathsf{L}\{\eta_k(t)\}$ of the time function main coordinate $\xi_k(t)$ and $\eta_k(t)$- unknown normal chain coordinates of the system main chains for forced vibrations, we can use Cramer approach by similar way as in the paragraph 5.

8.4. Forced eigen modes of the subsystems of the main chains of a fractional order double DNA helix chain system forced vibrations

In this part we start by two subsystems of fractional order differential equations (66) and (67) expressed by eigen normal chains coordinates $\xi_k=\varphi_{k,1}-\varphi_{k,2}$ and $\eta_k=\varphi_{k,1}+\varphi_{k,2}$, and we can rewrite these subsystems in the following form:

$$\frac{2\mathbf{J}}{K}\ddot{\xi}_{\mathbf{k}} - \xi_{\mathbf{k+1}} + 2\xi_{\mathbf{k}}[1+\mu-\kappa] - \xi_{\mathbf{k-1}} + \kappa_{\sigma}\mathrm{D}_{t}^{\sigma}\left[-\xi_{k-1,} + 2(1-\kappa)\xi_{k} - \xi_{k+1}\right] = ,$$

$$= h_{0,k,1}\cos\Omega_{k.1}t - h_{0,k,2}\cos\Omega_{k.2}t$$

$$k = 1,2,3,\ldots,n$$

(92)

$$\frac{2\mathbf{J}}{K}\ddot{\eta}_{\mathbf{k}} - \eta_{\mathbf{k+1}} + 2\eta_{\mathbf{k}}(1+\mu) - \eta_{\mathbf{k-1}} + \kappa_{\sigma}\mathrm{D}_{t}^{\sigma}\left[-\eta_{k-1,} + 2\eta_{k} - \eta_{k+1}\right] = ,$$

$$= h_{0,k,1}\cos\Omega_{k.1}t + h_{0,k,2}\cos\Omega_{k.2}t$$

$$k = 1,2,3,\ldots,n$$

(93)

Without loosing generality, we focused our next interest to consider two subsystems of the fractional order differential equations in the following form:

$$\frac{2\mathbf{J}}{K}\ddot{\xi}_{\mathbf{k}} - \xi_{\mathbf{k+1}} + 2\xi_{\mathbf{k}}[1+\mu-\kappa] - \xi_{\mathbf{k-1}} + \kappa_{\sigma}\mathrm{D}_{t}^{\sigma}\left[-\xi_{k-1,} + 2(1-\kappa)\xi_{k} - \xi_{k+1}\right] = \begin{cases} h_{0,1,1}\cos\Omega_{1.1}t & k=1 \\ 0 & k\neq 1 \end{cases}$$

$$k = 1,2,3,\ldots,n$$

(94)

$$\frac{2\mathbf{J}}{K}\ddot{\eta}_{\mathbf{k}} - \eta_{\mathbf{k+1}} + 2\eta_{\mathbf{k}}(1+\mu) - \eta_{\mathbf{k-1}} + \kappa_{\sigma}\mathrm{D}_{t}^{\sigma}\left[-\eta_{k-1,} + 2\eta_{k} - \eta_{k+1}\right] = \begin{cases} h_{0,1,1}\cos\Omega_{1.1}t & k=1 \\ 0 & k\neq 1 \end{cases}$$

$$k = 1,2,3,\ldots,n$$

(95)

Previous two subsystems are for the case of fractional order forced vibrations of a double DNA helix chain system excited by one single frequency external couple $\mathrm{M}_{0,1,1}\cos\Omega_{1,1}t$, with amplitude $\mathrm{M}_{0,1,1}$ and frequency $\Omega_{1,1}$, applied to the first mass particle in the first chain of a double DNA helix chain system.

First series (94) and second series (95) of the previous system (94-95) of the fractional order differential equations for forced vibrations are decoupled and independent. *Then, we can conclude that new coordinates ξ_k and η_k are main coordinates of fractional order double DNA helix chain model system for forced vibration regimes and that we obtain two fictive decoupled eigen single* fractional order *chains of the double DNA fractional order model. This is also one of the fundamental conclusion as an important property of the fractional order homogeneous model of forced vibrations in a* fractional order double DNA homogeneous helix.

Systems of the fractional order differential equations (94)-(95) contains two separate subsystems of fractional order differential equations expressed by *coordinates of* ξ_k *and* η_k which are main *coordinates of a fractional order double DNA chain helix forced vibration model and separate DNA fractional order chain model into two independent fractional order main chains.*

For first main chain of the double DNA chain helix (94), the eigen amplitudes for free vibrations are in the form $A_k^{(s)} = C_s\sin k\varphi_s$ and generalized coordinates $\xi_k(t)$ of the first main chain for forced vibrations is possible to express by set of this eigen main chain main coordinates $\zeta_{s\xi}$ for free vibrations in the following form:

$$\xi_k(t) = \sum_{s=1}^{n} \zeta_{s\xi} \sin k\varphi_s \tag{96}$$

$$k = 1,2,3,....,n$$

as well as for other main chain of the double DNA chain helix (95) generalized coordinates $\eta_k(t)$ of the second main chain for forced vibrations is possible to express by set of this eigen main chain main coordinates $\zeta_{s\eta}$ for free vibrations in the following form:

$$\eta_k(t) = \sum_{s=1}^{n} \zeta_{s\eta} \sin k\varphi_s \tag{97}$$

Normal coordinates $\zeta_{s\xi}$ or normal modes of the first main chain for forced vibrations is possible to express in the similar form as for free vibrations, but introducing suppositions that unknown amplitudes C_s and phase α_s depend of initial conditions are not constant, but functions of time, $C_s(t)$ and phase $\alpha_s(t)$, and for fractional order system main coordinate are in the form

$$\zeta_{s\xi}(t) = C_s(t)\cos(\Omega_\xi t + \alpha_s(t)), s = 1,2,3,....,n \tag{98}$$

with known frequencies (see Refs. [25] by Hedrih and Hedrih , [29] by Rašković P. Danilo) and unknown time functions - amplitudes $C_s(t)$ and phase $\alpha_s(t)$ depending of time and initial conditions.

Then, we introduce expressions (96) and (97) and their corresponding second and fractional order derivative into subsystem of the fractional order differential equations (94) and (95), we obtain the following systems:

$$\frac{2\mathbf{J}}{K}\sum_{s=1}^{n}\ddot{\zeta}_{s\xi}\sin k\varphi_s - \sum_{s=1}^{n}\zeta_{s\xi}\sin(k-1)\varphi_s + 2[1+\mu-\kappa]\sum_{s=1}^{n}\zeta_{s\xi}\sin k\varphi_s - \sum_{s=1}^{n}\zeta_{s\xi}\sin(k+1)\varphi_s +$$

$$+ \kappa_\sigma \mathsf{D}_t^\sigma\left[-\sum_{s=1}^{n}\zeta_{s\xi}\sin(k-1)\varphi_s + 2(1-\kappa)\sum_{s=1}^{n}\zeta_{s\xi}\sin k\varphi_s - \sum_{s=1}^{n}\zeta_{s\xi}\sin(k+1)\varphi_s\right] = \begin{cases} h_{0,1,1}\cos\Omega_{1.1}t & k=1 \\ 0 & k\neq 1 \end{cases}$$

$$k = 1,2,3,.....,n$$

$$\tag{99}$$

$$\frac{2\mathbf{J}}{K}\sum_{s=1}^{n}\ddot{\zeta}_{s\eta}\sin k\varphi_s - \sum_{s=1}^{n}\zeta_{s\eta}\sin(k-1)\varphi_s + 2[1+\mu]\sum_{s=1}^{n}\zeta_{s\eta}\sin k\varphi_s - \sum_{s=1}^{n}\zeta_{s\eta}\sin(k+1)\varphi_s +$$

$$+ \kappa_\sigma \mathsf{D}_t^\sigma\left[-\sum_{s=1}^{n}\zeta_{s\eta}\sin(k-1)\varphi_s + 2\sum_{s=1}^{n}\zeta_{s\eta}\sin k\varphi_s - \sum_{s=1}^{n}\zeta_{s\eta}\sin(k+1)\varphi_s\right] =$$

$$= \begin{cases} h_{0,1,1}\cos\Omega_{1.1}t & k=1 \\ 0 & k\neq 1 \end{cases}$$

$$\tag{100}$$

$$k = 1,2,3,.....,n$$

After made a group sublimations of the some terms in previous equations (99), we obtain the following subsystem:

$$\sum_{s=1}^{n} \frac{2\mathbf{J}}{K} \left(\ddot{\zeta}_{s\xi} + 2\frac{K}{2\mathbf{J}} \langle [1 + \mu - \kappa] - \cos\varphi_s \rangle + \frac{K}{2\mathbf{J}} 2\kappa_\sigma \langle (1 - \kappa) - \cos\varphi_s \rangle \mathsf{D}_t^\sigma [\zeta_{s\xi}] \right) \sin k\varphi_s =$$

$$= \begin{cases} h_{0,1,1} \cos\Omega_{1.1} t & k = 1 \\ 0 & k \neq 1 \end{cases}$$

(101)

$k = 1,2,3,.....,n$

Then taking into account denotations

(102)

$$\kappa_{s\sigma\xi} = \frac{K}{2\mathbf{J}} \left(2\sin^2 \frac{\varphi_s}{2} + \mu - \kappa \right), \ s = 1,2,3,....,n$$

$$\omega_{s\xi}^2 = \frac{K}{2\mathbf{J}} \left(2\sin^2 \frac{\varphi_s}{2} + \mu - \kappa \right), \ s = 1,2,3,....,n$$

(103)

$$\omega_{s\sigma\xi}^2 = \kappa_{s\sigma\xi} \frac{K}{2\mathbf{J}} = \kappa_\sigma \frac{K}{\mathbf{J}} \left(2\sin^2 \frac{\varphi_s}{2} - \kappa \right), s = 1,2,3,....,n$$

(104)

previous subsystem of fractional order differential equation (101) is possible to rewrite in the following form:

$$\sum_{s=1}^{n} \frac{2\mathbf{J}}{K} \left(\ddot{\zeta}_{s\xi} + \omega_{s\xi}^2 \zeta_{s\xi} + \frac{K}{2\mathbf{J}} \kappa_{s\sigma\xi} \mathsf{D}_t^\sigma [\zeta_{s\xi}] \right) \sin k\varphi_s = \begin{cases} h_{0,1,1} \cos\Omega_{1.1} t & k = 1 \\ 0 & k \neq 1 \end{cases},$$

$$k = 1,2,3,.....,n$$

(105)

Taking into account that it is possible to develop (to express) right hand side into series according to $\sin k\varphi_s$ in the following series:

$$\begin{cases} h_{0,1,1} \cos\Omega_{1.1} t & k = 1 \\ 0 & k \neq 1 \end{cases} = \begin{cases} \sum_{s=1}^{n} \frac{2\mathbf{J}}{K} h_{0,1,1(s)} \sin k\varphi_s \cos\Omega_{1.1} t & k = 1 \\ 0 & k \neq 1 \end{cases}$$

(106)

where

$$h_{0,1,1(s)} = \frac{K}{2\mathbf{J}} \frac{\displaystyle\sum_{s=1}^{n} h_{0,1,1} \sin k\varphi_s}{\left\langle \displaystyle\sum_{s=1}^{n} \sum_{r=1}^{n} \sin k\varphi_s \sin k\varphi_r \right\rangle_{r=s}} \qquad k = 1$$

$$h_{0,1,1(s)} = 0 \qquad k \neq 1$$

(107)

equations (101) is possible to rewrite in the following form:

$$\sum_{s=1}^{n} \frac{2\mathbf{J}}{K} \left(\ddot{\zeta}_{s\xi} + \omega_{s\xi}^2 \zeta_{s\xi} + \omega_{s\sigma\xi}^2 \mathsf{D}_t^\sigma [\zeta_{s\xi}] - h_{0,1,1(s)} \cos\Omega_{1.1} t \right) \sin k\varphi_s = 0 \ , k = 1,2,3,.....,n$$

(108)

Then, taking into account that $\sin k\varphi_s \neq 0$ in general case, from (108) is possible to obtain the following subsystem of fractional order differential equations:

$$\ddot{\zeta}_{s\xi} + \omega^2_{s\xi}\zeta_{s\xi} + \omega^2_{s\sigma\xi}\mathsf{D}^\sigma_t[\zeta_{s\xi}] = h_{0,1,1(s)}\cos\Omega_{1.1}t \, , \; s = 1,2,3,....,n$$

(109)

where $\omega^2_{s\xi}$ are square of eigen circular frequencies determined by expression (103) and $\omega^2_{s\sigma\xi}$ corresponding eigen characteristic numbers expressing fractional order subsystem properties, determined by expression (104).

In analogous way, taking into account denotation

$$\kappa_{s\sigma\eta} = 2\kappa_\sigma\left(\frac{2\mathbf{J}}{K}\omega^2_{s\eta} - \mu\right) \quad , \; s = 1,2,3,....,n$$

(110)

$$\omega^2_{s\eta} = \frac{K}{2\mathbf{J}}\left(2\sin^2\frac{\varphi_s}{2} + \mu\right), \; s = 1,2,3,....,n$$

(111)

$$\omega^2_{s\sigma\eta} = 4\kappa_\sigma\frac{K}{2\mathbf{J}}\sin^2\frac{\varphi_s}{2}, \; s = 1,2,3,....,n$$

(112)

and by use (100), is possible to obtain the second subsystem of fractional order differential equations in the following form:

$$\ddot{\zeta}_{s\eta} + \omega^2_{s\xi}\zeta_{s\eta} + \omega^2_{s\sigma\eta}\mathsf{D}^\sigma_t[\zeta_{s\eta}] = h_{0,1,1(s)}\cos\Omega_{1.1}t \, , \; s = 1,2,3,....,n$$

(113)

where $\omega^2_{s\eta}$ square of eigen circular frequencies determined by expression (111) and $\omega^2_{s\sigma\eta}$ corresponding eigen characteristic numbers expressing fractional order subsystem properties, determined by expression (112).

Then we have system of fractional order differential equations (109)-(1113) describing system of $2n$ fractional order oscillators, containing two subsets of the main fractional order forced oscillators, each described by n fractional order differential equations. Each of these $2n$ fractional order differential equations, contain only one main eigen coordinate $\zeta_{s\xi}$ or $\zeta_{s\eta}$ of the system.

The system (109)-(1113) represent the main fractional order forced oscillators along independent system main coordinates $\zeta_{s\xi}$ or $\zeta_{s\eta}$, $s = 1,2,3,....,n$ each with one circular frequency of external excitation and one eigen circular frequency and one eigen characteristic number from one of the two sets of: $\omega_{s\xi}$ or $\omega_{s\eta}$ eigen circular frequencies determined by expression (103) or (111) and $\omega^2_{s\sigma\xi}$ or $\omega^2_{s\sigma\eta}$ corresponding eigen characteristic numbers expressing fractional order subsystem properties, determined by expression (104) or (112).

All of fractional order differential equations of the system (109)-(1113) are same type and is possible to solve by same way by use Laplace transform $\mathsf{L}\{\zeta_{s\xi}(t)\}$ and $\mathsf{L}\{\zeta_{s\eta}(t)\}$. Applying Laplace transform to the system (109)-(1113) of the fractional order differential equations, we obtain the following system of the equations:

$$\mathsf{L}\{\ddot{\zeta}_{s\xi}\} + \omega_{s\xi}^2 \mathsf{L}\{\zeta_{s\xi}(t)\} + \omega_{s\sigma\xi}^2 \mathsf{L}\{\mathsf{D}_t^\sigma[\zeta_{s\xi}]\} = h_{0,1,1(s)}\mathsf{L}\{\cos\Omega_{1,1}t\}, \qquad s = 1,2,3,....,n$$

(114)

$$\mathsf{L}\{\ddot{\zeta}_{s\eta}\} + \omega_{s\xi}^2 \mathsf{L}\{\zeta_{s\eta}(t)\} + \omega_{s\sigma\eta}^2 \mathsf{L}\{\mathsf{D}_t^\sigma[\zeta_{s\eta}]\} = h_{0,1,1(s)}\mathsf{L}\{\cos\Omega_{1,1}t\}, \qquad s = 1,2,3,....,n$$

(115)

Taking into account that

$$\mathsf{L}\left\{\frac{d^2\zeta_{s\xi}(t)}{dt^2}\right\} = p^2\mathsf{L}\{\zeta_{s\xi}(t)\} - [p\zeta_{0s\xi} + \dot{\zeta}_{0s\xi}], \qquad s = 1,2,3,....,n$$

(116)

$$\mathsf{L}\left\{\frac{d^2\zeta_{s\eta}(t)}{dt^2}\right\} = p^2\mathsf{L}\{\zeta_{s\eta}(t)\} - [p\zeta_{0s\eta} + \dot{\zeta}_{0s\eta}], \; s = 1,2,3,....,n$$

(117)

$$\mathsf{L}\{\cos\Omega_{1,1}t\} = \frac{p}{p^2 + \Omega_{1,1}^2}$$

(118)

$$\mathsf{L}\left\{\frac{d^\sigma\zeta_{s\xi}}{dt\omega}\right\} = p^\sigma\mathsf{L}\{\zeta_{s\xi}\} - \frac{d^{\sigma-1}\zeta_{s\xi}}{dt^{\varpi-1}}\bigg|_{t=0} = p^\sigma\mathsf{L}\{\zeta_{s\xi}\}, \; s = 1,2,3,....,n$$

(119)

$$\mathsf{L}\left\{\frac{d^\sigma\zeta_{s\eta}}{dt\omega}\right\} = p^\sigma\mathsf{L}\{\zeta_{s\eta}\} - \frac{d^{\sigma-1}\zeta_{s\eta}}{dt^{\varpi-1}}\bigg|_{t=0} = p^\sigma\mathsf{L}\{\zeta_{s\eta}\}, \; s = 1,2,3,....,n$$

(120)

and after introducing into system (118)-(119) for Laplace transform $\mathsf{L}\{\zeta_{s\xi}(t)\}$ and $\mathsf{L}\{\zeta_{s\eta}(t)\}$ of system double DNA helix chain eigen main coordinates $\zeta_{s\xi}$ and $\zeta_{s\eta}$ we obtain:

$$\mathsf{L}\{\zeta_{s\xi}\} = \frac{[p\zeta_{0s\xi} + \dot{\zeta}_{0s\xi}]}{(p^2 + \omega_{s\xi}^2 + \omega_{s\sigma\xi}^2 p^\sigma)} + \frac{h_{0,1,1(s)}}{(p^2 + \omega_{s\xi}^2 + \omega_{s\sigma\xi}^2 p^\sigma)}\frac{p}{p^2 + \Omega_{1,1}^2}, \; s = 1,2,3,....,n$$

(121)

$$\mathsf{L}\{\zeta_{s\eta}\} = \frac{[p\zeta_{0s\eta} + \dot{\zeta}_{0s\eta}]}{(p^2 + \omega_{s\eta}^2 + \omega_{s\sigma\eta}^2 p^\sigma)} + \frac{h_{0,1,1(s)}}{(p^2 + \omega_{s\eta}^2 + \omega_{s\sigma\eta}^2 p^\sigma)}\frac{p}{p^2 + \Omega_{1,1}^2}, \; s = 1,2,3,....,n$$

(122)

Then, for obtaining system double DNA helix chain eigen main coordinates $\zeta_{s\xi}(t)$ and $\zeta_{s\eta}(t)$ is necessary to applied inverse of Laplace transform to the expressions (121)-(122).

Then, we can write the following:

$$\zeta_{s\xi}(t) = \zeta_{s\xi,\text{hom}}(t) + \zeta_{s\xi,part}(t)$$

(123)

and

$$\zeta_{s\eta}(t) = \zeta_{s\eta,\text{hom}}(t) + \zeta_{s\eta,part}(t)$$

(124)

where

a* $\zeta_{s\xi,\text{hom}}(t)$ and $\zeta_{s\eta,\text{hom}}(t)$ are terms correspond to solutions of the homogeneous fractional order differential equations and solutions are in the following forms (see Appendix (A.1)-(A.3) and (B.1)-(B.16)):

$$\zeta_{s\xi,\text{hom}}(t) = \zeta_{s\xi}(0)\sum_{k=0}^{\infty}(-1)^k \omega_{s\sigma\xi}^{2k} t^{2k}\sum_{j=0}^{k}\binom{k}{j}\frac{(\mp 1)^j \omega_{s\sigma\xi}^{2j} t^{-\alpha j}}{\omega_{s\xi}^{2j}\Gamma(2k+1-\alpha j)}+$$

$$+\dot{\zeta}_{s\xi}(0)\sum_{k=0}^{\infty}(-1)^k \omega_{s\sigma\xi}^{2k} t^{2k+1}\sum_{j=0}^{k}\binom{k}{j}\frac{(\mp 1)^j \omega_{s\sigma\xi}^{-2j} t^{-\alpha j}}{\omega_{s\xi}^{2j}\Gamma(2k+2-\alpha j)}$$

(125)

$$\zeta_{s\eta,\text{hom}}(t) = \zeta_{s\eta}(0)\sum_{k=0}^{\infty}(-1)^k \omega_{s\sigma\eta}^{2k} t^{2k}\sum_{j=0}^{k}\binom{k}{j}\frac{(\mp 1)^j \omega_{s\sigma\eta}^{2j} t^{-\alpha j}}{\omega_{s\eta}^{2j}\Gamma(2k+1-\alpha j)}+$$

$$+\dot{\zeta}_{s\eta}(0)\sum_{k=0}^{\infty}(-1)^k \omega_{s\sigma\eta}^{2k} t^{2k+1}\sum_{j=0}^{k}\binom{k}{j}\frac{(\mp 1)^j \omega_{s\sigma\eta}^{-2j} t^{-\alpha j}}{\omega_{s\eta}^{2j}\Gamma(2k+2-\alpha j)}$$

(126)

b* $\zeta_{s\xi,par}(t)$ and $\zeta_{s\eta,par}(t)$ are terms correspond to particular solutions of the no homogeneous fractional order differential equations system (121)-(122) and solutions must to obtain as a inverse transform of the following expressions:

$$\zeta_{s\xi,par}(t) = L^{-1}L\{\zeta_{s\xi,par}\} = L^{-1}\left\{\frac{h_{0,1,1(s)}}{\left(p^2+\omega_{s\xi}^2+\omega_{s\sigma\xi}^2 p^{\sigma}\right)}\frac{p}{p^2+\Omega_{1,1}^2}\right\}, s=1,2,3,....,n$$

(127)

$$\zeta_{s\eta,pat}(t) = L^{-1}L\{\zeta_{s\eta,pat}\} = L^{-1}\left\{\frac{h_{0,1,1(s)}}{\left(p^2+\omega_{s\eta}^2+\omega_{s\sigma\eta}^2 p^{\sigma}\right)}\frac{p}{p^2+\Omega_{1,1}^2}\right\}, s=1,2,3,....,n$$

(128)

or in developed form

$$\zeta_{s\xi,par}(t) = L^{-1}L\{\zeta_{s\xi,par}\} = h_{0,1,1(s)}L^{-1}\left\{\frac{1}{p}\frac{1}{p^2+\Omega_{1,1}^2}\sum_{k=0}^{\infty}\frac{(-1)^k \omega_{s\xi}^2}{p^{2k}}\sum_{j=0}^{k}\binom{k}{j}\frac{(\mp 1)^j p^{\alpha j}\omega_{s\sigma\xi}^{2(j-k)}}{\omega_{s\xi}^{2j}}\right\}$$

$$s=1,2,3,....,n$$

(129)

$$\zeta_{s\eta,pat}(t) = L^{-1}L\{\zeta_{s\eta,pat}\} = h_{0,1,1(s)}L^{-1}\left\{\frac{1}{p}\frac{1}{p^2+\Omega_{1,1}^2}\sum_{k=0}^{\infty}\frac{(-1)^k \omega_{s\eta}^2}{p^{2k}}\sum_{j=0}^{k}\binom{k}{j}\frac{(\mp 1)^j p^{\alpha j}\omega_{s\sigma\eta}^{2(j-k)}}{\omega_{s\eta}^{2j}}\right\}$$

$$s=1,2,3,....,n$$

(130)

9. Concluding remarks

At the end, we can conclude that new coordinates of ξ_k and η_k composed to generalized coordinates by the way $\xi_k = \varphi_{k,1} - \varphi_{k,2}$ and $\eta_k = \varphi_{k,1} + \varphi_{k,2}$. These coordinates are main coordinates of the main eigen chains of a double DNA helix chain system. Also we can conclude that it is possible to obtain two fictive decoupled and separated eigen single chains of the double DNA chain helix liner model as well as fractional order model. This is important fundamental conclusion as an important property of the linear model of vibrations in a double DNA helix.

Considered as a linear or fractional order mechanical system, *DNA molecule as a double helix chain system has its eigen circular frequencies and that is its characteristic. Mathematically it is possible to decuple it into two chains with their eigen circular frequencies which are different. This may correspond to different chemical structure (the order of base pairs) of the complementary chains of DNA. We are free to propose that each specific set of base pair order has its eigen circular frequencies and it changes when DNA chains are coupled in the system of double helix. DNA as a double helix in a living cell can be considered as nonlinear system but under certain condition its behavior can be describe by linear dynamics.*

By use superposition's of these solutions for the case that external excitations are with same amplitudes and frequencies from system differential equations, we can see that for this case external one frequency excitations in one eigen main chain appear pure free vibrations with eigen subset of circular frequencies of its free vibrations, and in other appear forced vibrations. This conclusion is possible to generalize for same multi-frequency external excitations applied in which of the pair material particle in both chains. This conclusion is possible to extend to the fractional order double helix DNA chain system forced vibrations.

This solutions may correspond with process of binding the enzyme to the specific part of the DNA molecule. Enzyme has a role of inducer of forced vibrations. In the transcription process only one chain is used as a template for transcription other chain is control. The part of DNA chain witch is template has to make more movements than the other chain.

Dynamical absorption on the first pair of the main coordinates of the main chains appear on the resonate circular frequencies of the set of the double DNA helix chain system with one less pair of the material particles in comparison with the considered real system.

Resonant state that appear only in one main chain may be important for selecting the specific sequence for transcription and we suggest that every sequence of DNA that encodes the specific protein has its own resonate circular frequencies different from the sequences that encode other proteins.

Dynamical absorption on the second pair of the main coordinates of the main chains appear on the resonate circular frequencies of the set of the double DNA helix chain system with two less pairs of the material particles in comparison with considered system.

This mathematical fact is important to consider in the light of the interruption or break of the double DNA helix chain **system on the specific places where the transcription process starts and ends.**

Acknowledgements

References

[1] Arsuaga, J., Tan, KZ., Vazquez, M., Sumners, D.W., Harvey, CS. (2002) 'Investigation of viral DNA packaging using molecular mechanics models', *Biophys Chem.,* Vol. 101 −102, pp. 475–484.

[2] Bao, G. (2002) 'Mechanics of biomolecules', *J Mech Phys Solids.,* Vol. 50, pp.2237-2274.

[3] Bačlić, B. S., Atanacković, T., (2000), M., *Stability and creep of a fractional derivative order viscoelastic Rod*, Bulletin T, CXXI de L'Academie Serbe des Sciences st de Arts - 2000, Class des Sciences mathematques et naturelles Sciences mathematiques, No. 25, 115-131.

[4] Brukner, I., Susic, S., Dlakic, M., Savic, A. and Pongor, S. (1994) 'Physiological concentrations of magnesium ions induces a strong macroscopic curvature in GGGCCC-containing DNA', *J. Mol. Biol.,* Vol. 236, pp.26– 32.

[5] Bryant, Z., Stone, M.D., Gore, J., Smith, S.B., Cozzarelli, N.R. and Bustamante, C. (2003) 'Structural transitions and elasticity from torque measurements on DNA', *Nature,* Vol. 424, pp.338-341.

[6] Cadoni, M., De Leo, R., Demelio, S. and Gaeta, G. (2008) 'Twist solitons in complex macromolecules: From DNA to polyethylene', *Int J Non-Linear Mech.,* Vol.43, No.10, pp.1094-1107.

[7] Cocco, S.J., Marko, F. and Monasson, R. (2002) 'Theoretical models for single-molecule DNA and RNA experiments: from elasticity to unzipping', *C. R. Physique.,* Vol. 3, pp.569–584.

[8] De Leo, R. and Demelio, S. (2008) 'Numerical analysis of solitons profiles in a composite model for DNA torsion dynamics', *Int J Non-Linear Mech.,* Vol. 43, No. 10, pp.1029-1039.

[9] Eslami-Mossallam, B. and. Ejtehadi, MR (2009) 'Asymmetric elastic rod model for DNA', *Phys Rev E Stat Nonlin Soft Matter Phys.,*Vol. 80, (1 Pt 1) 011919.

[10] Frontali, C., Dore, E., Ferrauto, A., Gratton, E., Bettini, A., Pozzan, M.R and Valdevit, E. (1979) 'An absolute method for the determination of the persistence length of native DNA from electron micrographs', *Biopolymers,* Vol. 18, pp.1353– 1357.

[11] Gaeta, G. (1992) 'Solitons in planar and helicoidal Yakushevich model of DNA dynamics', *Phys. Lett. A.,* Vol. 168, Iss.5-6, pp.383-390.

[12] González, J.A. and Martín-Landrove, M. (1994) 'Solitons in a nonlinear DNA model', *Phys. Lett. A,,* Vol. 191, No. 5-6, pp. 409-415.

[13] Gore, J., Bryant, Z.,. Nöllmann, M., LE, M.U., Cozzarelli, N.R. and Bustamante, C. (2006) 'DNA overwinds when stretched', *Nature,Vol.* 442, pp.836-839.

[14] Hedrih (Stevanović) K., (2006), Modes of the Homogeneous Chain Dynamics, Signal Processing, Elsevier, 86(2006), 2678-2702.

[15] Hedtrih (Stevanović) K., (2008), Dynamics of coupled systems, Nonlinear Analysis: Hybrid Systems, Volume 2, Issue 2, June 2008, Pages 310-334.

[16] Hedrih (Stevanović) K., (2005), Partial Fractional Order Differential Equations of Transversal Vibrations of Creep-connected Double Plate Systems, in Monograph - **Fractional Differentiation and its Applications,** Edited by Alain Le Mahaute, J. A. Tenreiro Machado, Jean Claude Trigeassou and Jocelyn Sabatier, p. 780, U-Book, Printed in Germany, pp. 289-302.

[17] Hedrih (Stevanović K., (2008), Main chains and eigen modes of the fractional order hybrid multipendulum system dynamics, IOP PUBLISHING PHYSICA SCRIPTA, Phys. Scr. **78** (2008) 000000 (12pp) doi:10.1088/0031-8949/78/8/000000

[18] Hedtrih (Stevanović) K., (2008), *Dynamics of multipendulum systems with fractional order creep elements, Special Issue Vibration and Chaos,* Journal of Theoretical and Applied Mechanics, Quaterly, (Warsaw, Poland) No.3 Vol. 46, pp. 483-509.

[19] Hedrih (Stevanović) Katica (2009)**,** *Considering Transfer of Signals through Hybrid Fractional Order Homogeneous Structure***, Keynote Lecture**, AAS-09, Ohird, Makedonija, posvecen profesoru Pane Vidincevu, prvom profesoru automatike i rachnarskih mashina u Makedoniji Special session, Applied Automatic Systems , Proceedings of selected AAS 2009 Papers. Edited by G. Dimirovski, Skopje –Istambul , 2009, ISBN -13-978-9989-2175-6-2, National Library of R. Makedonia, Skopje, Copright«2009Authors and ETAI Society, pp. 19-24.

[20] Hedrih   (Stevanović K., (2008), The fractional order hybrid system vibrations, Monograph, **Advances in Nonlinear Sciences**, ANN, 2008, Vol. 2, pp. 226-326.

[21] Hedrih (Stevanović), K., *Discrete Continuum Method*, Symposium, Recent Advances in Analytical Dynamics Control, Stability and Differential Geometry, Proceedings Mathematical institute SANU Edited by Vladan Djordjević, p.151, 2002, pp.30-57. ISBN 86-80593-32-X.   http://www.mi.sanu.ac.yu/publications.htm

[22] Hedrih (Stevanović) K., (2004), *Discrete Continuum Method,* COMPUTATIONAL MECHANICS, **WCCM** VI in conjunction with **APCOM**'04, *Sept. 5-10, 2004, Beijing, China,* © 2004 Tsinghua University Press & Springer-Verlag, pp. 1-11, CD. IACAM International Association for Computational Mechanics – www. iacm.info

[23] Hedrih (Stevanović) K. and Filipovski A., (2002), *Longitudinal Creep Vibrations of a Fractional Derivative Order Rheological Rod with Variable Cross Section*, Facta Universitatis, Series Mechanics, Automatics Control and Robotics, Vo. 3, No. 12, 2002**,** pp. 327-350. (in English**).**YU ISSN 0354-2009**.**

[24] Katica (Stevanović) Hedrih and Andjelka N. Hedrih, (2009), Eigen main chain modes of the double DNA fractional order chain helix vibrations, Proc. IConSSM 2009, M1-03, CD, pp. 1-15.

[25] Hedrih (Stevanović) K., Hedrih A. N., Eigen modes of the double DNA chain helix vibrations, Journal of Theoretical and Applied Mechanics (JTAM), no. 1, vol. 48, 2010., pp. 219-231

[26] N.Kovaleva, L.Manevich, V. Smirnov Analitical study of coarse-grained model of DNA. 9th conference on Dinamical systems theory and applications, December 17-20, 2007, Lodz, Poland

[27] N.Kovaleva, L.Manevich, Localized nonlinear oscillation of DNA molecule.8th conference on Dinamical systems theory and applications, December 12-15, 2005, Lodz, Poland

[28] Peck, L.J and Wang, J.C. (1981) 'Sequence dependence of the helical repeat of DNA in solution', *Nature,* Vol. 292, pp.375-378.

[29] Rašković P. Danilo, (1965), Teorija oscilacija (Theory of Oscillations), Naučna knjiga, 1965, 503.
[30] Tabi, C.B., Mohamadou, A., and Kofané, (T. C. 2009) 'Modulational instability and exact soliton solutions for a twist-opening model of DNA dynamics', *Phys. Lett A.,* Vol. 373, No. 29, pp.2476-2483.
[31] Tung, CS. and. Harvey S.C. (1984) 'A moecular mechanical model to predict the heix twists angles of B-DNA', *Nucleic Acids Res.,* Vol. 12, No.7, pp.3343-3356.
[32] Yakushevich, L., Savin, A. and Manevitch, L. (2002) 'Nonlinear dynamics of topological solitons in DNA', *Phys. Rev. E.* Vol. 66, pp.016614.
[33] Zhou, Z. and Lai, P-Y. (2001) 'On the consistency of two elastic models for double-stranded DNA', *Chem. Phys. Lett.,* Vol. 346, No. 5-6, pp.449-454.

APPENDIX

NOMENCLATURE

DNA – Deoxyribonucleic acid (DNA)

$\varphi_{k,1}[rad]$ - generalized coordinate – angles of the k-th base of the first chain of the double DNA chain helix;

$\varphi_{k,2}[rad]$ - generalized coordinate – angles of the k-th base of the second chain of the double DNA chain helix;

$\mathbf{J}_{k,1}[kgm^2]$- is the axial moment of mass inertia of the k-th base of the first chain of the double DNA chain helix;

$\mathbf{J}_{k,2}[kgm^2]$- is the axial moment of mass inertia of the k-th base of the second chain of the double DNA chain helix;

$\dot{\varphi}_{k,1}[\text{rads}^{-1}]$ - angular velocity of the k-th base of the first chain of the he double DNA chain helix;

$\mathbf{J}_{k,1} = m_\alpha r_\alpha^2$, $\mathbf{J}_{k,12} = m_\beta r_\beta^2$ [kgm^2] - the base pair the axial moments of mass inertia ;

m_α [kg]- the value of the base mass

r_α [m] - the length

$\mathbf{J}_{k,1} = m_\alpha r_\alpha^2$ [kgm^2] - the corresponding axial moment of mass inertia for all possible base pair authors accepted as in the Reference [17].

$K_{k,i}$, $i = 1,2$ [KJmol^{-1}]- parameters characterize the energy of interaction of the k-th base with the ($k+1$)-th one along
the i-th chain $i = 1,2$.

$K_{k,i} = K = 6 \times 10^3 [\text{KJmol-1}]$- for the calculation that the most appropriate value is close /

ξ_k, η_k [rad], $k = 1,2,3,.....,n$ - main orthogonal coordinates of the eigen main chains of the double DNA chain helix;

$\xi_k = \varphi_{k,1} - \varphi_{k,2}$ and $\eta_k = \varphi_{k,1} + \varphi_{k,2}$, $k = 1,2,3,.....,n$ - functional dependence between main orthogonal coordinates ξ_k and η_k of the eigen main chains and generalized coordinates $\varphi_{k,1}$ and $\varphi_{k,2}$ [rad] of the double DNA chain helix;

$\omega_{\alpha\beta2}$ [$\sec^{-1}$] - are frequencies of rotational motions of the bases, in similar and opposite directions accordingly, of the k -th base of the first chain of the
        double DNA chain helix;

$\omega_{\alpha\beta1}$ [$\sec^{-1}$] - are frequencies of rotational motions of the bases, in similar and opposite directions accordingly, of the k -th base of the first chain of the
        double DNA chain helix;

$K_{k,1} = K_{k,2} = K$ - for the case of homogeneous double DNA chain helix;

$\mathbf{J}_{k,1} = \mathbf{J}_{k,2} = \mathbf{J}$ [kgm^2] - for the case of homogeneous double DNA chain helix;

A_k - amplitude

u=JK$^{-1}\omega^2$- eigen characteristic number of the homogeneous double DNA chain helix;

k= $K_{\alpha\beta}$ 2K^{-1}\{1- $\omega_{\alpha\beta2}$ $\omega_{\alpha\beta1}$ $^{-1}$1)$\left(r_\alpha - r_\beta\right)^2$ - parameter of the homogeneous double DNA chain helix;

μ= $K_{\alpha\beta}r_\alpha\left(r_\alpha - r_\beta\right)$K^{-1} - parameter of the homogeneous double DNA chain helix;

$\omega_{s\xi}^2$ [$\sec^{-2}$], $s = 1,2,3,4...,n$ - set of the n eigen circular frequencies of the first eigen main chain of the homogeneous double DNA chain helix;

$\omega_{s\eta}^2$ [$\sec^{-2}$], $s = 1,2,3,4...,n$ - set of the n eigen circular frequencies of the first eigen main chain of the homogeneous double DNA chain helix;

$\omega_{s\xi}^2$ and $\omega_{s\eta}^2$, $s = 1,2,3,4...,n$ -two subsets of the set of the homogeneous double DNA chain helix;

APPENDIX A*

Expansion of the Laplace transform into series.

$$L\{\xi_2\} = \frac{p\varphi_{0i} + \dot{\varphi}_{0i}}{2\left(p^2 + \omega_{0\alpha}^2 p^\alpha + \widetilde{\omega}_0^2 + \omega_{00}^2\right)} \tag{A.1}$$

$$L\{\xi_2(t)\} = \frac{p\varphi_{01} + \dot{\varphi}_{01}}{2p^2\left[1 + \frac{\omega_{0\alpha}^2}{p^2}\left(p^\alpha + \frac{\widetilde{\omega}_0^2 + \omega_{00}^2}{\omega_{0\alpha}^2}\right)\right]} = \left(\varphi_{01} + \frac{\dot{\varphi}_{01}}{p}\right)\frac{1}{2p}\left[\frac{1}{1 + \frac{\omega_{0\alpha}^2}{p^2}\left(p^\alpha + \frac{\widetilde{\omega}_0^2 + \omega_{00}^2}{\omega_{0\alpha}^2}\right)}\right]$$

$$L\{\xi_2(t)\} = \left(\varphi_{01} + \frac{\dot{\varphi}_{01}}{p}\right)\frac{1}{2p}\sum_{k=0}^{\infty}\frac{(-1)^k \omega_{0\alpha}^{2k}}{p^{2k}}\left(p^\alpha + \frac{\widetilde{\omega}_0^2 + \omega_{00}^2}{\omega_{0\alpha}^2}\right)^k \tag{A.2}$$

$$L\{\xi_2(t)\} = \left(\varphi_{01} + \frac{\dot{\varphi}_{01}}{p}\right)\frac{1}{2p}\sum_{k=0}^{\infty}\frac{(-1)^k \omega_{0\alpha}^{2k}}{p^{2k}}\sum_{j=0}^{k}\binom{k}{j}\frac{p^{\alpha j}\omega_{0\alpha}^{2(j-k)}}{\left(\widetilde{\omega}_0^2 + \omega_{00}^2\right)^j} \tag{A.3}$$

APPENDIX B*

Solution of a fractional order differential equation of a fractional order creep oscillator with single degree of freedom

The fractional order differential equations obtained and considered cases of eigen fractional order partial oscillators of the hybrid fractional order multichain system are in mathematical analogy same fractional order differential equation with corresponding unknown time-functions. We can use notation $T(t)$ and all previous derived fractional order differential equations of eigen fractional order partial oscillators with one degree pf freedom, correspond to the hybrid fractional order multi-chain system dynamics with sixth degree of freedom, we can rewrite it in the following form:

$$\ddot{T}(t) \pm \omega_\alpha^2 T^{(\alpha)}(t) + \omega_0^2 T(t) = 0 \qquad (B.1)$$

This fractional order differential equation (B.1) on unknown time-function $T(t)$, can be solved applying Laplace transforms (see Refs. [3] by Bačlić and Atanacković (2000), [23] by Hedrih (Stevanović) and Filipovski (2002)). Upon that fact Laplace transform of solution is in form:

$$\mathsf{T}(p) = \mathsf{L}[T(t)] = \frac{pT(0) + \dot{T}(0)}{p^2 + \omega_0^2 \left[1 \pm \dfrac{\omega_\alpha^2}{\omega_0^2} \mathbf{R}(p) \right]} \qquad (B.2)$$

where $\mathsf{L}[D_t^\alpha[T(t)]] = \mathbf{R}(p)\mathsf{L}[\mathsf{T}(t)]$ is Laplace transform of a fractional derivative $\dfrac{d^\alpha T(t)}{dt^\alpha}$ for $0 \le \alpha \le 1$. For creep rheological material those Laplace transforms the form:

$$\mathsf{L}[D_t^\alpha[T(t)]] = \mathbf{R}(p)\mathsf{L}[T(t)] - \frac{d^{\alpha-1}}{dt^{\alpha-1}}T(0) = p^\alpha \mathsf{L}[T(t)] - \frac{d^{\alpha-1}}{dt^{\alpha-1}}T(0) \qquad (B.3)$$

where the initial value are:

$$\left. \frac{d^{\alpha-1}T(t)}{dt^{\alpha-1}} \right|_{t=0} = 0 \qquad (B.4)$$

so, in that case Laplace transform of time-function is given by following expression:

$$\mathsf{L}\{T(t)\} = \frac{pT_0 + \dot{T}_0}{\left[p^2 \pm \omega_\alpha^2 p^\alpha + \omega_0^2 \right]} \qquad (B.5)$$

For boundary cases, when material parameters α take following values: $\alpha = 0$ i $\alpha = 1$ we have the two special simple cases, whose corresponding fractional-differential equations and solutions are known. In these cases fractional-differential equations are:

1* $\ddot{T}(t) \pm \tilde{\omega}_{0\alpha}^2 T^{(0)}(t) + \omega_0^2 T(t) = 0$ for $\alpha = 0$ $\qquad (B.6)$

where $T^{(0)}(t) = T(t)$, and

2* $\ddot{T}(t) \pm \omega_{1\alpha}^2 T^{(1)}(t) + \omega_0^2 T(t) = 0$ for $\alpha = 1$ $\qquad (B.7)$

where $T^{(1)}(t) = \dot{T}(t)$.

The solutions to equations (B.6) and (B.7) are:

1* $T(t) = T_0 \cos t \sqrt{\omega_0^2 \pm \tilde{\omega}_{0\alpha}^2} + \dfrac{\dot{T}_0}{\sqrt{\omega_0^2 \pm \tilde{\omega}_{0\alpha}^2}} \sin t \sqrt{\omega_0^2 \pm \tilde{\omega}_{0\alpha}^2}$ $\qquad (B.8)$

for $\alpha = 0$.

2* a.

(B.9)

$$T(t) = e^{\mp\frac{\omega_{1}^2}{2}t}\left\{T_0 \cos t\sqrt{\omega_0^2 - \frac{\omega_{1\alpha}^4}{4}} + \frac{\dot{T}_0}{\sqrt{\omega_0^2 - \frac{\omega_{1\alpha}^4}{4}}}\sin t\sqrt{\omega_0^2 - \frac{\omega_{1\alpha}^4}{4}}\right\}$$

for $\alpha = 1$ and for $\omega_0 > \frac{1}{2}\omega_{1\alpha}^2$. (for soft creep) or for strong creep:

2* b.

(B.10)

$$T(t) = e^{\mp\frac{\omega_{1\alpha}^2}{2}t}\left\{T_0 Ch\, t\sqrt{\frac{\omega_{1\alpha}^4}{4} - \omega_0^2} + \frac{\dot{T}_0}{\sqrt{\frac{\omega_{1\alpha}^4}{4} - \omega_0^2}}Sh\, t\sqrt{\frac{\omega_{1\alpha}^4}{4} - \omega_0^2}\right\}$$

for $\alpha = 1$ and for $\omega_0 < \frac{1}{2}\omega_{1\alpha}^2$.

For critical case:

2* c. $T(t) = e^{\mp\frac{\omega_{1\alpha}^2}{2}t}\left\{T_0 + \frac{2\dot{T}_0}{\omega_{1\alpha}^2}t\right\}$ for $\alpha = 1$ and $\omega_0 = \frac{1}{2}\omega_{1\alpha}^2$.   (B.11)

Fractional-differential equation (B.1) for the general case, when α is real number from interval $0 < \alpha < 1$ can be solved by using Laplace's transformation. By using that is:

$$\mathsf{L}\left\{\frac{d^\alpha T(t)}{dt^\alpha}\right\} = p^\alpha \mathsf{L}\{T(t)\} - \frac{d^{\alpha-1}T(t)}{dt^{\alpha-1}}\bigg|_{t=0} = p^\alpha \mathsf{L}\{T(t)\}$$ (B.12)

and by introducing for initial conditions of fractional derivatives in the form (B.3), and after taking Laplace's transform of the equation (B.1), we obtain a corresponding equation. *By analyzing previous Laplace transform (B.12) of solution we can conclude that we can consider two cases.*

For the case when $\omega_0^2 \neq 0$, the Laplace transform solution can be developed into series by following way:

(B.13)

$$\mathsf{L}\{T(t)\} = \frac{pT_0 + \dot{T}_0}{p^2\left[1 + \frac{\omega_\alpha^2}{p^2}\left(\pm p^\alpha + \frac{\omega_0^2}{\omega_\alpha^2}\right)\right]} = \left(T_0 + \frac{\dot{T}_0}{p}\right)\frac{1}{p}\frac{1}{1 + \frac{\omega_\alpha^2}{p^2}\left(\pm p^\alpha + \frac{\omega_0^2}{\omega_\alpha^2}\right)}$$

$$\mathsf{L}\{T(t)\} = \left(T_0 + \frac{\dot{T}_0}{p}\right)\frac{1}{p}\sum_{k=0}^{\infty}\frac{(-1)^k\omega_\alpha^{2k}}{p^{2k}}\left(\pm p^\alpha + \frac{\omega_0^2}{\omega_\alpha^2}\right)^k$$ (B.14)

$$\mathsf{L}\{T(t)\} = \left(T_0 + \frac{\dot{T}_0}{p}\right)\frac{1}{p}\sum_{k=0}^{\infty}\frac{(-1)^k\omega_\alpha^{2k}}{p^{2k}}\sum_{j=0}^{k}\binom{k}{j}\frac{(\mp 1)^j p^{\alpha j}\omega_\alpha^{2(j-k)}}{\omega_o^{2j}}$$ (B.15)

In writing (B.15) it is assumed that expansion leads to convergent series. The inverse Laplace transform of previous Laplace transform of solution (B.15) in term-by-term steps is based on known theorem, and yield the following solution of differential equation (B.1) of time function in the following form of time series:

$$T(t) = \mathsf{L}^{-1}\mathsf{L}\{T(t)\}$$

$$T(t) = T_0\sum_{k=0}^{\infty}(-1)^k\omega_\alpha^{2k}t^{2k}\sum_{j=0}^{k}\binom{k}{j}\frac{(\mp 1)^j\omega_\alpha^{2j}t^{-\alpha j}}{\omega_o^{2j}\Gamma(2k+1-\alpha j)} + \dot{T}_0\sum_{k=0}^{\infty}(-1)^k\omega_\alpha^{2k}t^{2k+1}\sum_{j=0}^{k}\binom{k}{j}\frac{(\mp 1)^j\omega_\alpha^{-2j}t^{-\alpha j}}{\omega_o^{2j}\Gamma(2k+2-\alpha j)}$$

(B.16)

TANGENT SPACES OF POSITION VECTORS AND ANGULAR VELOCITIES OF THEIR BASIC VECTORS IN DIFFERENT COORDINATE SYSTEMS

Katica R. (Stevanović) Hedrih

Institute Mathematical Institute SANU Belgrade, Department for Mechanics
11 000-Belgrade, ul. Knez Mihailova 36/III
and Faculty of Mechanical Engineering, University of Niš.
Priv. address: 18000-Niš, ul. Vojvode Tankosića 3/22, Serbia, e-mail:
khedrih@eunet.rs

ABSTRACT. *Angular velocities of the basic vectors of tangent spaces of the position vectors of mass particles of the discrete rheonomic mechanical system are obtained in different coordinate systems. Starting from real three dimensional coordinate systems of Descartes orthogonal three dimensional system type with fixed coordinates axis as a reference, by different coordinate transformations for each position vector of corresponding mass particle in discrete rheonomic mechanical system, basic vectors of position vector tangent three dimensional spaces are obtained in different curvilinear coordinate systems suitable to the corresponding geometrical scleronomic or rheonomic constraints applied to the considered rheonomic system. For each basic vector of the basic triedar of position vector tangent space of each mass particle of the discrete rheonomic mechanical system, angular velocity vectors of basic vector rotations are determined.*

Then, after consideration and analysis of the number and properties of the geometrical scleronomic and rheonomic constraints applied to the mass particles of the considered discrete rheonomic mechanical system, number of system degree of mobility as well as number of system degree of freedom are determined. Corresponding number of independent coordinates are chosen and corresponding rheonomic coordinates are introduced. By use extended set of the generalized coordinates contained corresponding number of independent coordinates and corresponding number of rheonomic coordinates, position vectors of the mass particles of the discrete rheonomic mechanical system, are separated into two subsets.

First subset contain position vectors of the mass particle, keep their three dimensional tangent space each with three basic vectors.

Second subset contain position vectors of the mass particle, each depending, in general case, of the all generalized coordinates, independent and rheonomic. Then, each of the position vectors are with p-dimensional tangent spaces and with p basic vectors.

Keywords: *Position vectors, tangent space, basic vectors, angular velocity, rheonomic constraint, mobility, velocity of basic vector extension, p-dimensional tangent spaces.*

1. Introduction

Let consider a discrete system with N mass particles wirh mass m_α, and with corresponsing position in real three dimensional space determined by geometrical point $N_{(\alpha)}, \alpha = 1,2,3,...,N$ (see Figure 1). For begining we take that positions of the material points, as well as corresponding geometrical points coordinates are determined by coordinates in fixed orthogonal Descartes coordinate system with three coordinates as denoted by $N_{(\alpha)}\left(x_{(\alpha)}, y_{(\alpha)}, z_{(\alpha)}\right). \alpha = 1,2,3,...,N$, where O is fixed coordinate origin, and Ox, Oy and Oz fixed oriented coordinate strain lines-coordinate axes. Coordinates of the position vector of each material point are equal to coordinate of the geometrical point which determine mass particle position in the space. For Descartes coordinate system for position of the each mass particle we can write:
$\vec{\rho}_{(\alpha)}\left(x_{(\alpha)}, y_{(\alpha)}, z_{(\alpha)}\right) = x_{(\alpha)}\vec{i} + y_{(\alpha)}\vec{j} + z_{(\alpha)}\vec{k}$, $\alpha = 1,2,3,...,N$.

Let, now, to consider previus discrete system with N mass particles wirh mass m_α, and with corresponsing position in real three dimensional space determined by same geometrical points $N_{(\alpha)}, \alpha = 1,2,3,...,N$ in generalized coordinate system of curvilinear coordinates $\left(q_{(\alpha)}^1, q_{(\alpha)}^2, q_{(\alpha)}^3\right)$ $\alpha = 1,2,3,...,N$ corresponding to mass particle positions. For same geometrical points coordinates in considered two coordinate systems are: $N_{(\alpha)}\left(x_{(\alpha)}, y_{(\alpha)}, z_{(\alpha)}\right). \alpha = 1,2,3,...,N$ and $N_{(\alpha)}\left(q_{(\alpha)}^1, q_{(\alpha)}^2, q_{(\alpha)}^3\right)$ $\alpha = 1,2,3,...,N$ .. Formule of coordinate transformation from previous coordinate system with fixed axes and ne curvilinear coordinate system are:

$$
\begin{aligned}
x_{(\alpha)} &= x_{(\alpha)}\left(q_{(\alpha)}^1, q_{(\alpha)}^2, q_{(\alpha)}^3\right) \\
y_{(\alpha)} &= y_{(\alpha)}\left(q_{(\alpha)}^1, q_{(\alpha)}^2, q_{(\alpha)}^3\right) \\
z_{(\alpha)} &= z_{(\alpha)}\left(q_{(\alpha)}^1, q_{(\alpha)}^2, q_{(\alpha)}^3\right)
\end{aligned}
\tag{1}
$$

Position vectors of each mass particle and corresponding geometrical points are invariant geometrical objects in both coordinate systems, but their coordinates in considered coordinate systems are not equal to coordinates of the corresponding geometrical point. In generalized coordinate system geometrical points $N_{(\alpha)}, \alpha = 1,2,3,...,N$ have following coordinates: $\left(q_{(\alpha)}^1, q_{(\alpha)}^2, q_{(\alpha)}^3\right)$ $\alpha = 1,2,3,...,N$ and

coordinate   of   position   vectors   of   these   geometrical   points   are
$\left(\rho_{(\alpha)}{}^1, \rho_{(\alpha)}{}^2, \rho_{(\alpha)}{}^3\right), \alpha = 1,2,3,...,N$. For position vectors we can write:

$$\vec{\rho}_{(\alpha)}\left(x_{(\alpha)}, y_{(\alpha)}, z_{(\alpha)}\right) = x_{(\alpha)}\vec{i} + y_{(\alpha)}\vec{j} + z_{(\alpha)}\vec{k} \overset{def = inv.vektor}{=} \vec{\rho}_{(\alpha)}\left(q_{(\alpha)}{}^1, q_{(\alpha)}{}^2, q_{(\alpha)}{}^3\right) \qquad (2)$$

$$\vec{\rho}_{(\alpha)}\left(q_{(\alpha)}{}^1, q_{(\alpha)}{}^2, q_{(\alpha)}{}^3\right) = \rho_{(\alpha)}{}^1\left(q_{(\alpha)}{}^1, q_{(\alpha)}{}^2, q_{(\alpha)}{}^3\right)\vec{g}_{(\alpha)1} + \rho_{(\alpha)}{}^2\left(q_{(\alpha)}{}^1, q_{(\alpha)}{}^2, q_{(\alpha)}{}^3\right)\vec{g}_{(\alpha)2} + \rho_{(\alpha)}{}^3\left(q_{(\alpha)}{}^1, q_{(\alpha)}{}^2, q_{(\alpha)}{}^3\right)\vec{g}_{(\alpha)3}$$
$$\alpha = 1,2,3,...,N$$
(3)

For first example in polar-cylindrical coordinate system geometrical points have
the following coordinates: $N_{(\alpha)}\left(r_{(\alpha)}, \varphi_{(\alpha)}, z_{(\alpha)}\right)$ $\alpha = 1,2,3,...,N$ and position vectors
$\vec{\rho}_{(\alpha)}\left(r_{(\alpha)}, \varphi_{(\alpha)}, z_{(\alpha)}\right)$ of corresponding geometrical point are: $r_{(\alpha)}, 0, z_{(\alpha)}$ and we can write:

$$\vec{\rho}_{(\alpha)}\left(r_{(\alpha)}, \varphi_{(\alpha)}, z_{(\alpha)}\right) = r_{(\alpha)}\vec{r}_{o(\alpha)} + 0 \cdot \vec{c}_{0(\alpha)} + z_{(\alpha)}\vec{k} \equiv r_{(\alpha)}\vec{r}_{o(\alpha)} + z_{(\alpha)}\vec{k} \qquad (4)$$
$$\alpha = 1,2,3,...,N$$

where $\vec{r}_{o(\alpha)}, \vec{c}_{0(\alpha)}$ and $\vec{k}, \alpha = 1,2,3,...,N$ are basic unit vectors of tangent space of
corresponding position vector in polar-cylindrical coordinate system.

For second example in spherical coordinate system geometrical points have the
following coordinates: $N_{(\alpha)}\left(\rho_{(\alpha)}, \varphi_{(\alpha)}, \vartheta_{(\alpha)}\right)$ $\alpha = 1,2,3,...,N$ and position vectors
$\vec{\rho}_{(\alpha)}\left(\rho_{(\alpha)}, \varphi_{(\alpha)}, \vartheta_{(\alpha)}\right)$ of corresponding geometrical point are: $\rho_{(\alpha)}, 0, 0$ and we can write:

$$\vec{\rho}_{(\alpha)}\left(\rho_{(\alpha)}, \varphi_{(\alpha)}, \vartheta_{(\alpha)}\right) = \rho_{(\alpha)}\vec{\rho}_{0(\alpha)} + 0 \cdot \vec{c}_{0(\alpha)} + 0 \cdot \vec{v}_{0(\alpha)} \equiv \rho_{(\alpha)}\vec{\rho}_{0(\alpha)} \qquad (5)$$
$$\alpha = 1,2,3,...,N$$

where $\vec{\rho}_{0(\alpha)}, \vec{c}_{0(\alpha)}$ and $\vec{v}_{0(\alpha)}, \alpha = 1,2,3,...,N$ are basic unit vectors of tangent space of
corresponding position vector in polar-cylindrical coordinate system.
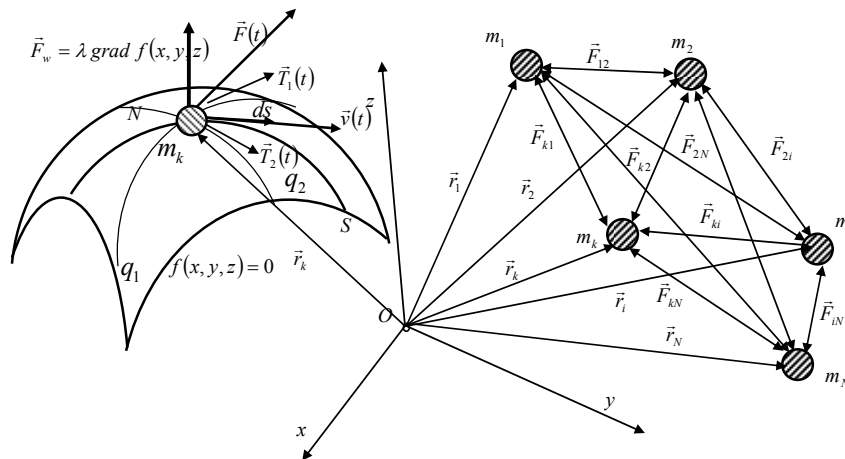
Figure 1. Discrete material system with N mass particles and gepmetrical
rheonomic constraints

2. Basic vectors of the position vector three-dimensional tangent space in generalized curvilinear coordinate systems

In real two-dimensional coordinate systems, position vector tangent spaces are tro-dimensional and the basic vectors of the tangent spaces of each position vector of each mass particle we denote with $\vec{g}_{(\alpha)i}$, $\alpha = 1,2,3,...,N$, $i = 1,2,3$ (see Figure 2). These vectors are in tangent directions to the corresponding curvilinear coordinate line and I general are not unit vectors. Basic vectors is possible to obtain by following way (for detail see Refs. [2], [3] and [4]):

$$\vec{g}_{(\alpha)i} = \frac{\partial \vec{\rho}_{(\alpha)}}{\partial q_{(\alpha)}^i}, \quad \alpha = 1,2,3,...,N, \quad i = 1,2,3 \tag{6}$$

or by formula coordinate transformation and by following expressions:

$$\vec{g}_{(\alpha)1} = \frac{\partial \vec{\rho}_{(\alpha)}}{\partial q_{(\alpha)}^1} = \frac{\partial x_{(\alpha)}\left(q_{(\alpha)}^1, q_{(\alpha)}^2, q_{(\alpha)}^3\right)}{\partial q_{(\alpha)}^1}\vec{i} + \frac{\partial y_{(\alpha)}\left(q_{(\alpha)}^1, q_{(\alpha)}^2, q_{(\alpha)}^3\right)}{\partial q_{(\alpha)}^1}\vec{j} + \frac{\partial z_{(\alpha)}\left(q_{(\alpha)}^1, q_{(\alpha)}^2, q_{(\alpha)}^3\right)}{\partial q_{(\alpha)}^1}\vec{k}$$

$$\vec{g}_{(\alpha)2} = \frac{\partial \vec{\rho}_{(\alpha)}}{\partial q_{(\alpha)}^2} = \frac{\partial x_{(\alpha)}\left(q_{(\alpha)}^1, q_{(\alpha)}^2, q_{(\alpha)}^3\right)}{\partial q_{(\alpha)}^2}\vec{i} + \frac{\partial y_{(\alpha)}\left(q_{(\alpha)}^1, q_{(\alpha)}^2, q_{(\alpha)}^3\right)}{\partial q_{(\alpha)}^2}\vec{j} + \frac{\partial z_{(\alpha)}\left(q_{(\alpha)}^1, q_{(\alpha)}^2, q_{(\alpha)}^3\right)}{\partial q_{(\alpha)}^2}\vec{k} \tag{7}$$

$$\vec{g}_{(\alpha)3} = \frac{\partial \vec{\rho}_{(\alpha)}}{\partial q_{(\alpha)}^3} = \frac{\partial x_{(\alpha)}\left(q_{(\alpha)}^1, q_{(\alpha)}^2, q_{(\alpha)}^3\right)}{\partial q_{(\alpha)}^3}\vec{i} + \frac{\partial y_{(\alpha)}\left(q_{(\alpha)}^1, q_{(\alpha)}^2, q_{(\alpha)}^3\right)}{\partial q_{(\alpha)}^3}\vec{j} + \frac{\partial z_{(\alpha)}\left(q_{(\alpha)}^1, q_{(\alpha)}^2, q_{(\alpha)}^3\right)}{\partial q_{(\alpha)}^3}\vec{k}$$

Contravariant coordinates of the position vectors is possible to obtain by following formulas:

$$\rho_{(\alpha)}^1\left(q_{(\alpha)}^1, q_{(\alpha)}^2, q_{(\alpha)}^3\right) = \frac{1}{\Delta}\left[\frac{\partial y_{(\alpha)}\left(q_{(\alpha)}^1, q_{(\alpha)}^2, q_{(\alpha)}^3\right)}{\partial q_{(\alpha)}^2}\frac{\partial z_{(\alpha)}\left(q_{(\alpha)}^1, q_{(\alpha)}^2, q_{(\alpha)}^3\right)}{\partial q_{(\alpha)}^3} - \frac{\partial y_{(\alpha)}\left(q_{(\alpha)}^1, q_{(\alpha)}^2, q_{(\alpha)}^3\right)}{\partial q_{(\alpha)}^3}\frac{\partial z_{(\alpha)}\left(q_{(\alpha)}^1, q_{(\alpha)}^2, q_{(\alpha)}^3\right)}{\partial q_{(\alpha)}^2}\right]x_{(\alpha)}\left(q_{(\alpha)}^1, q_{(\alpha)}^2, q_{(\alpha)}^3\right) -$$

$$- \frac{1}{\Delta}\left[\frac{\partial x_{(\alpha)}\left(q_{(\alpha)}^1, q_{(\alpha)}^2, q_{(\alpha)}^3\right)}{\partial q_{(\alpha)}^2}\frac{\partial z_{(\alpha)}\left(q_{(\alpha)}^1, q_{(\alpha)}^2, q_{(\alpha)}^3\right)}{\partial q_{(\alpha)}^3} - \frac{\partial x_{(\alpha)}\left(q_{(\alpha)}^1, q_{(\alpha)}^2, q_{(\alpha)}^3\right)}{\partial q_{(\alpha)}^3}\frac{\partial z_{(\alpha)}\left(q_{(\alpha)}^1, q_{(\alpha)}^2, q_{(\alpha)}^3\right)}{\partial q_{(\alpha)}^2}\right]y_{(\alpha)}\left(q_{(\alpha)}^1, q_{(\alpha)}^2, q_{(\alpha)}^3\right) -$$

$$- \frac{1}{\Delta}\left[\frac{\partial x_{(\alpha)}\left(q_{(\alpha)}^1, q_{(\alpha)}^2, q_{(\alpha)}^3\right)}{\partial q_{(\alpha)}^2}\frac{\partial y_{(\alpha)}\left(q_{(\alpha)}^1, q_{(\alpha)}^2, q_{(\alpha)}^3\right)}{\partial q_{(\alpha)}^3} - \frac{\partial x_{(\alpha)}\left(q_{(\alpha)}^1, q_{(\alpha)}^2, q_{(\alpha)}^3\right)}{\partial q_{(\alpha)}^3}\frac{\partial y_{(\alpha)}\left(q_{(\alpha)}^1, q_{(\alpha)}^2, q_{(\alpha)}^3\right)}{\partial q_{(\alpha)}^2}\right]z_{(\alpha)}\left(q_{(\alpha)}^1, q_{(\alpha)}^2, q_{(\alpha)}^3\right)$$

$$\rho_{(\alpha)}^2\left(q_{(\alpha)}^1, q_{(\alpha)}^2, q_{(\alpha)}^3\right) = -\frac{1}{\Delta}\left[\frac{\partial y_{(\alpha)}\left(q_{(\alpha)}^1, q_{(\alpha)}^2, q_{(\alpha)}^3\right)}{\partial q_{(\alpha)}^1}\frac{\partial z_{(\alpha)}\left(q_{(\alpha)}^1, q_{(\alpha)}^2, q_{(\alpha)}^3\right)}{\partial q_{(\alpha)}^3} - \frac{\partial y_{(\alpha)}\left(q_{(\alpha)}^1, q_{(\alpha)}^2, q_{(\alpha)}^3\right)}{\partial q_{(\alpha)}^3}\frac{\partial z_{(\alpha)}\left(q_{(\alpha)}^1, q_{(\alpha)}^2, q_{(\alpha)}^3\right)}{\partial q_{(\alpha)}^1}\right]x_{(\alpha)}\left(q_{(\alpha)}^1, q_{(\alpha)}^2, q_{(\alpha)}^3\right) +$$

$$+ \frac{1}{\Delta}\left[\frac{\partial x_{(\alpha)}\left(q_{(\alpha)}^1, q_{(\alpha)}^2, q_{(\alpha)}^3\right)}{\partial q_{(\alpha)}^1}\frac{\partial z_{(\alpha)}\left(q_{(\alpha)}^1, q_{(\alpha)}^2, q_{(\alpha)}^3\right)}{\partial q_{(\alpha)}^3} - \frac{\partial x_{(\alpha)}\left(q_{(\alpha)}^1, q_{(\alpha)}^2, q_{(\alpha)}^3\right)}{\partial q_{(\alpha)}^3}\frac{\partial z_{(\alpha)}\left(q_{(\alpha)}^1, q_{(\alpha)}^2, q_{(\alpha)}^3\right)}{\partial q_{(\alpha)}^1}\right]y_{(\alpha)}\left(q_{(\alpha)}^1, q_{(\alpha)}^2, q_{(\alpha)}^3\right) -$$

$$- \frac{1}{\Delta}\left[\frac{\partial x_{(\alpha)}\left(q_{(\alpha)}^1, q_{(\alpha)}^2, q_{(\alpha)}^3\right)}{\partial q_{(\alpha)}^1}\frac{\partial y_{(\alpha)}\left(q_{(\alpha)}^1, q_{(\alpha)}^2, q_{(\alpha)}^3\right)}{\partial q_{(\alpha)}^3} - \frac{\partial x_{(\alpha)}\left(q_{(\alpha)}^1, q_{(\alpha)}^2, q_{(\alpha)}^3\right)}{\partial q_{(\alpha)}^3}\frac{\partial y_{(\alpha)}\left(q_{(\alpha)}^1, q_{(\alpha)}^2, q_{(\alpha)}^3\right)}{\partial q_{(\alpha)}^1}\right]z_{(\alpha)}\left(q_{(\alpha)}^1, q_{(\alpha)}^2, q_{(\alpha)}^3\right)$$

$$\rho_{(\alpha)}^3\left(q_{(\alpha)}^1, q_{(\alpha)}^2, q_{(\alpha)}^3\right) = \frac{1}{\Delta}\left[\frac{\partial y_{(\alpha)}\left(q_{(\alpha)}^1, q_{(\alpha)}^2, q_{(\alpha)}^3\right)}{\partial q_{(\alpha)}^1}\frac{\partial z_{(\alpha)}\left(q_{(\alpha)}^1, q_{(\alpha)}^2, q_{(\alpha)}^3\right)}{\partial q_{(\alpha)}^2} - \frac{\partial y_{(\alpha)}\left(q_{(\alpha)}^1, q_{(\alpha)}^2, q_{(\alpha)}^3\right)}{\partial q_{(\alpha)}^2}\frac{\partial z_{(\alpha)}\left(q_{(\alpha)}^1, q_{(\alpha)}^2, q_{(\alpha)}^3\right)}{\partial q_{(\alpha)}^1}\right]x_{(\alpha)}\left(q_{(\alpha)}^1, q_{(\alpha)}^2, q_{(\alpha)}^3\right) -$$

$$- \frac{1}{\Delta}\left[\frac{\partial x_{(\alpha)}\left(q_{(\alpha)}^1, q_{(\alpha)}^2, q_{(\alpha)}^3\right)}{\partial q_{(\alpha)}^1}\frac{\partial z_{(\alpha)}\left(q_{(\alpha)}^1, q_{(\alpha)}^2, q_{(\alpha)}^3\right)}{\partial q_{(\alpha)}^2} - \frac{\partial x_{(\alpha)}\left(q_{(\alpha)}^1, q_{(\alpha)}^2, q_{(\alpha)}^3\right)}{\partial q_{(\alpha)}^2}\frac{\partial z_{(\alpha)}\left(q_{(\alpha)}^1, q_{(\alpha)}^2, q_{(\alpha)}^3\right)}{\partial q_{(\alpha)}^1}\right]y_{(\alpha)}\left(q_{(\alpha)}^1, q_{(\alpha)}^2, q_{(\alpha)}^3\right) +$$

$$+ \frac{1}{\Delta}\left[\frac{\partial x_{(\alpha)}\left(q_{(\alpha)}^1, q_{(\alpha)}^2, q_{(\alpha)}^3\right)}{\partial q_{(\alpha)}^1}\frac{\partial y_{(\alpha)}\left(q_{(\alpha)}^1, q_{(\alpha)}^2, q_{(\alpha)}^3\right)}{\partial q_{(\alpha)}^2} - \frac{\partial x_{(\alpha)}\left(q_{(\alpha)}^1, q_{(\alpha)}^2, q_{(\alpha)}^3\right)}{\partial q_{(\alpha)}^2}\frac{\partial y_{(\alpha)}\left(q_{(\alpha)}^1, q_{(\alpha)}^2, q_{(\alpha)}^3\right)}{\partial q_{(\alpha)}^1}\right]z_{(\alpha)}\left(q_{(\alpha)}^1, q_{(\alpha)}^2, q_{(\alpha)}^3\right)$$

where

$$\Delta_{(\alpha)} = \begin{vmatrix} \dfrac{\partial x_{(\alpha)}\left(q_{(\alpha)}{}^1,q_{(\alpha)}{}^2,q_{(\alpha)}{}^3\right)}{\partial q^1} & \dfrac{\partial y_{(\alpha)}\left(q_{(\alpha)}{}^1,q_{(\alpha)}{}^2,q_{(\alpha)}{}^3\right)}{\partial q^1} & \dfrac{\partial z_{(\alpha)}\left(q_{(\alpha)}{}^1,q_{(\alpha)}{}^2,q_{(\alpha)}{}^3\right)}{\partial q^1} \\[2ex] \dfrac{\partial x_{(\alpha)}\left(q_{(\alpha)}{}^1,q_{(\alpha)}{}^2,q_{(\alpha)}{}^3\right)}{\partial q^2} & \dfrac{\partial y_{(\alpha)}\left(q_{(\alpha)}{}^1,q_{(\alpha)}{}^2,q_{(\alpha)}{}^3\right)}{\partial q^2} & \dfrac{\partial z_{(\alpha)}\left(q_{(\alpha)}{}^1,q_{(\alpha)}{}^2,q_{(\alpha)}{}^3\right)}{\partial q^2} \\[2ex] \dfrac{\partial x_{(\alpha)}\left(q_{(\alpha)}{}^1,q_{(\alpha)}{}^2,q_{(\alpha)}{}^3\right)}{\partial q^3} & \dfrac{\partial y_{(\alpha)}\left(q_{(\alpha)}{}^1,q_{(\alpha)}{}^2,q_{(\alpha)}{}^3\right)}{\partial q^3} & \dfrac{\partial z_{(\alpha)}\left(q_{(\alpha)}{}^1,q_{(\alpha)}{}^2,q_{(\alpha)}{}^3\right)}{\partial q^3} \end{vmatrix} \neq 0$$

$$N\left(q^1(t),q^2(t),q^3(t)\right) \qquad \vec{\rho}\left(q^1,q^2,q^3\right)$$

$$\vec{\rho}\left(q^1(t),q^2(t),q^3(t)\right) = \rho^1\vec{g}_1 + \rho^2\vec{g}_2 + \rho^3\vec{g}_3$$

$$\vec{g}_1 = \frac{\partial\vec{\rho}}{\partial q^1}$$

$$\vec{g}_2 = \frac{\partial\vec{\rho}}{\partial q^2}$$

$$\vec{g}_3 = \frac{\partial\vec{\rho}}{\partial q^3}$$

$$\omega_p = \omega_p\left(q^1(t),q^2(t),q^3(t),\dot{q}^1(t),\dot{q}^2(t),\dot{q}^3(t)\right)$$
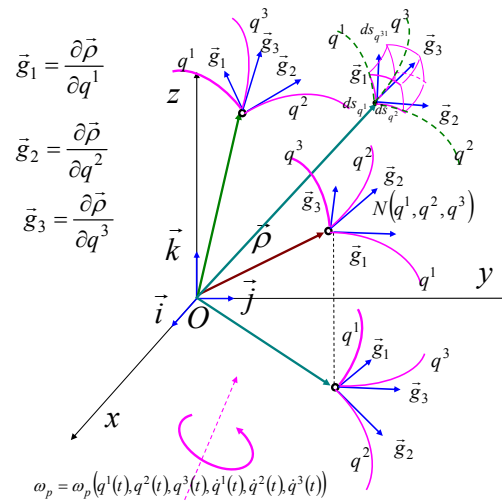
Figure 2. A position vectors and its three-dimensional space with corresponding curvilinear coordinate system and tangent space with corresponding three basic vectors of the position vector tangent spaces along mass particle motion through time

3. Change of the basic vectors of the position vector three-dimensional tangent space in generalized curvilinear coordinate systems

Without loosing generality, we consider change of basic vectors of the a position vector of one mass particle during mass particle motion through real space and described in three-dimensional space. Also we focused our attention to the orthogonal curvilinear coordinate system. For that case change (first derivative) with time of the basic vectors of tangent space of a position vector are:

$$\frac{d\vec{g}_1}{dt} = \overset{*}{\vec{g}}_1 + \left[\vec{\omega}_{p1},\vec{g}_1\right] = \vec{g}_1\left(\Gamma_{11}^1\dot{q}^1 + \Gamma_{12}^1\dot{q}^2 + \Gamma_{13}^1\dot{q}^3\right) + \vec{g}_2\left(\Gamma_{11}^2\dot{q}^1 + \Gamma_{12}^2\dot{q}^2 + \Gamma_{13}^2\dot{q}^3\right) + \vec{g}_3\left(\Gamma_{11}^3\dot{q}^1 + \Gamma_{12}^3\dot{q}^2 + \Gamma_{13}^3\dot{q}^3\right)$$

$$\frac{d\vec{g}_2}{dt} = \overset{*}{\vec{g}}_2 + \left[\vec{\omega}_{p2},\vec{g}_2\right] = \left(\Gamma_{21}^1\vec{g}_1 + \Gamma_{21}^2\vec{g}_2 + \Gamma_{21}^3\vec{g}_3\right)\dot{q}^1 + \left(\Gamma_{22}^1\vec{g}_1 + \Gamma_{22}^2\vec{g}_2 + \Gamma_{22}^3\vec{g}_3\right)\dot{q}^2 + \left(\Gamma_{23}^1\vec{g}_1 + \Gamma_{23}^2\vec{g}_2 + \Gamma_{23}^3\vec{g}_3\right)\dot{q}^3$$

$$\frac{d\vec{g}_3}{dt} = \overset{*}{\vec{g}}_3 + [\vec{\omega}_{p3}, \vec{g}_3] = \left(\Gamma_{31}^1\vec{g}_1 + \Gamma_{31}^2\vec{g}_2 + \Gamma_{31}^3\vec{g}_3\right)\dot{q}^1 + \left(\Gamma_{32}^1\vec{g}_1 + \Gamma_{32}^2\vec{g}_2 + \Gamma_{32}^3\vec{g}_3\right)\dot{q}^2 + \left(\Gamma_{33}^1\vec{g}_1 + \Gamma_{33}^2\vec{g}_2 + \Gamma_{33}^3\vec{g}_3\right)\dot{q}^3$$

(8)

After analysis of the obtained derivatives of the basic vectors of position vector tangent spaces in three-dimensional orthogonal curvilinear coordinate systems we can separate two sets of the terms in obtained expressions (8). First set correspond to the relative derivative of the corresponding basic vectors in the following forms:

$$\overset{*}{\vec{g}}_1 = \vec{g}_1\left(\Gamma_{11}^1\dot{q}^1 + \Gamma_{12}^1\dot{q}^2 + \Gamma_{13}^1\dot{q}^3\right)$$

$$\overset{*}{\vec{g}}_2 = \vec{g}_2\left(\Gamma_{21}^2\dot{q}^1 + \Gamma_{22}^2\dot{q}^2 + \Gamma_{23}^2\dot{q}^3\right) \qquad (9)$$

$$\overset{*}{\vec{g}}_3 = \vec{g}_3\left(\Gamma_{31}^3\dot{q}^1 + \Gamma_{32}^3\dot{q}^2 + \Gamma_{33}^3\dot{q}^3\right)$$

These vectors present vector forms of extensions of the corresponding basic vectors and in scalar form is possible to express relative change of the intensity – dilatation of the basic vectors in direction of its previous kinetic state. In differential form is possible to write:

$$d\varepsilon_1 = \frac{d|\vec{g}_1|}{|\vec{g}_1|} = \Gamma_{11}^1 dq^1 + \Gamma_{12}^1 dq^2 + \Gamma_{13}^1 dq^3$$

$$d\varepsilon_2 = \frac{d|\vec{g}_2|}{|\vec{g}_2|} = \Gamma_{31}^2 dq^1 + \Gamma_{32}^2 dq^2 + \Gamma_{33}^2 dq^3 \qquad (10)$$

$$d\varepsilon_3 = \frac{d|\vec{g}_{31}|}{|\vec{g}_3|} = \Gamma_{31}^3 dq^1 + \Gamma_{32}^3 dq^2 + \Gamma_{33}^3 dq^3$$

From analysis of the obtained derivatives of the basic vectors of position vector tangent spaces in three-dimensional orthogonal curvilinear coordinate systems we can separate second set of the terms in obtained expressions (8). Second set correspond to the rotation change of the corresponding basic vectors in the following forms:

$$[\vec{\omega}_{p1}, \vec{g}_1] = \vec{g}_2\left(\Gamma_{11}^2\dot{q}^1 + \Gamma_{12}^2\dot{q}^2 + \Gamma_{13}^2\dot{q}^3\right) + \vec{g}_3\left(\Gamma_{11}^3\dot{q}^1 + \Gamma_{12}^3\dot{q}^2 + \Gamma_{13}^3\dot{q}^3\right)$$

$$[\vec{\omega}_{p2}, \vec{g}_2] = \vec{g}_1\left(\Gamma_{21}^1\dot{q}^1 + \Gamma_{22}^1\dot{q}^2 + \Gamma_{23}^1\dot{q}^3\right) + \vec{g}_3\left(\Gamma_{21}^3\dot{q}^1 + \Gamma_{22}^3\dot{q}^2 + \Gamma_{23}^3\dot{q}^3\right) \quad (11)$$

$$[\vec{\omega}_{p3}, \vec{g}_3] = \vec{g}_1\left(\Gamma_{31}^1\dot{q}^1 + \Gamma_{32}^1\dot{q}^2 + \Gamma_{33}^1\dot{q}^3\right) + \vec{g}_2\left(\Gamma_{31}^2\dot{q}^1 + \Gamma_{32}^2\dot{q}^2 + \Gamma_{33}^2\dot{q}^3\right)$$

where we introduce notation $\vec{\omega}_{p1}$, $\vec{\omega}_{p2}$ and $\vec{\omega}_{p3}$ for vectors of the angular velocities of the corresponding basic vectors of the position vector tangent space. When curvilinear coordinate system is not orthogonal and angles between three basic vectors are changeable with time these angular velocities are different for each basic vector. When basic vectors are orthogonal and without change orthogonal relation, all three angular velocity are same.

For the case of the discrete mechanical system N mass particles for each vector position of each mass particle is necessary, by analogous way as presented in previous part, is possible to determine change of the basic vectors of tangent space of position vectors. For that case for first basic vector of each position vector tangent space, we can write:

$$\frac{d\vec{g}_{(\alpha)1}}{dt} = \vec{g}_{(\alpha)1}\left(\Gamma^1_{(\alpha)11}\dot{q}_{(\alpha)}^{\;1} + \Gamma^1_{(\alpha)12}\dot{q}_{(\alpha)}^{\;2} + \Gamma^1_{(\alpha)13}\dot{q}_{(\alpha)}^{\;3}\right) + \vec{g}_{(\alpha)2}\left(\Gamma^2_{(\alpha)11}\dot{q}_{(\alpha)}^{\;1} + \Gamma^2_{(\alpha)12}\dot{q}_{(\alpha)}^{\;2} + \Gamma^2_{(\alpha)13}\dot{q}_{(\alpha)}^{\;3}\right) +$$
$$+ \vec{g}_{(\alpha)3}\left(\Gamma^3_{(\alpha)11}\dot{q}_{(\alpha)}^{\;1} + \Gamma^3_{(\alpha)12}\dot{q}_{(\alpha)}^{\;2} + \Gamma^3_{(\alpha)13}\dot{q}_{(\alpha)}^{\;3}\right)$$

$$\alpha = 1,2,3,...,N \qquad\qquad (12)$$

After analysis of the obtained derivatives of the basic vectors of position vector tangent spaces for each mass particle, in three-dimensional orthogonal curvilinear coordinate systems, we can separate two sets of the terms in obtained expression (11) and corresponding for other two sets of the basic vectors. First set correspond to the relative derivative of the corresponding basic vectors in the following forms:

$$\overset{*}{\vec{g}}_{(\alpha)1} = \vec{g}_{(\alpha)1}\left(\Gamma^1_{(\alpha)11}\dot{q}_{(\alpha)}^{\;1} + \Gamma^1_{(\alpha)12}\dot{q}_{(\alpha)}^{\;2} + \Gamma^1_{(\alpha)13}\dot{q}_{(\alpha)}^{\;3}\right), \alpha = 1,2,3,...,N$$
$$\overset{*}{\vec{g}}_{(\alpha)2} = \vec{g}_{(\alpha)2}\left(\Gamma^2_{(\alpha)21}\dot{q}_{(\alpha)}^{\;1} + \Gamma^2_{(\alpha)22}\dot{q}_{(\alpha)}^{\;2} + \Gamma^2_{(\alpha)23}\dot{q}_{(\alpha)}^{\;3}\right), \alpha = 1,2,3,...,N \qquad (13)$$
$$\overset{*}{\vec{g}}_{(\alpha)3} = \vec{g}_{(\alpha)3}\left(\Gamma^3_{(\alpha)31}\dot{q}_{(\alpha)}^{\;1} + \Gamma^3_{(\alpha)32}\dot{q}_{(\alpha)}^{\;2} + \Gamma^3_{(\alpha)33}\dot{q}_{(\alpha)}^{\;3}\right), \alpha = 1,2,3,...,N$$

These vectors present vector forms of extensions of the corresponding basic vectors and in scalar form is possible to express relative changes of the intensities – dilatations of the basic vectors in direction of their previous kinetic state. In differential form is possible to write:

$$d\varepsilon_{(\alpha)1} = \frac{d\left|\vec{g}_{(\alpha)1}\right|}{\left|\vec{g}_{(\alpha)1}\right|} = \Gamma^1_{(\alpha)11}\dot{q}_{(\alpha)}^{\;1} + \Gamma^1_{(\alpha)12}\dot{q}_{(\alpha)}^{\;2} + \Gamma^1_{(\alpha)13}\dot{q}_{(\alpha)}^{\;3} \;, \alpha = 1,2,3,...,N$$

$$d\varepsilon_{(\alpha)2} = \frac{d\left|\vec{g}_{(\alpha)2}\right|}{\left|\vec{g}_{(\alpha)2}\right|} = \Gamma^2_{(\alpha)21}\dot{q}_{(\alpha)}^{\;1} + \Gamma^2_{(\alpha)22}\dot{q}_{(\alpha)}^{\;2} + \Gamma^2_{(\alpha)23}\dot{q}_{(\alpha)}^{\;3} \;, \alpha = 1,2,3,...,N \quad (14)$$

$$d\varepsilon_{(\alpha)3} = \frac{d\left|\vec{g}_{(\alpha)3}\right|}{\left|\vec{g}_{(\alpha)3}\right|} = \Gamma^3_{(\alpha)31}\dot{q}_{(\alpha)}^{\;1} + \Gamma^3_{(\alpha)32}\dot{q}_{(\alpha)}^{\;2} + \Gamma^3_{(\alpha)33}\dot{q}_{(\alpha)}^{\;3} \;, \alpha = 1,2,3,...,N$$

From analysis of the obtained derivatives of the basic vectors of position vector tangent spaces for each mass particle in three-dimensional orthogonal curvilinear coordinate systems, we can separate second sets of the terms in obtained expressions (8). Second set correspond to the rotation change of the corresponding basic vectors in the following forms:

$$\left[\vec{\omega}_{(\alpha)p1}, \vec{g}_{(\alpha)1}\right] = \vec{g}_{(\alpha)2}\left(\Gamma^2_{(\alpha)11}\dot{q}_{(\alpha)}^{\;1} + \Gamma^2_{(\alpha)12}\dot{q}_{(\alpha)}^{\;2} + \Gamma^2_{(\alpha)13}\dot{q}_{(\alpha)}^{\;3}\right) + \vec{g}_{(\alpha)3}\left(\Gamma^3_{(\alpha)11}\dot{q}_{(\alpha)}^{\;1} + \Gamma^3_{(\alpha)12}\dot{q}_{(\alpha)}^{\;2} + \Gamma^3_{(\alpha)13}\dot{q}_{(\alpha)}^{\;3}\right)$$

$$\left[\vec{\omega}_{(\alpha)p2}, \vec{g}_{(\alpha)2}\right] = \vec{g}_{(\alpha)1}\left(\Gamma^1_{(\alpha)21}\dot{q}_{(\alpha)}^{\;1} + \Gamma^1_{(\alpha)22}\dot{q}_{(\alpha)}^{\;2} + \Gamma^1_{(\alpha)23}\dot{q}_{(\alpha)}^{\;3}\right) + \vec{g}_{(\alpha)3}\left(\Gamma^3_{(\alpha)21}\dot{q}_{(\alpha)}^{\;1} + \Gamma^3_{(\alpha)22}\dot{q}_{(\alpha)}^{\;2} + \Gamma^3_{(\alpha)23}\dot{q}_{(\alpha)}^{\;3}\right)$$

$$\left[\vec{\omega}_{(\alpha)p3}, \vec{g}_{(\alpha)3}\right] = \vec{g}_{(\alpha)1}\left(\Gamma^1_{(\alpha)31}\dot{q}_{(\alpha)}^{\;1} + \Gamma^1_{(\alpha)32}\dot{q}^{\;2} + \Gamma^1_{(\alpha)33}\dot{q}_{(\alpha)}^{\;3}\right) + \vec{g}_{(\alpha)2}\left(\Gamma^2_{(\alpha)31}\dot{q}_{(\alpha)}^{\;1} + \Gamma^2_{(\alpha)32}\dot{q}_{(\alpha)}^{\;2} + \Gamma^2_{(\alpha)33}\dot{q}_{(\alpha)}^{\;3}\right)$$
$$\alpha = 1,2,3,...,N \qquad\qquad (15)$$

where we introduce notation $\vec{\omega}_{(\alpha)p1}$, $\vec{\omega}_{(\alpha)p2}$ and $\vec{\omega}_{(\alpha)p3}$ for vectors of the angular velocities of the corresponding basic vectors of the position vector tangent spaces. When basic

vectors are orthogonal and without change orthogonal relation, all three angular velocity are same.

For example 1*: in polar-cylindrical curvilinear coordinate system by expressions (8), (9), (10) and (11) we can write (see Figure 3.a*):

$$\frac{d\vec{g}_1}{dt} = \frac{d\vec{g}_r}{dt} = \dot{\varphi}\left(-\vec{i}\sin\varphi + \vec{j}\cos\varphi\right) = \frac{d\vec{r}_0}{dt} = \dot{\varphi}\vec{c}_0 = \frac{1}{r}\dot{\varphi}\vec{g}_\varphi = \left[\vec{\omega}_{\mathrm{Pr}}, \vec{g}_r\right]$$

$$\frac{d\vec{g}_2}{dt} = \frac{d\vec{g}_\varphi}{dt} = \dot{r}\vec{c}_0 + r\frac{d\vec{c}_0}{dt} = \dot{r}\vec{c}_0 - r\dot{\varphi}\,\vec{r}_0 = \overset{*}{\vec{g}}_\varphi + \left[\vec{\omega}_{P\varphi}, \vec{g}_\varphi\right]$$

$$\frac{d\vec{g}_3}{dt} = \frac{d\vec{g}_z}{dt} = \frac{d\vec{k}}{dt} = 0$$

$$\overset{*}{\vec{g}}_r = 0\,, \qquad\qquad d\varepsilon_r = \frac{d\left|\vec{g}_\varphi\right|}{\left|\vec{g}_\varphi\right|} = \frac{dr}{r}\,, \qquad\qquad \vec{\omega}_{\mathrm{Pr}} = \dot{\varphi}\vec{k}$$

$$\overset{*}{\vec{g}}_\varphi = \dot{r}\vec{c}_0 = \frac{\dot{r}}{r}\vec{g}_\varphi\,, \qquad \vec{\omega}_{P\varphi} = \dot{\varphi}\vec{k}\,, \qquad \overset{*}{\vec{g}}_z = 0\,, \qquad \vec{\omega}_{Pz} = 0$$

Angular velocities of the basic vectors of each position vector tangent space of mass particle motion in polar-cylindrical curvilinear coordinate systems are: $\vec{\omega}_{(\alpha)P} = \dot{\varphi}_{(\alpha)}\vec{k}$, $\alpha = 1,2,3,...,N$.
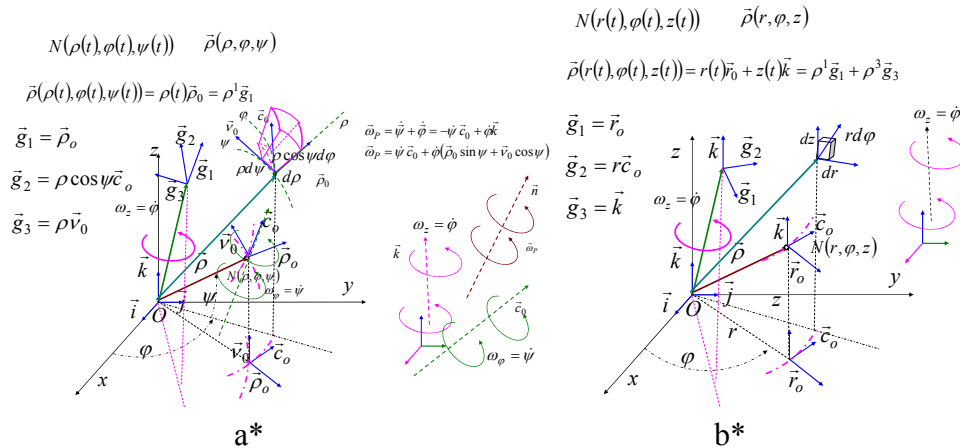
Figure 3. A position vectors and its three-dimensional spaces with corresponding curvilinear coordinate system and tangent space with corresponding three basic vectors of the position vector tangent spaces along mass particle motion through time
a* polar-cylindrical curvilinear coordinate system; b* spherical curvilinear coordinate system

For example 2*: in spherical curvilinear coordinate system by expressions (8), (9), (10) and (11), we can write (see Figure 3.b*):

$$\frac{d\vec{g}_1}{dt} = \frac{d\vec{g}_\rho}{dt} = \dot{\varphi}\vec{c}_0\cos\psi + \dot{\psi}\vec{v}_0 = \frac{1}{\rho}\dot{\varphi}\vec{g}_\varphi + \frac{1}{\rho}\dot{\psi}\vec{g}_\psi$$

$$\frac{d\vec{g}_2}{dt} = \frac{d\vec{g}_\varphi}{dt} = \vec{c}_0\left(\dot{\rho}\cos\psi - \rho\dot{\psi}\sin\psi\right) - \dot{\varphi}\left(\vec{\rho}_0\cos\psi - \vec{v}_0\sin\psi\right)\rho\cos\psi$$

$$\frac{d\vec{g}_3}{dt} = \frac{d\vec{g}_\psi}{dt} = \dot{\rho}\vec{v}_0 + \rho\left(-\dot{\varphi}\vec{c}_0\sin\psi - \dot{\psi}\vec{\rho}_0\right)$$

$$\overset{*}{\vec{\rho}}_\rho = 0 \ , \qquad \left[\vec{\omega}_{P\rho},\vec{\rho}_\rho\right] = \dot{\psi}\vec{v}_0 + \dot{\varphi}\vec{c}_0\cos\psi$$

$$\vec{\omega}_{P\rho} = \dot{\psi}\vec{c}_0 + \dot{\varphi}\vec{k} = -\frac{\dot{\psi}}{\rho\cos\psi}\vec{g}_\varphi + \dot{\varphi}\left(\vec{g}_\rho\sin\psi + \frac{1}{\rho}\vec{g}_\psi\cos\psi\right)$$

$$\overset{*}{\vec{g}}_\varphi = \vec{c}_0(\dot{\rho}\cos\psi - \rho\dot{\psi}\sin\psi) = \frac{1}{\rho\cos\psi}(\dot{\rho}\cos\psi - \rho\dot{\psi}\sin\psi)\vec{g}_\varphi$$

$$\left[\vec{\omega}_{P\varphi},\vec{g}_\varphi\right] = \left[-\dot{\psi}\vec{c}_0 + \dot{\varphi}(\vec{\rho}_0\sin\psi + \vec{v}_0\cos\psi),\vec{c}_0\rho\cos\psi\right] = -\dot{\varphi}(\vec{\rho}_0\cos\psi - \vec{v}_0\sin\psi)\rho\cos\psi$$

$$\vec{\omega}_{P\varphi} = -\dot{\vec{\psi}} + \dot{\vec{\varphi}} = \dot{\psi}\vec{c}_0 + \dot{\varphi}\vec{k} = -\frac{\dot{\psi}}{\rho\cos\psi}\vec{g}_\varphi + \dot{\varphi}\left(\vec{g}_\rho\sin\psi + \frac{1}{\rho}\vec{g}_\psi\cos\psi\right)$$

$$\frac{d\vec{g}_3}{dt} = \frac{d\vec{g}_\psi}{dt} = \dot{\rho}\vec{v}_0 + \rho\left(-\dot{\varphi}\vec{c}_0\sin\psi - \dot{\psi}\vec{\rho}_0\right)$$

$$\overset{*}{\vec{g}}_\psi = \dot{\rho}\vec{v}_0 = \frac{\dot{\rho}}{\rho}\vec{g}_\psi \ ,$$

$$\left[\vec{\omega}_{P\psi},\vec{g}_\psi\right] = -\dot{\varphi}\vec{g}_\varphi tg\,\psi - \dot{\psi}\vec{g}_\psi = \left[-\dot{\psi}\vec{c}_0 + \dot{\varphi}(\vec{\rho}_0\sin\psi + \vec{v}_0\cos\psi),\rho\vec{v}_0\right]$$

$$\vec{\omega}_{P\psi} = -\dot{\vec{\psi}} + \dot{\vec{\varphi}} = \dot{\psi}\vec{c}_0 + \dot{\varphi}\vec{k} = -\frac{\dot{\psi}}{\rho\cos\psi}\vec{g}_\varphi + \dot{\varphi}\left(\vec{g}_\rho\sin\psi + \frac{1}{\rho}\vec{g}_\psi\cos\psi\right)$$

Angular velocities of the basic vectors of each position vector tangent space of mass particle motion in spherical curvilinear coordinate systems are:

$$\vec{\omega}_{(\alpha)P} = -\dot{\vec{\psi}}_{(\alpha)} + \dot{\vec{\varphi}}_{(\alpha)} = \dot{\psi}_{(\alpha)}\vec{c}_{0(\alpha)} + \dot{\varphi}_{(\alpha)}\vec{k}$$
$$\vec{\omega}_{(\alpha)P} = -\dot{\psi}_{(\alpha)}\vec{c}_{0(\alpha)} + \dot{\varphi}_{(\alpha)}\left(\vec{\rho}_{0(\alpha)}\sin\psi_{(\alpha)} + \vec{v}_{0(\alpha)}\cos\psi_{(\alpha)}\right) \text{'}$$
$$\alpha = 1,2,3,...,N$$

4. Dimensional extension of the position vector tangent spaces of the reheonomic mechanical system in generalized curvilinear coordinate systems

Considered discrete mechanical system is constrained by G geometrical stationary constraints in the form:

$$f_\beta\left(q_{(1)}{}^1, q_{(1)}{}^2, q_{(1)}{}^3, q_{(2)}{}^1, q_{(2)}{}^2, q_{(2)}{}^3, ..., q_{(N)}{}^1, q_{(N)}{}^2, q_{(N)}{}^3\right) = 0 \ , \ \beta = 1,2,3....G$$

(16)

and by R geometrical rheonomic constraints in the form (see ref. [3]):

$$f_\gamma\left(q_{(1)}{}^1, q_{(1)}{}^2, q_{(1)}{}^3, q_{(2)}{}^1, q_{(2)}{}^2, q_{(2)}{}^3, ..., q_{(N)}{}^1, q_{(N)}{}^2, q_{(N)}{}^3, \phi_\gamma(t)\right) = 0 \ , \ \gamma = 1,2,3....R$$

(17)

Considered system is rheonomic system with $p = 3N - G$ degree of the system mobility, and with $n = 3N - G - R$ degrees of the freedom. For the n n generalized independent coordinates we take q^i , $i = 1,2,3,....,n$. Also we introduce additional subsystem of the R rheonomic coordinates $q^{0\gamma} = q^{n+\gamma} = \phi_\gamma(t)$, $\gamma = 1,2,3....R$ which correspond to number of

rheonomic constraints. Then we have extended system of the generalized curvilinear coordinates q^i, $i = 1,2,3,....,n,...,n+\gamma,......,n+R$. Then we know that subsystem of R rheonomic coordinates $q^{0\gamma} = q^{n+\gamma} = \phi_\gamma(t)$, $\gamma = 1,2,3....R$ contain known rheonomic coordinates as functions of the time. But, force of the rheonomic constraints change are unknown (see Ref. [1]).

Let now taking into account that first n coordinates of the position vectors of the mass particles are independent generalized coordinates. Extended system of the generalized coordinates containing independent coordinates q^i, $i = 1,2,3,....,n$ and rheonomic coordinates $q^{0\gamma} = q^{n+\gamma} = \phi_\gamma(t)$, $\gamma = 1,2,3....R$ is possible to list in the form:

$$q^1 = q_{(1)}{}^1,$$
$$q^2 = q_{(1)}{}^2,$$
$$q^3 = q_{(1)}{}^3,$$
$$q^4 = q_{(2)}{}^1,$$
$$q^5 = q_{(2)}{}^2,$$
$$q^6 = q_{(2)}{}^3,.$$
$$.......,$$
$$q^{n-2} = q_{(n)}{}^1,$$
$$q^{n-1} = q_{(n)}{}^2,$$
$$q^n = q_{(n)}{}^3$$

(18)

$$q^{0\gamma} = q^{n+\gamma} = \phi_\gamma(t), \gamma = 1,2,3....R \tag{19}$$

On the basic of the listed system (19) we can conclude that in considered case, we use coordinates of the positions vectors of the first $K \leq \dfrac{n}{3} = \dfrac{1}{3}(3N - G - R)$ mass particle as generalized independent coordinates.

Then on the basic of previous for the coordinates of the geometrical point which correspond to the mass particle positions at arbitrary moment of the motion, we can write:

$$N_1\left(q^1 = q_{(1)}{}^1, q^2 = q_{(1)}{}^2, q^3 = q_{(1)}{}^3\right),$$
$$N_2\left(q^4 = q_{(2)}{}^1, q^5 = q_{(2)}{}^2, q^6 = q_{(2)}{}^3\right),$$

(20)

$$............................,$$
$$N_K\left(q^{3K-2} = q_{(K)}{}^1, q^{3K-1} = q_{(K)}{}^2, q^{3K} = q_{(K)}{}^3\right)$$
$$N_{K+j}\left(q_{(K+j)}{}^1\left(q^1,q^2,.......q^n,q_{n+1},.........,q^{n+R}\right), q_{(K+j)}{}^2\left(q^1,q^2,.......q^n,q_{n+1},.........,q^{n+R}\right), q_{(K+j)}{}^3\left(q^1,q^2,.......q^n,q_{n+1},.........,q^{n+R}\right)\right)$$
$$j = 1,2,3,..., (N-K)$$

$$\vec{\rho}_1\left(q^1 = q_{(1)}{}^1, q^2 = q_{(1)}{}^2, q^3 = q_{(1)}{}^3\right),$$
$$\vec{\rho}_2\left(q^4 = q_{(2)}{}^1, q^5 = q_{(2)}{}^2, q^6 = q_{(2)}{}^3\right),$$
$$............................., \qquad\qquad (21)$$
$$\vec{\rho}_K\left(q^{3K-2} = q_{(K)}{}^1, q^{3K-1} = q_{(K)}{}^2, q^{3K} = q_{(K)}{}^3\right)$$
$$\vec{\rho}_{K+j}\left(q^1, q^2, ...q^n, q_{n+1}, ..., q^{n+R}\right), \quad j = 1,2,3,...,(N-K)$$

We cam see that in extended system of generalized coordinates we can identified two sets of the position vectors of the mass particles, one set contain the K, $K \leq \dfrac{n}{3} = \dfrac{1}{3}(3N - G - R)$ position vectors of the mass particles depending of three generalized coordinates, and second set contain the $N - K \geq \dfrac{G+R}{3}$, $K \leq \dfrac{n}{3} = \dfrac{1}{3}(3N - G - R)$ position vectors of the mass particles depending of all $p = 3N - G$ generalized coordinates in general case, or more then of three generalized coordinates.

Also we can conclude that in extended system of generalized coordinates, we can identified two sets of the position vectors of the mass particles, one set contain the K, $K \leq \dfrac{n}{3} = \dfrac{1}{3}(3N - G - R)$ position vectors of the mass particles with three-dimensional tangent space and each with three basic vectors of this tangent spaces, and second set contain the $N - K \geq \dfrac{G+R}{3}$, $K \leq \dfrac{n}{3} = \dfrac{1}{3}(3N - G - R)$ position vectors of the mass particles with extended dimension of the tangent space and to each tangent space correspond $p = 3N - G$ basic vectors in general case, or more then three basic vectors of the tangent space..

5. Concluding remarks

By introducing system of generalized independent coordinates, or extended system of generalized curvilinear coordinates depending of numbers of geometrical scleronomic and rheonmic constraints in the mathematical description of the discrete mechanical system motion we reduce total number of the system coordinate, but we introduce extension of the position vector tangent spaces fro three dimensional into more dimensional the three but maximal dimensional is equal to the total numbed of the coordinates accepted in extended system of the coordinates.

Also, we show that each position vector of the mass particle described by coordinates in curvilinear coordinate system have in tangent space basic vectors which rotate with angular velocity depending of the functional dependence position vector coordinates with respect to time.

First set of the basic vectors $\vec{g}_{(\alpha)i}$, $\alpha = 1,2,3,...,K \leq \dfrac{n}{3}$, $i = 1,2,3$ of the position

vectors of corresponding firs $K \leq \dfrac{n}{3} = \dfrac{1}{3}(3N - G - R)$ mass particles correspond to three-

dimensional tangent spaces, and are same as before coordinate restriction.

Second set of the basic vectors $\vec{g}_{(\alpha)j}$, $\alpha = K+1.K+2,......,N;$ $K > \dfrac{n}{3}$,

$j = 1,2,3,.....,n,.....,p$, of the $N - K$, $K \leq \dfrac{n}{3} = \dfrac{1}{3}(3N - G - R)$ position vectors of

corresponding second sets of the mass particles correspond to ($p = 3N - G$)--
dimensional tangent spaces, and are new in comparison with these obtained before
coordinate restriction. For position vectors from this second set, we can write
$$\vec{\rho}_{K+j}\left(q^1,q^2,.......q^n,q^{n+1},........,q^{n+R}\right), \quad j = 1,2,3,...,(N-K)$$
and for corresponding basic vectors of the tangent space
$$\vec{g}_{(\alpha)j} = \frac{\partial \vec{\rho}_{(\alpha)}}{\partial q^j}, \quad \alpha = K+1.K+2,......,N; \quad K > \frac{n}{3}, \quad j = 1,2,3,.....,n,.....,p,$$

Also, by use previous obtained results for angular velocity of the basic vectors of
position vector tangent space and corresponding vectors of the mass particle velocity and
acceleration on the generalized coordinate system is possible to analyze present Coriolis
force present in the mass particle motion in curvilinear coordinate system, Some
presentation for polar-cylindrical system and spherical system are presented in Figure 4. a*
and b*.
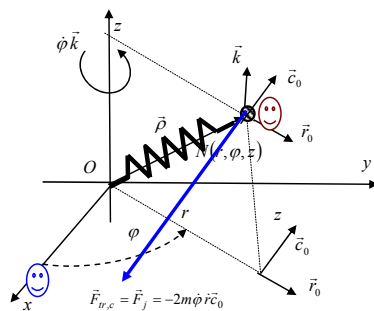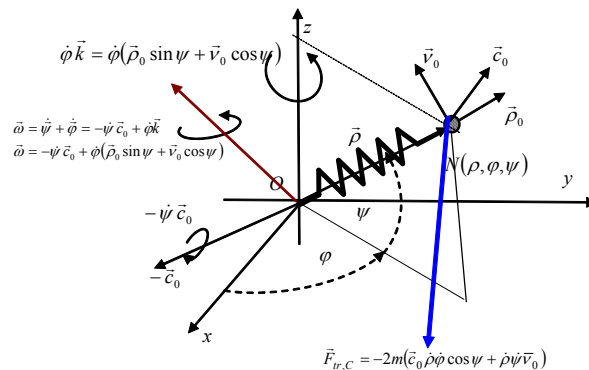
Figure 4. a*   Figure 4.b*

Figure 4.a* Description of the material particle mass m motion in the cylindrical polar
coordinate system by use coordinate transformation: Presentation of the Coriolis' inertia forces
$\vec{F}_{jcir} = \vec{F}_{tr,C} = -m\vec{a}_C = -2m[\vec{\omega}_p, \vec{v}_r] = -2m\dot{\varphi}\dot{r}\vec{c}_0$ induced by rotation motion of the cylindrical-polar
coordinate system in comparison with fixed – no moving reference Descartes's coordinate system:
relative motion of the material rarticle along radii $\vec{v}_{rel} = \vec{v}_r = \dot{r}\vec{r}_0$ and precession motion of the
coordinate system in the form of rotation motion with angular velocity $\vec{\omega} = \dot{\varphi}\vec{k}$.

Figure 4.b*. Description of the material particle mass m motion in the spherical coordinate system by use coordinate transformation. Presentation of the Coriolis' inertia forces $\vec{F}_{tr,Cp} = -2m\left(\vec{c}_0\dot{\rho}\dot{\varphi}\cos\psi + \dot{\rho}\dot{\psi}\vec{v}_0\right)$ induced by rotation motion of the spherical coordinate system in comparison with fixed – no moving reference Descartes's coordinate system: relative motion of the material particle along radii $\vec{v}_{rel} = \vec{v}_r = \dot{\rho}\vec{\rho}_0$ and precession motion of the coordinate system in the form of rotation motion with angular velocity $\vec{\omega} = -\dot{\vec{\psi}} + \dot{\vec{\varphi}} = \dot{\psi}\,\vec{c}_0 + \dot{\varphi}\vec{k} = -\dot{\psi}\,\vec{c}_0 + \dot{\varphi}\left(\vec{\rho}_0\sin\psi + \vec{v}_0\cos\psi\right)$.

References

[1] Hedrih (Stevanović), K., (1994), Snaga promene reonomnih veza, (The Power of the Rheonomic Constraints Change), Zbornik radova Jugoslovenskog društva za mehaniku, Simpozijum iz Opšte mehanike, Novi Sad, 1994, pp. 177-184.

[2] Hedrih (Stevanović) R. Katica , (2010), Visibility or appearance of nonlinearity, Tensor, N.S. Vol. 72, No. 1 (2010), pp. 14-33, #3. Tensor Society, Chigasaki, Japan, ISSN 0040-3504.

[3] Rašković P. Danilo, *Analitička mehanika*, Mašinski fakultet Kragujevac, 1974.

[4] Rašković P. Danilo, *Osnovi tenzorskog računa*, Mašinski fakultet Kragujevac, 1974.

ANALYSIS OF THE VECTOR ROTATORS OF A RIGID BODY NONLINEAR DYNAMICS ABOUT TWO AXES WITHOUT SECTION

Katica R. (Stevanović) Hedrih[1], Ljiljana Veljović[2]

[1] Mathematical Institute SANU Belgrade, Department for Mechanics
11 000-Belgrade, ul. Knez Mihailova 36/III, and Faculty of Mechanical Engineering, University of Niš. Priv. address: 18000-Niš, ul Vojvode Tankosića 3/22, Serbia, e-mail: khedrih@eunet.rs
[2] Faculty of Mechanical Engineering, University of Kragujevac, Serbia, 3400-Kragujevac, ul. Sestre Janic 6. e-mail: veljovicljilja@yahoo.co.uk

ABSTRACT. *Vector expressions, based on the mass moment vectors for axis and pole, introduced by Hedrih (Stevanović) K., for linear momentum and angular momentum of a heavy rigid body dynamics about two axes without section are derived, as well as their derivatives. In the vector expressions of the derivatives of linear momentum and angular momentum appear members with component vector multiplications in the form of pure by kinematical vectors named by us rotators. These vector rotators are orthogonal to the corresponding axis of rigid body coupled rotations and are functions of corresponding angular velocity and angular accelerations. Vector rotators rotate around corresponding axis with angular velocity different then component angular velocity of the rigid body component rotation in general case. In this paper a series of the research results according vector rotators are presented analytically and graphically. For the special case that heavy rigid disk is eccentrically and skew positioned on the self rotation axis which rotate in the horizontal plane around vertical axis with constant angular velocity on a distance, the nonlinear differential equation of the system dynamics in the gravitational field and corresponding equations of the phase trajectory as well as expressions of the kinematical vector rotators and expression of their relative angular velocity are expressed in the function of angular coordinate of disk self rotation. By use these derived expressions, series of graphical presentation of vector rotators and their properties transformation with changes of distance between axes, disk eccentricity and angle of skew disk position are presented.*

Keywords: *Rigid body, coupled rotation, axes without section, mass moment vectors, rotators, gravitational field, angular velocity, angular acceleration, graphical presentation.*

1. Mass moment vectors for the axis to the pole

The monograph [1], IUTAM extended abstract [3] and monograph paper [5] as well as series of the published papers [2], [4], [7] contain definitions of three mass moment vectors coupled to an axis passing through a certain point as a reference pole. The References [8]. [9] and [10] contain results of nonlinear dynamics of gyro-rotors which dynamics contain coupled rotations around two axes without intersections.

Now, we start with necessary definitions of mass momentum vectors.

Definitions of selected mass moment vectors for the axis and the pole, which are used in this paper are:

1* Vector $\vec{S}_{\vec{n}}^{(O)}$ of the body mass linear moment for the axis, oriented by the unit vector $\vec{n}$, through the point – pole O, in the form (see Figure 1):

$$\vec{S}_{\underline{n}}^{(O)} \overset{def}{=} \iiint\limits_{V} [\vec{n}, \vec{\rho}] dm = [\vec{n}, \vec{\rho}_C] M \;, \qquad dm = \sigma dV \;; \tag{1}$$

where $\vec{\rho}$ is the position vector of the elementary body mass particle dm in point N, between pole O and mass particle position N.

2* Vector $\vec{J}_{\underline{n}}^{(O)}$ of the body mass inertia moment for the axis, oriented by the unit vector $\vec{n}$, through the point – pole O, in the form:

$$\vec{J}_{\underline{n}}^{(O)} \overset{def}{=} \iiint\limits_{V} [\vec{\rho}, [\vec{n}, \vec{\rho}]] dm \tag{2}$$

For special cases, the details can be seen in [1-7]. In the previously cited references, the spherical and deviational parts of the mass inertia moment vector and the inertia tensor are analysed. In monograph [1] knowledge about the change (rate) in time and, the derivatives of the mass moment vectors of the body mass linear moment, the body mass inertia moment for the pole and a corresponding axis for different properties of the body, is shown, on the basis of results from the first author's Reference [1].
This expression

$$\vec{J}_{\underline{n}}^{(O)} = \vec{J}_{\underline{n}}^{(O_1)} + [\vec{\rho}_O, \vec{S}_{\underline{n}}^{(O_1)}] + [\vec{M}_C^{(O_1)}, [\vec{n}, \vec{\rho}_O]] + [\vec{\rho}_O, [\vec{n}, \vec{\rho}_O]] M \tag{3}$$

is **the vector form of the theorem** for the relation of material body mass inertia moment vectors, $\vec{J}_{\underline{n}}^{(O)}$ and $\vec{J}_{\underline{n}}^{(O_1)}$, for two parallel axes through two corresponding points, pole O and pole O_1. We can see that all the members in the last expression have the same structure. These structures are: $[\vec{\rho}_o, [\vec{n}, \vec{r}_C]] M$, $[\vec{r}_C, [\vec{n}, \vec{\rho}_o]] M$ and $[\vec{\rho}_o, [\vec{n}, \vec{\rho}_o]] M$.

In the case when the pole O_1 is the centre C of the body mass, the vector $\vec{r}_C$ (the position vector of the mass centre with respect to the pole O_1) is equal to zero, whereas the vector $\vec{\rho}_O$ turns into $\vec{\rho}_C$ so that the last expression (3) can be written in the following form:

$$\vec{J}_{\underline{n}}^{(O)} = \vec{J}_{\underline{n}}^{(C)} + [\vec{\rho}_C, [\vec{n}, \vec{\rho}_C]] M \tag{4}$$

This expression (4) *represents the vector form of the theorem of the rate change of the mass inertia moment vector for the axis and the pole, when the axis is translated from the pole at the mass centre C to the arbitrary point, pole O.*

The *Huygens-Steiner theorems* (see Refs. [1] and [5]) for the body mass axial inertia moments, as well as for the mass deviational moments, emerged *from this theorem* (4) on the change of the vector $\vec{J}_{\underline{n}}^{(O)}$ of the body mass inertia moment at point O for the axis oriented by the unit vector $\vec{n}$ passing trough the mass center C, and when the axis is moved by translate to the other point O.

Mass inertia moment vector $\vec{J}_{\underline{n}}^{(O)}$ for the axis to the pole is possible to decompose in two parts: first $\vec{n}(\vec{n}, \vec{J}_{\underline{n}}^{(O)})$ collinear with axis and second $\vec{D}_{\underline{n}}^{(O)}$ normal to the axis. So we can write:

$$\vec{J}_{\underline{n}}^{(O)} = \vec{n}(\vec{n}, \vec{J}_{\underline{n}}^{(O)}) + \vec{D}_{\underline{n}}^{(O)} = J_{\underline{n}}^{(O)} \vec{n} + \vec{D}_{\underline{n}}^{(O)} \tag{5}$$

Collinear component $\vec{n}\left(\vec{n}, \vec{J}_{\vec{n}}^{(O)}\right)$ to the axis corresponds to the axial mass inertia moment $J_{\vec{n}}^{(O)}$ of the body. Second component, $\vec{D}_{\vec{n}}^{(O)}$, orthogonal to the axis, we denote by the $\vec{D}_{O}^{(\vec{n})}$, and it is possible to obtain by both side double vector products by unit vector $\vec{n}$ with mass moment vector $\vec{J}_{\vec{n}}^{(O)}$ in the following form:

$$\vec{D}_{\vec{n}}^{(O)} = \left[\vec{n}, \left[\vec{J}_{\vec{n}}^{(O)}, n\right]\right] = \vec{J}_{\vec{n}}^{(O)}\left(\vec{n}, \vec{n}\right) - \vec{n}\left(\vec{n}, \vec{J}_{\vec{n}}^{(O)}\right) = \vec{J}_{\vec{n}}^{(O)} - J_{O}^{\vec{n}}\vec{n} \tag{6}$$

In case when rigid body is balanced with respect to the axis the mass inertia moment vector $\vec{J}_{\vec{n}}^{(O)}$ is collinear to the axis and there is no deviational part. In this case axis of rotation is main axis of body inertia. When axis of rotation is not main axis then mass inertial moment vector for the axis contains deviation part $\vec{D}_{\vec{n}}^{(O)}$. That is case of rotation unbalanced rotor according to axis and bodies skew positioned to the axis of rotation.

Figure 1. Arbitrary position of rigid body coupled rotations around two axes without intersection. System is with two degrees of mobility (two freedom or one degrees of freedom and one rheonomic constraint) where φ_1 and φ_2 are generalized coordinates Fixed coordinate system and two moveable coordinate systems $O_1\xi_1\eta_1\zeta_1 = O_1\xi_1\eta_1 z$ and $O_2\xi_2\eta_2\zeta_2 = O_2\xi_2\eta_2 z_2$ that are rotating with

component angular velocities of rigid body coupled rotations: independent generalized (/or rheonomic) coordinates are φ_1 coordinate of precission rotation and φ_2 coordinate around self rotation axis. Vector rotators $\vec{R}_{01}$, $\vec{R}_{011}$ and $\vec{R}_{022}$ are presented.

2. Derivatives of linear momentum and angular momentum of rigid body coupled rotations around two axes without intersection

Let us to consider rigid body rotation around two axes first oriented by unit vector $\vec{n}_1$ with fixed position and second oriented by unit vector $\vec{n}_2$ which is rotating around fixed axis with angular velocity $\vec{\omega}_1 = \omega_1 \vec{n}_1$. Axes of rotation are without intersection. Rigid body is positioned on the moving rotating axis oriented by unit vector $\vec{n}_2$ and rotate around self rotating axis with angular velocity $\vec{\omega}_2 = \omega_2 \vec{n}_2$ and around fixed axis oriented by unit vector $\vec{n}_1$ with angular velocity $\vec{\omega}_1 = \omega_1 \vec{n}_1$. Then, axes of rigid body coupled rotations are without intersection. The shortest orthogonal distance between axes is defined by lenght $\overline{O_1 O_2}$ and it is perpendicular to both axes that is to the direction of angular velocities $\vec{\omega}_1 = \omega_1 \vec{n}_1$ and $\vec{\omega}_2 = \omega_2 \vec{n}_2$. This vector is $\vec{r}_0 = \overrightarrow{O_1 O_2}$ (see Figure 1): $\vec{r}_0 = r_0 \dfrac{[\vec{n}_1, \vec{n}_2]}{\left\|[\vec{n}_1, \vec{n}_2]\right\|} = r_0 \vec{u}_{01}$ and it can be seen on Fig.1. Velocity of mass particle dm is: $\vec{v} = [\vec{\omega}_1, \vec{r}_0] + [\vec{\omega}_1 + \vec{\omega}_2, \vec{\rho}]$.

By using expressions for linear momentum (see Refs. [1], [11], [12] and [10]) and after taking in account derivatives of parts, the derivative of linear momentum of rigid body coupled rotations around two axes without intersection, we can write the folowing vector expression:

$$\frac{d\vec{K}}{dt} = \dot{\omega}_1[\vec{n}_1, \vec{r}_0]M + \omega_1^2[\vec{n}_1, [\vec{n}_1, \vec{r}_0]]M + \dot{\omega}_1\vec{S}_{\vec{n}_1}^{(O_2)} + \omega_1^2[\vec{n}_1, \vec{S}_{\vec{n}_1}^{(O_2)}] +$$
$$+ \dot{\omega}_2\vec{S}_{\vec{n}_2}^{(O_2)} + \omega_2^2[\vec{n}_2, \vec{S}_{\vec{n}_2}^{(O_2)}] + 2\omega_1\omega_2[\vec{n}_1, \vec{S}_{\vec{n}_2}^{(O_2)}]$$

(7)

After analysis structure of linear momentum derivative terms, we can see that there are possible to introduce pure kinematic vectors depending on component angular velocitie and component angular accelerations of component coupled rotations that is useful to express derivatives of linear moment in following form

$$\frac{d\vec{K}}{dt} = \vec{R}_{01}[[\vec{n}_1, \vec{r}_0]]M + \vec{R}_{011}\left|\vec{S}_{\vec{n}_1}^{(O_2)}\right| + \vec{R}_{022}\left|\vec{S}_{\vec{n}_2}^{(O_2)}\right| + 2\omega_1\omega_2[\vec{n}_1, \vec{S}_{\vec{n}_2}^{(O_2)}]$$

(8)

By using vector expressions for angular momentum after taking in account derivatives of parts, the derivative of angular momentum of rigid body coupled rotations around two axes without intersection and after analysis structure of angular momentum derivative terms, we can see, as in previous chapter for the derivatives of linear momentum, that there is possible to introduce pure kinematic vectors-rotators depending on angular

velocities and angular accelerations of component coupled rotations and that to express derivatives of angular momentum in following shorther form:

$$\frac{d\vec{L}_{O_1}}{dt} = \vec{\chi}_{12}(\vec{r}_0, \vec{\rho}_C, M, \dot{\omega}_1, \dot{\omega}_2, \omega_1, \omega_2, \vec{n}_1, \vec{n}_2) + \dot{\omega}_1 \vec{n}_1 r_0^2 M + 2\omega_1 \omega_2 [\vec{n}_1, \vec{J}_{\vec{n}_2}^{(O_2)}]$$

$$+ \dot{\omega}_1 (\vec{n}_1, \vec{J}_{\vec{n}_1}^{(O_2)},)\vec{n}_1 + \dot{\omega}_2 (\vec{n}_2, \vec{J}_{\vec{n}_2}^{(O_2)},)\vec{n}_2 + \vec{R}_1 |\vec{D}_{\vec{n}_1}^{(O_2)}| + \vec{R}_2 |\vec{D}_{\vec{n}_2}^{(O_2)}|$$

$$(9)$$

where

$$\vec{S}_{\vec{n}_1}^{(O_2)} = \iiint_V [\vec{n}_1, \vec{\rho}] dm$$

and

$$\vec{S}_{\vec{n}_2}^{(O_2)} = \iiint_V [\vec{n}_2, \vec{\rho}] dm$$

are correspond body mass linear moment of the rigid body for the axes oriented by direction of component angular velocities of coupled rotations through the movable pole O_2 on self rotating axis;

$$\vec{J}_{\vec{n}_1}^{(O_2)} \overset{def}{=} \iiint_V [\vec{\rho}, [\vec{n}_1, \vec{\rho}]] dm$$

and

$$\vec{J}_{\vec{n}_2}^{(O_2)} \overset{def}{=} \iiint_V [\vec{\rho}, [\vec{n}_2, \vec{\rho}]] dm$$

are corresponding rigid body mass inertia moment vectors for the axes oriented by directions of component rotations through the pole O_2 on self rotating axes. For detail see ref. [10].

In previous expressions (8) and (9) we introduce following notations: $\vec{R}_{01}, \vec{R}_{011}$, $\vec{R}_{022}$, $\vec{R}_1$ and $\vec{R}_2$. These vectors are vector rotators which intensity depends of angular velocity and angular acceleration of corresponding component rotation.

3. Vector rotators of a rigid body coupled rotations around two axes without intersection

We can see that in previous expressions (8) and (9) for derivative of linear momentum and angular momentum are introduced the vectors $\vec{R}_{01}, \vec{R}_{011}$, $\vec{R}_{022}$, $\vec{R}_1$ and $\vec{R}_2$. Let us to consider vector forms and properties of these vectors.

$$\vec{R}_{01} = \dot{\omega}_1 \vec{u}_{01} + \omega_1^2 \vec{v}_{01} , \quad \vec{R}_{01} = \dot{\omega}_1 \left[\vec{n}_1, \frac{\vec{r}_0}{r_0} \right] + \omega_1^2 \left[\vec{n}_1, \left[\vec{n}_1, \frac{\vec{r}_0}{r_0} \right] \right], \quad \vec{R}_{011} = \dot{\omega}_1 \vec{u}_{011} + \omega_1^2 \vec{v}_{011}$$

$$\vec{R}_{011} = \dot{\omega}_1 \frac{\vec{S}_{\vec{n}_1}^{(O_2)}}{|\vec{S}_{\vec{n}_1}^{(O_2)}|} + \omega_1^2 \left[\vec{n}_1, \frac{\vec{S}_{\vec{n}_1}^{(O_2)}}{|\vec{S}_{\vec{n}_1}^{(O_2)}|} \right] = \dot{\omega}_1 \frac{[\vec{n}_1, \vec{\rho}_C]}{|[\vec{n}_1, \vec{\rho}_C]|} + \omega_1^2 \frac{[\vec{n}_1, [\vec{n}_1, \vec{\rho}_C]]}{|[\vec{n}_1, \vec{\rho}_C]|}, \quad \vec{R}_{022} = \dot{\omega}_1 \vec{u}_{022} + \omega_1^2 \vec{v}_{022}$$

$$\vec{R}_{022} = \dot{\omega}_2 \frac{\vec{S}_{\vec{n}_2}^{(O_2)}}{\left|\vec{S}_{\vec{n}_2}^{(O_2)}\right|} + \omega_2^2 \left[\vec{n}_2, \frac{\vec{S}_{\vec{n}_2}^{(O_2)}}{\left|\vec{S}_{\vec{n}_2}^{(O_2)}\right|}\right] = \dot{\omega}_2 \frac{[\vec{n}_2, \vec{\rho}_C]}{\left|[\vec{n}_2, \vec{\rho}_C]\right|} + \omega_1^2 \frac{[\vec{n}_2, [\vec{n}_2, \vec{\rho}_C]]}{\left|[\vec{n}_2, \vec{\rho}_C]\right|}$$

$$(11)$$

$$\vec{R}_1 = \dot{\omega}_1 \frac{\vec{D}_{\vec{n}_1}^{(O_2)}}{\left|\vec{D}_{\vec{n}_1}^{(O_2)}\right|} + \omega_1^2 \left[\vec{n}_1, \frac{\vec{D}_{\vec{n}_1}^{(O_2)}}{\left|\vec{D}_{\vec{n}_1}^{(O_2)}\right|}\right] = \dot{\omega}_1 \vec{u}_1 + \omega_1^2 \vec{v}_1$$

$$\vec{R}_2 = \dot{\omega}_2 \frac{\vec{D}_{\vec{n}_2}^{(O_2)}}{\left|\vec{D}_{\vec{n}_2}^{(O_2)}\right|} + \omega_2^2 \left[\vec{n}_2, \frac{\vec{D}_{\vec{n}_2}^{(O_2)}}{\left|\vec{D}_{\vec{n}_2}^{(O_2)}\right|}\right] = \dot{\omega}_2 \vec{u}_2 + \omega_2^2 \vec{v}_2$$

a*   b*
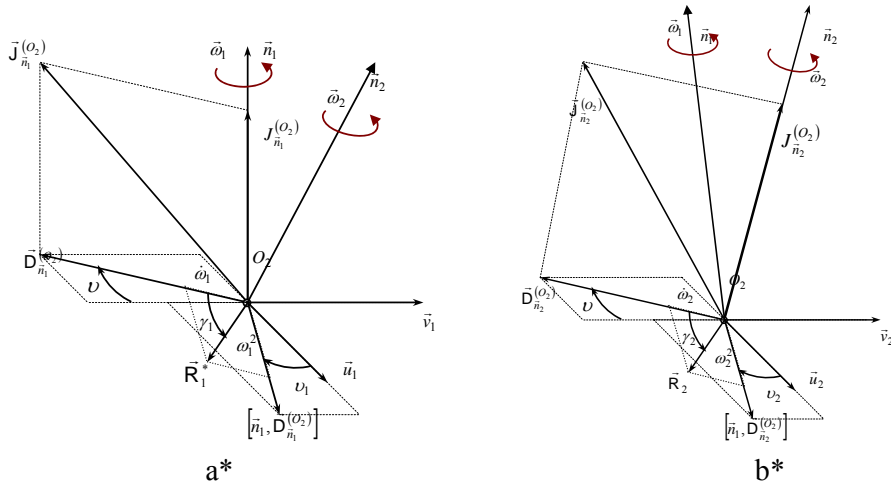
Figure 2. Vector rotators $\vec{R}_1$ (a*) and $\vec{R}_2$ (b*) in relations to corresponding mass moment vectors $\vec{J}_{\vec{n}_1}^{(O_2)}$ and $\vec{J}_{\vec{n}_2}^{(O_2)}$, and their corresponding deviational components $\vec{D}_{\vec{n}_1}^{(O_2)}$ and $\vec{D}_{\vec{n}_2}^{(O_2)}$ as well as to corresponding deviational planes.

Three vector rotators $\vec{R}_{01}$, $\vec{R}_{011}$ and $\vec{R}_1$ from the set (11) are orthogonal to the direction of the first fixed axis oriented by unit vector $\vec{n}_1$ and two vector rotators $\vec{R}_{022}$ and $\vec{R}_2$ are orthogonal to the self rotation axis. But, first vector rotator $\vec{R}_{01}$ is coupled for pole O_1 on the fixed axis and second and third vector rotators, $\vec{R}_{011}$ and $\vec{R}_{022}$, are coupled for the pole O_2 at self rotation axis and for corresponding direction oriented by directions of component angular velocities of coupled rotations. Intensities of three first rotators are equal and are expressed by angular velocity and angular acceleration of the first component rotation, and intensities of two vector rotators $\vec{R}_{022}$ and $\vec{R}_2$ are expressed by angular

velocity and angular acceleration of the second component rotation, and are in the following forms:

$$\mathsf{R}_{01} = \mathsf{R}_{011} = \sqrt{\dot{\omega}_1^2 + \omega_1^4} \qquad \text{and} \qquad \mathsf{R}_{022} = \sqrt{\dot{\omega}_2^2 + \omega_2^4}$$

(12)

Rotators from first set are rotated around axis through pole O_2 in direction of first component rotation angular velocity and depend of angular velocity ω_1 and angular acceleration $\dot{\omega}_1$. There are two vectors of such type and all trees have equal intensity. Rotators from second set are rotated around axis in direction of second component rotation and depend of angular velocity ω_2 and angular acceleration $\dot{\omega}_2$. There are two vectors of such type and they have equal intensity.

4. Relative angular velocity of vector rotators of a rigid body coupled rotations around two axes without intersection

Let's introduce notation γ_1, and γ_2 denote difference between corresponding component angles of rotation φ_1 and φ_2 of the rigid body component rotations and corresponding absolute angles of pure kinematics vector rotators $\vec{\mathsf{R}}_{01}, \vec{\mathsf{R}}_{011}, \vec{\mathsf{R}}_{022}, \vec{\mathsf{R}}_1$ and $\vec{\mathsf{R}}_2$, about corresponding axis oriented by unit vector $\vec{n}_1$, and $\vec{n}_2$ through pole O_2 (see Fig. 2). These angles are determined by following relations:

$$\gamma_1 = arc\, tg\, \frac{\dot{\varphi}_1^2}{\ddot{\varphi}_1} \qquad\qquad \gamma_2 = arc\, tg\, \frac{\dot{\varphi}_2^2}{\ddot{\varphi}_2}$$

and

(13)

Angular velocity of relative kinematics vectors rotators $\vec{\mathsf{R}}_{01}, \vec{\mathsf{R}}_{011}, \vec{\mathsf{R}}_{022}, \vec{\mathsf{R}}_1$ and $\vec{\mathsf{R}}_2$ which rotate about axes in corresponding directions in relation to the component angular velocities of the rigid body component rotations through pole O_2 are:

$$\dot{\gamma}_1 = \frac{\dot{\varphi}_1\left(2\ddot{\varphi}_1^2 - \dot{\varphi}_1\dddot{\varphi}_1\right)}{\ddot{\varphi}_1^2 + \dot{\varphi}_1^4} \qquad\qquad \dot{\gamma}_2 = \frac{\dot{\varphi}_2\left(2\ddot{\varphi}_2^2 - \dot{\varphi}_2\dddot{\varphi}_2\right)}{\ddot{\varphi}_2^2 + \dot{\varphi}_2^4}$$

(14)

5. Concluding remarks

First main result presented in this paper is successful application the vector method by use mass moment vectors for investigation of the rigid body coupled rotation around two axes without intersections and vector decomposition of the dynamic structure into series of the vector parameters useful for analysis of the coupled rotation kinetic properties.

By introducing mass moment vectors and vector rotators we expensed linear momentum and angular momentum, as well as their derivatives with respect to time for the case of the rigid body coupled rotations around two axes without intersections.

Appearance, as it is visible, of the vector rotators, their intensity and their directions as well as their relative angular velocity of rotation around component directions parallel to components of the coupled rotations is very important for understanding mechanisms of coupled rotations as well as kinetic pressures on shaft bearings of both shaft.

Special attentions are focused to the vector rotators, as well as to the absolute and relative angular velocities of their rotations.

References

[1] Hedrih (Stevanović), K., (2001), Vector Method of the Heavy Rotor Kinetic Parameter Analysis and Nonlinear Dynamics, University of Niš 2001,Monograph, p. 252, YU ISBN 86-7181-046-1.

[2] Hedrih (Stevanović) K., (1993), *The mass moment vectors at n-dimensional coordinate system*, Tensor, Japan, Vol 54 (1993), pp. 83-87.

[3] Hedrih (Stevanović) K., (1992), *On some interpretations of the rigid bodies kinetic parameters,* XVIIIth ICTAM HAIFA, Apstracts, pp. 73-74.

[4] Hedrih (Stevanović) K., (1993), Same *vectorial interpretations of the kinetic parameters of solid material lines*, ZAMM. Angew.Math. Mech. 73(1993) 4-5, T153-T156.

[5] Hedrih (Stevanović), K. (1998), Vectors of the Body Mass Moments, Monograph paper, Topics from Mathematics and Mechanics, Mathematical institute SANU, Zbornik radova 8(16), 1998, pp. 45-104.

[6] Hedtrih (Stevanović) K., (2008), Dynamics of coupled systems, Nonlinear Analysis: Hybrid Systems, Volume 2, Issue 2, June 2008, Pages 310-334.

[7] Hedrih (Stevanović) K., (2001), *Derivatives of the Mass Moment Vectors at the Dimensional Coordinate System N*, dedicated to memory of Professor D. Mitrinović, Facta Universitatis Series Mathematics and Informatics, 13 (1998), pp. 139-150. (1998, published in 2001. Edited by G. Milovanović).\

[8] Katica (Stevanović) Hedrih and Ljiljana Veljović, (2008), *Nonlinear dynamics of the heavy gyro-rotor with two skew rotating axes*, Journal of Physics: Conference Series, 96 (2008) 012221 DOI:10.1088/1742-6596/96/1/012221, IOP Publishing http://www.iop.org/EJ/main/-list=current/

[9] Hedrih (Stevanović) K. and Veljović Lj., (2010), The Kinetic Pressure of the Gzrorotor Eigen Shaft Bearings and Rotators, The Third International Conference Nonlinear Dynamics – 2010, pp. 78-83

[10] Hedrih (Stevanović) K. and Veljović Lj., (2010), Vector Rotators of a Rigid Body Dynamics with Coupled Rotations around Axes without Intersection, Mathematical Problem in Engineering, (MPE/351269: Accepted, in press)

[11] Rašković, D.,(1972), Mehanika III–Dinamika, (*Mechanics II –Dynamics)*, Naučna knjiga, 1972, p. 424.

[12] Rašković P. Danilo, (1965), Teorija oscilacija (Theory of Oscillations), Naučna knjiga, 1965, 503.

Energy analysis of vibro-impact systems based on oscillator moving freely along curvilinear routes and non-ideal relations

Srdjan Jović*, Vladimir Raičević*

*Faculty of Technical Sciences, Kosovska Mitrovica
38 220 Kosovska Mitrovica, Kralja Petra I br. 149/12, Serbia
e-mail: jovic003@yahoo.com
Tel: 028 42 3579

Abstract: This work is based on the analysis of vibro-impact system motion, moving freely along non-ideal lines-rough curvilinear paths in vertical plane in the shapes of: parabola, cicloid and circle. Non-ideal caracter of the relation is due to the Coloumb's type friction force with coefficient $\mu = tg\,\alpha_0$. The oscilator is composed by one heavy mass particle (the observed systems have one degree of freedom of motion) whose free motion was limited by one or two stabile elongation limiters. The analyitical-numerical results for certain kinetic parameters of the observed vibro-impact systems are basis for the visualization of the motion analysis and energy analysis, which are subject of this analytical research. In this paper the methodology of the energy transfer investigation among the elements of the observed vibro-impact system is presented.

The Applied methodology : Free motion of the heavy mass particle was divided to the corresponding intervals. Each motion interval corresponds one differential equation from the group of ordinary homogenious non-linear differential second order equations. This differential equation was solved in analytical form. The differential motion equation for corresponding motion conditions is matched to initial motions coditions, impact conditions to elongations limiters and conditions of alteration of motions directions causing the alternation of direction of friction force. By solving the differential equation of motion analyticaly we came to analytica; expression for phase trajectory equation in plane $(\varphi, \dot{\varphi})$, that is neccessary for energy analysis of dynamics of vibro-impact systems together with the energy equation curves. The graphic visualization of the energy curves and motion analysis of representative point of system kinetic state during the kinetic (dynamics) is done by using software package MathCad and user's package CorelDraw.

Application: Based on vibro-impact systems there are constructed various vibration machines, where working part has to perform periodic impacts for realization of technology processes. In general, vibro-impact systems are applied in transportation systems, construction machines, casting machines, vibro-devices etc.

Keywords: Heavy mass particle, rough parabola, rough cicloid, rough circle, friction, impact limiters, vibro-impact, phase trajectory, singular points, large initial conditions, total energy, kinetic and potential energy, analytical expression, graphical presentation, representative point, differential equations.

1. Introduction

The investigation of vibro-impact processes to the dynamics of the systems and properties and specifications of non-linear phenomena with discontinious conditions were made by many researcher all around the world. Based to the previous knoledge ablut the theory of vibro-impact systems, and to the original works by: František Peterka, Katica (Stevanović) Hedrih, Alz Nayfeh et al., Dimentberg M.F and Menyailov A.I., Foole S. and Bishop S., Lieber P. and Jensen, D., Luo G.W. and Xie J.H., Nordmark A.B., Pavlovskaia E. and Wiercigroch M., and other, it can be concluded that there is greater interest today for investigation of energy transfer within complex systems and non-linear modes. That is the reason of importance of energy analysis of the dynamics of vibro-impact processes in vibro-impact systems with one or more degrees of freedom as well as non-ideal relations.

The problems of dynamics of vibro-impact systems represent separate area of applied theory of oscilations. The theory of vibro-impact systems is specially important for engineering practice for wide application of vibro-impact astions, used for realization of the technology processes. The collisions occured in the procedure of kinemtaic couples oscilation motions cause increased dynamic impact loadings,

decreasing durability and liability of the system, as well as alternating dissipative system features. The studies about vibo-impact systems and vibro-impact actions are essential because of some very harmful impacts to the gaps and wearing in kinetic systems. The investigation of such vibro-impact actions is important for achievement of expected motion regimes and system stability, i.e. regulation of the system motion.

The introducing theory for this paper were taken from the nooks of D. Rašković, where the motion of mechanic system in ideal conditions and without limitations was analyzed, as well as the motion of curvilinear oscilator in the presence of sliding Columb's friction, than from the papers by Katica (Stevanović) Hedrih referring to the movement of heavy mass particle along rough curvilinear path. In order to perform the analysis of the dynamics of vibro-impact system with curvilinear paths and non-ideal relations, an explanation of free oscilation of heavy mass particle along curvilinear paths and non-ideal links must be done first.

2.   Free mass particle oscilations along curvilinear paths and non-ideal links

Vibro-impact system represents the dynamic system with oscilation motion in the periods with impacts occurances. In

order to study the motion and energy analyze of the corresponding vibro-impact system, non-impact motion i.e. motion between the impacts, must be analyzed first. Non-impact motion is described by differentail (double) motion equations and by double phase trajectories equations, *free oscilations of heavy mass particle along curvilinear rough lines and vertical planes and with non-ideal links,* as well as the particular examples of motions along the rough parabolic line, rough cicloid line and rough circle line, based on the results from prof.dr Katica (Stevanović) Hedrih [10-11].

2.1. Free motion of heavy mass particle along rough curbilinear line

Let us study free motion (oscilation) of heavy mass particle M, mass *m*, along rough curvilinear line with sliding *Coulomb*'s friction force and coefficient type μ (Fig.*1*).
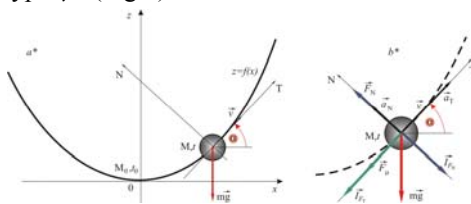
Fig. 1. Free motion of heavy mass particle along curvilinear path: a* derived position of heavy mass particle; b* force plan

Curvilinear line equation situated in vertical plane *Oxz* is written in a form $z = f(x)$. By using the principle of dynamic equilibrium, with acting forces presented on Fig. 1 b*, the vector's equation of motion of heavy mass particle along curvilinear path can be written in a form :

$$\left(-m\ddot{s}\vec{T}\right)+\left(-m\frac{v^2}{R_k}\vec{N}\right)+mg\left(-\sin\alpha\vec{T}-\cos\alpha\vec{N}\right)+F_N\vec{N}-\mu F_N\frac{\vec{v}}{|v|}=0$$

After scalar multiplication of this vector equation with unit vectors $\vec{T}$ and $\vec{N}$ and

by completing of obtained scalar vectors equations one differential (double) equation of motion of heavy mass particle is obtained, as a function of curvilinear (arc) coordinate s, $\left(ds = dx\sqrt{1+z'^2}\right)$, in a form:

$$\ddot{s} + g\sin\alpha \pm \mu\left(\frac{v^2}{R_k} + g\cos\alpha\right) = 0 \tag{1}$$

BY solving of differential (double) equation of motion (1) we get (double) phase trajectory equation

$$\dot{x}^2(x) = e^{-\int\frac{2}{\sqrt{1+z'^2}}\left[\frac{d}{dx}\sqrt{1+z'^2}\pm\mu\frac{z^*}{\sqrt{1+z'^2}}\right]dx}. \tag{2}$$
$$\cdot\left[-2g\int\frac{1}{\left(1+z'^2\right)}\left(z'\pm\mu\right)e^{\int\frac{2}{\sqrt{1+z'^2}}\left[\frac{d}{dx}\sqrt{1+z'^2}\pm\mu\frac{z^*}{\sqrt{1+z'^2}}\right]dx}dx+C\right]$$

The equations (1) and (2) are basis for formation of diffrential (double) motion equations and (double) phase trajectory equations for any shape of curvilinear line. In this papere there are considered rough parabolic, cycloid and circle lines.

2.1.1. Free motion of heavy mass particle along parabolic rough line is presented on Fig. 2.

Based on the theory conducted for motion of heavy mass particle along rough curvilinear line in general, the analysis of this motion is special case.
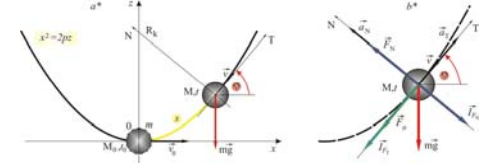
Fig.2. a* initial and derived position of heavy mass particle; b* force plan

The general equation of parabola has a form $x^2 = 2pz$, where $2p[m]$- is parabola parameter equal to quadric distance of focus from the top of parabola. The observed system has one degree of

freedom of motion. For generalized coordinate we take parameter φ (the angle between tangence direction with the direction that is paralel to axis Ox). Based on equations (1) and (2) and the general parabola equation, using many mathematic operations, the differential (double) equation of motion and phase trajectory of heavy mass particle equation along parabolic rough line (as a function of generalized coordinate φ) were obtained.

$$\ddot{\varphi} + (3tg\varphi \pm \mu)\dot{\varphi}^2 + \frac{g\cos^3\varphi}{p}(\sin\varphi \pm \mu\cos\varphi) = 0, \begin{cases} za\ v > 0 \\ za\ v < 0 \end{cases} \quad (3)$$

$$\dot{\varphi}^2 = \cos^6\varphi\left(-\frac{g}{p\cos^2\varphi} + Ce^{\mp 2\mu\varphi}\right) \begin{cases} za\ v > 0 \\ za\ v < 0 \end{cases} \quad (4)$$

Where C - integration constant depending of initial motion conditions (valid also in equations for cicloid and circle lines). The integral constant has some alternation in dependence of period of motion of heavy mass particle along parabolic rough line, limited by points at phase trajectory where the the velocity is equal to zero. That alteration is related to the alternation of the direction of heavy mass particle motion, i.e. alternation of velocity direction of heavy mass particle causing the alternation of friction force.

2.1.2. Free motion of heavy mass particle along cicloid rough line **is presented on Fig.3.**

Based on the theory conducted for the motion of heavy mass particle along the curvilinear rough line in general, the analysis of this motion represents the special case.
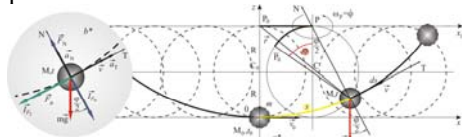
Fig.3. a* the initial and derived position of heavy mass particle; b* force plan

The observed system has one degree of freedom of motion. For generalized coordinate we adopt parameter φ (angle between direction $M\overline{P_0}$ and vertical line), which defines the position of heavy mass particle M, positioned on the circle of seni diameter R, moving equaly along the axes Ox. Heavy mass particle in this case describes the line representing geometry clear cicloid path. Based on equations (1) and (2) together with parametrs of cicloide equation $x = R(\varphi + \sin\varphi)$ and $z = R(1 - \cos\varphi)$, and using chain of mathematic operations we get differential (double) equation of motion and (double) equation of phase trajectory of heavy mass particle along cicloid rough line (as a function of generalized coordinate φ).

$$\ddot{\varphi} - \dot{\varphi}^2\left(\frac{1}{2}tg\frac{\varphi}{2} \mp \mu\right) + \left(tg\frac{\varphi}{2} \pm \mu\right)\frac{g}{2R} = 0, \quad (5)$$

$$\begin{cases} za\ v = 2R\cos\frac{\varphi}{2}\dot{\varphi} > 0 \\ za\ v = 2R\cos\frac{\varphi}{2}\dot{\varphi} < 0 \end{cases}$$

$$\dot{\varphi}^2 = -\frac{\left(\frac{g}{2R}\right)}{1+4\mu^2}\frac{1}{\cos^2\frac{\varphi}{2}}\left[(\pm 3\mu)\sin\varphi - (1-2\mu^2)\cos\varphi + \frac{1+4\mu^2}{2} + Ce^{\mp 2\mu\varphi}\right]$$

$$\begin{cases} za\ v = 2R\cos\frac{\varphi}{2}\dot{\varphi} > 0 \\ za\ v = 2R\cos\frac{\varphi}{2}\dot{\varphi} < 0 \end{cases} \quad (6)$$

where C - is integration constant

2.1.3. Free motion of heavy mass particle along circle rough line is presented on Fig.4.

The angle φ represents generalized coordinate of the observed non-conservative mechanical system with one degree of freedom of motion.

By using the coordinate system of references with axes in direction of perpendicular and tangent, and based to the procedure conducted for the motion of heavy mass particle along rough curvilinear path (1), the differential (double) equation of motion of heavy mass particle along the

circle rough line can be written in a form of:

$$\ddot{\varphi} \pm \dot{\varphi}^2 tg\alpha_0 + \frac{g}{R\cos\alpha_0}\sin(\varphi \pm \alpha_0) = 0$$

$$\begin{cases} za\ \dot{\varphi} > 0 \\ za\ \dot{\varphi} < 0 \end{cases},$$
(7)
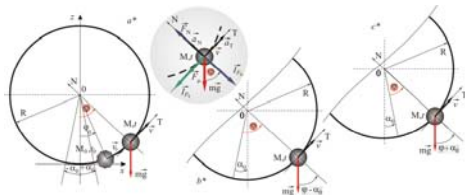
Fig. 4. a*the initial and derived position of heavy mass particle , force plan; b* and c* presentation of the „relative" equilibrium positions with alternation properties $\pm\alpha_0$

By solving the equation (7) we get (double) phase trajectory equation of heavy mass *particle moving along circle rough line*

$$\dot{\varphi}(\varphi)^2 = \frac{2g}{(1+4tg^2\alpha_0)R\cos\alpha_0}[\cos(\varphi\pm\alpha_0) - 2tg\alpha_0\sin(\varphi\pm\alpha_0)] + Ce^{\mp 2\varphi tg\alpha_0}$$

$$\begin{cases} za\ \dot{\varphi} > 0 \\ za\ \dot{\varphi} < 0 \end{cases}$$
(8)

where C - integrating constant.

3. Vibro-impact system based on oscilator moving freely along curvilinear paths and non-ideal connections

The dynamics of vibro-impact systems based on oscilator with free motion along non-ideal links-rough curvilinear lines, in shape of parabola and circle was analyzed by application of analytical method of „ adjustment" and phase plane method. Also, for the part of oscilator there are used one or two heavy mass particles – pellets, moving freely along rough curvilinear route with sliding *Coulomb*'s type friction force. The system becomes vibro-impact system when one or two elongation limiters for each are positioned

and concerned as mobile and stabile limiters.

3.1. Vibro-impact system based on oscillator moving freely along parabolic rough line

Heavy mass particle moving along parabolic rough line in vertical plane, with sliding Coulomb's type friction force coefficient $\mu = tg\alpha_0$, with one elongation limiter on the right and one elongation limiter on the left side (Fig.5).
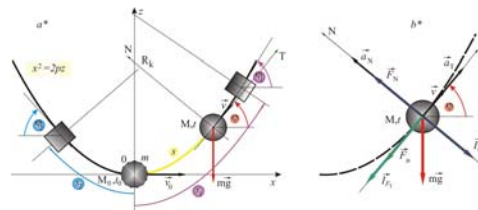
Fig.5. The system with two stabile elongation limiters, based on oscilator with one pellet:
a* initial and derived position of the pellet;
b* force plan

The positions of the limiters are determined by arc coordinates $s_{ul,1} = s_1(\varphi_1)$ and $s_{ul,2} = s_2(\varphi_2)$ are measured from the equilibrium position of heavy mass particle. The arc (curvilinear) coordinates are given in as a function of the angle φ.

For the complete description of the dynamics of heavy mass particle, the differential (double) equation of motion (3) is coupled to:
a* initial conditions
$s_{(0)}(\varphi_{(0)}) = s_0(\varphi_0)$ and
$v_{(0)}(\varphi_{(0)}, \dot{\varphi}_{(0)}) = \dot{s}_{(0)}(\varphi_{(0)}, \dot{\varphi}_{(0)}) = v_0(\varphi_0, \dot{\varphi}_0)$;
b* angular elongation limitation conditions, and impact conditions
$s_{ul,i} = s_i(\varphi_i)$, $s_{ul,(i+1)} = s_{(i+1)}(\varphi_{(i+1)})$,
$\dot{s}_{odl,i}(\dot{\varphi}_{odl,i}) = -k\dot{s}_{ul,i}(\dot{\varphi}_{ul,i})$,

$$\dot{s}_{odl,(i+1)}\left(\dot{\varphi}_{odl,(i+1)}\right) = -k s_{ul,(i+1)}\left(\dot{\varphi}_{ul,(i+1)}\right),$$
$$i = 1,2,3,...,n,$$

where: k- impact coefficient in the range between $k = 0$, for ideal plastci impact, and $k = 1$, for ideal elastic impact; n- number of impacts until arrestment of heavy mass particle on the parabolic rough line, or until the interval where heavy mass particle continues to move without impact to the limiter.

Free motion of heavy mass particle along parabolic rough line is divided to the corresponding intervals and subintervals of motion:

The first; From the initial moment of motion to the impact into the right elongation limiter; **The second;** From the right elongation limiter to the impact to the left elongation limiter, until the direction alternation (motion intervals limited by friction force direction alternation)

The motion analysis is conducted by using the phase trajectory equation (4) with corresponding argument in dependance of motion interval.

3.1.1 Grafic visualization of the phase portrait of heavy mass perticle in the observed vibro-impact system

Based on real values of kinetic and geometry parameters of the system,

$$\varphi_1 = \frac{\pi}{4}[rad], \varphi_2 = -\frac{\pi}{6}[rad], \varphi_0 = 0, \dot{\varphi}_0 = 7\left[\frac{rad}{s}\right],$$

$$p = 1[m], \alpha_0 = 0,05, g = 9,81\left[\frac{m}{s^2}\right]$$

$$m = 0,2[kg] \ \text{i}$$

The phase portrait of heavy mass particle moving along parabolic rough line is showed (Fig.6).
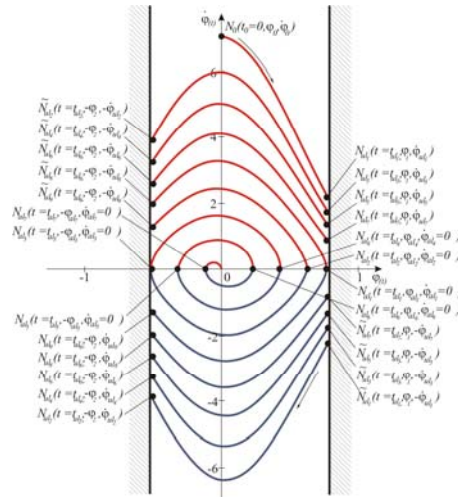
Fig. 6. Phase portrait of heavy mass particle moving along the parabolic rough line with sliding Coulomb's type friction coefficient $\mu = tg\,\alpha_0$ with limited elongations in a plane $(\varphi, \dot{\varphi})$

3.1.2 Graphic visualization of energy analysis of the observed vibro-impact system

By using the analytical expressions for the peripendicular pressure force $F_{N,i}$, power originated of sliding *Coulomb's* type friction force $P_{\mu,i}$ to the heavy mass particle on the parabolic rough line, kinetic energy $E_{k,i}$, potential energy $E_{p,i}$ and total mechanical energy E_i, $(i = 1,2,..,n.)$,

$$F_{N,i} = mg\cos\varphi + mp\cos^3\varphi\left(-\frac{g}{p\cos^2\varphi} + C_i e^{\mp 2\mu\varphi}\right)$$

,

$$P_{\mu,i} = -\mu F_{N,i}\dot{s} = -\mu F_{N,i}\frac{p}{\cos^3\varphi}\dot{\varphi} =$$

$$= -\mu mp\left(g\cos\varphi + p\cos^3\varphi\left(-\frac{g}{p\cos^2\varphi} + C_i e^{\mp 2\mu\varphi}\right)\right)\sqrt{-\frac{g}{p\cos^2\varphi} + C_i e^{\mp 2\mu\varphi}},$$

$$Ek_i(\varphi) = \frac{1}{2}mv_i^2 = \frac{1}{2}m\frac{p^2}{\cos^6\varphi}\dot{\varphi}_i^2 = \frac{1}{2}mp^2\left(-\frac{g}{p\cos^2\varphi} + C_i e^{\mp 2\mu\varphi}\right),$$

$$Ep_i(\varphi) = \frac{1}{2}\frac{mgp}{\cos^2\varphi} \quad \text{and}$$

$$E_i(\varphi) = Ek_i(\varphi) + Ep_i(\varphi) =$$

$$= \frac{1}{2}mp^2\left(-\frac{g}{p\cos^2\varphi} + C_i e^{\mp 2\mu\varphi}\right) + \frac{1}{2}\frac{mgp}{\cos^2\varphi}$$

,
For every separate branch of the phase portrait, there is a graphic of alternation of F_N, P_μ, E_k, E_p and E from the initial moment of motion until the moment when heavy mass particles returns into equilibrium position (*Fig.7-11*).
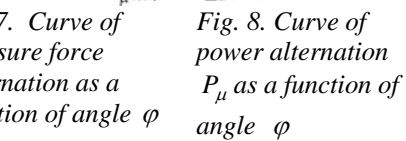
Fig. 9. Graphic presentation of kinetic energy alternation in plane (Ek, φ)

Fig. 10. . Graphic presentation of potential energy alternation in plane (Ep, φ)

Fig.7. Curve of pressure force alternation as a function of angle φ

Fig. 8. Curve of power alternation P_μ *as a function of angle* φ
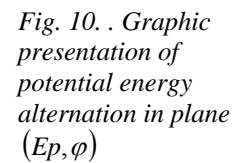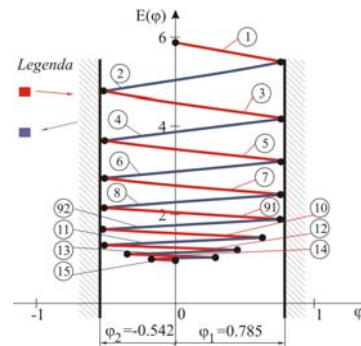
Fig.11.Graphic presentation of total mechanical energy alternation in plane (E, φ)

3.2. Vibroimpact system based on oscillator moving freely along cicloid rough line

Heavy mass particle is moving along cicloid rough line in vertical plane, with sliding Coloumb's type friction coefficient $\mu = tg\,\alpha_0$, with elongation limiter on the left and on the right side (Fig.12). The limiters positions are determined by arc coordinates $s_{ul,1} = s_1(\varphi_1)$ and $s_{ul,2} = s_2(\varphi_2)$ and measured from the equilibrium position of heavy mass particle. The arc (curvilinear) coordinates are given as a function of the angle φ.

For the complete description of the dynamics of heavy mass particle there are conditions matched to the differential (double) motion equation:

a* initial conditions

$$s_{(0)}(\varphi_{(0)}) = s_0(\varphi_0) \quad \text{and}$$
$$v_{(0)}(\varphi_{(0)}, \dot\varphi_{(0)}) = \dot{s}_{(0)}(\varphi_{(0)}, \dot\varphi_{(0)}) = v_0(\varphi_0, \dot\varphi_0);$$

b* angular elongation limitation conditions, and collision conditions

$$s_{ul,i} = s_i(\varphi_i)\ ,\ s_{ul,(i+1)} = s_{(i+1)}(\varphi_{(i+1)}),$$
$$\dot{s}_{odl,i}(\dot\varphi_{odl,i}) = -k\dot{s}_{ul,i}(\dot\varphi_{ul,i}),$$
$$\dot{s}_{odl,(i+1)}(\dot\varphi_{odl,(i+1)}) = -k s_{ul,(i+1)}(\dot\varphi_{ul,(i+1)}),$$
$$i = 1,2,3,...,n\ ,$$

where: k- is impact coefficient within the range from $k = 0$, for ideal plastic impact, to $k = 1$, for ideal elastic impact; n- number of impacts until the heavy mass particle stopping on the parabolic rough line or to the interval where heavy mass particle continues to move without impact to the limiter.
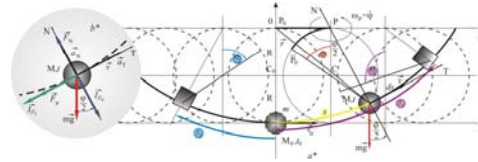
Fig. 12. System with two stabile elongation limiters, based on oscilator with one pellet: a* initial and derived position of the pellet; b* force plan

Free motion of heavy mass particle along cicloid rough line is divided into corresponding motion intervals and sub intervals:

The first; From the initial moment of motion to the impact into the right elongation limiter; **The second;** From the right elongation limiter to the impact to the left elongation limiter, etc., until the direction alternation (motion intervals limited by friction force direction alternation)

The motion analysis is conducted by using the phase trajectory equation (6) with corresponding argument in dependance of motion interval.

3.2.1 Grafic visualization of the phase portrait of heavy mass perticle in the observed vibro-impact system

Based on real values of kinetic and geometry parameters of the system,

$$\varphi_1 = \frac{\pi}{4}[rad], \varphi_2 = -\frac{\pi}{6}[rad], \varphi_0 = 0, \dot\varphi_0 = 8\left[\frac{rad}{s}\right],$$

$$R = 0,05[m], \alpha_0 = 0,05, g = 9,81\left[\frac{m}{s^2}\right], m = 0,2[kg].$$

The phase portrait of heavy mass particle moving along cicloid rough line is showed (Fig.13).
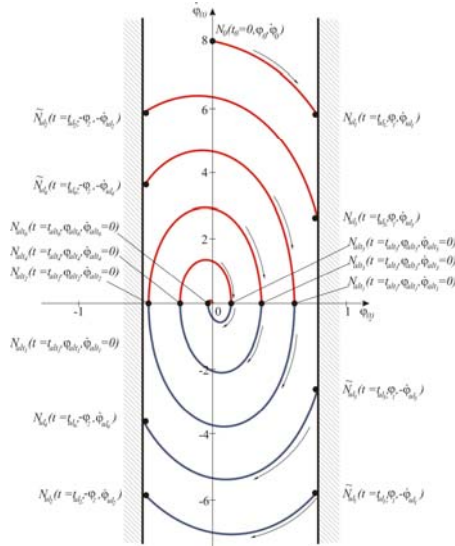
Fig. 13. Phase portrait of heavy mass particle moving along thecicloid rough line with sliding Coulomb's type friction coefficient $\mu = tg\,\alpha_0$ *with limited elongations in a plane* $(\varphi, \dot{\varphi})$

3.2.2 Graphic visualization of energy analysis of the observed vibro-impact system

By using the analytical expressions for the peripendicular pressure force $F_{N,i}$, power originated of sliding *Coulomb's* type friction force $P_{\mu,i}$ of the heavy mass particle on the parabolic rough line, kinetic energy $E_{k,i}$, potential energy $E_{p,i}$ and total mechanical energy E_i , $(i=1,2,\ldots,n.)$,

E_i , $(i=1,2,\ldots,n.)$,

$$F_{N,i} = mg\cos\frac{\varphi}{2} + m2R\cos\frac{\varphi}{2}\cdot$$

$$\cdot\left(-\frac{\left(\frac{g}{2R}\right)}{1+4\mu^2}\frac{1}{\cos^2\frac{\varphi}{2}}\left[(\pm 3\mu)\sin\varphi - (1-2\mu^2)\cos\varphi + \frac{1+4\mu^2}{2} + C_i e^{\mp 2\mu\varphi}\right]\right),$$

$$P_{\mu,i} = -\mu F_{N,i}2R\cos\frac{\varphi}{2}\dot{\varphi} = -\mu F_{N,i}2R\cos\frac{\varphi}{2}\cdot$$

$$\cdot\sqrt{-\frac{\left(\frac{g}{2R}\right)}{1+4\mu^2}\frac{1}{\cos^2\frac{\varphi}{2}}\left[(\pm 3\mu)\sin\varphi - (1-2\mu^2)\cos\varphi + \frac{1+4\mu^2}{2} + C_i e^{\mp 2\mu\varphi}\right]},$$

$$Ek_i(\varphi) = 2mR^2\cos^2\frac{\varphi}{2}\dot{\varphi}_i^2(\varphi) = 2mR^2\cos^2\frac{\varphi}{2}\cdot$$

$$\cdot\left(-\frac{\left(\frac{g}{2R}\right)}{1+4\mu^2}\frac{1}{\cos^2\frac{\varphi}{2}}\left[(\pm 3\mu)\sin\varphi - (1-2\mu^2)\cos\varphi + \frac{1+4\mu^2}{2} + C_i e^{\mp 2\mu\varphi}\right]\right),$$

$$Ep_i(\varphi) = mgR(1-\cos\varphi) \quad \text{i}$$

$$E_i(\varphi) = Ek_i(\varphi) + Ep_i(\varphi) = 2mR^2\cos^2\frac{\varphi}{2}\cdot$$

$$\cdot\left(-\frac{\left(\frac{g}{2R}\right)}{1+4\mu^2}\frac{1}{\cos^2\frac{\varphi}{2}}\left[(\pm 3\mu)\sin\varphi - (1-2\mu^2)\cos\varphi + \frac{1+4\mu^2}{2} + C_i e^{\mp 2\mu\varphi}\right]\right) +$$

$$+ mgR(1-\cos\varphi).$$

For every separate branch of the phase portrait, there is a graphic presentation of alternation of F_N , P_μ , E_k , E_p and E from the initial moment of motion until the moment when heavy mass particles returns into equilibrium position (*Fig.14-18*).
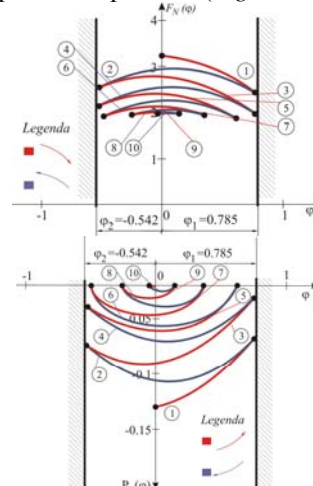
Fig.14. Curve of   Fig. 15. Curve of
pressure force   power alternation
alternation as a P_μ as a function of

function of angle φ *angle* φ

3.3. *Vibroimpact system based on oscillator moving freely along circle rough line*

Heavy mass particle is moving along circle rough line in vertical plane, with sliding Coloumb's type friction coefficient $\mu = tg\alpha_0$, with one elongation limiter on the right side (Fig.19). The limiter position is determined by the angle δ measured from the equilibrium position of heavy mass particle i.e. from the vertical line driven through the center of the circle.

Fig. 16. Graphic presentation of kinetic energy alternation in plane (Ek, φ)

Fig. 17. . Graphic presentation of potential energy alternation in plane (Ep, φ)
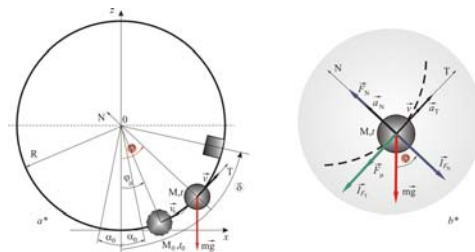
Fig. 19. System with one stabile elongation limiter, based on oscilator with one pellet: a* initial and derived position of the pellet; b* force plan

Fig.18.Graphic presentation of total

mechanical energy alternation in plane (E, φ)

For the complete description of the dynamics of heavy mass particle there are conditions matched to the differential (double) motion equation:

a^* initial conditions $\varphi_{(0)} = \varphi_0$ and

$\dot{\varphi}_{(0)} = \dot{\varphi}_0$;

b^* angular elongation limitation conditions, and collision conditions

$$\varphi_{ul_i} = \delta \ , \qquad \dot{\varphi}_{odl_i} = -k\dot{\varphi}_{ul_i} ,$$
$$i = 1,2,3,...,n \ ,$$

where: k- is impact coefficient within the range from $k = 0$, for ideal plastic impact, to $k = 1$, for ideal elastic impact; n- number of impacts until the heavy mass particle stopping on the circle rough line or to the interval where heavy mass particle continues to move without impact to the limiter.

Free motion of heavy mass particle along circle rough line is divided into corresponding motion intervals and sub intervals limited by direction of the friction force alternation.

The motion analysis is conducted by using the phase trajectory equation (8) with corresponding argument in dependance of motion interval.

3.3.1 Grafic visualization of the phase portrait of heavy mass perticle in the observed vibro-impact system

Based on real values of kinetic and geometry parameters of the system,

$$\delta = \frac{\pi}{4}[rad], \varphi_0 = \frac{\pi}{12}[rad], \dot{\varphi}_0 = 3,8\left[\frac{rad}{s}\right], R = 0,5[m],$$

$$\alpha_0 = 3, g = 9,81\left[\frac{m}{s^2}\right], m = 0,2[kg].$$

The phase portrait of heavy mass particle moving along circle rough line is showed (Fig.20.).
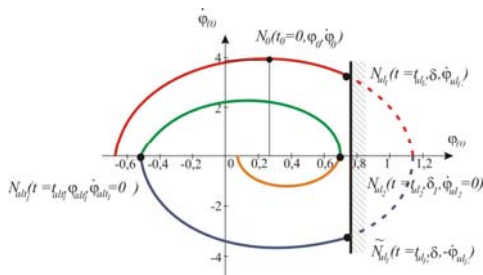
Fig. 20. Phase portrait of heavy mass particle moving along the circle rough line with sliding Coulomb's type friction coefficient $\mu = tg\,\alpha_0$ with limited elongations in a plane $(\varphi, \dot{\varphi})$

For the selected initial conditions and friction coefficient 3 (high degree of resistance), in the observed case there were one impact and one oscillation until the moment of arrestment.

The conditions needed for the heavy mass particle to have several impacts into angular elongation limiter in the observed vibro-impact system are:

$$\varphi_0 < \delta \quad \text{and}$$

$$\sqrt{2\frac{g}{R}(1-\cos\delta)} < \dot{\varphi}_0 < \sqrt{4\frac{g}{R} - 2\frac{g}{R}(1-\cos\delta)}$$

.

It can be concluded that for the lower friction coefficient and larger initial velocity, there are larger number of impacts and oscilations before the arrestment of heavy mass particle along rough circle line.

In order to get better graphic visualization of the motion analysis and energy analysis of the observed vibro-impact system the values for sliding friction coefficient will be changed (instead of $\alpha_0 = 3$ there is $\alpha_0 = 0,05$) and also for initial velocity of heavy mass particle (instead of $\dot{\varphi}_0 = 3,8\left[\frac{rad}{s}\right]$ there is $\dot{\varphi}_0 = 7\left[\frac{rad}{s}\right]$).

The rest of kinetic and geometry parameters remained the same.

Fazni portret teške materijalne tačke koja se kreće po kružnoj hrapavoj liniji u ovom slučaju data je na (sl.21).
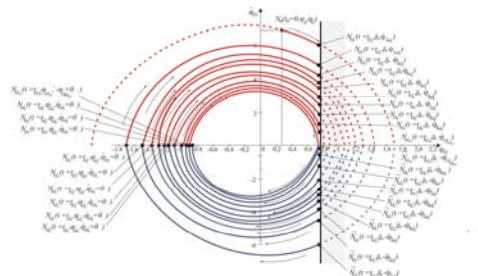
Fig. 21. Phase portrait of heavy mass particle moving along rough circle line with sliding Coulomb's type friction coefficient $\mu = 0,05$ with limited elongations in a plane $(\varphi, \dot{\varphi})$

3.3.2 Graphic visualization of energy analysis of the observed vibro-impact system

By using the analytical expressions for the peripendicular pressure force $F_{N,i}$, power originated of sliding *Coulomb's* type friction force $P_{\mu,i}$ of the heavy mass particle on the parabolic rough line, kinetic energy $E_{k,i}$, potential energy $E_{p,i}$ and total mechanical energy E_i ,

E_i , $\left(i=1,2,...,n.\right)$,

$F_{N,i} = mg\cos\varphi + mR \cdot$

$\cdot\left(\dfrac{2g}{\left(1+4tg^2\alpha_0\right)R\cos\alpha_0}\left[\cos\left(\varphi\pm\alpha_0\right)-2tg\alpha_0\sin\left(\varphi\pm\alpha_0\right)\right]+C_i e^{\mp 2\varphi tg\alpha_0}\right),$

$P_{\mu,i} = -\mu F_{N,i}R\dot\varphi = -\mu F_{N,i}R \cdot$

$\cdot\left\{-\sqrt{\dfrac{2g}{\left(1+4tg^2\alpha_0\right)R\cos\alpha_0}\left[\cos\left(\varphi\pm\alpha_0\right)-2tg\alpha_0\sin\left(\varphi\pm\alpha_0\right)\right]+C_i e^{\mp 2\varphi tg\alpha_0}}\right\},$

$Ek_i(\varphi) = \dfrac{1}{2}mR^2\dot\varphi_i^2(\varphi) = \dfrac{1}{2}mR^2 \cdot$

$\cdot\left(\dfrac{2g}{\left(1+4tg^2\alpha_0\right)R\cos\alpha_0}\left[\cos\left(\varphi\pm\alpha_0\right)-2tg\alpha_0\sin\left(\varphi\pm\alpha_0\right)\right]+C_i e^{\mp 2\varphi tg\alpha_0}\right),$

$Ep_i(\varphi) = mgR\left(1-\cos\varphi\right)$ and

$E_i(\varphi) = Ek_i(\varphi) + Ep_i(\varphi) = \dfrac{1}{2}mR^2 \cdot$

$\cdot\left(\dfrac{2g}{\left(1+4tg^2\alpha_0\right)R\cos\alpha_0}\left[\cos\left(\varphi\pm\alpha_0\right)-2tg\alpha_0\sin\left(\varphi\pm\alpha_0\right)\right]+C_i e^{\mp 2\varphi tg\alpha_0}\right)+$

$+mgR\left(1-\cos\varphi\right).$

For every separate branch of the phase portrait, there is a graphic presentation of alternation of F_N , P_μ , E_k , E_p and E from the initial moment of motion until the moment when heavy mass particles returns into equilibrium position (*Fig.22-26*).
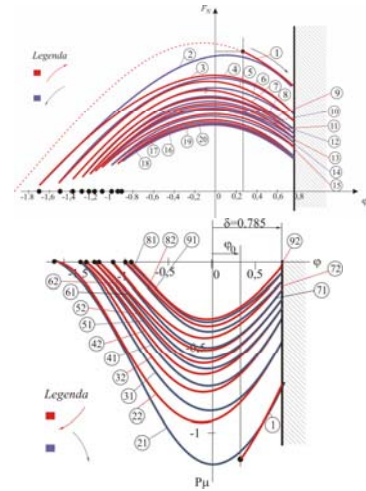
Fig.22. Curve of pressure force alternation as a function of angle φ

Fig. 23. Curve of power alternation P_μ as a function of angle φ
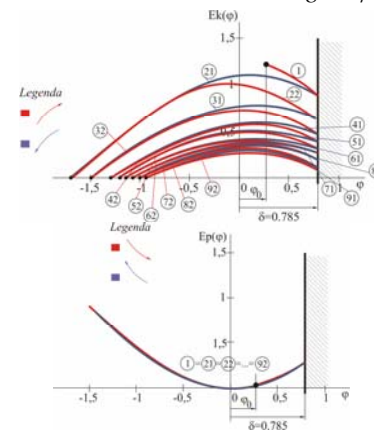
Fig. 24. Graphic presentation of kinetic energy alternation in plane $\left(Ek,\varphi\right)$

Fig. 25. Graphic presentation of potential energy alternation in plane $\left(Ep,\varphi\right)$
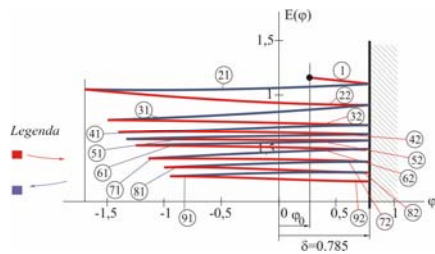
Fig. 26. Graphic presentation of total mechanical energy alternation in plane (E, φ)

Fig. 27. Clock mechanism

4.   The application of vibro-impact systems to the construction of vibro-machines

Vibro-impact motion is necessary for the technology process in many devices. In the next paragraph there are presented schematic presentations of vibro-impact machines () for the conducting the presented motion analysis and energy analysis of the observed vibro-impact systems with appropriate graphic visualization by the corresponding dynamic models. It should be mentioned that this paper represents the sequal of the paper in reference [14], but with difference that the paper referred to the straight line oscilator which can be also included as a special case of heavy mass particle motion along rough curvilinear route (the oscilation motion is enabled by elastic spring force instead of gravity).
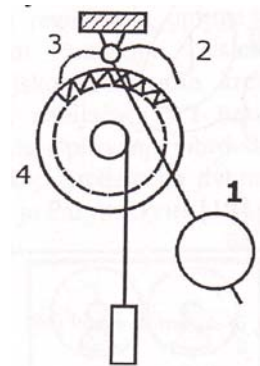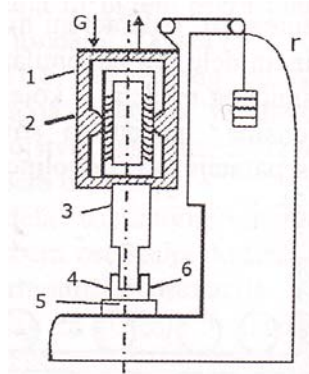
Fig. 28. Machine for ultra sound cutting
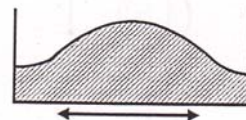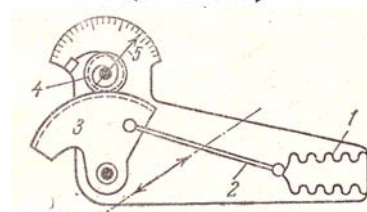
Fig. 29. Sieve   Fig. 30. Measuring   aparture

Fig. 33. Plane analog mechanism

Fig. 31. Schematic presentation of the vibro-impact system with curvilinear motion of heavy mass particle
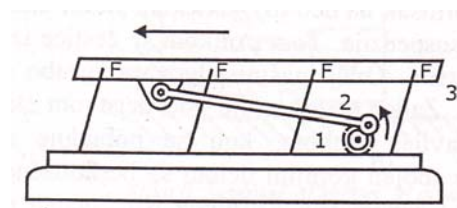
Fig. 34. Vibro-transporter
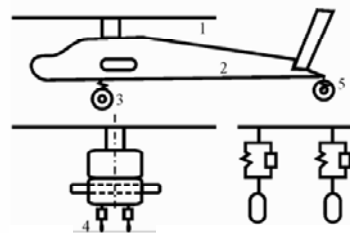
Fig. 35. Helicopter
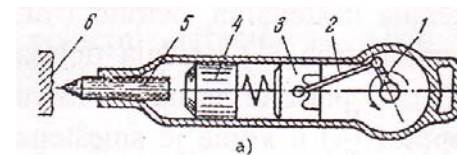
Fig. 36. Manual vibro-impact hammer

Fig. 32. The example of the mechanism for technical realization in the constructions such as elevators, holding tools etc.
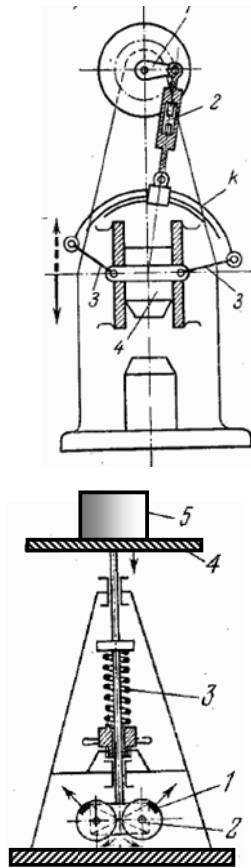
Fig. 37.
Vibroimpact
Hammer

Fig. 38.
Vibroimpact
platform
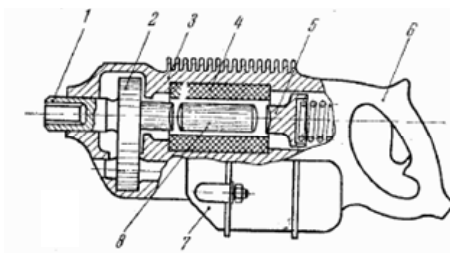
Fig. 39. Manual stroke-rotary hammer
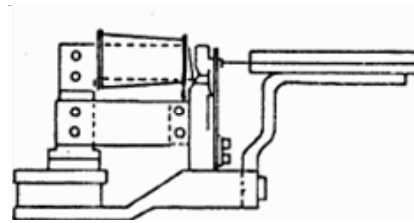
Fig. 40. Printer
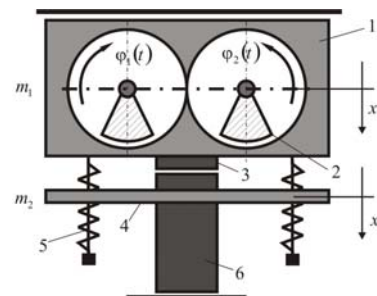
Fig. 41. Vibro-rammer

5. Concluding remarks

Non-linearity of the observed vibro-impact systems originate by the discontinuity of heavy mass particle angular velocity moving along rough curvilinear routes. Discontinuities of the angular velocity occure at the moment of impact of heavy mass particle into angular elongation limiters set on the right and on the left side, at the moment of direction alternation of motion of heavy mass particle (when the alternation occures) causing angular velocity and friction force alternation. This non-linearity is described mathematically for heavy mass particle by regular differential equation, more precisely by the second member, representing square angular velocity of generalized coordinate $\dot{\varphi}^2$. This corresponds to the case known in literature as a case of „turbulent" damping.

It should be pointed out that in observed vibro-impact systems there are trigger coupled singularities, i.e.

phenomena of bifurcation of equilibrium positions, because of the influence of sliding Coloumb's type friction force and angular velocity direction alternation.

For considered vibro-impact systems there is a common conclusion that non-impact motion represents free supressed oscilations of the dynamic system with one degree of freedom. Rough curvilinear lines are mutual detaining bond. Free oscillations of heavy mass particle along rough curvilinear lines, representing vibro-impact systems are divided into corresponding motion intervals and sub-intervals. Each interval or sub-interval are matched to differential motion equation from the group of regular homogenous non-linear differential equations.

Differential (double) motion equations for corresspponding interval and sub-intervals are coupled with initial motion conditions, imact conditions into elongation limiters and direction alternation conditions, which cause alternations of the friction force direction.

By analytic solving of differential (doble) motion equations, the analytical expressions for phase trajectories in plane $(\varphi, \dot{\varphi})$, are made, which are necessary for energy analysis, together with equation of curves of mechanical dependance for the energy analysis of the dynamics of vibro-impact systems.

The authors presented a good quality graphic visualization of the curves of alternations of the components of mechanical energies of vibro-impact system dynamics and motion analysis of representative point of system kinetic state during the kinetic (dynamics), by application of the analytical expressions and software package MathCad and user's package CorelDraw.

By the phase portraite analysis and graphic of kinetic energy E_K, potential energy E_P, total mechanical energy E, Pressure force F_N and power originated of

the sliding Coloumb's type friction force alternations, for all examples of free motion of heavy mass perticles along rough curvilinear lines, with one degree of freedom, it can be concluded:

The perpendicular pressure force on rough parabola, cicloid and circle line doesn't change its value.

* In the moment of impact of heavy mass particle into elongation limiter (any position), when the impact is ideal eleastic, the intensity of motion velocity is not changed.

* In the state of heavy mass particle direction alternation, the velocity is equal to zero. .

In the case of mutually retaining bond in the point of alternation pressure force has local minimum, and corresponding friction force alternates its direction.

The friction force direction is altered: in the point where angular velocity of heavy mass particle is equal to zero and at the point of impact of heavy mass particle into elongation limiter.

Power alternation, due to sliding friction Coloumb's type force follows the graphic of friction force alternation, but the power is always with negative argument and in the following representative points has lower values (decreasing from the higher lewel to the lower level). In heavy mass particle motion along rough curvilinear lines with elongation limiters, assuming that the impact is ideal elasctic, from the initail moment to the moment when the particle returned into equilibrium position, maximum value of power of sliding Coloumb's type force decreases constantly, no matter how many degrees of freedom are there in the observed system.

Kinetic energy, depending explicitely of angular velocity of heavy mass particle, permanently changed and its maximum value in the sequence motion intervals is decreased.

Potential energy depends of elongation, identical for all identical motion intervals, due to the fact that it depends of heavy mass particle weight and generalized coordinates, and the impact doesn't have influence to the potential energy, for it is due to the action of the conservative forces to the system.

Total mechanical energy of the system is constantly decreasing, i.e. in every following motion interval, the total mechanical energy of the system dynamics has lower value (at the point of impact into elongation limiter and point of angular velocity alternation).

In the fourth section of this paper, there is presented a series of models of technology processes, with real engineering constructions. The selected models are characteristic, presented in scientific monographies of the leading scientists and researchers from the field of vibro-impact dynamics. In every real model, the motion and energy analysis of the corresponding vibro-impact system can be done, by application of the methodology presented in this paper, being continuation of the author's own research presented in reference [14].

REFERENCES

[1]   Babickii V. I., Kolovskii M.Z., *Vibrations of linear system with limiters, and excited by random excitation*, *Mehanika tverdogo tela*, No 3,1967. (in Russian).

[2]   Babickii V. I.: *Theory of vibro-impact systems*, Moskva, "Nauka", 1978. (in Russian).

[3]   Babickii V. I., Kolovskii M.Z., *Investigation of the vibro-impact systems by resonant regimes*, *Mehanika tverdogo tela*, No 4,1976. (in Russian).

[4]   Bapat, C. N., Popplewell N., *Several Similar Vibroimpact Systems*, *Journal of Sound and Vibration,* 1987, 113 (1), pp. 17-28.

[5]   Bačlić, B. S., Atanacković, T. M., *Stability and creep of a fractional derivative order viscoelastic Rod*, Bulletin T, CXXI de L'Academie Serbe des Sciences st de Arts - 2000, Class des Sciences mathematques et naturelles Sciences mathematiques, No. 25, 115-131.

[6]   Bapat, C. N., *Impact-Pair under Periodic Exitation*, Journal of Sound and Vibration, 1988, 120 (1), pp. 53-61.

[7]   Dimentberg M., *Pseudolinear vibro-impact systems: Non-white random excitation*, Nonlinear Dynamics, Volume 9, Number 4/ April, 1996, pp. 327-332.

[8]   Hedrih (Stevanović) K., (2004), *Discrete Continuum Method,* COMPUTATIONAL MECHANICS, WCCM VI in conjunction with APCOM'04, *Beijing, China,* © 2004 Tsinghua University Press & Springer-Verlag, pp. 1-11, CD.

[9] Hedrih (Stevanović) K., (2006), *Modes of the Homogeneous Chain Dynamics*, Signal Processing, Elsevier, 86(2006), 2678-2702.. ISSN:0165-1684. www.sciencedirect.com/science/journal

[10] Hedrih (Stevanović) K., *Free and forced vibration of the heavy material particle along line with friction*: Direct and inverse task of the theory of vibrorheology, 7th EUROMECH Solid Mechanics Conference, J. Ambrósio et.al. (eds.), Lisbon, Portugal, September 7-11, 2009, CD –MS-24, Paper 348, pp. 1-20.

[11] Hedrih (Stevanović) K., *Vibrations of a Heavy Mass Particle Moving along a Rough Line with Friction of Coulomb Type*, ©Freund Publishing House Ltd., International Journal of Nonlinear Sciences & Numerical Simulation 10(11): 1705-1712, 2009. Vol.11, No.3 March 2010, pp. 203-210.

[12] Hedrih (Stevanović) K., *Discontinuity of kinetic parameter properties in nonlinear dynamics of mechanical systems*, Invited Keynote Lecture, Proceedings of the 9th Brazilian Conference on Dynamics, Control and Their Applications, DINCON , Serra Negra, 2010, pp. 8-40. (SP - ISSN 2178-3667).

[13] Hedrih (Stevanović) Katica (2009), *Phase plane method applied to the optimal control in nonlinear dynamical systems – Heavy material particle oscillations along rough circle line with friction*: Phase portraits and optimal control 10th conference on

DYNAMICAL SYSTEMS THEORY AND APPLICATIONS, December 7-10, 2009. Łódź, Polan (submitted)

[14] Hedrih (Stevanović) K., Jović S., *Models of Technological Processes on the Basis of Vibro-impact Dynamics*, Scientific Technical Review, Vol.LIX,No.2,2009,pp.51-72.

[15] Hedrih (Stevanović) K., Raičević V., Jović S., *Vibro-impact of a Heavy Mass Particle Moving along a Rough Circle with Two Impact Limiters*, ©Freund Publishing House Ltd., International Journal of Nonlinear Sciences & Numerical Simulation ISSN: 1565-1339, Volume 11, NO.3, pp.211-224, 2010.

[16] Hedrih (Stevanović) K., Raičević V., Jović S., *„VIBROIMPACT SYSTEM DYNAMICS: HEAVY MATERIAL PARTICLE OSCILLATIONS ALONG ROUGH CIRCLE WITH TWO SIDE MOVING IMPACT LIMITS"*, The Symposium DyVIS (Dynamics of Vibroimpact Systems) ICoVIS - 2th International Conference on Vibroimpact Systems, *6-9 January 2010.* School of Mechanical Engineering & Automation Northeastern University, Shenyang, Liaoning Province, P. R. China, pp.79-86.

[17] Hedrih (Stevanović) K., Raičević V., Jović S., *Phase Trajectory Portrait of the Vibro-imact Forced Dynamics of Two Mass Particles along Rough Circle*, 3rd International Conference on *Nonlinear*

Science and Complexity, Ankara, Turkey, Çankaya Üniversitesi, 28-31 Jul, 2010 (to appear).

[18] Hedrih (Stevanović) K., Raičević V., Jović S., *The phase portrait of the vibro-imact dynamics of two mass particle motions along rough circle*, 3 rd International conference "Nonlinear Dynamics – 2010", Kharkov, Ukraine, 21-24 Septembar, 2010, pp.84-89.

[19] Hedrih (Stevanović) K., Jović S., *„Vibroimpact system dynamics: Heavy material particle oscillations along rough circle with one side impact limit" ,* 10th Conference on Dynamical systems- theory and applications (DSTA) Lodz, Decembar 7-10, 2009 Poland. Procedings Volume 1, pp.213-220.

[20] Hedrih (Stevanović) K., Jović S., *„Energy of the vibroimpact system dynamics: Heavy material particle oscillations along rough circle with one side impact limit"*, 6-th IFAC INTERNATIONAL WORKSHOP on Knowledge and technology transfer in/to developing countries: automation and infrastructure, Hotel Metropol Resort, Ohrid Republic of Macedonia, Septembar 26-29, 2009 (is uploaded to the DECOM-TT 2009 web site with ID number D65).

[21] Hedrih (Stevanović) K., Jović S., *„Energy of the vibro-impact systems with Coulomb's type frictions"*, ESMC Lisbon 2009 Minisymosium MS-24 Kinetics, Control and Vibrorheology

KINCONVIB-2009, 7-11 Septembar 2009. pp. 43-47.

[22] Jović S., (2009). *Energijska analiza dinamike vibroudarnih sistema*, magistarski rad, str. 239, odbranjen 06. Novembra 2009. Fakultet tehničkih nauka u Kosovskoj Mitrovici Univerziteta u Prištini.

[23] Jović S., (2010). *Energijska analiza dinamike vibroudarnih sistema sa krivolinijskim putanjama i neidealnim vezama*, doktorska disertacija, str. 335, bila na uvid javnosti, očekuje se odbrana do završetka kalendarske godine. Fakultet tehničkih nauka u Kosovskoj Mitrovici Univerziteta u Prištini.

[24] Hinrichs N., Oestreich M., Popp K., 1997, *Dynamics of oscillators with impact and friction*, *Chaos, Solitons and Fractals*, **8**, 4, 535-558

[25] Kobrinskii A. E., Kobrinskii A. A., *Vibroudarni sistemi*, Moskva, Nauka, 1973

[26] Mitić Sl., *Стабилност детерминистичких и стохастичких процеса у виброударним системима*, 1994. Mašinski fakultet Niš, doktorska disertacija, mentor Hedrih (Stevanović) K..

[27] Mitić Sl., Hedrih K., *Pregled savremenih saznanja o vibroudarnim sistemima*, I deo-Klasifikacija vibroudarnih sistema sa dinamičkim modelima, str. 758-763.,br. 11-12, Tehnika, obl.Mašinstvo, godina XV-1991.

[28] Mitić Sl., Hedrih K., *Pregled savremenih saznanja o vibroudarnim sistemima*, II deo-Pregled metoda istraživanja, str. 231-235.,br. 3-4, Tehnika,

obl. Mašinstvo, godina XVI-1992.

[29] Mitić Sl., Hedrih K., *Pregled savremenih saznanja o vibroudarnim sistemima*, III deo-Fazne trajektorije regulisanih vibroudarnih procesa kod jednodimenzionih udarnih prigušivača, 8 str., Tehnika, obl. Mašinstvo, godina XVIII-1994, 43, br. 1-2, M1-M5.

[30] Mitić Sl., Hedrih K., *Pregled savremenih saznanja o vibroudarnim sistemima*, IV deo-Fazne trajektorije vibroudarnih procesa u torzionom oscilatoru sa medjusobno kruto vezanim udarnim masama, 8 str., Tehnika, obl. Mašinstvo, godina XVIII-1994,43, br.7, M25-M29.

[31] Pavlovskaia E., Wiercigroch M., 2003, *Periodic solution finder for an impact oscillator with a drift*, *Journal of Sound and Vibration*, **267**, 4, 893-911

[32] Pavlovskaia E., Wiercigroch M., Woo K.-C., Rodger A.A., 2003, *Modelling of ground moling dynamics by an impact oscillator with a frictional slider*, *Meccanica*, **38**, 1, 85-97.

[33] Peterka F., 1996, *Bifurcations and transition phenomena in an impact oscillator*, *Chaos, Solitons and Fractals*, **7**, 10, 1635-1647.

[34] Peterka F., *Laws of Impact Motion of Mechanical Systems with one Degree of Freedom*: Part I - Theoretical Analysis of n- Multiple (1/n) - Impact Motions, Acta Technica CSAV, 1974, No 4, pp 462-473.

[35] Peterka F., *Laws of Impact Motion of Mechanical Systems with one Degree of Freedom*: Part II - Resalts of Analogue Computer Modelling of the Motion, Acta Technica CSAV, 1974, No 5, pp 569-580

[36] Ragulskene V. L.: *Stereomehaničeskoi modeli udara*,Vibrotehnika, 1 (1), 1967.

[37] Rašković P. D., *Teorija oscilacija*, Naučna knjiga, 1965, str. 503.

[38] Stoker, J. J., (1950), *Nonlinear Vibrations,* Interscience Publish.

[39] Tung P.C., Shaw S. W., *A Method for the Improvement of Impact Printer Performance, Journal of Vibration*, Acoustics, Stress and Reliability in Design, oct. 1988, Vol. 110, pp.528-532.

A NEW DIRECT TIME INTEGRATION METHOD FOR THE EQUATIONS OF MOTION IN STRUCTURAL DYNAMICS

John T. Katsikadelis

Institute of Structural Analysis and Aseismic Research
School of Civil Engineering, national Technical University of Athens
Zografou Campus, 15773, Athens, Greece
e-mail: jkats@ central.ntua.gr

Abstract. A direct time integration method is presented for the solution of the equations of motion describing the dynamic response of structural linear and nonlinear multi-degree of freedom systems. It applies also to equations with variable coefficients. The proposed method is based on the concept of the analog equation, which converts the coupled N equations into a set of single term uncoupled second order ordinary quasi-static differential equations under appropriate fictitious loads unknown in the first instance. The fictitious loads are established from the integral representation of the solution of the substitute single term equations. The method is simple to implement. It is unconditionally stable and accurate. Several examples are presented, which demonstrate the efficiency of the method. The method can be extended to equations of order higher than two.

1. Introduction

In dynamic analysis the equations of motion are obtained by considering the dynamic equilibrium of the external, internal and inertia forces, namely

$$\mathbf{f}_I(t) + \mathbf{f}_D(t) + \mathbf{f}_S(t) = \mathbf{p}(t)$$

which may be written as

$$\mathbf{M}\ddot{\mathbf{u}} + \mathbf{f}_D(\dot{\mathbf{u}}) + \mathbf{f}_S(\mathbf{u}) = \mathbf{p}(t) \tag{1}$$

where $\mathbf{f}_I(t) = \mathbf{M}\ddot{\mathbf{u}}$ are the inertia forces, $\mathbf{f}_D(t) = \mathbf{f}_D(\dot{\mathbf{u}})$ the damping forces, $\mathbf{f}_S(t) = \mathbf{f}_S(\mathbf{u})$ the elastic forces and $\mathbf{p}(t)$ are the external excitation forces; $\mathbf{u} = \mathbf{u}(t)$ is the displacement vector. The problem consists in establishing the time history $\mathbf{u} = \mathbf{u}(t)$, where $t \in [0,T]$, $T > 0$, satisfying Eq. (1) with the initial conditions

$$\mathbf{u}(0) = \mathbf{u}_0, \quad \dot{\mathbf{u}}(0) = \dot{\mathbf{u}}_0 \tag{2}$$

The forces $\mathbf{f}_D(\dot{\mathbf{u}})$ and $\mathbf{f}_S(\mathbf{u})$ are in general non linear functions of their arguments. For linear problems they are given as $\mathbf{f}_D(t) = \mathbf{C}\dot{\mathbf{u}}$ and $\mathbf{f}_S(t) = \mathbf{K}\mathbf{u}$ and Eq. (1) becomes

$$\mathbf{M}\ddot{\mathbf{u}} + \mathbf{C}\dot{\mathbf{u}} + \mathbf{K}\mathbf{u} = \mathbf{p}(t) \tag{3}$$

where $\mathbf{M}$, $\mathbf{C}$ and $\mathbf{K}$ are the mass, damping and stiffness matrix of the structure, respectively.

In the last fifty years, significant advances have been made in the development and application of numerical methods to the solution of the equations of motion governing the dynamic behavior of structural systems. Many methods have been proposed either in the time or in frequency domain. The reader is advised to relevant literature, where extensive surveys of the various numerical solution methods and computational procedures for linear and nonlinear structural systems subjected to dynamic loads are presented, e.g. Hughes [1], Dokainish and Subbaraj [2], Subbaraj and Dokainish [3].

In this paper a new direct time integration method is presented based on the principle of the Analog Equation [4]. According to this principle the system of the N coupled equations of motion, linear or nonlinear, are replaced by a set of uncoupled linear single term quasi-static equations each of which includes only one unknown displacement and are subjected to appropriate unknown fictitious external loads. These fictitious loads are established numerically from the integral representation of the solution and the requirement that the equations of motion are satisfied at discrete times. The method is easy to implement. Numerical examples, including linear as well as non linear systems, are treated and the results are compared with those obtained by exact or other numerical methods. The method is accurate and unconditionally stable. The solution applies also to equations with variable coefficients as it is the case of time dependent mass, damping or stiffness.

2. The one-degree-of-freedom system

2.1. The AEM solution

For the linear one-degree-of-freedom system the initial value problem (2), (3) becomes

$$m\ddot{u} + c\dot{u} + ku = p(t) \tag{4}$$

$$u(0) = u_0, \qquad \dot{u}(0) = \dot{u}_0 \tag{5}$$

Let $u = u(t)$ be the sought solution. Then, if the operator d^2 / dt^2 is applied to it we have

$$\ddot{u} = q(t) \tag{6}$$

where $q(t)$ is a fictitious source, unknown in the first instance. Eq. (6) is the analog equation of (4). It indicates that the solution of Eq. (4) can be obtained by solving Eq. (6) with the initial conditions (5), if the $q(t)$ is first established. This is achieved as following.

Using the Laplace transform method we can obtain the solution of Eq. (6) in integral from

$$u(t) = u(0) + \dot{u}(0)t + \int_0^t q(\tau)(t - \tau)d\tau \tag{7}$$

Thus the initial value problem of Eqs (4), (5) is transformed into the equivalent Volterra integral equation for $q(t)$.
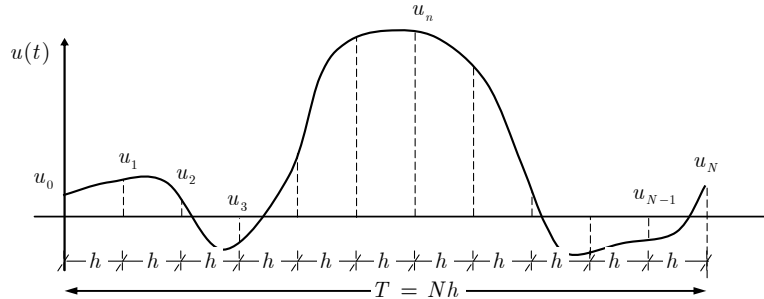
Figure 1. Discretization of the interval $[0, T]$ into N equal intervals $h = T / N$

Eq. (7) can be solved numerically within a time interval $[0, T]$ as following.

The interval $[0, T]$ is divided into N equal intervals $\Delta t = h$, $h = T / N$, in which $q(t)$ is assumed to vary according to a certain law, e.g. constant, linear etc. In this analysis $q(t)$ is assumed to be constant and equal to a weighted value in the interval h. That is

$$q_r^m = \alpha q_{r-1} + \beta q_r \tag{8}$$

where α, β are constants satisfying a constraint of the form

$$f(\alpha, \beta) = 1 \tag{9}$$

The values of these constants influence the stability, the convergence and the accuracy of the resulting numerical scheme.

Hence, Eq. (7) at instant $t = nh$ can be written as

$$
\begin{aligned}
u_n = u_0 &+ nh\dot{u}_0 \\
&+ \left[q_1^m \int_0^h (nh - \tau)d\tau + q_2^m \int_h^{2h} (nh - \tau)d\tau + \cdots + q_n^m \int_{(n-1)h}^{nh} (nh - \tau)d\tau \right]
\end{aligned}
\tag{10}
$$

which after evaluation of the integrals yields

$$
\begin{aligned}
u_n &= u_0 + nh\dot{u}_0 + c_1 \sum_{r=1}^{n-1} \big[2(n-r) + 1 \big] q_r^m + c_1 q_n^m \\
&= u_{n-1} + h\dot{u}_0 + 2c_1 \sum_{r=1}^{n-1} q_r^m + c_1 q_n^m
\end{aligned}
\tag{11}
$$

where

$$c_1 = \frac{h^2}{2} \tag{12}$$

The velocity is obtained by direct differentiation of Eq. (7) making use of the Leibnitz rule for the integral. Thus we have

$$\dot{u}(t) = +\dot{u}(0) + \int_0^t q(\tau)d\tau \tag{13}$$

Using the same discretization for the interval $[0, T]$ to approximate the integral in Eq. (13), we have

$$\dot{u}_n = \dot{u}_0 + c_2 \sum_{r=1}^{n-1} q_r^m + c_2 q_n^m \tag{14}$$
$$= \dot{u}_{n-1} + c_2 q_n^m$$

where

$$c_2 = h \tag{15}$$

Solving Eq. (14) for $\displaystyle\sum_{r=1}^{n-1} q_r^m$ and substituting in Eq. (11) gives

$$u_n = u_{n-1} + h\dot{u}_n - c_1 q_n^m \tag{16}$$

By virtue of Eq. (8), Eqs (16) and (14) can be further written as

$$\beta c_1 q_n - h\dot{u}_n + u_n = -\alpha c_1 q_{n-1} + u_{n-1} \tag{17}$$

$$-\beta c_2 q_n + \dot{u}_n = \dot{u}_{n-1} + \alpha c_2 q_{n-1} \tag{18}$$

Moreover, Eq. (4) at time $t = nh$ is written as

$$m q_n + c \dot{u}_n + k u_n = p_n \tag{19}$$

Eqs (17), (18) and (19) can be combined as

$$\begin{bmatrix} m & c & k \\ \beta c_1 & -h & 1 \\ -\beta c_2 & 1 & 0 \end{bmatrix} \begin{Bmatrix} q_n \\ \dot{u}_n \\ u_n \end{Bmatrix} = \begin{bmatrix} 0 & 0 & 0 \\ -\alpha c_1 & 0 & 1 \\ \alpha c_2 & 1 & 0 \end{bmatrix} \begin{Bmatrix} q_{n-1} \\ \dot{u}_{n-1} \\ u_{n-1} \end{Bmatrix} + \begin{Bmatrix} 1 \\ 0 \\ 0 \end{Bmatrix} p_n \tag{20}$$

Since $m \neq 0$, the coefficient matrix in Eq. (20) is not singular for sufficient small h and the system can be solved successively for $n = 1, 2, \ldots$ to yield the solution u_n and the derivatives $\dot{u}_n$, $\ddot{u}_n = q_n$ at instant $t = nh \leq T$. For $n = 1$, the value q_0 appears in the right hand side of Eq. (20). This quantity can be readily obtained from Eq. (4) for $t = 0$. This yields

$$q_0 = \left(p_0 - c\dot{u}_0 - ku_0 \right) / m \tag{21}$$

Eq. (20) can be also written as

$$\mathbf{U}_n = \mathbf{A}\mathbf{U}_{n-1} + \mathbf{b}\bar{p}_n, \qquad n = 1, 2, \ldots N \tag{22}$$

in which

$$\mathbf{U}_n = \begin{Bmatrix} q_n \\ \dot{u}_n \\ u_n \end{Bmatrix}, \qquad \mathbf{A} = \begin{bmatrix} 1 & 2\xi\omega & \omega^2 \\ \beta c_1 & -h & 1 \\ -\beta c_2 & 1 & 0 \end{bmatrix}^{-1} \begin{bmatrix} 0 & 0 & 0 \\ -\alpha c_1 & 0 & 1 \\ \alpha c_2 & 1 & 0 \end{bmatrix} \tag{23a,b}$$

$$\mathbf{b} = \begin{bmatrix} 1 & 2\xi\omega & \omega^2 \\ \beta c_1 & -h & 1 \\ -\beta c_2 & 1 & 0 \end{bmatrix}^{-1} \begin{Bmatrix} 1 \\ 0 \\ 0 \end{Bmatrix} \tag{23c}$$

where $\bar{p}_n = p_n / m$; $\omega = \sqrt{m / k}$ is the eigenfrequency and $\xi = c / 2m\omega$ the damping ratio. The recurrence formula (22) can be employed to construct the solution algorithm. However, the solution procedure can be further simplified. Thus, applying Eq. (22) for $n = 1, 2, \ldots$ we have

$$\begin{aligned} \mathbf{U}_1 &= \mathbf{A}\mathbf{U}_o + \mathbf{b}\bar{p}_1 \\ \mathbf{U}_2 &= \mathbf{A}\mathbf{U}_1 + \mathbf{b}\bar{p}_2 \\ &= \mathbf{A}(\mathbf{A}\mathbf{U}_o + \mathbf{b}\bar{p}_1) + \mathbf{b}\bar{p}_2 \\ &= \mathbf{A}^2\mathbf{U}_o + \mathbf{A}\mathbf{b}\bar{p}_1 + \mathbf{b}\bar{p}_2 \\ \cdots = &\; \cdots\cdots\cdots\cdots\cdots\cdots\cdots \\ \mathbf{U}_n &= \mathbf{A}^n\mathbf{U}_o + (\mathbf{A}^{n-1}\bar{p}_1 + \mathbf{A}^{n-2}\bar{p}_2 + \ldots \mathbf{A}^0\bar{p}_n)\mathbf{b} \end{aligned} \tag{24}$$

Apparently, the last of Eqs (24) gives the solution vector $\mathbf{U}_n$ at instant $t_n = nh$ using only the known vector $\mathbf{U}_0$ at $t = 0$. The matrix $\mathbf{A}$ and the vector $\mathbf{b}$ are computed only once.

2.2 Stability of the numerical scheme

The matrix $\mathbf{A}$ is the amplification matrix. In order that the solution is stable $\mathbf{A}^n$ must be bounded. This is true if

$$\lim_{n\to\infty} \mathbf{A}^n = 0 \tag{25}$$

which is satisfied if the spectral radius of $\mathbf{A}$

$$\rho(\mathbf{A}) = \max\left\{ |\rho_1|, |\rho_2|, |\rho_3| \right\} \leq 1 \tag{26}$$

If $\rho(\mathbf{A}) < 1$ the method is strongly stable.
We examine the case where Eq. (9) is of the form $\alpha + \beta = 1$, that is the constraint is linear. The eigenvalues of $\mathbf{A}$ are

$$\rho_1 = 0 \tag{27a}$$

$$\rho_2 = \frac{4(2b-1)s\xi + 4 - s^2}{4 + 2bs^2 + 8\beta s\xi} + i\frac{+s\sqrt{16(1-\xi^2) - 8s\xi(1-2b) - s^2(1-2b)^2}}{4 + 2bs^2 + 8\beta s\xi} \qquad (27b)$$

$$\rho_3 = \frac{4(2b-1)s\xi + 4 - s^2}{4 + 2bs^2 + 8\beta s\xi} - i\frac{+s\sqrt{16(1-\xi^2) - 8s\xi(1-2b) - s^2(1-2b)^2}}{4 + 2bs^2 + 8\beta s\xi} \qquad (27c)$$

where it has been set $s = h\omega$.
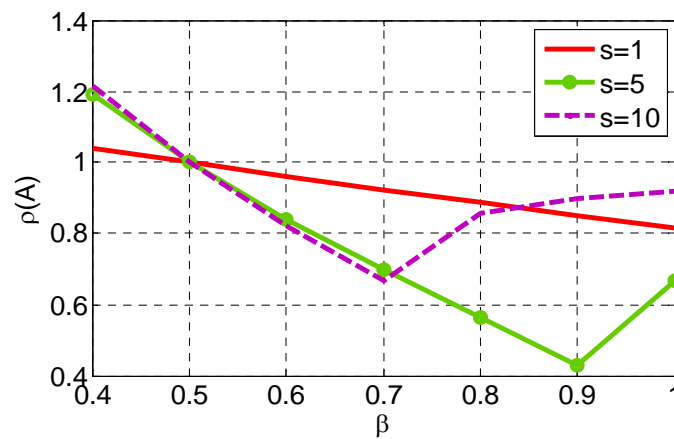
Figure 2. Spectral radius $\rho(A)$ versus parameter β for various values of $s = h\omega$ ($\xi = 0$).

We distinguish the following cases

(i) $\xi = 0$. It can be shown that for $\beta = 1/2$ we have

$$\left|\rho_2\right| = \left|\rho_3\right| = 1 \qquad (28a)$$

while for $\beta > 1/2$

$$\left|\rho_2\right| = \left|\rho_3\right| < 1 \qquad (28b)$$

This is shown in Fig. 2.

(ii) $0 < \xi < 1$. Fig. 3 shows the variation of the spectral radius versus the values of β for various values of ξ. We see that for $\xi > 0.125$ the method is strongly stable for any value of β in the interval $[0,1]$. Apparently, for a given set of values of s and ξ a region of values of β can be established for which strong stability is ensured.
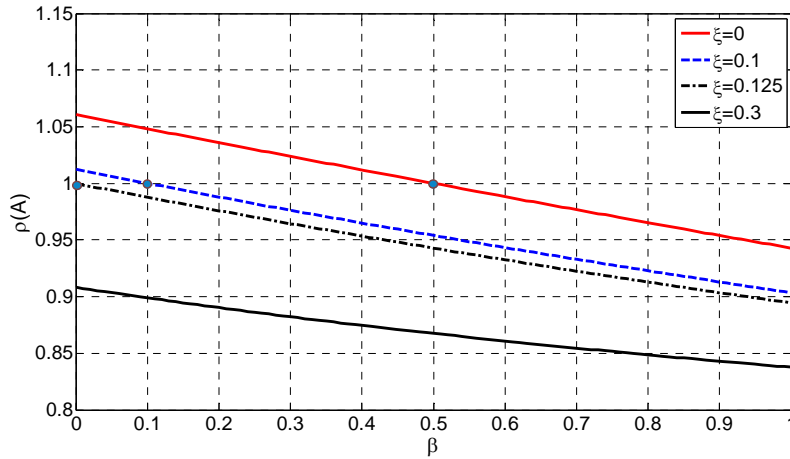
Figure 3. Spectral radius versus parameter β for various of the damping ratio ξ ($s = 5$).

2.3 Error analysis and convergence

The error is due to the approximation of the integrand in the integral of Eq. (7) in the n integration interval $[(n-1)h, nh]$

$$\int_{t_0}^{t_1} f(\tau)d\tau, \quad t_0 = (n-1)h, \ t_1 = nh \tag{29}$$

where

$$f(\tau) = q(\tau)(t_1 - \tau) \tag{30}$$

which in this analysis is approximated as

$$\tilde{f}(\tau) = q^m(t_1 - \tau) \tag{31}$$

Expanding $f(\tau)$ and $\tilde{f}(\tau)$ in Taylor series at $\tau = t_0$ and evaluating the integral of $f(\tau) - \tilde{f}(\tau)$ in the interval $[t_0, t_1]$ we find

$$\int_{t_0}^{t_1} [f(\tau) - \tilde{f}(\tau)]d\tau = (q_0 - q_0^m)h^2 + (q_1 - q_0 + q_0^m)\frac{h^2}{2}$$
$$= \frac{3}{2}q_0^m h^2 \tag{32}$$

Therefore the convergence of the algorithm is $O(h^2)$.

2.4 Accuracy

For free vibrations, the numerical solution can be written in terms of the eigenvalues

$$u_n = c_1' \rho_2^n + c_2' \rho_3^n \qquad (\rho_3 = 0) \qquad (33)$$

It can be shown that for $0 \le \xi < 1$, $0.5 \le \beta < 1$ and $0 < s$ the eigenvalues ρ_2, ρ_3 are complex conjugate and the solution of Eq. (33) can be written as

$$u_n = r^n (c_1 \sin n\theta + c_2 \cos n\theta) \qquad (34)$$

where $r = \sqrt{a^2 + b^2}$, $\qquad \theta = \tan^{-1}(b/a)$, $\qquad a = \mathrm{Re}(\rho_2)$, $\quad b = \mathrm{Im}(\rho_2)$

The corresponding exact solution is given as

$$u_n = e^{-\xi \omega t_n} (\overline{c}_1 \sin \omega_D t_n + c_2 \cos \omega_D t_n), \quad \omega_D = \sqrt{1 - \xi^2}, \quad t_n = nh \qquad (35)$$
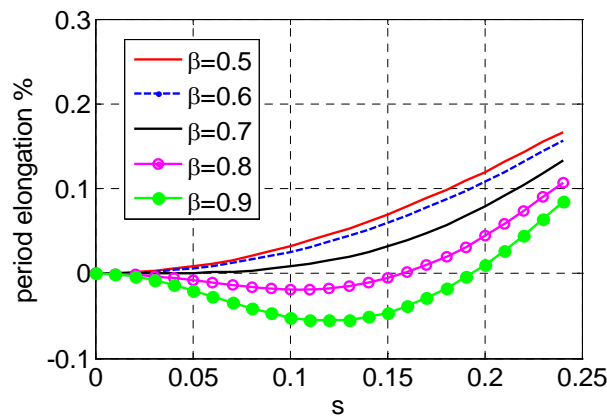
Figure 4. Period elongation versus s for various values of the parameter ($\xi = 0$).

Comparison of these two solutions could show the accuracy of the numerical scheme. However, to avoid a rather complicated investigation, the period elongation and the amplitude decay of the free undamped vibration can be defined as measures of the relative accuracy. Thus, if T and $\overline{T}$ are the exact and the approximate periods, respectively, we define the period elongation

$$pe = \frac{\overline{T} - T}{T} = \frac{s}{\theta} - 1 \qquad (36)$$

Fig. 4 shows the dependence of the period elongation on $s = \omega h$ for various values of β. Apparently, s should be small to avoid period elongation. Since for $\xi = 0$, $\beta = 1/2$ it is $|\rho_2| = |\rho_3| = 1$, we obtain $r^n = 1$. Thus, there is no amplitude decay, provided that $\beta = 1/2$.

2.5 Numerical examples

Following the steps of the previous solution procedure a MATLAB program has been written and various example problems have been solved.
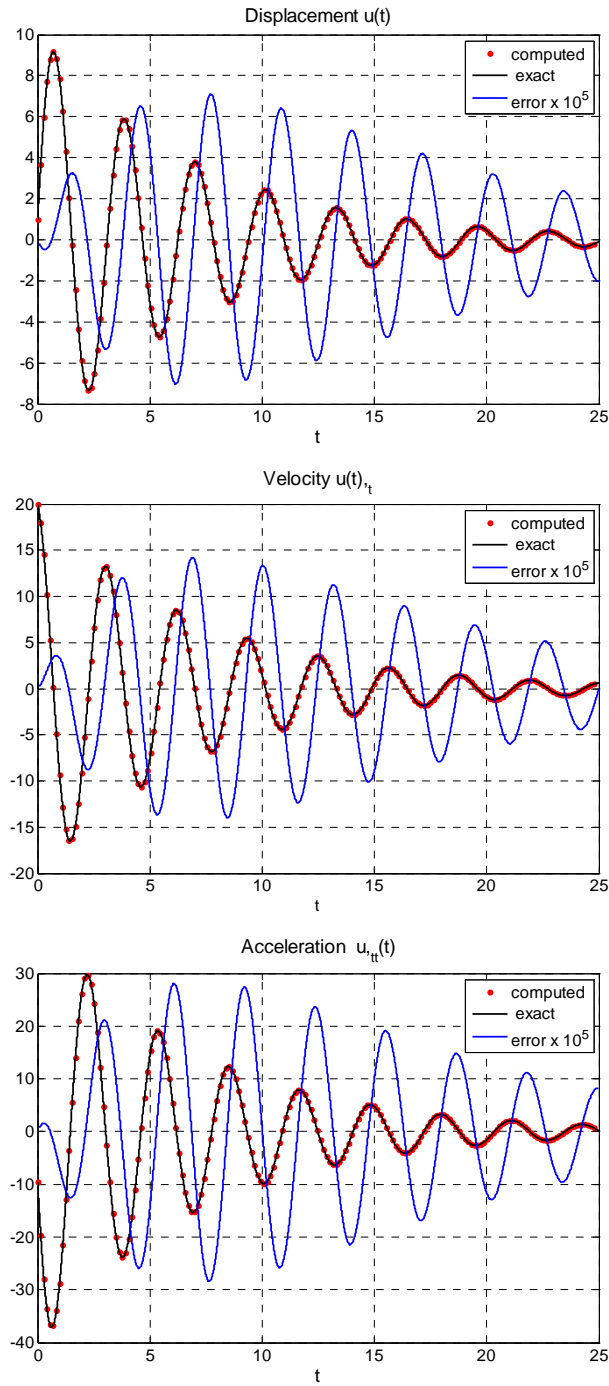
Figure 5. Displacement, velocity, acceleration and respective errors in Example 1, Case (i)

Example 1. Free and forced damped vibrations. Error discussion
Eq. (4) has been solved with data: $m = 1$, $\xi = 0.07$, $\omega = 2$, $u_0 = 1$, $\dot{u}_0 = 20$, $T = 25$, $h = 1/500$, $\beta = 0.5$. Case (i) $p(t) = 0$; case (ii) $p(t) = p_0 H(t)$, $p_0 = 10$; $H(t)$ is the Heaviside function.

The analytical solution is

$$u(t) = \left[\frac{\dot{u}(0) + u(0)\xi\omega}{\omega_D} \sin\omega_D t + u(0)\cos\omega_D t \right] e^{-\xi\omega t}$$

$$+ \frac{p_0}{k}\left[1 - \left(\cos\omega_D t + \frac{\xi}{\sqrt{1-\xi^2}}\sin\omega_D t \right) e^{-\xi\omega t} \right] \tag{37}$$

where $\omega_D = \omega\sqrt{1-\xi^2}$. Fig. 5 and Fig. 6 show the obtained solution together with the error $e = u - u_{exact}$ for the two load cases. Moreover, in Fig. 7 the variation of the computed error $e = e(h)$, $h(k) = 1/500k$, $k = 1,2,\ldots,8$ has been plotted, which verifies that the convergence is of $O(h^2)$.
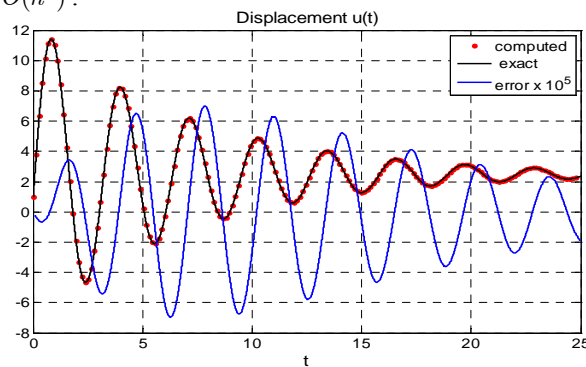
Figure 6. Displacement and error in Example 1, Case (ii)
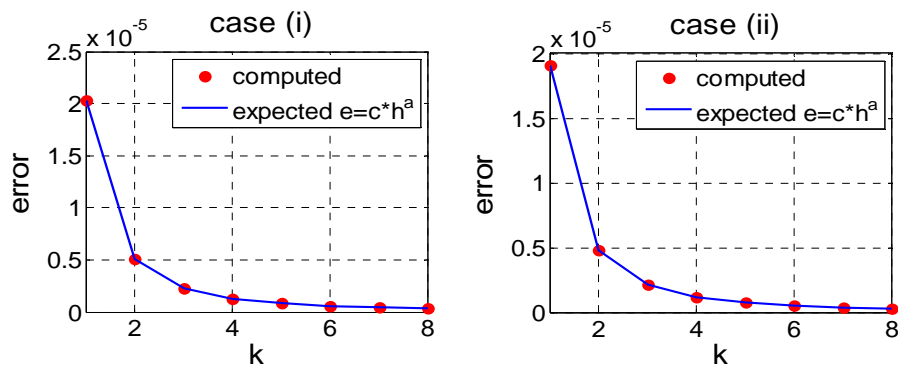
Figure 7. Computed and expected error $e = e(h)$ in Example 1; $h(k) = 1/500k$, $k = 1,2,\ldots,8$

$$e = ch^2, \quad c = e(1)/h(1).$$

3. Variable coefficients

So far we have developed the method for the solution of the equation of motion with constant coefficients. Obviously, if the coefficients m, c and k are functions of the independent variable t, the previously described solution procedure remains the same except that the elements m, c, k in the first row of the coefficient matrix in the left hand side of Eq. (20) depend on time. Therefore, this coefficient matrix in the respective solution algorithm must be reevaluated in each step. In the following, the efficiency of the method is demonstrated by solving an equation with variable coefficients.
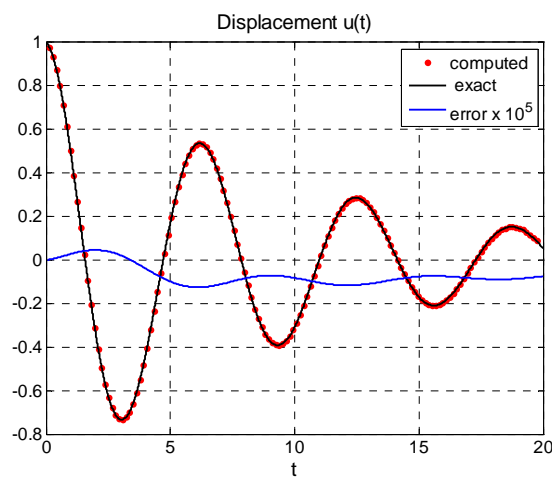
Figure 8. Solution u and error $u - u_{exact}$ in Example 2.

Example 2.
We consider the initial value problem

$$(1 + t^2)\ddot{u} + t\dot{u} + e^{1/(1+t)}u = p(t), \qquad u_0 = 1, \ \dot{u}_0 = -0.1 \qquad (38)$$

where
$$p(t) = -0.01e^{-0.1t}[(99 + 10t + 99t^2)\cos t + (-20 + 100t - 20t^2)\sin t - 100e^{1/(1+t)}\cos t].$$

The equation admits an exact solution $u_{exact}(t) = e^{-0.1t}\cos t$. The solution for $T = 20$ is shown in Fig. 8 as compared with the exact one.

4. Multi-degree-of-freedom systems

The developed solution algorithm can be applied to systems of N linear equations of motion describing the response of multi-degree-of-freedom systems. The initial value problem is described by Eq. (3) with initial conditions (2)

The solution procedure described in Section 2 may be also applied to this case provided that the coefficients m, c, k and the quantities $u_0, \dot{u}_0, u_n, \dot{u}_n, q_n, p_n$ are replaced with the coefficients matrices $\mathbf{M}, \mathbf{C}, \mathbf{K}$ and the vectors $\mathbf{u}_0, \dot{\mathbf{u}}_0, \mathbf{u}_n, \dot{\mathbf{u}}_n, \mathbf{q}_n, \mathbf{p}_n$, respectively, and the scalar operations by matrix operations. Thus Eqs (17), (18) and (19) become

$$
\begin{bmatrix}
\mathbf{M} & \mathbf{C} & \mathbf{K} \\
\dfrac{c_1}{2}\mathbf{I} & -h\mathbf{I} & \mathbf{I} \\
-\dfrac{c_2}{2}\mathbf{I} & \mathbf{I} & \mathbf{0}
\end{bmatrix}
\begin{Bmatrix}
\mathbf{q}_n \\
\dot{\mathbf{u}}_n \\
\mathbf{u}_n
\end{Bmatrix}
=
\begin{bmatrix}
\mathbf{0} & \mathbf{0} & \mathbf{0} \\
-\dfrac{c_1}{2}\mathbf{I} & \mathbf{0} & \mathbf{I} \\
\dfrac{c_2}{2}\mathbf{I} & \mathbf{I} & \mathbf{0}
\end{bmatrix}
\begin{Bmatrix}
\mathbf{q}_{n-1} \\
\dot{\mathbf{u}}_{n-1} \\
\mathbf{u}_{n-1}
\end{Bmatrix}
+
\begin{Bmatrix}
\mathbf{I} \\
0 \\
0
\end{Bmatrix}
\mathbf{p}_n
\tag{39}
$$

$$
\mathbf{q}_0 = \mathbf{M}^{-1}(\mathbf{p}_0 - \mathbf{C}\dot{\mathbf{u}}_0 - \mathbf{K}\mathbf{u}_0), \qquad \det(\mathbf{M}) \neq 0
\tag{40}
$$

Eq. (39) is solved for $n = 1, 2, \ldots$
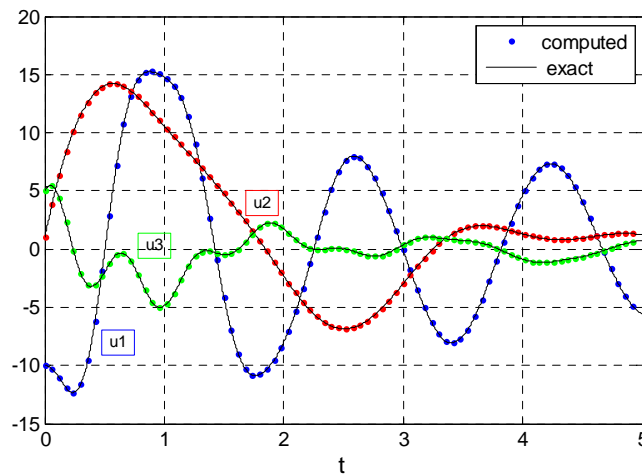
Figure 9. Solution $\mathbf{u} = \begin{Bmatrix} u_1 & u_2 & u_3 \end{Bmatrix}^T$ in Example 3.

Example 3.
We consider the initial value problem for the system of three equations

$$
\begin{bmatrix}
52 & 10 & 20 \\
10 & 150 & 30 \\
20 & 30 & 441
\end{bmatrix}
\begin{Bmatrix}
\ddot{u}_1 \\
\ddot{u}_2 \\
\ddot{u}_3
\end{Bmatrix}
+
\begin{bmatrix}
31.3093 & 26.0236 & 72.3331 \\
26.0236 & 176.1373 & 60.5706 \\
72.3331 & 60.5706 & 579.9713
\end{bmatrix}
\begin{Bmatrix}
\dot{u}_1 \\
\dot{u}_2 \\
\dot{u}u_3
\end{Bmatrix}
$$
$$
+
\begin{bmatrix}
1472 & 407 & 5553 \\
407 & 1001 & 4154 \\
5553 & 4154 & 43516
\end{bmatrix}
\begin{Bmatrix}
u_1 \\
u_2 \\
u_3
\end{Bmatrix}
=
\begin{Bmatrix}
1 \\
1 \\
1
\end{Bmatrix}
10H(t)
\tag{41}
$$

with initial conditions

$$\mathbf{u}_0 = \{-10 \quad 1 \quad 5\}^T, \quad \dot{\mathbf{u}}_0 = \{0 \quad 50 \quad 20\}^T \tag{42}$$

A proportional damping matrix $\mathbf{C}$ has been constructed with modal damping coefficients $\xi_1 = 0.3, \, \xi_2 = 0.05, \, \xi_3 = 0.09$. This ensures orthogonality of the damping matrix with respect to the modes ϕ_i of the free undamped vibrations. Thus the exact solution can be obtained using the modal superposition method. Results for $T = 5$ are shown in Fig. 9.

5. Nonlinear equations of motion

The solution procedure developed previously for the linear equations can be straightforward extended to nonlinear equations.
The nonlinear initial value problem for multi-degree of freedom systems is described as

$$\mathbf{M}\ddot{\mathbf{u}} + \mathbf{F}(\dot{\mathbf{u}}, \mathbf{u}) = \mathbf{p}(t) \tag{43}$$

$$\mathbf{u}(0) = \mathbf{u}_0, \, \dot{\mathbf{u}}(0) = \dot{\mathbf{u}}_0 \tag{44}$$

where $\mathbf{M}$ is $N \times N$ known coefficient matrix with $\det(\mathbf{M}) \neq 0$; $\mathbf{F}(\dot{\mathbf{u}}, \mathbf{u})$ is an $N \times 1$ vector, whose elements are nonlinear functions of the components of $\mathbf{u}, \dot{\mathbf{u}}$; $\mathbf{p}(t)$ is the vector of N given load functions and $\mathbf{u}_0, \dot{\mathbf{u}}_0$ given constant vectors.

The solution procedure is similar to that for the linear systems. Thus Eq. (43) for $t = 0$ gives the initial acceleration vector

$$\mathbf{q}_0 = \mathbf{M}^{-1}[\mathbf{p}_0 - \mathbf{F}(\dot{\mathbf{u}}_0, \mathbf{u}_0)], \qquad \mathbf{q}_0 = \ddot{\mathbf{u}} \tag{45}$$

Subsequently we apply Eq. (43) for $t = t_n$

$$\mathbf{M}\mathbf{q}_n + \mathbf{F}(\dot{\mathbf{u}}_n, \mathbf{u}_n) = \mathbf{p}_n \tag{46}$$

Apparently, the second and third of Eqs (39) are valid in this case and can be written as

$$\begin{bmatrix} -h\mathbf{I} & \mathbf{I} \\ \mathbf{I} & \mathbf{0} \end{bmatrix} \begin{Bmatrix} \dot{\mathbf{u}}_n \\ \mathbf{u}_n \end{Bmatrix} = \begin{bmatrix} \mathbf{0} & \mathbf{I} \\ \mathbf{I} & \mathbf{0} \end{bmatrix} \begin{Bmatrix} \dot{\mathbf{u}}_{n-1} \\ \mathbf{u}_{n-1} \end{Bmatrix} + \begin{bmatrix} \dfrac{c_1}{2}\mathbf{I} \\ -\dfrac{c_2}{2}\mathbf{I} \end{bmatrix} \mathbf{q}_n + \begin{bmatrix} -\dfrac{c_1}{2}\mathbf{I} \\ \dfrac{c_2}{2}\mathbf{I} \end{bmatrix} \mathbf{q}_{n-1} \tag{47}$$

Eqs (46) and (47) are combined and solved for $\mathbf{q}_n, \dot{\mathbf{u}}_n, \mathbf{u}_n$ with $n = 1, 2, \ldots ..$

Example 4.
The method is employed to solve the initial value problem for the Duffing equation

$$\ddot{u} + 0.2\dot{u} + u + u^3 = p(t) \tag{48}$$

$$u(0) = 0, \quad \dot{u}(0) = 1 \tag{49}$$

For $\quad p(t)e^{-\xi t}[(\xi^2 \sin t - 2\xi \cos t - \sin t) - C(\xi \sin t - \cos t) + B \sin t + A e^{-2\xi t}(\sin t)^3]$

Eq. (48) admits an exact solution $u_{exact}(t) = e^{-0.1t}\sin t$. The solution for $T = 25$ is shown in Fig. 10.
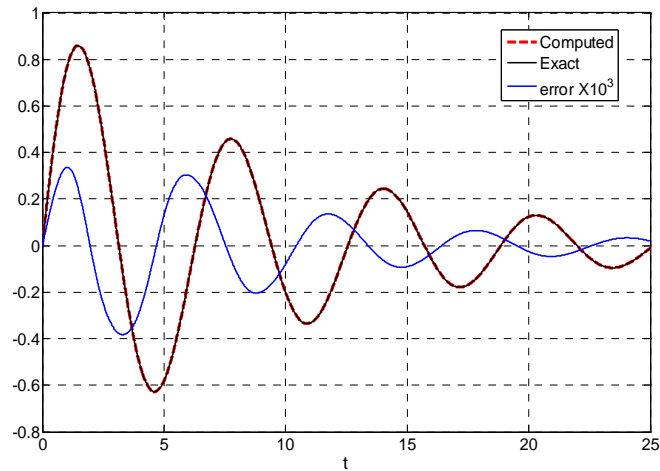
Figure 10. Solution u and error $u - u_{exact}$ in Example 4.

Example 5.
In this example we solve the initial value problem

$$ml_0\ddot{u} + EAu\left[2 - \frac{1}{\sqrt{x^2 + (1 + \delta_0 - v)^2}} - \frac{1}{\sqrt{x^2 + (1 + \delta_0 + v)^2}}\right] = 0 \quad (50a)$$

$$ml_0\ddot{v} + EA\left[2v + \frac{1 + \delta_0 - v}{\sqrt{x^2 + (1 + \delta_0 - v)^2}} - \frac{1 + \delta_0 + v}{\sqrt{x^2 + (1 + \delta_0 + v)^2}}\right] = 0 \quad (50b)$$

$$\begin{Bmatrix} u(0) \\ v(0) \end{Bmatrix} = \begin{Bmatrix} 0.066 \\ 0.050 \end{Bmatrix}, \qquad \begin{Bmatrix} \dot{u}(0) \\ \dot{v}(0) \end{Bmatrix} = \begin{Bmatrix} 0 \\ 0 \end{Bmatrix} \qquad (51)$$

The employed data are: $A = 3.14 \text{cm}^2$, $l_0 = 3.00\text{m}$, $m = 3\text{kNm}^{-1}\text{sec}^2$, $g = 9.81\text{m}/\text{sec}^2$, $\delta_0 = 0.065\,\text{m}$, $E = 2 \times 10^7 \text{kN}/\text{m}^2$. Fig. 11 shows the time histories of $u(t)$ and $v(t)$ as compared with those obtained with the mean acceleration method.
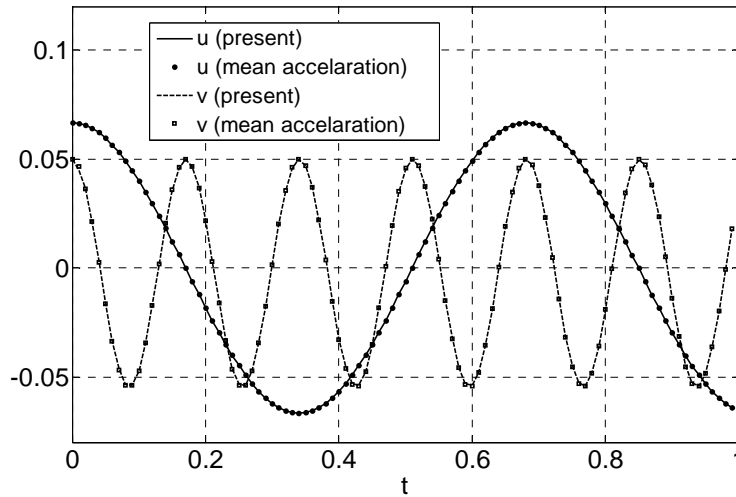
Figure 11. Displacements $u(t)$ and $v(t)$ in Example 5

6. Conclusions

An integral equation method has been developed for the numerical solution of second order linear and nonlinear differential equations. The coefficients may be variable. The resulting numerical scheme is applied to the solution of the equations of motion arising in structural dynamics. The method is simple to implement. It is unconditionally stable and accurate. Several examples are presented, which illustrate the method and demonstrate its efficiency. The method can be readily extended to equations of order higher than two.

References

[1] Hughes TJR (1987) *The finite element method*, Englewood Cliffs, NJ, USA: Prentice Hall Inc.
[2] Dokainish MA and Subbaraj K (1989) A Survey of Direct Time-integration Methods in Computational Structural Dynamics, *Computer and Structures*, **32**, pp.1371-1386.
[3] Subbaraj K and Dokainish MA (1989) A Survey of Direct Time-integration Methods in Computational Structural Dynamics, *Computer and Structures*, **32**, pp. 1387-1401.
[4] Katsikadelis JT (1994) The Analog Equation Method - A Powerful BEM-based Solution Technique for Solving Linear and Nonlinear Engineering Problems. In: Brebbia C.A. (ed.), *Boundary Element Method XVI*, pp.167-182, *Proceedings of 16th International Boundary Element Method Conference*, Southampton, UK, July 12-15, Computational Mechanics Publications.

BRACHISTOCHRONIC MOTION OF A VARIABLE MASS SYSTEM

A. Obradović[1], S. Šalinić[2], O. Jeremić[1], Z. Mitrović[1]

[1] Faculty of Mechanical Engineering,
University of Belgrade, Kraljice Marije 16, 11120 Belgrade 35
e-mail: aobradovic@mas.bg.ac.rs
[2] Faculty of Mechanical Engineering
University of Kragujevac, Dositejeva 19, 36000 Kraljevo
e-mail: salinic.s@ptt.rs,   salinic.s@mfkv.kg.ac.rs

Abstract. A mechanical system consisting of rigid bodies and material particles, of which some particles are with variable masses, is considered. Laws of variation of the masses of the points and relative velocity of particles separating from the points are well-known. The system is moving in an arbitrary field of known potential and nonpotential forces. Applying Pontryagin's Maximum Principle and singular optimal control theory, brachistochronic motion is determined. A two-point boundary value problem, due to nonlinearity of equations in a general case, is needed to be solved using some of the numerical procedures. Here the Shooting method is used, where the missing boundary conditions are chosen so as to be the physical variables (velocity and mass). The field where they are found can be approximately estimated, which is not the case with the conjugate vector coordinates being of purely mathematical nature. The paper also presents the manner of brachistrochronic motion realization without the action of active control forces. It is realized by subsequent imposition to the system a corresponding number of independent ideal holonomic mechanical constraints. The constraints must be in accordance with the previously determined brachistochronic motion of the system. The method is illustrated by an example of determining the brachistochronic motion of the system with three degrees of freedom and method of its realization. The system consists of one rigid body to which two points of variable masses are attached, where the system is moving in a vertical plane. Brachistochronic motion is realized by the help of two ideal holonomic constraints.

1. Introduction

The problem of a brachistochronic motion of mechanical systems is a very topical area of research as evidenced from literature cited. Research is inspired not only by the expansion of existing fundamental knowledge in this area, but also by various engineering applications (see e.g., [1-7]). Thus in [8-16] the brachistochronic motion of a particle in the presence of resistance forces (forces of dry friction, viscous friction) is analyzed, while in [6,17,18] the brachistochronic motion of a particle on a surface is considered. In [18] it was shown that results from [8,10,13] represent special cases of the brachistochronic motion of a particle on a surface. Note that in [6] the problem of optimization of a bobsled travelling on a path was solved as the problem of a brachistochronic motion of a particle on a surface, whereas [7] considers the brachistochrone problem for a steerable particle moving on a 1D curved surface
with application to ski racing. The next important group of references comprises the papers that consider the problem of brachistochronic motion of a rigid body [1-3,5,19] and system of rigid bodies [21-23]. Furthermore, in [24-27] the brachistochronic motion of mechanical systems with nonholonomic constrains is analyzed. Also, a certain number of references

can be singled out [14,28-31], where the solution of the classical brachistochrone problem (cycloid) was used with the aim of testing various numerical methods in solving nonlinear engineering optimization problems. References [32,33] consider the problem of brachistochronic motion of a variable mass particle.

This paper considers the mechanical systems that consist of constant-mass rigid bodies and variable-mass particles. It is started from the assumption that such mechanical systems are moving in the arbitrary field of known potential and nonpotential forces. Pontryagin's Maximum Principle [34] and singular optimal control theory [35] is applied in solving the brachistrochrone problem. Considerations in this paper represent a continuation of research commenced in paper [27].

2. Problem statement

The motion of mechanical system with n-degrees of freedom within which there are ℓ variable-mass particles is considered. The system configuration is determined by generalized coordinates $\overline{q} = (q^1, q^2, \ldots, q^n)$. Laws of variation of the masses are well-known:

$$m_\rho = m_\rho(t), \quad \rho = 1, \ldots, \ell \tag{1}$$

as well as relative velocity of particles separating from the points

$$\vec{v}_\rho^{rel} = \vec{v}_\rho^{rel}(\overline{q}, \dot{\overline{q}}, t), \qquad \rho = 1, \ldots, \ell. \tag{2}$$

Since the system motion is under the imposition of holonomic scleronomic mechanical constraints, kinetic energy has the form

$$T = \frac{1}{2} a_{ij} \dot{q}^i \dot{q}^j, \qquad i, j = 1, \ldots, n \tag{3}$$

where covariant coordinates of metric tensor, taking into account (1), are

$$a_{ij} = a_{ij}(\overline{q}, t), \qquad i, j = 1, \ldots, n. \tag{4}$$

Let the system move in the field of known potential forces with potential energy

$$\Pi = \Pi(\overline{q}, t) \tag{5}$$

and let the system be also acted upon by arbitrary known nonpotential forces, whose generalized forces are

$$Q_i^w = Q_i^w(\overline{q}, \dot{\overline{q}}, t), \qquad i = 1, \ldots, n. \tag{6}$$

Differential equations of motion of such variable-mass system in the form of Lagrange's equations of the second kind [36] have the form

$$\frac{d}{dt} \frac{\partial T}{\partial \dot{q}^i} - \frac{\partial T}{\partial q^i} = -\frac{\partial \Pi}{\partial q^i} + Q_i^w + Q_i^{\mathrm{var}} + Q_i^c \tag{7}$$

where generalized forces Q_i^{var} have the following form

$$Q_i^{\text{var}}(\overline{q},\dot{\overline{q}},t) = \sum_{\rho=1}^{\ell} \dot{m}_\rho (\vec{v}_\rho + \vec{v}_\rho^{\,rel}) \frac{\partial \vec{r}_\rho}{\partial q^i}, \tag{8}$$

while Q_i^c represent generalized control forces. Their determination represents an essential part of solving the problem of brachistochronic motion of the mechanical system. They can be generalized active forces and/or reactions of constraints, depending on the manner of brachistochronic motion realization. In accordance with the original postulates of brachistochronic motion [20] their power equals zero

$$Q_i^c \dot{q}^i = 0, \qquad i = 1,\ldots,n . \tag{9}$$

Thus based on (3), (7) and (9), there exists linear dependence of the second derivatives of generalized coordinates

$$a_{ij}\ddot{q}^j \dot{q}^i = \left(-\dot{a}_{ij}\dot{q}^j + \frac{\partial T}{\partial q^i} - \frac{\partial \Pi}{\partial q^i} + Q_i^w + Q_i^{\text{var}} \right)\dot{q}^i, \quad i,j=1,\ldots,n. \tag{10}$$

Let the initial values of generalized coordinates and total mechanical energy of the system be specified

$$t_0 = 0, \quad \overline{q}(t_0) = \overline{q}_0, \quad T(\overline{q}_0,\dot{\overline{q}}_0,t_0) + \Pi(\overline{q}_0,t_0) = E_0 \tag{11}$$

as well as terminal values of generalized coordinates at unknown instant of time t_1

$$\overline{q}(t_1) = \overline{q}_1 . \tag{12}$$

Solving the problem of brachistochronic motion of a variable-mass mechanical system, whose differential equations are (7), consists in determining the control forces $Q_i^c = Q_i^c(t)$ and the system motions corresponding to them, so that the system transfers for the shortest time from the state described by (11) into the state described by (12).

2. Brachistochronic motion as a problem of optimal control

Linear constraint (10) allows for another derivative of generalized coordinate to be expressed via the others. Let it be, without limiting the generality

$$\ddot{q}^n = \Phi + \Phi_s \ddot{q}^s \qquad s = 1,\ldots,n-1 \tag{13}$$

where:

$$\Phi(\overline{q},\dot{\overline{q}},t) = \frac{\left(-\dot{a}_{ij}\dot{q}^j + \frac{\partial T}{\partial q^i} - \frac{\partial \Pi}{\partial q^i} + Q_i^w + Q_i^{\text{var}} \right)\dot{q}^i}{a_{in}\dot{q}^i},$$

$$\Phi_s(\overline{q},\dot{\overline{q}},t) = \frac{-a_{is}\dot{q}^s}{a_{in}\dot{q}^i}, \quad i,j=1,\ldots,n; \ s=1,\ldots,n-1. \tag{14}$$

Introducing the control

$$u^s = \ddot{q}^s \qquad s = 1,\ldots,n-1 \tag{15}$$

differential equations of the first kind in the problem of optimal control can be, incorporating the rheonomic coordinate, written in the form

$$\dot{q}^i = y^i, \; \dot{q}^{n+1} = 1, \; \dot{y}^s = u^s, \; \dot{y}^n = \Phi + \Phi_s u^s. \tag{16}$$

Taking into account the form of functional in a time minimization problem

$$J = \int_{t_0}^{t_1} dt, \tag{17}$$

In solving the problem by the help of Pontrryagin's Maximum Principle [34], it is necessary to form Pontryagin's function

$$H = \lambda_0 + \lambda_i \dot{y}^i + \kappa_s u^s + \kappa_n (\Phi + \Phi_s u^s) + \lambda_{n+1}, \quad i = 1,\ldots,n, \; s = 1,\ldots,n-1 \tag{18}$$

where λ_0, λ_i, λ_{n+1}, and κ_i are coordinates of the conjugate vector. A costate system of differential equations corresponds to them

$$\dot{\lambda}_i = -\frac{\partial H}{\partial q^i} = -\kappa_n \left(\frac{\partial \Phi}{\partial q^i} + \frac{\partial \Phi_s}{\partial q^i} u^s \right)$$

$$\dot{\lambda}_{n+1} = -\frac{\partial H}{\partial q^{n+1}} = -\kappa_n \left(\frac{\partial \Phi}{\partial q^{n+1}} + \frac{\partial \Phi_s}{\partial q^{n+1}} u^s \right) \tag{19}$$

$$\dot{v}_i = -\frac{\partial H}{\partial y^i} = -\lambda_i - \kappa_n \left(\frac{\partial \Phi}{\partial y^i} + \frac{\partial \Phi_s}{\partial y^i} u^s \right), \quad i = 1,\ldots,n, \; s = 1,\ldots,n-1$$

Pontryagin's function (18) depends linearly on the control

$$H = H_0 + H_s u^s \quad s = 1,\ldots,n-1 \tag{20}$$

In the optimal control theory such case is referred to as singular [35] because the corresponding condition of a maximum principle

$$\frac{\partial H}{\partial u^s} = H_s = 0 \quad s = 1,\ldots,n-1 \tag{21}$$

does not allow for determining the optimal controls. Instead, one obtains a constraint between parts of the conjugate vector coordinates

$$\kappa_s = -\kappa_n \Phi_s \qquad s = 1,\ldots,n-1 \tag{22}$$

In order to determine optimal controls, it is necessary to further differentiate the relation (21) with respect to time in accordance with (16) and (19). Applying the formalism of Poisson brackets [36]

$$\dot{H}_s = \{H, H_s\} = \{H_s, H_0\} + \{H_s, H_z\} u^z = 0, \qquad s, z = 1,\ldots,n-1 \tag{23}$$

and taking into account the fact that for multidimensional singular controls [35]

$$\{H_s, H_z\} = 0, \quad s, z = 1, \ldots, n-1 \tag{24}$$

it is obtained that

$$\{H_s, H_0\} = 0, \quad s = 1, \ldots, n-1 \tag{25}$$

From (25), taking into account (22), another constraint between the coordinates of conjugate vector can be established

$$\lambda_s = \lambda_s(\overline{q}, \overline{y}, t, \lambda_n, \kappa_n) \quad s = 1, \ldots, n-1 \tag{26}$$

Further differentiation yields:

$$\{\{H_s, H_0\}, H_0\} + \{\{H_s, H_0\}, H_z\}u^z = 0, \quad s, z = 1, \ldots, n-1 \tag{27}$$

Limiting to the singular controls of the first order [35], the linear system of equations (27) using the relations (22) and (26) yields optimal controls

$$u^s = u^s(\overline{q}, \overline{y}, t, \lambda_n, \kappa_n), \quad s = 1, \ldots, n-1 \tag{28}$$

Substituting (28) in (16) and (19) one obtains the system of (2n+2) differential equations of the first kind in normal form

$$
\begin{aligned}
\dot{q}^i &= \dot{q}^i(\overline{q}, \overline{y}, t, \lambda_n, \kappa_n), \\
\dot{y}^i &= \dot{y}^i(\overline{q}, \overline{y}, t, \lambda_n, \kappa_n), \\
\dot{\lambda}_n &= \dot{\lambda}_n(\overline{q}, \overline{y}, t, \lambda_n, \kappa_n), \\
\dot{\kappa}_n &= \dot{\kappa}_n(\overline{q}, \overline{y}, t, \lambda_n, \kappa_n), \quad i = 1, \ldots, n
\end{aligned}
\tag{29}
$$

where differential equations, whose solutions are (22) and (26), were eliminated from (19). In a general case, due to nonlinearity (29), a two-point boundary value problem should be solved by applying some of the numerical methods. If the Shooting method is used [37], it is necessary to adjust the choice of the missing boundary conditions such that one can approximately estimate their field. In this regard, it should be avoided, whenever it is possible, having any of the coordinates of conjugate vector among them, because they are of purely mathematical character and as such difficult to estimate the field. Therefore, it is suitable here to perform backward numerical integration in the interval $[t_0, t_1]$. At terminal point the maximum principle can be utilized for the case of unspecified interval $[t_0, t_1]$

$$H(t_1) = 0 \tag{30}$$

Since final velocities $y^i(t_1)$ are not specified, nor is the rheonomic coordinate $q^{n+1}(t_1)$, it follows from the transversality conditions that:

$$\kappa_i(t_1) = 0, \; i = 1, \ldots, n, \quad \lambda_{n+1}(t_1) = 0 \tag{31}$$

Taking into account that $\lambda_0 = -1$ (according to the maximum principle $\lambda_0 = const \leq 0$) as well as the relations (12),(18),(26),(30) and (31), it is possible to establish in the analytical form the dependence

$$\lambda_n(t_1) = \lambda_n(\overline{y}_1, t_1) \tag{32}$$

which, along with the fact that

$$\kappa_n(t_1) = 0 \tag{33}$$

completely excludes the necessity to estimate the fields for $\lambda_n(t_1)$ and $\kappa_n(t_1)$ in backward shooting procedure.

The backward shooting procedure consists of choosing $n+1$ values of generalized velocities $y^i(t_1)$ and duration t_1 of the time interval $[t_0, t_1]$, so that $n+1$ values (11) of generalized coordinates and mechanical energy are shot.

There remains the discussion on transversality conditions at the initial point:

$$\lambda_i(t_0)\delta q^i(t_0) + \kappa_i(t_0)\delta y^i(t_0) + \lambda_{n+1}(t_0)\delta q^{n+1}(t_0) = 0 \quad i = 1,\ldots,n \ . \tag{34}$$

Based on specified values (11) it follows

$$\delta q^i(t_0) = 0 , \qquad \delta q^{n+1}(t_0) = 0, \quad a_{ij}(t_0)y^i(t_0)\delta y^i(t_0) = 0, \quad j,i = 1,\ldots,n . \tag{35}$$

Substituting (14) in (22), it is obtained

$$\kappa_i(t_0)\delta y^i(t_0) = \kappa_n(t_0)a_{ij}(t_0)y^j(t_0)\delta y^i(t_0) \quad i, j = 1,\ldots,n \ . \tag{36}$$

Directly substituting (35) and (36) in (34), it is evident that transversality conditions at the initial point are satisfied. Numerical solving of the system (29) yields

$$\overline{q} = \overline{q}(t), \ \dot{\overline{q}} = \dot{\overline{q}}(t), \ \lambda_n = \lambda_n(t), \ \kappa_n = \kappa_n(t) \tag{37}$$

and based on (13), (28) it is also obtained

$$\ddot{\overline{q}} = \ddot{\overline{q}}(t) \tag{38}$$

which enables too final determination of the control forces (7)

$$Q_i^c = Q_i^c(t) \tag{39}$$

Control forces (39) can be realized in various ways, combining active forces and/or reactions of constraints. The most approximate to the original brachistochrone problem is realization of motion by subsequent imposition to the system a corresponding number of independent ideal stationary constraints, without the action of active forces. The constraints must be in accordance with the brachistochronic motion (37).

Let the ideal holonomic stationary independent constraints, in accordance with (37), be imposed to the system

$$\varphi^s(\overline{q}) = 0, \ rank\left[\frac{\partial \varphi^s}{\partial q^i}\right] = n - 1, \ s = 1,\ldots,n-1 \tag{40}$$

In that case, generalized control forces read

$$Q_i^c = \mu_s \frac{\partial \varphi_s}{\partial q^i}, \quad i = 1,\ldots,n; \quad s = 1,\ldots,n-1 \tag{41}$$

where from, if necessary, based on (37), (39) and (40), multipliers of constraints can be also determined

$$\mu_s = \mu_s(t) \quad s = 1, \ldots, n-1 \tag{42}$$

More information on such manner of control can be found in []. The form of constraints (40) is most often chosen to be performed by the simplest construction. One of the manners for the case of motion control of mechanical systems, especially of a rigid body, is imposition of guides to the specified number of particles whose motion is determined by numerical relations.

3. Example

The rod AB of mass m, of length 2ℓ and radius of inertia $i_{Cz} = \ell$ moves in a vertical plane, where the Oy axis is directed upward (see Fig.1).
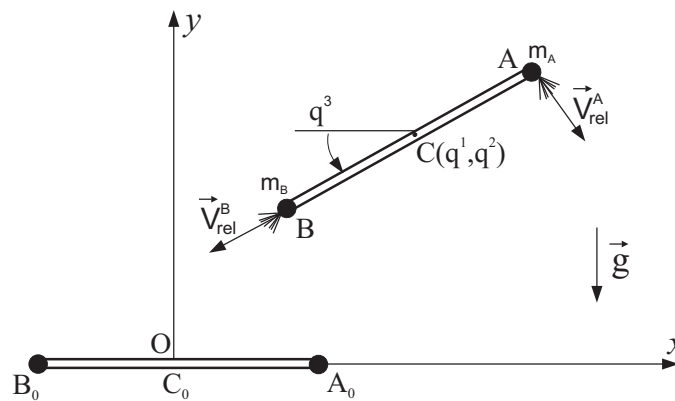
Figure 1. Variable-mass mechanical system

At both ends of the rod there are two variable-mass points, whose masses change according to the Law

$$m_A(t) = m_B(t) = m - kt \tag{43}$$

where $k = const > 0$. The particles are separating by relative velocities of constant intensities $(v = const > 0)$

$$v_{rel}^B = v_{rel}^A = v \tag{44}$$

It is needed to determine the brachistochronic motion of the system and present its realization without the action of active forces if at the initiation of motion (11) $(E_0 > 0)$ is specified:

$$t_0 = 0, \quad q^1(t_0) = q^2(t_0) = q^3(t_0) = 0,$$

$$\frac{3m}{2}\left[\left(\dot{q}^1(t_0)\right)^2 + \left(\dot{q}^2(t_0)\right)^2 + \left(\dot{q}^3(t_0)\right)^2\right] = E_0, \tag{45}$$

while at the end of motion (12)

$$t_1 = ?, \quad q^1(t_1) = q^2(t_1) = \ell, \quad q^3(t_1) = \frac{\pi}{2} \tag{46}$$

Differential equations of motion (7) of this system are:

$$(3m - kt)\ddot{q}^1 = kv(\cos q^3 - \sin q^3) + Q_1^c$$
$$(3m - kt)\ddot{q}^2 = kv(\cos q^3 + \sin q^3) - (3m - kt)g + Q_2^c \tag{47}$$
$$(3m - kt)\ell^2\ddot{q}^3 = kv\ell + Q_3^c$$

so that the relations (14) obtain the form

$$\Phi = \frac{1}{\ell^2 \dot{q}^3}\left[-g + \frac{kv}{3m-kt}\left(\cos q^3(\dot{q}^1 + \dot{q}^2) + \sin q^3(\dot{q}^2 - \dot{q}^1) + \ell\dot{q}^3\right)\right],$$
$$\Phi_1 = -\frac{\dot{q}^1}{\ell^2 \dot{q}^3}, \quad \Phi_2 = -\frac{\dot{q}^2}{\ell^2 \dot{q}^3} \tag{48}$$

The problem is solved for the following numerical values of the parameters:

$$\ell = 1m, \quad m = 1kg, \quad E_0 = 30J, \quad v = 1\frac{m}{s}, \quad k = 1\frac{kg}{s}. \tag{49}$$

The missing values of boundary conditions are:

$$\dot{q}^1(t_1) = 1.14877\frac{m}{s}, \quad \dot{q}^1(t_2) = 1.30177\frac{m}{s}, \tag{50}$$
$$\dot{q}^1(t_3) = 2.94686s^{-1}, \quad t_1 = 0.532857s$$

The trajectories of points A, B, and C are shown in Fig.2.
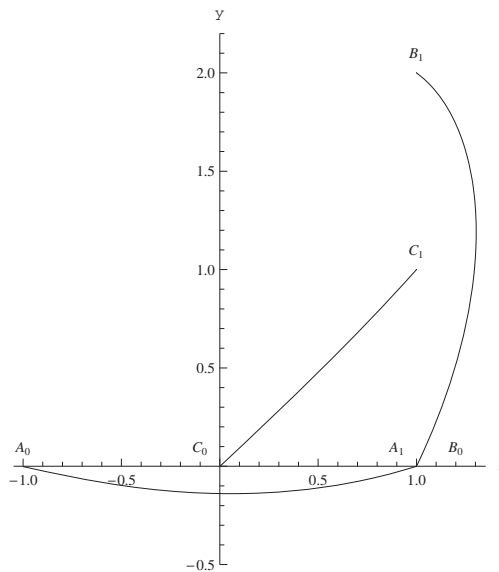
Figure 2: Trajectories of points A, B, and C

4. Conclusions

This paper is a continuation of research from [27] for the case of brachistochronic motion of a variable-mass system. Like in [27], the manner of motion control is presented without the action of active forces. The novelty in this paper is the numerical solving procedure for the two-point boundary value problem of maximum principle, based on shooting method, where costate variables were avoided as the missing boundary conditions. The number of missing boundary conditions is the least possible, such as $n-$ generalized velocities and time t_1, which yields $n+1$ conditions. Their values can be approximately estimated.

References
[1] Legeza V P (2008) Quickest-descent curve in the problem of rolling of a homogeneous cylinder, *International Applied Mechanics*, **44**(12), pp.1430-1436.
[2] Legeza V P (2010) Conditions for pure rolling of a heavy cylinder along a brachistochrone, *International Applied Mechanics*, **46**(6), pp.730-735.
[3] Legeza V P (2010) Brachistochrone for a rolling cylinder, *Mechanics of Solids* , **45**(1), pp.27-33.
[4] Gershman M D and Nagaev R F (1979) The oscillation brachistochrone problem, *Mechanics of Solids* , **14**(2), pp.9-17.
[5] Djukic Dj (1976) The brachistochronic motion of a gyroscope mounted on the gimbals, *Theoretical and Applied Mechanics* , **2**, pp.37-40.
[6] Maisser P (1998) Brachystochronen als zeitkrzeste Fahrspuren von Bobschlitten, *Zeitschrift fur Angewandte Mathematik und Mechanik* / ZAMM, **78**(5), pp.311-319.
[7] Hennessey M P and Shakiban Ch (2010) Brachistochrone on a 1D curved surface using optimal control, *ASME Journal of Dynamic Systems Measurement and Control*, **132**, p.034505
[8] Ashby N, Brittin W E, Love W F and Wyss W (1975) Brachistochrone with Coulomb friction, *American Journal of Physics*, **43**(10), pp.902-906.

[9] Gershman M D and Nagaev R F (1976) O frikcionnoj brakhistokhrone, *Izvestiya Akademii Nauk: Mekhanika Tverdogo Tela* , **4**, pp.85-88.

[10] Van der Heijden A M A and Diepstraten J D (1975) On the brachystochrone with dryfriction, *International Journal of Non-linear Mechanics*, **10**, pp.97-112.

[11] Lipp S C (1997) Brachistochrone with Coulomb friction, *SIAM Journal on Control and Optimization*, **35**(2), pp.562-584.

[12] Parnovsky A S (1998) Some generalisations of brachistochrone problem, *Acta Physica Polonica. Series A: General Physics, Physics of Condensed Matter, Optics and Quantum Electronics, Atomic and Molecular Physics, Applied Physics*, **93**(SUPPL), pp.S55-S64.

[13] Vratanar B and Saje M (1998) On the analytical solution of the brachistochrone problem in a non-conservative field, *International Journal of Non-linear Mechanics*, **33**(3), pp.489-505.

[14] Wensrich C M (2004) Evolutionary solutions to the brachistochrone problem with Coulomb friction, *Mechanics Research Communications*, **31**, pp.151-159.

[15] Hayen J C (2005) Brachistochrone with Coulomb friction, *International Journal of Non-linear Mechanics*, **40,** pp.1057-1075.

[16] Šalinić S (2009) Contribution to the brachistochrone problem with Coulomb friction, *Acta Mechanica*, **208**(1-2), pp.97-115.

[17] Djukić Dj (1976) The brachistochronic motion of a material point on surface, *Rivista di Matematica della Università di Parma*, **(4)**2, pp.177-183.

[18] Čović V and Vesković M (2008) Brachistochrone on a surface with Coulomb friction, *International Journal of Non-linear Mechanics*, **43**(5), pp.437-450.

[19] Akulenko L D (2009) The brachistochrone problem for a disc, *Journal of Applied Mathematics and Mechanics*, **73**(4), pp.371-378.

[20] Čović V, Lukačević M and Vesković M (2007) *On Brachistochronic Motions*, Budapest University of Technology and Economics, Budapest

[21] Čović V and Lukačević M (1999) Extension of the Bernoulli's case of a brachistochronic motion to the multibody system in the form of a closed kinematic chain, *FACTA UNIVERSITATIS, Series:Mechanics, Automatic Control and Robotics*, **2**(9), pp.973-982.

[22] Čović V and Vesković M (2002) Extension of the Bernoulli's case of brachistochronic motion to the multibody system having the form of a kinematic chain with external constraints, *European Journal of Mechanics. A: Solids*, **21,** pp.347-354.

[23] Čović V and Vesković M (2009) Brachistochronic motion of a multibody system with Coulomb friction, *European Journal of Mechanics. A: Solids*, **28**(9), pp.882-890.

[24] Djukić Dj (1979) On the brachistochronic motion of a dynamic system, *Acta Mechanica*, **32,** pp.181-186.

[25] Zekovic D (1990) On the brachistochronic motion of mechanical systems with non-holonomic , non-linearand rheonomic constraints, *Journal of Applied Mathematics and Mechanics*, **54**(6), pp.931-935.

[26] Zekovic D and Covic V (1993) On the brachistochronic motion of mechanical systems with linear nonholonomic nonhomogeneous constraints, *Mechanics Research Communications*, **20**(1), pp.25-35.

[27] Obradović A, Čović V , Vesković M and Dražić M (2010) Brachistochronic Motion of a Nonholonomic Rheonomic Mechanical System, *Acta Mechanica*, **214**(3-4), pp.291-304.

[28] Dooren R V and Vlassenbroeck J (1980) A new look at the brachistochrone problem, *Zeitschrift fur Angewandte Mathematik und Physik / ZAMP*, **31**, pp.785-790.

[29] Julstrom B A (2003) Evolutionary algorithms for two problems from the calculus of variations, In: *Lecture Notes in Computer Science, Genetic and Evolutionary Computation-GECCO*, Springer-Verlag Berlin Heidelberg, pp.2402-2403.

[30] Razzaghi M and Sepehrian B (2004) Single-term walsh series direct method for the solution of nonlinear problems in the calculus of variations, *Journal of Vibration and Control*, **10**, pp.1071-1081.

[31] Cruz P A F and Torres D F M (2007) Evolution strategies in optimization problems, *Proceedings of the Estonian Academy of Sciences, Physics, Mathematics*, **56**(4), pp.299-309.

[32] Ivanov A I (1968) On the brachistochrone of a variable mass point with constant relative rates of particle throwing away and adjoining, *Doklady Akademii Nauk Ukrainskoi SSR Ser.A*, pp.683-686.

[33] Russalovskaya A V, Ivanov G I and Ivanov A I (1973) On brachistochrone of the variable mass point during motion with friction with an exponential rule of mass rate flow, *Doklady Akademii Nauk Ukrainskoi SSR Ser.A*, pp.1024-1026.

[34] Pontryagin L S, Boltyanskii V G, Gamkrelidze R V and Mishchenko E F (1962) *The Mathematical Theory of Optimal Processes*, John Wiley & Sons, New Jersey.

[35] Gabasov R and Kirillova F M (1973) *Singular Optimal Controls*, Nauka, Moscow.

[36] Gantmacher F (1975) *Lectures in Analytical Mechanics*, Mir Publications, Moscow.

[37] Stoer J and Bulirsch J (1993) *Introduction to Numerical Analysis*, Springer-Verlag.

Vibro-impact system based on oscillator, with two heavy mass particles moving along a rough parabola

Srdjan Jović[1] and Vladimir Raičević[1]

[1]Faculty of Technical Sciences, Kosovska Mitrovica, University of Priština
38 220 Kosovska Mitrovica, Ul. Kralja Petra I br. 149/12, Serbia,
e-mail: jovic003@gmail.com

ABSTRACT. The paper is based on an analysis of vibro-impact system motion based on oscillator with two degrees of freedom moving in a parabola rough line in the vertical plane. Oscillator consists of two heavy mass particles whose free motion is limited by two fixed elongation limiters. Analytical and numerical results for the specific kinetic parameters of observed vibro-impact systems are the basis for visualization of the energy analysis which was subject of this analytical research. This paper deals with the methodology study of energy transfer between elements of the observed vibro-impact system. The process of determining time interval and angle at which there is an impact of heavy mass particles appeared and the determination of their incoming and outgoing velocities immediately before and after the impact was studied here.

Free movement of heavy mass particles was divided into appropriate intervals. Each motion interval corresponds to the differential equation of motion which belongs to a group of ordinary non-linear homogeneous second order differential equations with variable coefficients. These differential equations are solved in analytical form. Differential equations of motion for the corresponding motion intervals are matched with the corresponding initial conditions of motion, impact conditions to the elongation limiters, impact conditions of heavy mass particles, and alternation conditions of the direction that cause an alternation of friction force direction. By the analytical solution of differential equations of motion, we came to the analytical expression for the equation of phase trajectory in plane $(\varphi_i, \dot{\varphi}_i)$, $i = 1,2$ -number of degrees of freedom, with energy equation curves necessary for energy analysis of the dynamics of vibro-impact system. Graphical visualization and analysis of the energy curves and representative kinetics state point of the system during the kinetics (dynamics) was performed using the software package MathCad and the users package CorelDraw.

Keywords: Heavy mass particle, rough parabola, friction, two impact limiters, pellet, vibro-impact, phase trajectory, singular points, large initial conditions, total energy, kinetic and potential energy, analytical expression, graphical presentation, representative point.

1. Introduction

Investigation of the vibro-impact system dynamics and nonlinear phenomena in the presence of certain discontinuity represents the area of interest of numerous researchers from all over the world. Theoretical knowledge of vibro-impact systems (see references [1-5]) are of particular importance to engineering practice because of the wide application of vibro-impact effects that are used for technological process. Based on knowledge of the theory of vibro-impact systems and relying on the original works on this subject by the authors: František Peterka [6-8], Katica (Stevanovic) Hedrih [9-16], Alz Nayfeh and his associates [17,18], Fool S., Bishop S. [19], Luo G.W., Xie JH [20], Nordmark A.B. [21], Pavlovskaia E., Wiercigroch M. [22,23] et al., we can say that today there is an increasing interest for the study of energy transfer within complex systems and non-linear modes. This is the reason for importance of vibro-impact processes dynamics analysis in vibro-impact systems with one or more degrees of freedom of motion.

The necessary theoretical knowledge, which leads us to this paper are from the books by D. Rašković [24-25] in which he analyzes the motion of mechanical systems in ideal conditions and without constrains, as well as curvilinear oscillators motion in the presence of sliding Coulomb-type friction and from the paper published by Katica (Stevanovic) Hedrih [13-14] related to the heavy mass particle motion along the rough curvilinear paths. In these papers, there is a basic mathematical description of the movement of heavy mass particles by rough curvilinear line, and special cases of motion of heavy mass particles along the circular rough line, cycloid rough line and parabolic rough line.

In previous works [26-31] authors analyzed several variants of vibro-impact system with one and two degrees of freedom, based on the oscillator moving along a rough circle, sliding Coulomb-type friction and limited elongation. Referring to them, the vibro-impact system with two degrees of freedom, moving along rough parabola in the vertical plane and sliding Coulomb-type friction Coulomb's coefficient with limited angular elongation (Figure 1) was studied in this paper.

Oscillator consists of two heavy mass particles (pellets 1 and 2) mass m_1 i m_2, exposed to gravity. These mass particles are moving along rough parabola in vertical plane on which the two sided impact limiters of elongation (constraints) were placed. The impact limiter positions were determined by the angle δ_1 for the limiter of elongation set on the right, and δ_2 for the impact limiter of elongation positioned on the left side. The angles δ_1 and δ_2 were measured from the equilibrium position of the mass particles, through the vertical center of the circular line. The angular elongations of the first and second mass particles at arbitrary time t were marked by φ_1 and φ_2 and measured from the equilibrium position. At the initial time the material points were at position φ_{10} and φ_{20} from the equilibrium position 0-0, with initial angular velocities, $\dot{\varphi}_{10}$ and $\dot{\varphi}_{20}$.
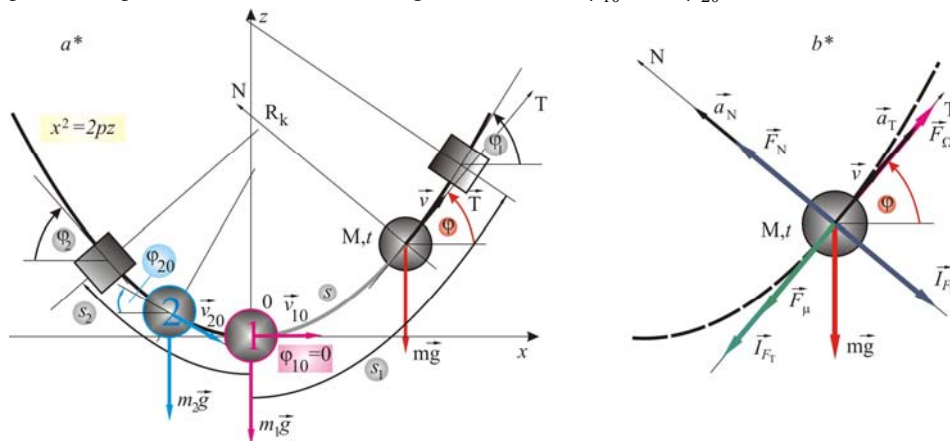
Fig. 1. Oscillator moving along rough parabola in vertical plane, with limited elongations $\varphi_{ul,1} = \delta_1$ and $\varphi_{ul,2} = \delta_2$: a* initial heavy mass particles position, b* active, reactive and innertial forces plan.

Let's discuss the properties of the oscillation of the first and second heavy mass particles in a parabola rough line with limited elongation, so the system becomes vibro-

impact with two-sided impact limiter. The differential equations of motion of heavy mass particles for each interval of motion are requested. The motion interval is interval from impact to impact, from collision to collision and motion interval when the friction force direction alternation appears. The friction force direction alternation is associated with the alternation of angular velocity direction alternation of motion of heavy mass particle, as well as impact velocity alternation of heavy mass particles into angular elongation limiter and heavy mass particles mutual impacts. Differential equations are matched to the initial motion conditions, system elongation limitation conditions, heavy mass particles impact conditions, and friction force direction alternation conditions. Also, it was necessary to determine, for heavy mass particles in particular, the equation of phase trajectories in phase planes $(\varphi_1, \dot{\varphi}_1)$ and $(\varphi_2, \dot{\varphi}_2)$, and the equation curves for constant energy with the corresponding graphical visualization and motion analysis of the same representative point of the kinetic state of the system during the kinetics (dynamics). It was also necessary to conduct the analysis of total mechanical energy alternation for each heavy mass particle as a part of the system as a parameter of mechanical energy decrease in each characteristic motion interval.

The operating conditions for such observed vibro-impact system are:

$$\varphi_{10} > \varphi_{20} ; \qquad \dot{\varphi}_{10} > \dot{\varphi}_{20} . \qquad (1)$$

2. Differential Equation of Vibrations of a Mass Particle Motion along Curvilinear Rough Parabola

The obsreved vibro-impact system has two degrees of freedom, so the corresponding governing non-linear differential equations of motion are presented as:

$$\ddot{\varphi}_1 + (3tg\,\varphi_1 \pm \mu)\dot{\varphi}_1^2 + \frac{g\cos^3\varphi_1}{p}(\sin\varphi_1 \pm \mu\cos\varphi_1) = 0, \qquad \begin{cases} for\ v_1 > 0 \\ for\ v_1 < 0 \end{cases}$$

$$(2)$$

$$\ddot{\varphi}_2 + (3tg\,\varphi_2 \pm \mu)\dot{\varphi}_2^2 + \frac{g\cos^3\varphi_2}{p}(\sin\varphi_2 \pm \mu\cos\varphi_2) = 0, \qquad \begin{cases} for\ v_2 > 0 \\ for\ v_2 < 0 \end{cases}$$

$$(3)$$

for $\mu = tg\,\alpha_0$ - sliding Coulomb-type friction coefficient, φ_1, φ_2 - generalized coordinates for monitoring the motion of first, second and third heavy mass particles.

This system of double differential non-linear equations is coupled by inital motion conditions:

a* the first heavy mass particle (pellet 1), in further text marked with subscript -1 $\qquad \varphi_{1(0)} = \varphi_{10}$ and $\qquad \dot{\varphi}_{1(0)} = \dot{\varphi}_{10}$;

$$(4)$$

b* the second heavy mass particle (pellet 2), in further text marked with subscript -2

$$\varphi_{2(0)} = \varphi_{20} \quad and \qquad \dot{\varphi}_{2(0)} = \dot{\varphi}_{20}; \qquad (5)$$

At the initial moment of motion, heavy mass particles were given the positive initial angular velocity $(\dot{\varphi}_1 > 0, \dot{\varphi}_2 > 0)$.

The first integral of governing non-linear differential equations (2) and (3) are representing the phase trajectory equations of heavy mass particles moving along the rough parabola line.

For the first heavy mass particle 1

$$\dot{\varphi}_1^2 = \cos^6 \varphi_1 \left(-\frac{g}{p\cos^2 \varphi_1} + C_1 e^{\mp 2\mu\varphi_1} \right) \qquad \begin{cases} for \ v_1 > 0 \\ for \ v_1 < 0 \end{cases}$$

For the second heavy mass particle 2

$$\dot{\varphi}_2^2 = \cos^6 \varphi_2 \left(-\frac{g}{p\cos^2 \varphi_2} + C_2 e^{\mp 2\mu\varphi_2} \right) \qquad \begin{cases} for \ v_2 > 0 \\ for \ v_2 < 0 \end{cases}$$

where C_1 and C_2 are integration constants depending of the initial conditions of motion.

3. Motion analysis of vibro-impact system

The analysis of heavy mass particles vibrations was conducted for each motion interval. For the certain motion interval the corresponding vibration of the first and second mass particles were analyzed.

Pellet 1, with mass m_1, is moving in the interval from impact to the pellet 2 with mass m_2, to the impact to the angular elongation limiter, or to direction alternation point of the first mass particle 1 (when it appears).

Pellet 2, $m_2 = 0,2 [kg]$ is moving within the interval of motion from the impact with pellet 1, $m_1 = 0,2 [kg]$ to the impact to the angular elongation limiter positioned on the left side, or to the direction alternation point of heavy mass particle 2 motion (when it appears).

Heavy mass particle 1 –the first motion interval represents the interval from the initial moment to the first impact of the pellet 1 to the angular elongation limiter positioned to the right side.

Heavy mass particle 1 is moving according to the rule

$$\dot{\varphi}_{11}^2 = \cos^6 \varphi_1 \left(-\frac{g}{p\cos^2 \varphi_1} + C_{11} e^{-2\mu\varphi_1} \right)$$

By using the initial conditions (4) we get

$$C_{11}(\varphi_{10}, \dot{\varphi}_{10}) = \frac{e^{2\mu\varphi_0}}{\cos^2 \varphi_{10}} \left(\frac{\dot{\varphi}_{10}^2}{\cos^4 \varphi_{10}} + \frac{g}{p} \right)$$

The impact conditions are

$$t_1 = t_{1ul_1 -}, \qquad \varphi_{1ul_1}(t_{1ul_1 -}) = \delta_1, \qquad \dot{\varphi}_{1ul_1}(t_{1ul_1 -}) = \dot{\varphi}_{1ul_1 -}.$$

After the determination of constant C_{11}, the conditions for phase trajectory visualization were created (Fig.2) $\dot{\varphi}_{11} = f(\varphi_1)$ in the first interval to the first impact of heavy mass particle 1 into angular elongation limiter.

Parameter values are :

$$\delta_1 = \frac{\pi}{4}[rad], \varphi_{10} = 0[rad], \dot{\varphi}_{10} = 7\left[\frac{rad}{s}\right], p = 1[m], \alpha_0 = 0,15, \qquad g = 9,81\left[\frac{m}{s^2}\right]$$ and

$$m_1 = 0,2[kg]_.$$
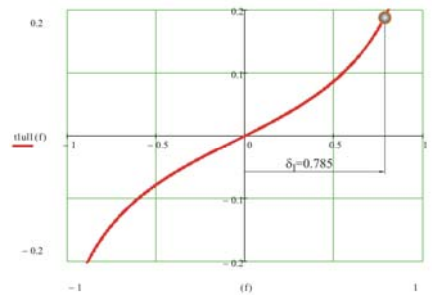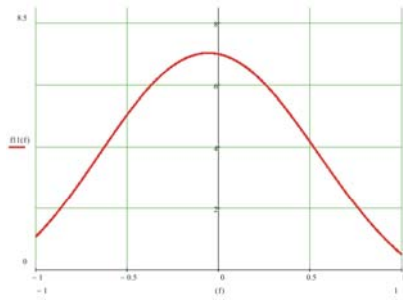
Fig. 2. Phase trajectory curve of heavy mass particle 1 in the first motion interval until first impact

Fig. 3. Heavy mass particle impact time into elongation limiter

Angular velocity of the firts impact to the limiter is determined as:

$$\dot{\varphi}_{1ul_1} = \sqrt{\cos^6 \delta_1 \left(-\frac{g}{p\cos^2 \delta_1} + C_{11}e^{-2\mu\delta_1} \right)}_.$$

The first impact appears at the moment t_{1ul_1} is analytically represented by

$$t_{1ul_1} = \int_{\varphi_{10}}^{\delta_1} \frac{d\varphi_1}{\sqrt{\cos^6 \varphi_1 \left(-\frac{g}{p\cos^2 \varphi_1} + C_{11}e^{-2\mu\varphi_1} \right)}}_.$$

(6)

Time t_{1ul_1} (*Fig.3*) was determined by numeric method or by using MathCad software for solving equation (6) and function $t = f(\varphi)$ graphic presentation.

Heavy mass particle 2- the first motion interval represents the interval form the initial time to the first impact of the heavy mass particle 2 to the heavy mass particle 1.

Heavy mass particle 2 is moving according the expression

$$\dot{\varphi}_{21}^2 = \cos^6 \varphi_2 \left(-\frac{g}{p\cos^2 \varphi_2} + C_{21}e^{-2\mu\varphi_2} \right)_.$$

By using the initial conditions (5) we get the following expression:

$$C_{21}(\varphi_{20}, \dot{\varphi}_{20}) = \frac{e^{2\mu\varphi_{20}}}{\cos^2 \varphi_{20}} \left(\frac{\dot{\varphi}_{20}^2}{\cos^4 \varphi_{20}} + \frac{g}{p} \right)_.$$

After the determination of the constant C_{21}, the conditions for phase trajectory visualization were created (Fig.4) $\dot{\varphi}_{21} = f(\varphi_2)$ in the first interval to the first impact of heavy mass particles.
Parameter values are:

$$\delta_2 = -\frac{\pi}{6}[rad], \varphi_{20} = -\frac{\pi}{12}[rad], \dot{\varphi}_{20} = 5\left[\frac{rad}{s}\right], p = 1[m], \alpha_0 = 0,15, \quad g = 9,81\left[\frac{m}{s^2}\right] \text{ and}$$

$$m_2 = 0,2[kg].$$
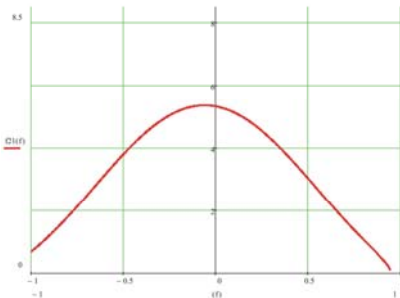
Fig. 4. Heavy mass particle 2 phase trajectory
curve, until the first impact
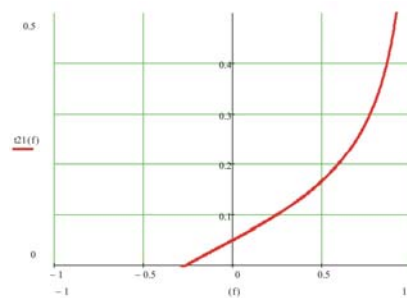
Fig.5 Time alternation vs angle φ_2

For further analysis the position of heavy mass particle 2 has to be determined when heavy mass particle 1 reaches elongation limiter. For this position the value of time t_{1ul_1} is determined (from the graphic presented on Fig.3). Time alternation t_{21} as a function of the angle φ_2 is defined by the equation

$$t_{21} = \int_{\varphi_{20}}^{\varphi_2} \frac{d\varphi_2}{\sqrt{\cos^6\varphi_2\left(-\dfrac{g}{p\cos^2\varphi_2} + C_{21}e^{-2\mu\varphi_2}\right)}}.$$

(7)

Time alternation curve $t_{21} = f(\varphi_2)$ (Fig.5) is defined by using MathCad software for function (7) graphic presentation.

On the graphic presentation $t_{21} = f(\varphi_2)$ given in Fig.5., value for time t_{1ul_1} is subtracted (by absolute value) from the time value $t_{21}(\varphi_{20})$. Angle $\varphi_2(t_{1ul_1})$ was defined on the x axis of a diagram of function $t_{21} = f(\varphi_2)$. Angle $\varphi_2(t_{1ul_1})$ represents the requested position of the heavy mass particle 2, when heavy mass particle 1 reaches the elongation limiter.

After the position $\varphi_2(t_{1ul_1})$ was defined, from the graphic presentation of the phase trajectory $\dot{\varphi}_{21} = f(\varphi_2)$ (*Fig.4*) we can read the angular velocity of heavy mass particle 2, when heavy mass particle 1 comes to the elongation limiter.

Heavy mass particle 1- the second motion interval represents the interval from the first impact into the elongation limiter to the first impact of heavy mass particles 1 and 2.

Phase trajectory equation for the second motion interval is

$$\dot{\varphi}_{12}^2 = \cos^6 \varphi_1 \left(-\frac{g}{p \cos^2 \varphi_1} + C_{12} e^{+2\mu\varphi_1} \right)$$

The initial angular velocity for this interval is

$$\dot{\varphi}_{1odl_1} = -k\dot{\varphi}_{1ul_1-} = -\dot{\varphi}_{1ul_1-},$$

with k – impact coefficient in the range from $k = 0$, for ideal plastic impact to, $k = 1$, for ideal elastic impact (referring to ideal elastic impact).

By using the initial conditions for this period

$$t_1 = t_{1ul_1+}, \qquad \varphi_1(t_{1ul_1+}) = \delta_1, \qquad \dot{\varphi}_1(t_{1ul_1+}) = \dot{\varphi}_{1odl_1} = -\dot{\varphi}_{1ul_1-},$$

The integration constant can be determined

$$C_{12} = \frac{e^{-2\mu\varphi_1}}{\cos^2 \varphi_1} \left(\frac{(\dot{\varphi}_{1ul_1})^2}{\cos^4 \varphi_1} + \frac{g}{p} \right)$$
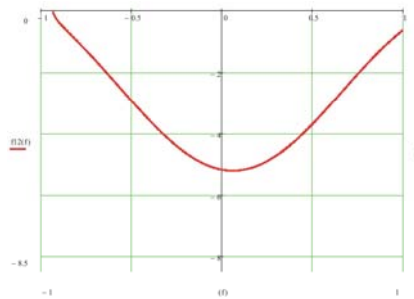
Fig. 6. Phase trajectory branch for heavy
mass particle 1 in the second motion interval
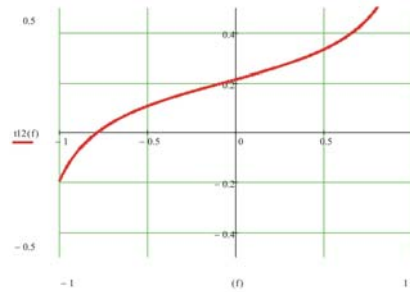
Fig. 7. Time alternation vs angle
$$(t_{12} = f(\varphi_1))$$

After the definition of constant C_{12} the conditions for the phase trajectory $\dot{\varphi}_{12} = f(\varphi_1)$ (*Fig.6*), for the second motion interval were defined. The time for the second motion interval of heavy mass particle 1 can be expressed as a function of generalized coordinate φ_1 as:

$$t_{12} = \int_{\delta_1}^{-\varphi_1} \frac{d\varphi_1}{-\sqrt{\cos^6 \varphi_1 \left(-\frac{g}{p \cos^2 \varphi_1} + C_{12} e^{+2\mu\varphi_1} \right)}}$$

The function $t_{12} = f(\varphi_1)$ can be presented by using MathCad software (Fig.7)

The first heavy mass particles impact happened in the second motion interval of mass particle 1 and in the first motion interval of mass particle 2.

Further analysis is focused on the definition of time necessary for the first impact appearance. After the first impact time definition t_{sud_1} angle φ_{sud_1} was determined, representing the basis for further heavy mass particles motion.

The condition for time definition t_{sud_1} is

$$s = s_{12}(t_{sud_1}) + s_{21}(t_{sud_1}) \quad \text{or} \quad (\delta_1 - \varphi_2(t_{1ul_1})) = \varphi_{12}(t_{sud_1}) + \varphi_{21}(t_{sud_1}). \tag{8}$$

Time t_{sud_1} was defined by relation

$$\left(t_{sud_1}\right)^2 + \frac{2\left(\dot{\varphi}_{1ul_1} + \dot{\varphi}_2\left(\varphi_2\left(t_{1ul_1}\right)\right)\right)}{\left(\ddot{\varphi}_{12} + \ddot{\varphi}_{21}\right)} t_{sud_1} - \frac{2\left(\delta_1 - \varphi_2\left(t_{1ul_1}\right)\right)}{\left(\ddot{\varphi}_{12} + \ddot{\varphi}_{21}\right)} = 0 \ . \tag{9}$$

Here the accelerations $\ddot{\varphi}_{12}$ and $\ddot{\varphi}_{21}$ were approximatelly determined, with enough accurance, as arithmetic mean values of average accelerations at subintervals of the given interval. For this specific case the interval $\left(\delta_1 - \varphi_2\left(t_{1ul_1}\right)\right)$ was divided into six equal subintervals.

For the obtained value of t_{sud_1} from the graphic presentation presented in Fig.7. or Fig.5 (the values must be corresponding) the angle of the first impact was defined φ_{sud_1}.

Value for angle φ_{sud_1} is used for determination of angular velocities of heavy mass particles 1 and 2 immediately before the first impact $\dot{\varphi}_{1sud_1,ul}$ and $\dot{\varphi}_{2sud_1,ul}$, from phase trajectories for the second motion interval for heavy mass particles 1 (Fig.6) and the first motion interval of heavy mass particle 2 (Fig.4).

Mass centres of material points are positioned on rough circle line, i.e., impact centers are positioned on the same axis. This is about the central impact.

The expressions for the explicite definition of angular velocity immediately after the impact by using amount of motion alternation law and Newton's hypotesis of relative angular velocities of mass particles are:

$$\dot{\varphi}_{2sud_1,odl} = \frac{m_1(1+k)}{m_1 + m_2}\dot{\varphi}_{1sud_1,ul} - \frac{m_2 - km_1}{m_1 + m_2}\dot{\varphi}_{2sud_1,ul},$$

$$\dot{\varphi}_{1sud_1,odl} = \frac{km_2 - m_1}{m_1 + m_2}\dot{\varphi}_{1sud_1,ul} + \frac{m_2(k+1)}{m_1 + m_2}\dot{\varphi}_{2sud_1,ul}.$$

Generalized coordinate φ_{sud_1} for the first impact, and velocities of heavy mass particles immediatelly after the impact $\dot{\varphi}_{1sud_1,odl}$, $\dot{\varphi}_{2sud_1,odl}$ represent the initial conditions of heavy mass particles in the following motion intervals.

Graphic visualization of conducted motion analysis for analyzed vibro-impact system based on oscillator moving along rough parabola, which consists of two ideal smooth pellets, will be shown in Fig.8 and Fig.9. Phase portrait of heavy mass particle 2 was given in Fig.8 and phase portrait of heavy mass particle 1 was given in Fig.9.
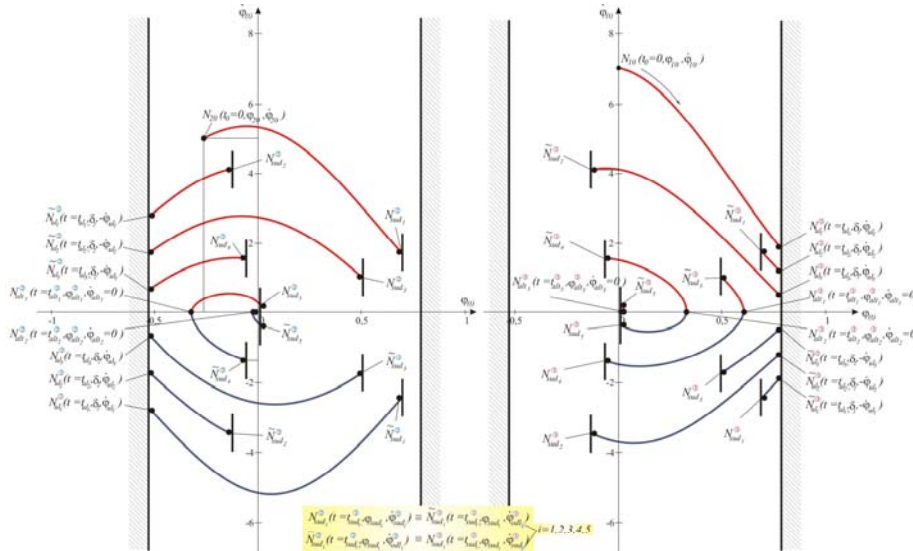
Fig. 8 *Phase portrait of heavy mass particle 2 (as part of an oscillator) moving along rough parabola line with sliding friction coefficient* $\mu = tg\alpha_0$ *with limited elongations in plane* $(\varphi,\dot\varphi)$ Fig. 9 *Phase portrait of heavy mass particle 1 (as part of an oscillator) moving along rough parabola line with sliding friction coefficient* $\mu = tg\alpha_0$ *with limited elongations in plane* $(\varphi,\dot\varphi)$

Based on the phase portraits of heavy mass particles, it can be seen that the value of angular velocities of heavy mass particle 1 impact into the elongation limiter placed on the right side and heavy mass particle 2 impact into the elongation limiter placed on the left side, alternately decreasing and increasing, and in general, if only even or only odd motion intervals were matched, it can be observed that the values of the initial angular velocity decreased.

4. Energy analysis of vibro-impact system

Energy analysis of the observed vibro-impact system consisting of heavy mass particles 1 and 2 was conducted so the graphic representations of alternations *Ek, Ep* and *E* for each branch of the phase portraits were performed. Graphic visualization of the energy alternations will be presented by figures (Fig.10) and (Fig.11) for the kinetic energies of the second and first heavy mass particle, (Fig.12) and (Fig.13) for the potential energy alternations of the second and first heavy mass particle and (Fig.14) and (Fig.15) for total mechanical energy of the second and first heavy mass particle.
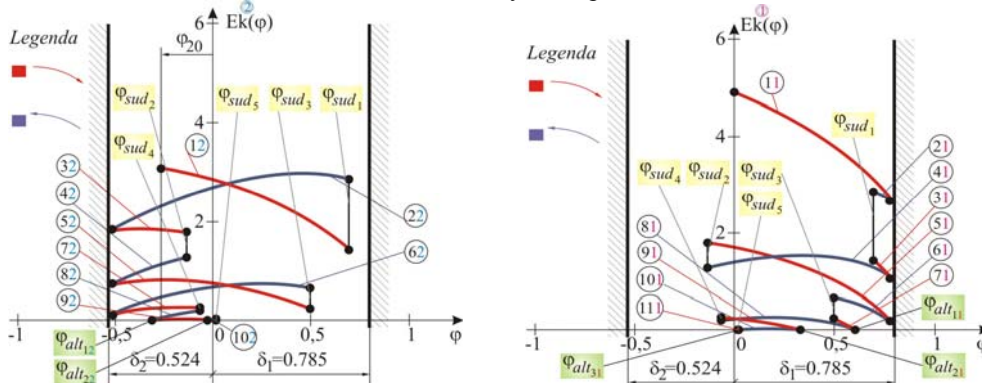
Fig. 10.- 11. Kinetic energy of heavy mass particle 2-1 in plane (Ek,φ).
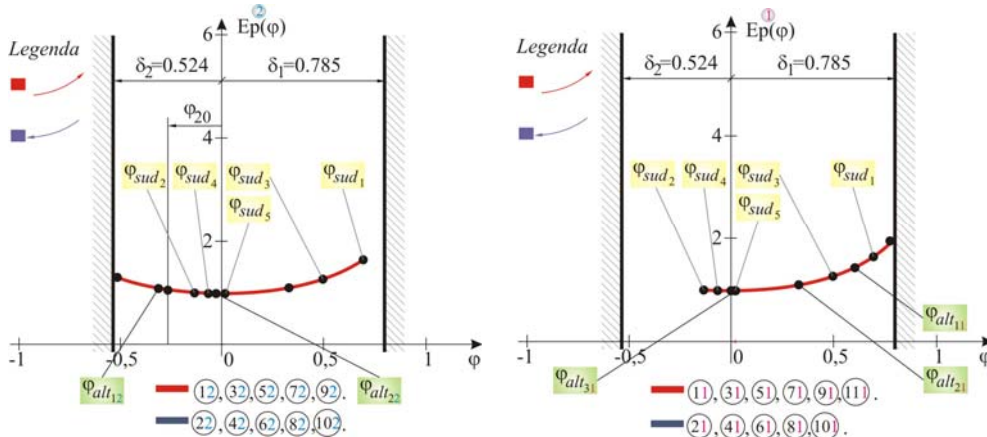
Fig. 12.- 13. Potential energy of heavy mass particle 2- 1 in plane (Ep, φ)
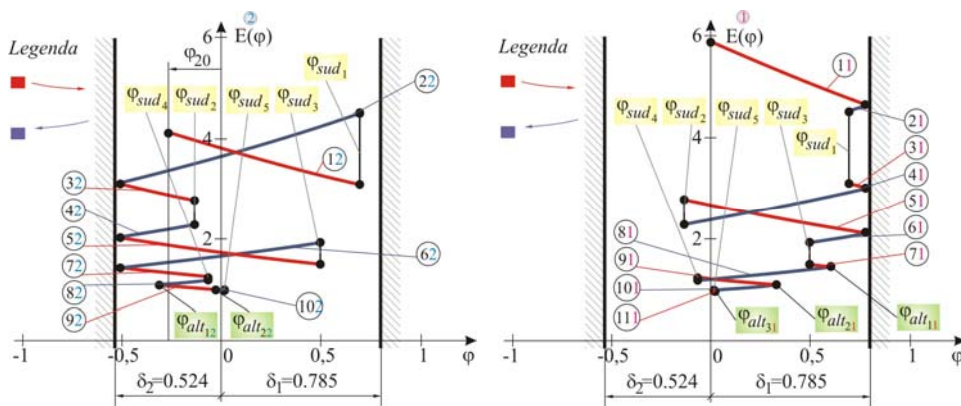
Fig. 14.-15. Total mechanical energy of heavy mass particle 2-1 in plane (E, φ)

5. Concluding Remarks

Non-linearity of the analyzed vibro-impact system is a result of discontinuity of heavy mass particles angular velocities moving along rough parabola. Discontinuities of angular velocities appeared at the moment of impact of first mass particle into elongation limiter set on the right, than at the moment of the motion direction alternation of the first and two heavy mass particles (when it appears) causing angular velocity and friction force alternations, and at the moment of heavy mass particles impact. This non-linearity is mathematically described for heavy mass particles by the system of governing non-linear differential equations, by the second part representing angular velocity square of generalized coordinate $\dot{\varphi}_1^2, \dot{\varphi}_2^2$. This corresponds to the case of "turbulent" supression.

It shoud also be noted that in analyzed vibro-impact system with two degrees of freedom, there is a trigger of coupled sigularities, i.e. phenomena of bifurcation of equilibrium positions, because of the influence of sliding Coulomb's friction force and angular velocities alternation of heavy mass particles.

Using analytical expressions for the phase trajectories branches of heavy mass particles, and after determining the integration constants, graphic visualization of heavy mass particles oscillation in the observed vibro-impact system with two degrees of freedom was presented. For graphic visualization, we used a software program MathCad.

The combination of analytical and numerical results in the process of getting the graphical performance of phase trajectories in different motion intervals of heavy mass particles, by using MathCad software and Corel Draw, phase portraits of heavy mass particles were obtained. On the phase portraits there are clearly visible phenomena of non-linearity of vibro-impact system with two degrees of freedom.

Furthermore, the energy analysis was performed for the observed vibro-impact system. The alternation of kinetic energy, potential energy and the total mechanical energy. It can be concluded that the observed vibro-impact system dissipation of the total mechanical energy is present, reduced pressure on the rough circle line and decrease the force that comes from the force of friction.

At the end, it is necessary to point out that using a software program MathCad and analytical expressions for the branches of phase trajectories at intervals between impacts and graphical determination of kinetic parameters of the state kinetics, in the process of impacts and velocity alternation, the visualization of vibro-impact dynamics is presented. A methodology that is easily applicable in engineering practice to analyze the dynamics of real vibro-impact systems is based on various visualizations. This methodology is gaining importance as an algorithm that facilitated the analysis of kinetic parameters of the dynamics vibro-impact system with two degrees of freedom.

References

[1]   Babickii V. I., Kolovskii M.Z., *Vibrations of linear system with limiters, and excited by random excitation*, *Mehanika tverdogo tela*, No 3,1967. (in Russian).
[2]   Babickii V. I.: *Theory of vibro-impact systems*, Moskva, "Nauka", 1978. (in Russian).
[3]   Babickii V. I., Kolovskii M.Z., *Investigation of the vibro-impact systems by resonant regimes*, *Mehanika tverdogo tela*, No 4,1976. (in Russian).
[4]   Bapat, C. N., Popplewell N., *Several Similar Vibroimpact Systems*, *Journal of Sound and Vibration,* 1987, 113 (1), pp. 17-28.
[5]   Stoker, J. J., (1950), *Nonlinear Vibrations,* Interscience Publish.
[6]   Peterka F., *Laws of Impact Motion of Mechanical Systems with one Degree of Freedom*: Part I - Theoretical Analysis of n- Multiple (1/n) - Impact Motions, Acta Technica CSAV, 1974, No 4, pp 462-473.
[7]   Peterka F., *Laws of Impact Motion of Mechanical Systems with one Degree of Freedom*: Part II - Resalts of Analogue Computer Modelling of the Motion, Acta Technica CSAV, 1974, No 5, pp 569-580.
[8]   Peterka F., 1996, Bifurcations and transition phenomena in an impact oscillator, Chaos, Solitons and Fractals, 7, 10, 1635-1647.
[9]   Hedrih (Stevanović) K., (2005), Nonlinear Dynamics of a Heavy Material Particle Along Circle which Rotates and Optimal Control, *Chaotic Dynamics and Control of Systems and Processes in Mechanics* (Eds: G. Rega, and F. Vestroni), p. 37-45. IUTAM Book, in Series *Solid Mechanics and Its Applications*, Editerd by G.M.L. Gladwell, Springer,. 2005, XXVI, 504 p., ISBN: 1-4020-3267-6. DOI 10.1007/1-4020-3268-4_4. ISBN 978-1-4020-3267-7 (Print) 978-1-4020-3268-4 (Online)
[10]   Hedrih (Stevanović) K., (2008), *The optimal control in nonlinear mechanical systems with trigger of the coupled singularities,* pp. 174-182, in the book: Advances in Mechanics : Dynamics and Control : Proceedings of the 14th International Workshop on Dynamics and Control / [ed. by F.L. Chernousko, G.V. Kostin, V.V. Saurin] : A.Yu. Ishlinsky Institute for Problems in Mechanics RAS. – Moscow : Nauka, 2008. –ISBN 978-5-02-036667-1

[11] Hedrih (Stevanović) K. (Serbia), *Homoclinic Orbits Layering in the Coupled Rotor Nonlinear Dynamics and Chaotic Clock Models*, SM17 – Multibody Dynamics (M. Geraldin and F. Pfeiffer), p. Lxiii – CD - SM10624, Mechanics of the 21st Century (21st ICTAM, Warsaw 2004) - CD ROM INCLUDED, edited by Witold Gutkowski and Tomasz A. Kowalewski, IUTAM, Springer 2005, ISBN 1-4020-3456-3, Hardcover., p. 421+CD. ISBN-13 978-1-4020-3456-5 (HB), ISBN-10 1-4020-3559-4(e-book), ISBN-13-978-1-4020-3559-3 (e-book). www. springeronline3.com.

[12] Hedrih (Stevanović) K., *A Trigger of Coupled Singularities*, MECCANICA, Vol.39, No. 3, 2004., pp. 295-314. International Journal of the Italian Association of Theoretical and Applied Mechanics,Meccanica, Publisher: Springer Science + Business Media B.V., Formerly Kluwer Academic Publishers B.V. ISSN: 0025-6455 (Paper) 1572-9648 (Online) DOI: 10.1023/B:MECC.0000022994.81090.5f, Issue: Volume 39, Number 3, Date: June 2004, Pages: 295 - 314

[13] Hedrih (Stevanović) K., *Free and forced vibration of the heavy material particle along line with friction*: Direct and inverse task of the theory of vibrorheology, 7th EUROMECH Solid Mechanics Conference, J. Ambrósio et.al. (eds.), Lisbon, Portugal, September 7-11, 2009, CD –MS-24, Paper 348, pp. 1-20.

[14] Hedrih (Stevanović) K., *Vibrations of a Heavy Mass Particle Moving along a Rough Line with Friction of Coulomb Type*, ©Freund Publishing House Ltd., International Journal of Nonlinear Sciences & Numerical Simulation ISSN: 1565-1339, Volume 11, NO.3, pp.203-210, 2010.

[15] Hedrih (Stevanović) K., *Discontinuity of kinetic parameter properties in nonlinear dynamics of mechanical systems*, Invited Keynote Lecture, Proceedings of the 9th Brazilian Conference on Dynamics, Control and Their Applications, DINCON , Serra Negra, 2010, pp. 8-40. (SP - ISSN 2178-3667).

[16] Hedrih (Stevanović) K. (2009), Phase plane method applied to the optimal control in nonlinear dynamical systems – Heavy material particle oscillations along rough circle line with friction: Phase portraits and optimal control 10th conference on DYNAMICAL SYSTEMS THEORY AND APPLICATIONS, December 7-10, 2009. Łódź, Poland (submitted).

[17] Nayfeh A.H., (1996), *Transfer of energy from high-frequency to Low-frequency modes*, Book of Abstracts, The Second International Conference "Asymptotics in Mechanics" St. Petersburg Marine Technical University, Russia, 13-16 October, 1996, pp. 44.

[18] Nayfeh A.H., and Balachandran B., *Applied Nonlinear Dynamics*, Wiley Interscience, 1995 .

[19] Foole S., Bishop S., *Bifurcation in Impact Oscillators*, UTAM, London, 1998.

[20] Luo G.W., Xie J.H., *Hopf Bifurcation of a Two-Degree-of-Freedom Vibro-impact System*, Journal of Sound and Vibration, 1998, 213 (3), pp.391-408.

[21] Nordmark A.B., (1991), *Nonperiodic Motion Caused by Grazing Incidence in an Impact Oscillator*, Journal of Sound and Vibration, 145(2), pp. 279-297.

[22] Pavlovskaia E., Wiercigroch M., 2003, Periodic solution finder for an impact oscillator with a drift, Journal of Sound and Vibration, 267, 4, 893-911.

[23] Pavlovskaia E., Wiercigroch M., Woo K.-C., Rodger A.A., 2003, Modelling of ground moling dynamics by an impact oscillator with a frictional slider, Meccanica, 38, 1, 85-97.

[24] Rašković D., *Mehanika - Dinamika (Dynamics)*, Naučna knjiga, 1972.

[25] Rašković D., Teorija oscilacija (Theory of oscillatins), Naučna knjiga, 1952.

[26] Hedrih (Stevanović) K., Raičević V., Jović S., *Vibro-impact of a Heavy Mass Particle Moving along a Rough Circle with Two Impact Limiters*, ©Freund Publishing House Ltd., International Journal of Nonlinear Sciences & Numerical Simulation ISSN: 1565-1339, Volume 11, NO.3, pp.211-224, 2010.

[27] Hedrih (Stevanović) K., Raičević V., Jović S., *„VIBROIMPACT SYSTEM DYNAMICS: HEAVY MATERIAL PARTICLE OSCILLATIONS ALONG ROUGH CIRCLE WITH TWO SIDE MOVING IMPACT LIMITS"*, The Symposium DyVIS (Dynamics of Vibroimpact Systems) ICoVIS -2th International Conference on Vibroimpact Systems, *6-9 January 2010*. School of Mechanical Engineering & Automation Northeastern University, Shenyang, Liaoning Province, P. R. China, pp.79-86.

[28] Hedrih (Stevanović) K., Jović S., *Models of Technological Processes on the Basis of Vibro-impact Dynamics*, Scientific Technical Review, Vol.LIX,No.2, 2009, pp.51-72.

[29] Hedrih (Stevanović) K., Raičević V., Jović S., Phase Trajectory Portrait of the Vibro-imact Forced Dynamics of Two Mass Particles along Rough Circle, 3rd International Conference on *Nonlinear Science and Complexity*, Ankara, Turkey, Çankaya Üniversitesi, 28-31 Jul, 2010 (to appear).

[30] Hedrih (Stevanović) K., Raičević V., Jović S., *The phase portrait of the vibro-imact dynamics of two mass particle motions along rough circle*, 3rd International conference "Nonlinear Dynamics – 2010", Kharkov, Ukraine, 21-24 Septembar, 2010, pp.84-89.

[31] Jović S., Raičević V., *Energy analysis of vibro-impact system dynamics based on a heavy mass particle free oscillations along curvilinear rough trajectories*, Scientific Technical Review, Vol.60, No.3-4, 2010, pp.9-21, M52=1,5 boda.

DYNAMIC MODELS OF BUILDINGS TO MITIGATE FLUCTUATIONS

**Vera Nikolić-Stanojević[1], Ćemal Dolićanin[1],
Ljiljana Veljović[2], Milica Obradović[2]**

[1] State Univesity of Novi Pazar, Serbia
e-mail: veranikolic1@gmail.com; rektorat@np.ac.rs
[2] Faculty of Mechanical Engineering in Kragujevac, Serbia
The University of Kragujevac
e-mail: veljovicljilja@yahoo.co.uk

Abstract. Dynamic suspension system for high-rise buildings has a role to reduce the oscillation of the highest floors of the effects of wind or the earthquake, and other adverse effects. It is a complex mechanical and mathematical problem.
The suspension system, which can be active and passive, to absorb and suppress all components of the forces that would lead to reduced life of the structure, comfort, housing and disruption of stability and security. Modeling of dynamic suspension system is reduced to the formation of physical and mathematical models that most adequately describes the real system. This paper presents a dynamic model for tall buildings. Given the numerical solution and the appropriate comments.

Key words: modeling, dynamic, intelligent building, dumping system.

1. Introduction

In recent years there are a lot of discussion about the category and the concept of "*intelligent building*", "*smart buildings"* or " *the next generation buildings*". This includes the use of technology and processes to create buildings that are safer and more productive for their users and that can apply all kinds of loads during the scheduled lifetime.

The concept of "intelligent building" was first introduced in the eighties in *Australia, Canada, China, Japan* and the *United States*. In fact, there is a race along with the construction of skyscrapers whose peaks are found in complex wind. Although to careful design in terms of aerodynamics, the problem of protection against the effects of weather is not solved. Intelligent design implies, in addition to the use of new standards such as XML and AEC-GB-XML and other system models to be tracked throughout the lifetime of the building and updated as necessary.

High buildings belong to the group of dynamical systems that influence the stability of the building in case of sudden, shock loads. The most common causes of horizontal and vertical oscillations of tall buildings are wind and tremors, i.e. earthquakes (Melbourne & Palmer, [27], 1002nd). Most unstable part of the tall building is its top - the highest intensity of oscilations is on the top floor. By adding the masses and building elements for depreciation or damping system such oscillations can be reduced.
In order to determine the boundaries of individual endurance, in terms of oscillations, experiments were carried out based on simulation of movement (Chen & Robertson, [6].

1973, Irwin [15] 1981, Goto [11], 1983, Shioya et al. 1992). In most cases the observed sinusoidal reasons. Isyumov, [14], 1993. showed that there are significant differences between these tests and the actual conditions. In fact there are axial, transversal and torsional oscillations, which can not adequately show the sine wave.

Based on these studies are conducted especially in North America, because it is subject to frequent hurricanes and typhoons, which set the limits can be exceeded because a certain period, the condition stabilizes and returns to its original (Isyumov, [14], 1993, Kareem [18.19] 1988th, Irwin, [16] 1986.etc.).

Structural systems that can mitigate the effects of wind are very different. For example, by *adding a system of pillars*, Figure 1a, one can increase the resistance of buildings, especially the effect of torque caused by lateral loads caused by wind. The building of 30 ... 40 floors, typically relying on a "*shear wall"* and the focal steel struts that are very effective in confronting the forces caused by earthquakes. For more solitary, central systems are becoming scarce. In these cases, installation of load-bearing walls or bars, usually at a distance of 2 ... 3 floors, it can be to alleviate that problem as one of the cargo transferred to the external structure. Installation of such systems has proven to be efficient in the world's highest buildings, such as the *Melbourne Tower* (500 m).Later, these systems have been modified using the *band walls / grid as a "virtual carriers"*, Figure 1b. so that achieves the same transmission power, but much simpler structure. This system was applied at the highest world of reinforced concrete building with 77 floors of *Plaza Rakyat*, (office building in *Kuala Lumpur*).
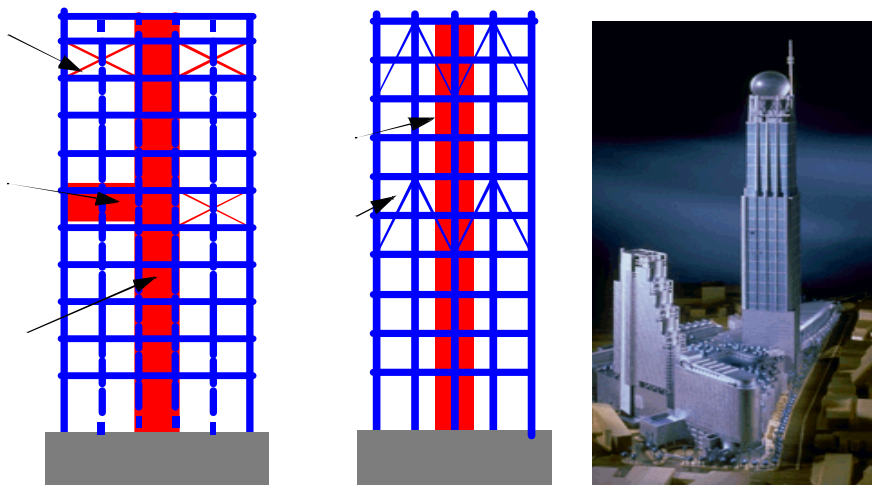
Figure 1. (a) Schematic representation of outrigger system. (b) Illustration of "virtual outrigger" system using belt trusses (Model of Plaza Rakyat)

A similar system was implemented with the so-called. *Vierendeel pads*, Figure 2, placed at 775 feet high building, at the *First Bank Place in Minneapolis* (Dorris, [9], 1991). The tower carried by the skeleton is in the form of a cross with four pillars of reinforced steel which is effective when it comes to large torsional moments. *Vierendeel* installation and trim, structural strength is more increased by 36%. Lining of the upper floors receive the cargo and transfer it to the massive pillars between the columns and beams (*the Sears Tower, World Trade Towers and Center John Hancock Center*). This concept has become popular and was applied and the *Shanghai World Finance Center*.

The *combination of tube* ("tube in tube") or a double system of pipes of steel and reinforced concrete (composite pipes) has proven very effective in protection from typhoons.

Vierendeel bandage

Super column
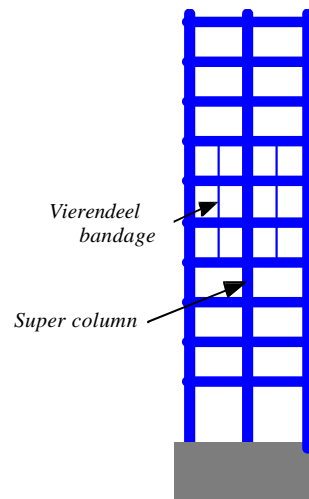
Figure 2. Schematic of Vierendeel bandage

Other solutions mainly based on increasing the mass of the upper floors. This method is applied to the *Washington National Airport Control Tower* so the rotation of the building (and Banavalkar Isyumov, [5], 1998).is neglected.

Aerodynamic modifications of the building proved to be very effective (Kwok and Isyumov, [24], 1998.) and it is usually called "*Cross-sectional*" shape. Researches (Kwok, [23], 1995.) have shown that various modifications can deliver significant reduction in the harmful effects of wind. Aerodynamics effect tests showed that there is some adjusting in the angles inside the building (Hayashida and Iwasa, [12], 1990.), Figure 3. The *angle modification* reflected a favorable angle to reduce the effects of weather along and inside the building. It is shown that the larger rounding buildings (closer to a circular shape) is very convenient.

| *Basic* | *Fins* | *Vented Fins* | *SlottedCorners* | *Chamfered Corners* |
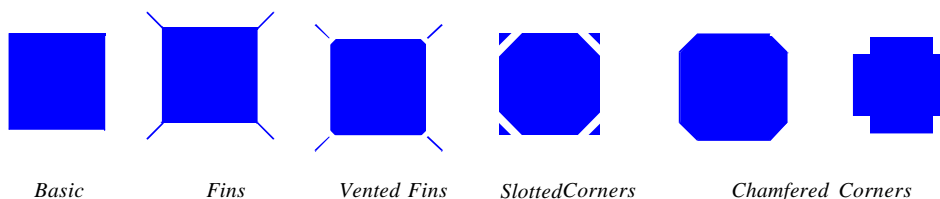
Figure 3. Aerodynamic Modifications to Square Building Shape

This method was applied at a height of 150 m, the *Yokohama Mitsubichi Heavy Industries Building*, and wind power is considerably reduced. But still there is a certain consensus (agreement) about the advantages of angular geometric modification, since some studies have also shown that modifications at the corners in some cases have been ineffective and

even had negative consequences (Miyashita et. al., [29], 1993, Kwok & Isyumov, [24], 1998).

Improved response in relation to the cross wind, in tall buildings, is given *by reduction in cross section with increasing altitude* (Shimada & Hibi, [33], 1995), Fig. 4. This was confirmed in some other works and the general conclusion is, if the top of the building more sculpted, the greater the influence of longitudinal and transverse wind is less (*Jin Mao building (Figure 4a) in China and Petronas Towers (Figure 4b) in Malaysia.*

a)   *b)*
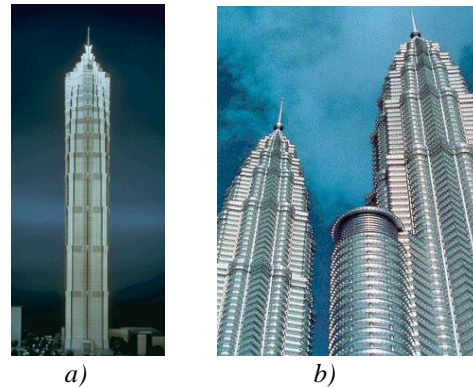
Figure 4. (a) Sketch of Jin Mao Building. (taken from Skidmore, Owings, and Merrill, LLP); (b) Photo of upper plan of Petronas Towers

One method in order to improve aerodynamics is to *add designed holes* (Miyashita, [29], 1993. Irwin, [17], 1998.), Figure 5. The holes completely through the building, especially those near the top, significantly reduce whirling wind power (Dulton & Isyumov, [10], 1990., Kareem, [18, 19], 1988). Effectiveness of this modification is impaired if the holes are on the lower levels of buildings.

However, this method may have a negative impact in terms of increasing whirling sound resonance imaging (Tamura, [36], 1997). Adding a hole was applied and *the Shanghai World Finance Center*. Diameter hole at the top of the tower is 51 m. In this case, is reached and the previous effect of reducing the cross section at the top of the building.
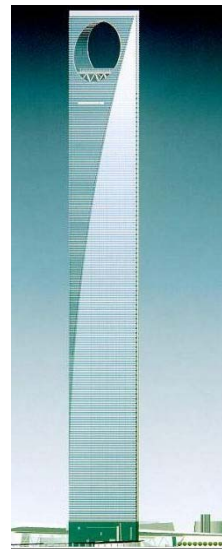
Figure 5. Shanghai World Financial Center)

The tall buildings Model can be represented as a system of two masses with two springs and ballasts (P. Horan, [31]) where the second mass, the mass of the last floor of a characteristic element of depreciation which is tied to it will depend on which elements are applied. This system works as a passive truck.

2. Display oscillator model

The tall buildings Model can be represented as a system of two masses with two springs and ballasts (P. Horan, [31]) where the second mass, the mass of the last floor of a characteristic element of depreciation which is tied to it will depend on which elements are applied. This system works as a passive truck..

If beside bearings, springs, ballasts, there is a system for control and automation at any time determines the output value depending on the size of input and previous output we get active tipper. System with passive tipper will give better acceleration and displacement reduction system in relation to the controlled system but worse results in the case of loads such as earthquake in comparison with the controlled system. Therefore, in practice, uncontrolled systems are rarely used. This example was first exposed to passive systems analysis and control system is carried out. In Figure 6 simplified model of a six-building is shown.
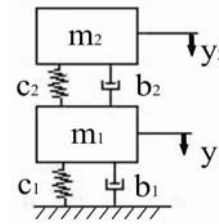
Figure 6. Model of a six- store building

System parameters are chosen based on the weight relationship μ.

$$\mu = \frac{m_2}{m_1} \qquad (2.1)$$

The optimal damping ratio for the mass m_1 (ξ_{1opt}) is chosen among these three recommended values from the literature [2, 28, 31], 0; 0.02; 0.05.

Based on the weight relationship μ and adopted the optimal damping relationships ξ_{1opt} for m_1, one can calculate the optimal damping ratio and the optimum ratio ξ_{2opt} frequency setting for the mass damper f_{2opt}, i.e. mass m_2 in the equation (Sadek):

$$f_{2opt} = \frac{1}{1+\mu} \cdot \left(1 - \xi_1 \sqrt{\frac{\mu}{1+\mu}} \right), [-]$$

$$\xi_{2opt} = \frac{\xi_1}{1+\mu} + \sqrt{\frac{\mu}{1+\mu}}, [-] \qquad (2.2)$$

The next step is reading the value of the optimal damping and optimal stiffness b_{2opt} and c_{2opt} for mass m_2 on the basis of weight relationship μ on diagram which is shown in Figure 7, (M. H. Chey, [28]).
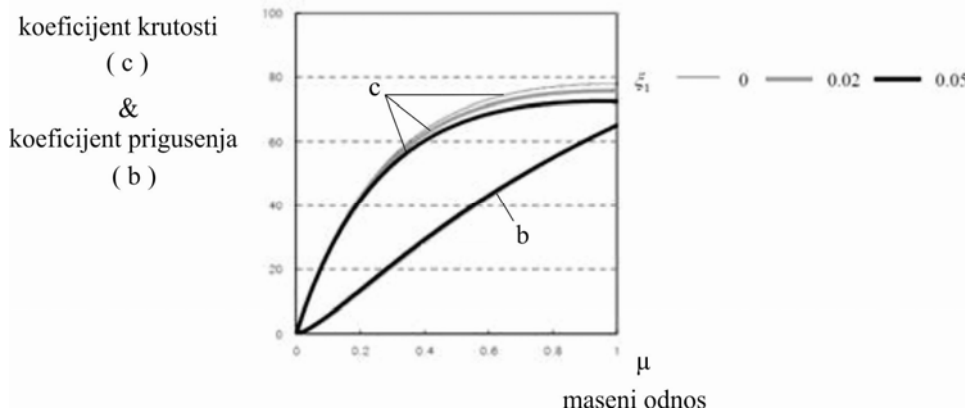
Figure 7. Diagram of the stiffness coefficient, damping coefficient - weight relationships

By using obtained optimal values for f_{2opt}, ξ_{2opt}, b_{2opt} and c_{2opt} frequency ω_1 for circular mass m_1 and damping ratio ξ_2 of the mass m_2 are obtained from equation::

$$c_{2opt} = m_2\omega_1^2 f_{2opt}^2 = \frac{m_2\omega_1^2\left(\xi_1\sqrt{\frac{\mu}{1+\mu}}-1\right)^2}{(1+\mu)^2} \Rightarrow \omega_1^2 = \frac{c_{2opt}}{m_2 f_{2opt}^2} = \frac{c_{2opt}(1+\mu)^2}{m_2\left(\xi_1\sqrt{\frac{\mu}{1+\mu}}-1\right)^2}$$

$$\Rightarrow \omega_1 = \frac{1}{f_{2opt}}\sqrt{\frac{c_{2opt}}{m_2}} = \frac{1+\mu}{\xi_1\sqrt{\frac{\mu}{1+\mu}}-1}\sqrt{\frac{c_{2opt}}{m_2}}$$

$$b_{2opt} = 2m_2\xi_2\omega_1 f_{2opt} \Rightarrow \xi_2 = \frac{b_{2opt}}{2m_2\omega_1 f_{2opt}}$$

(2.3)

It was necessary to determine the angular frequency ω_2 of mass m_2 from the equation:

$$f_2 = f_{2opt} = \frac{\omega_2}{\omega_1} \Rightarrow \omega_2 = \omega_1 \cdot f_{2opt}$$

(2.4)

Finally, the values of stiffness and damping parameters for both mass are obtained from the equation:

$$\omega_i^2 = \frac{c_i}{m_i} \Rightarrow c_i = m_i\omega_i^2 , \quad i = 1, 2 ; c_1 = m_1\omega_i^2 ; c_2 = m_2\omega_2^2$$

$$b_i = 2\xi_i\omega_i m_i , i = 1, 2 ; b_1 = 2\xi_1\omega_1 m_1 ; b_1 = 2\xi_1\omega_2 m_2$$

(2.5)

In this case, approved the masses m_1=203t i m_2=32.277t that gives μ=0.159. The optimal damping coefficient ξ_{1opt} for mass m_1 is 0.05.

By applying the above-described procedure, the following parameters were obtained for the system to be analyzed, Table 1, [2, 28, 31].

Table 1. System characteristics

mass		spring stiffness coefficient		damping coefficient	
m_1 [t=10^3 kg]	m_2 [t=103kg]	c_1 [kN/m]	c_2 [kN/m]	b_1 [kNs/m]	b_2 [kNs/m]
203	32.277	245.63	28.0185	22.33	16.6

2.1 Mathematical modeling of the system

For the oscillatory model, Figure 6, it can be written Lagrange second kind equations, [22, 32, 37] in the form of:

$$\frac{d}{dt}\left(\frac{\partial E_k}{\partial \dot{q}_i}\right) - \frac{\partial E_k}{\partial q_i} = Q_i^{(N)} - \frac{\partial E_p}{\partial q_i}, i = 1,..,s \qquad (2.6)$$

$$Q_i^{(N)} = -\frac{\partial \phi}{\partial q_i}$$

where s is the number of degrees of system freedom. For the given system there are two degrees of freedom, i.e. s = 2.
Independent movement of the mass are vertical movement so as adopt generalized coordinates are y_1 and y_2.
It is necessary to determine the kinetic, potential and dissipation energy of systems in order to write the Lagrange equations of motion.
The kinetic energy of the system is equal to the sum of the kinetic energies of bodies with mass m_1 and m_2 and it is a function of generalized speeds::

$$E_k = E_{k1} + E_{k2} \; ; \; E_{k1} = \frac{1}{2}m_1 \dot{y}_1^2 \; ; \; E_{k2} = \frac{1}{2}m_2 \dot{y}_2^2 \; ; \; E_k = \frac{1}{2}m_1 \dot{y}_1^2 + \frac{1}{2}m_2 \dot{y}_2^2 \qquad (2.7)$$

The potential energy of the system is a function of displacement, i.e. reflected in the generalized coordinates as follows:

$$E_p = E_{p1} + E_{p2} \; ; \; E_{p1} = \frac{1}{2}c_1 y_1^2 : E_{p2} = \frac{1}{2}c_2 (y_2 - y_1)^2 \; ; \; E_p = \frac{1}{2}c_1 y_1^2 + \frac{1}{2}c_2 (y_2 - y_1)^2 \qquad (2.8)$$

and the damping energy is:

$$\phi = \phi_1 + \phi_2 \; ; \; \phi_1 = \frac{1}{2}b_1 \dot{y}_1^2 \; ; \; \phi_2 = \frac{1}{2}b_2 \dot{y}_2^2 \; ; \; \phi = \frac{1}{2}b_1 \dot{y}_1^2 + \frac{1}{2}b_2 \dot{y}_2^2 \qquad (2.9)$$

Furthermore, it is necessary to find partial derivatives of the calculated energy. Partial derivatives of kinetic energy (2.7) per generalized speeds are:

$$\frac{\partial E_k}{\partial \dot{y}_1} = m_1 \dot{y}_1 \; ; \; \frac{\partial E_k}{\partial \dot{y}_2} = m_2 \dot{y}_2 \qquad (2.10)$$

and their derivatives by time:

$$\frac{d}{dt}\left(\frac{\partial E_k}{\partial \dot{y}_1}\right) = m_1 \ddot{y}_1 \quad ; \qquad \frac{d}{dt}\left(\frac{\partial E_k}{\partial \dot{y}_2}\right) = m_2 \ddot{y}_2 \tag{2.11}$$

Partial derivatives of kinetic energy in generalized coordinates are zero because the kinetic energy is not dependent on displacement; it depends from mass velocities only:

$$\frac{\partial E_k}{\partial y_1} = 0 \quad ; \qquad \frac{\partial E_k}{\partial y_2} = 0 \tag{2.12}$$

Partial derivatives of potential energy (3.3) in generalized coordinates are:

$$\frac{\partial E_p}{\partial y_1} = c_1 y_1 + c_2 (y_2 - y_1) \cdot (-1) = (c_1 + c_2) y_1 - c_2 y_2$$

$$\frac{\partial E_p}{\partial y_2} = c_2 (y_2 - y_1) \cdot 1 = -c_2 y_1 + c_2 y_2 \tag{2.13}$$

It is necessary to determine the generalized forces on the basis of statements of partial energy damping (2.9) by the generalized speeds:

$$Q_1^{(N)} = -\frac{\partial \phi}{\partial \dot{y}_1} = -b_1 \dot{y}_1 - b_2 (\dot{y}_2 - \dot{y}_1) \cdot (-1) = -(b_1 + b_2) \dot{y}_1 + b_2 \dot{y}_2$$

$$Q_2^{(N)} = -\frac{\partial \phi}{\partial \dot{y}_2} = -b_2 (\dot{y}_2 - \dot{y}_1) \cdot 1 = b_2 \dot{y}_1 - b_2 \dot{y}_2 \tag{2.14}$$

Based on the calculated energies and partial statements of their respective sizes Lagrange equations can be written in the form of:

$$\frac{d}{dt}\left(\frac{\partial E_k}{\partial \dot{y}_1}\right) - \frac{\partial E_k}{\partial y_1} = Q_1 - \frac{\partial E_p}{\partial y_1}$$

$$\frac{d}{dt}\left(\frac{\partial E_k}{\partial \dot{y}_2}\right) - \frac{\partial E_k}{\partial y_2} = Q_2 - \frac{\partial E_p}{\partial y_2} \tag{2.15}$$

Substituting the calculated values it is obtained Lagrange equations that describe the monitored system:

(1) $\qquad\qquad m_1 \ddot{y}_1 + (b_1 + b_2) \dot{y}_1 - b_2 \dot{y}_2 + (c_1 + c_2) y_1 - c_2 y_2 = 0$

(2) $\qquad\qquad m_2 \ddot{y}_2 - b_2 \dot{y}_1 + b_2 \dot{y}_2 - c_2 y_1 + c_2 y_2 = 0$
$\hfill (2.16)$

The equations of motion can be written in matrix form as:

$$\begin{bmatrix} m_1 & 0 \\ 0 & m_2 \end{bmatrix} \cdot \begin{Bmatrix} \ddot{y}_1 \\ \ddot{y}_2 \end{Bmatrix} + \begin{bmatrix} b_1+b_2 & -b_2 \\ -b_2 & +b_2 \end{bmatrix} \cdot \begin{Bmatrix} \dot{y}_1 \\ \dot{y}_2 \end{Bmatrix} + \begin{bmatrix} c_1+c_2 & -c_2 \\ -c_2 & +c_2 \end{bmatrix} \cdot \begin{Bmatrix} y_1 \\ y_2 \end{Bmatrix} = 0 \tag{2.17}$$

where **M**, **B** i **C** are mass matrix, damping and stiffness matrix, respectively, ie.:

$$\mathbf{M} = \begin{bmatrix} m_1 & 0 \\ 0 & m_2 \end{bmatrix}, \mathbf{B} = \begin{bmatrix} b_1+b_2 & -b_2 \\ -b_2 & +b_2 \end{bmatrix}, \mathbf{C} = \begin{bmatrix} c_1+c_2 & -c_2 \\ -c_2 & +c_2 \end{bmatrix} \tag{2.18}$$

Hamilton's equations, [22, 32, 37], are:

$$d\left(\sum_{i=1} p_i \dot{y}_i - L\right) = \sum_{i=1}\left[(Q_i - \dot{p}_i)dy_i + \dot{y}_i dp_i\right] - \frac{\partial L}{\partial t} dt$$

$$L = E_k - E_p$$

$$p_i = \frac{\partial L}{\partial \dot{y}_i} = \frac{\partial\left(E_k - E_p\right)}{\partial \dot{y}_i} = \frac{\partial E_k}{\partial \dot{y}_i}$$
(2.19)

where L is a function of Lagrange and p_i is generalized impulse. Hamilton function H is represented by the expression:

$$H = \sum_{i=1} p_i \dot{y}_i - L$$
(2.20)

$$dH = \sum_{i=1}\left[(Q_i - \dot{p}_i)dy_i + \dot{y}_i dp_i\right] - \frac{\partial L}{\partial t} dt$$

Characteristic functions for the reference system are still determined and that is:

$$L = E_k - E_p = \frac{1}{2}m_1 \dot{y}_1^2 + \frac{1}{2}m_2 \dot{y}_2^2 - \frac{1}{2}c_1 y_1^2 - \frac{1}{2}c_2 (y_2 - y_1)^2$$

$$p_1 = \frac{\partial L}{\partial \dot{y}_1} = m_1 \dot{y}_1 \Rightarrow \dot{y}_1 = \frac{p_1}{m_1} \Rightarrow \dot{y}_1^2 = \frac{p_1^2}{m_1^2} \; ; \; p_2 = \frac{\partial L}{\partial \dot{y}_2} = m_2 \dot{y}_2 \Rightarrow \dot{y}_2 = \frac{p_2}{m_2} \Rightarrow \dot{y}_2^2 = \frac{p_2^2}{m_2^2}$$
(2.21)

$$H = \sum_{i=1}^{n} p_i \dot{y}_i - L = p_1 y_1 + p_2 y_2 - L \; ; \; H = \frac{1}{2}\frac{p_1^2}{m_1} + \frac{1}{2}\frac{p_2^2}{m_2} + \frac{1}{2}c_1 y_1^2 + \frac{1}{2}c_2 (y_2 - y_1)$$

The Hamilton function (2.20) derivatives by generalized coordinates and generalized impulses are:

$$\frac{\partial H}{\partial y_1} = c_1 y_1 + c_2 (y_2 - y_1) \cdot (-1) = (c_1 + c_2)y_1 - c_2 y_2$$

$$\frac{\partial H}{\partial y_2} = c_2 (y_2 - y_1) \cdot 1 = -c_2 y_1 + c_2 y_2$$

$$\frac{\partial H}{\partial p_1} = \frac{1}{2m_1} \cdot 2p_1 = \frac{p_1}{m_1}$$
(2.22)

$$\frac{\partial H}{\partial p_2} = \frac{1}{2m_2} \cdot 2p_2 = \frac{p_2}{m_2}$$

Hamilton's equations in canonical form are obtained based on terms:

$$\dot{y}_i = \frac{\partial H}{\partial p_i} \; ; \qquad \dot{p}_i = Q_i - \frac{\partial H}{\partial y_i}$$
(2.23)

For the considered system the canonical form of equations is obtained in a form:

$$\dot{y}_1 = \frac{\partial H}{\partial p_1} = \frac{p_1}{m_1}$$

$$\dot{p}_1 = Q_1 - \frac{\partial H}{\partial y_1} = -(b_1 + b_2)\dot{y}_1 + b_2 \dot{y}_2 - (c_1 + c_2)y_1 + c_2 y_2 = -(b_1 + b_2)\frac{p_1}{m_1} + b_2 \frac{p_2}{m_2} - (c_1 + c_2)y_1 + c_2 y_2$$

$$\dot{y}_2 = \frac{\partial H}{\partial p_2} = \frac{p_2}{m_2}$$
(2.24)

$$\dot{p}_2 = Q_2 - \frac{\partial H}{\partial y_2} = b_2 \dot{y}_1 - b_2 \dot{y}_2 + c_2 y_1 - c_2 y_2 = b_2 \frac{p_1}{m_1} - b_2 \frac{p_2}{m_2} + c_2 y_1 - c_2 y_2$$

The **state matrix of system** by taking into account the main coordinates are determined by the *Hamilton generalized coordinates and generalized momentum:*

$$q_1 = y_1 \qquad \dot{q}_1 = \dot{y}_1$$
$$q_2 = y_2 \qquad \dot{q}_2 = \dot{y}_2$$
$$q_3 = p_1 \qquad \dot{q}_3 = \dot{p}_1 \tag{2.25}$$
$$q_4 = p_2 \quad \Rightarrow \quad \dot{q}_4 = \dot{p}_2$$

The state matrix of system is:

$$\{\dot{q}\} = A\{q\} \tag{2.26}$$

So the state matrix of system based on the canonical Hamilton equations for modeled system can be written:

$$
\begin{Bmatrix} \dot{q}_1 \\ \dot{q}_2 \\ \dot{q}_3 \\ \dot{q}_4 \end{Bmatrix}
=
\begin{bmatrix}
0 & 0 & \dfrac{1}{m_1} & 0 \\
0 & 0 & 0 & \dfrac{1}{m_2} \\
-(c_1+c_2) & c_2 & \dfrac{-(b_1+b_2)}{m_1} & \dfrac{b_2}{m_2} \\
c_2 & -c_2 & \dfrac{b_2}{m_1} & \dfrac{-b_2}{m_2}
\end{bmatrix}
\cdot
\begin{Bmatrix} q_1 \\ q_2 \\ q_3 \\ q_4 \end{Bmatrix}
\tag{2.27}
$$

Substituting the data of the mass, stiffness coefficients and damping coefficients from Table 1 in equation (2.26) the matrix A becomes:

$$
A =
\begin{bmatrix}
0 & 0 & 4.926\text{e-}6 & 0 \\
0 & 0 & 0 & 3.0982\text{e-}5 \\
-273.65\text{e+}3 & 28.0185\text{e+}3 & -0.1918 & 0.5143 \\
28.0185\text{e+}3 & -28.0185\text{e+}3 & 0.0818 & -0.5143
\end{bmatrix}
\tag{2.28}
$$

To determine the stability of the system Ljapunov stability method [22, 32, 37] is used. According to Ljapunov criteria it is necessary to determine the matrix D such that satisfies the condition:

$$A^T D + DA = Q \tag{2.29}$$

The matrix Q in previous equation is non positive unit matrix, i.e.,

$$
Q = -I = -
\begin{bmatrix}
1 & 0 & 0 & 0 \\
0 & 1 & 0 & 0 \\
0 & 0 & 1 & 0 \\
0 & 0 & 0 & 1
\end{bmatrix}
=
\begin{bmatrix}
-1 & 0 & 0 & 0 \\
0 & -1 & 0 & 0 \\
0 & 0 & -1 & 0 \\
0 & 0 & 0 & -1
\end{bmatrix}
\tag{2.30}
$$

It is known that the system is stable if the determinant of the matrix D and all major minors are greater than or equal to zero [7, 8, and 30].

The matrix D is obtained by solving matrix equations or it can be easily obtained in *MatLab* by using the command:

D=lyap(A,I) where the identity matrix I is I = – Q. I = eye (4.4).
For analyzing system it is obtained that the dynamic matrix D is matrix with following values:

$$D = \begin{bmatrix} 0.0000 & 0.0000 & -0.0000 & 0.0000 \\ 0.0000 & 0.0000 & -0.0000 & -0.0000 \\ -0.0000 & -0.0000 & 9.55005 & 0.1503 \\ 0.0000 & -0.0000 & 0.1503 & 0.4281 \end{bmatrix} \cdot 1e+10 \tag{2.31}$$

The matrix D determinant is:

$$\det|D| = 1.2908 \cdot 10^{21} > 0 \tag{2.32}$$

and order appropriate major minors determinants are respectively:

$$D_0 = 1.9909 > 0 \; ; \quad D_1 = 8.8730 > 0 \; ; \quad D_2 = 5.9811 \cdot 10^{11} > 0 \tag{2.33}$$

So it can be concluded that analyzed system is stable.

2.2 Own system frequency definition

By solving the frequency equation their own system frequency are obtained. Frequency equation is in the form, [20, 26, and 34]:

$$\det(\lambda I - A) = 0 \tag{2.34}$$

$$\begin{bmatrix} \lambda & 0 & 0 & 0 \\ 0 & \lambda & 0 & 0 \\ 0 & 0 & \lambda & 0 \\ 0 & 0 & 0 & \lambda \end{bmatrix} - \begin{bmatrix} 0 & 0 & 4.926e\text{-}6 & 0 \\ 0 & 0 & 0 & 3.0982e\text{-}5 \\ -273.65e\text{+}3 & 28.0185e\text{+}3 & -0.1918 & 0.5143 \\ 28.0185e\text{+}3 & -28.0185e\text{+}3 & 0.0818 & -0.5143 \end{bmatrix} = \begin{bmatrix} \lambda & 0 & -4.926e\text{-}6 & 0 \\ 0 & \lambda & 0 & -3.0982e\text{-}5 \\ 273.65e\text{+}3 & -28.0185e\text{+}3 & \lambda+0.1918 & -0.5143 \\ -28.0185e\text{+}3 & 28.0185e\text{+}3 & -0.0818 & \lambda+0.5143 \end{bmatrix}$$

$$\det(\lambda I - A) = \lambda \cdot \begin{vmatrix} \lambda & 0 & -3.0982e\text{-}5 \\ -28.0185e\text{+}3 & \lambda+0.1918 & -0.5143 \\ 28.0185e\text{+}3 & -0.0818 & \lambda+0.5143 \end{vmatrix} - 0.000004926 \cdot \begin{vmatrix} 0 & \lambda & -3.0982e\text{-}5 \\ 273.65e\text{+}3 & -28.0185e\text{+}3 & -0.5143 \\ -28.0185e\text{+}3 & 28.0185e\text{+}3 & \lambda+0.5143 \end{vmatrix}$$

$$\det(\lambda I - A) = \lambda^4 + 0.7061\lambda^3 + 2.2726\lambda^2 + 0.7178\lambda + 1.0503 \tag{2.35}$$

Thus we obtain the characteristic determinants of polynomial (2.35) by an unknown λ.

The characteristic polynomial can also be obtained on an easier way via MATLAB if one enters values for the matrix A in the main window and press command:

characteristic polynom = poly (A)

By solving the characteristic polynom by λ its own frequency (2.36) are obtained.

Own frequencies, we can also determine from Matlab using the command: frequency = eig (A)

The obtained values of its own frequency for a given model are:

$\lambda_1 = -0.2086 + 1.1664 \, i \; ; \; \lambda_2 = -0.2086 - 1.1664 \, i \; ; \; \lambda_3 = -0.1445 + 0.8528 \, i \; ;$
$\lambda_4 = -1445 \, -0.8528$ \hfill (2.36)

2.3 The transfer function of the system

In order to define the system transfer function, it is necessary to determine the damping factors and appropriate frequencies. By using MatLab programs and commands:

$$[w_n, \xi] = damp(A)$$

damping factors are obtained:

$$\xi_1 = 0.1760 \;\; ; \;\; \xi_2 = 0.1760 \;\; , \xi_3 = 0.1671 \;\; ; \;\; \xi_1 = 0.1671 \tag{2.37}$$

The appropriate frequencies for the system are respectively:

$$w_{n1} = 1.1849 \; ; \; w_{n2} = 1.1849 \; ; \; w_{n3} = 0.8649 \; ; \; w_{n1} = 0.8649 \tag{2.38}$$

By using obtained values for the frequency and damping of the observed system *transfer functions* can be written *in the form of polynomials* based on the formula:

$$H(S) = \frac{1}{S^2 + 2\xi w_n S + w_n{}^2} \tag{2.39}$$

The transfer functions of the observed model are:

$$H_1(S) = \frac{1}{S^2 + 0.4171\,S + 1.404} \;\; ; \;\; H_1(S) = \frac{1}{S^2 + 0.4171\,S + 1.404}$$

$$H_3(S) = \frac{1}{S^2 + 0.28905\,S + 0.74805} \;\; ; \;\; H_4(S) = \frac{1}{S^2 + 0.28905\,S + 0.74805} \tag{2.40}$$

To express transfer function through the transmission zeros and poles, it is necessary to determine the zeros and poles first of all:

$$z_1 = 0 \;\; ; \;\; p_1 = -0.20855 + 1.1651 \;\; ; \;\; p_1{}^* = -0.20855 - 1.165i \;\; ; \;\; k_1 = 1$$

$$z_2 = 0 \;\; ; \;\; p_2 = -0.20855 + 1.1651 \;\; ; \;\; p_2{}^* = -0.20855 - 1.165i \;\; ; \;\; k_2 = 1$$

$$z_3 = 0 \;\; ; \;\; p_3 = -0.1445 + 0.853\,i \;\; ; \;\; p_3{}^* = -0.1445 - 0.853\,i \;\; ; \;\; k_3 = 1 \tag{2.41}$$

$$z_4 = 0 \;\; ; \;\; p_4 = -0.20855 + 1.1651 \;\; ; \;\; p_4{}^* = -0.20855 - 1.1651 \;\; ; \;\; k_4 = 1$$

Now, the transfer function is:

$$H_i(S) = \frac{k_i}{(S - p_i) \cdot (S - p_i{}^*)} \tag{2.42}$$

By applying calculated zeros and poles at the above formula transfer functions are obtained:

$$H_1(S) = \frac{k_1}{(S-p_1)\cdot(S-p_1^*)} = \frac{1}{(S+0.20855-1.165i)\cdot(S+0.20855+1.165i)}$$

$$H_2(S) = \frac{k_2}{(S-p_2)\cdot(S-p_2^*)} = \frac{1}{(S+0.20855-1.165i)\cdot(S+0.20855+1.165i)}$$

$$H_3(S) = \frac{k_3}{(S-p_3)\cdot(S-p_3^*)} = \frac{1}{(S+0.1445-0.853i)\cdot(S+0.1445+0.853i)}$$

(2.43)

$$H_4(S) = \frac{k_4}{(S-p_4)\cdot(S-p_4^*)} = \frac{1}{(S+0.1445-0.853i)\cdot(S+0.1445+0.853i)}$$

To draw a layout of the poles in *MatLab* one need to enter the transfer function and the set commands:
zeros = roots (num); poles = roots (den);
hold on;
plot(real(poles),   imag(poles),'x');
It can be seen on Figure 8. that all poles are in the left side and it is concluded that the *observed system is stable*.
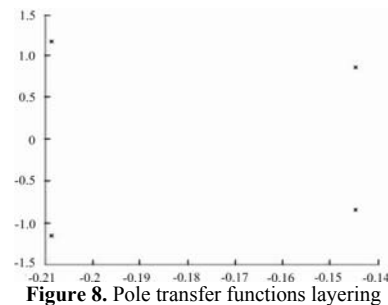
Figure 8. Pole transfer functions layering

Based on the derived transfer function, system responses to unit step function are shown in Figure 9.

Time t, s   *Time t, s*
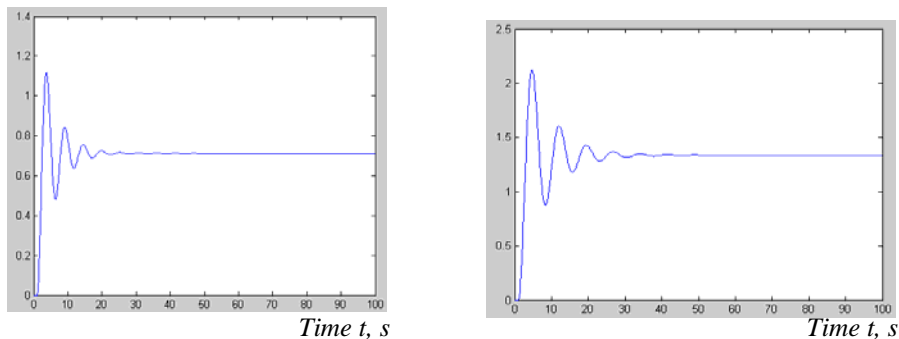
Figure 9. System responses to unit step function

It can be seen in Figure 9 that in the case without loads there is a big jump and a relatively long time to reach steady state - about the 40s.

That is why it is necessary to automate the system to reduce overshoot and oscillatory interval shortening and achieving faster response system and reach steady state. In further work in this field, it may review the effects of management on the first transmission function and automating and semi-automating dumping systems..

Semi–active type works by changing the coefficient of viscous damping system on various ways. Basic characteristic of semi-suspension system is that it is activated only in the time

interval when the relative velocity of the piston dampers and the required force are of the same sign.

Differential control can reduce the overshoot but leads to zero steady state which is also undesirable. Proportional control can reduce the oscillation amplitude to such an extent as is permissible reduction in output. Responses to the appropriate management systems are shown in Figure 10.
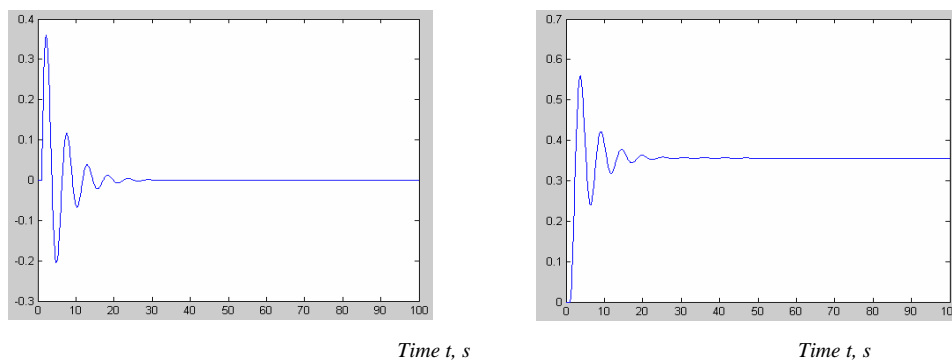
Time t, s   *Time t, s*
Figure 10. Semi–Active System responses to unit step function

It can be seen that there is a smaller jump and a shorter time during system reaches steady state - about the 20s (twice shorter).

The active suspension system achieves the effect of management present whenever the movement of suspension system. Active systems differ from passive by the presence of actuator which generates a variable force that compensates disturbances acting on the system.

This system is achieved by placing the order PID controller with transfer functions and the closure of the unit negative feedback. The parameters of the proportional, integral and differential control and simulation are combined to test the response until the shape does not get as close as first-order system is so skip it and eliminate the oscillations. System response is shown in Figure 11 and it can be seen that system became stable very fast.
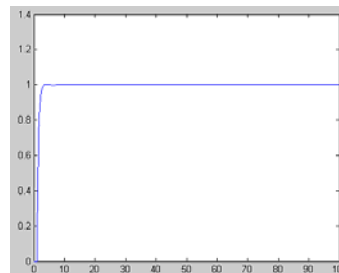
Figure 11. Active System responses to unit step function

Conclusion

This paper has presented a number of different techniques used to reduce vibration (movement) of objects. It was shown how to control the movement of the object, in order to improve the performance of high buildings, under the gusts of wind.

Among the numerous methods it may be listed *damping systems*, i.e. oscillatory systems that are *installed in building*.

One such system is shown in this work and for it are derived the appropriate equations and obtained solutions for the oscillation frequency, transfer functions and responses of the

system.

Based on the results, it can be concluded that the proposed model describes the real problem and that the system is stable. This means that it can recommend the installation of such oscillatory systems in real facilities to protect against wind and earthquake shock caused by the earthquake.

Since the time of the stabilization system is relatively long (40s), for further research it is recommended to applicate of more sophisticated damping system (automated) where corrections can be made during working life.

References

[1]   Aizawa, S., Ohtake, K., Yamamoto, M., Azuma, T., Miyazaki, M., and S. Fujimori. (1997), The Characteristics of Wind Fluctuation and the Results of Structural Control at Porte Kanazawa, *Summaries of Technical Papers of Annual Meeting*, AIJ, B-2: 937-938 (In Japanese).

[2]   Ahsan Kareem, Tracy Kijewski, Yukio Tamura, Mitigation of Motions of Tall Buildings with Specific Examples of Recent Applications, one stady, 2002.

[3]   Baker, W.P., Brown, C.D., and R.C. Sinn. (July 1998), Belt Wall/Core Interacting System for 77-Story Plaza Rakyat Tower, *Proceedings of Structural Engineers World Congress*, San Francisco, CD-ROM: T114-3.

[4]   Banavalkar, P. (1990), Structural Systems to Improve Wind Induced Dynamic Performance of High Rise Buildings, *Journal of Wind Engineering and Industrial Aerodynamics,* 36: 213-224.

[5]   Banavalkar, P. V. and N. Isyumov. (July 1998), Tuned Mass Damping System to Control Wind-Induced Accelera- tions of Washington National Airport Air Traffic Tower Control Tower, *Proceedings of Structural Engineers World Congress*. San Francisco, CD-ROM: T179-2.

[6]   Chen, P.W. and L.E. Robertson. (1973), Human Perception Threshold of Horizontal Motion, *Journal of Structural Division*, ASCE, 98: 1681-1695.

[7]   Dolicanin C**.** Соловьев Ю.Петрович, *Differential geometry*, ETF in Pristina, Pristina, 1993.

[8]   Dolicanin C., Mathematics II, *University textbook*, Pristina, 1995

[9]   Dorris, V. K. (29 July 1991), Configuration Poses Challenges, *Engineering News-Record*: 24-25.

[10]   Dutton, R. and N. Isyumov. (1990), Reduction of Tall Building Motion by Aerodynamic Treatments, *Journal of Wind Engineering and Industrial Aerodynamics*, 36(2): 739-747.

[11]   Goto, T. (1983), Studies on Wind-Induced Motion of Tall Buildings Based on Occupants' Reactions, *Journal of Wind Engineering and Industrial Aerodynamics,* 13.

[12]   Hayashida, H., and Y. Iwasa. (1990), Aerodynamic Shape Effects on Tall Building for Vortex Induced Vibration, *Journal of Wind Engineering and Industrial Aerodynamics,* 33(1-2): 237-242.

[13]   Hayashida, H., Mataki, Y., and Y. Iwasa. (1992), Aerodynamic Damping Effects of Tall Building for a Vortex Induced Vibration, *Journal of Wind Engineering and Industrial Aerodynamics,* 43(3): 1973-1983.

[14]   Isyumov, N. (17-19 May 1993), Criteria for Acceptable Wind-Induced Motions of Tall Buildings, *International Conference on Tall Buildings*, Council on Tall Buildings and Urban Habitat, Rio de Janerio.

[15]   Irwin, A. (1981), Perception, Comfort and Performance Criteria for Human Beings Exposed to Whole Body Pure Yaw Vibration and Vibration Containing Yaw and Translational Components, *Journal of Sound and Vibration*, 76(4).

[16]   Irwin, A. (1986), Motion in Tall Buildings, *Proceedings of Conference on Tall Buildings, Second Century of the Sky- scraper*, Chicago.

[17]   Irwin, P., Breukelman, B., Williams, C., and M. Hunter. (July 1998), Shaping and Orienting Tall Buildings for Wind, *Proceedings of Structural Engineers World Congress*, San Francisco, CD-ROM: T114-1.

[18]   Kareem, A. (1988a), Wind-Induced Response of Buildings: A Serviceability Viewpoint, *Proceedings of National Engineering Conference*, American Institute of Steel Construction, Miami Beach, FL.

[19]   Kareem, A. (1988b), Aerodynamic Loads on Buildings: A Compendium of Measured PSD on a Host of Building Shapes and Configurations, *Unpublished Wind Tunnel Study*, University of Houston.

[20]   Katica (Stevanovic) Hedrih, Vera Nikolic-Stanojevic: A model of gear transmission: fractional order system dynamics, (Research Article), *Mathematical Problems in Engineering*, Received 24 January 2010; Revised 2   March 2010; Accepted 6 May 2010 m, (http://www.hindawi.com/journals/mpe/aip. 972873. html),   http://www.hindawi.com/journals/mpe/aip.6.html.

[21]   Kitamura, H., Tamura, Y., and T. Ohkuma. (May 1995), Wind Resistant Design & Response Control in Japan Part III: Structural Damping & Response Control, *Proceedings of 5th World Congress Council on Tall Buildings and Urban Habitat,* Amsterdam.

[22]   Kojić M. Dynamics, Theory and examples, Scientific book, Belgrade, 1993.

[23]   Kwok, K.C.S. (Jan. 1995), Aerodynamics of Tall Buildings, *A State of the Art in Wind Engineering: International Association for Wind Engineering*, *Ninth International Conference on Wind Engineering*, New Delhi.

[24]   Kwok*, K.C.S. and N.* Isyumov. (July 1998), Aerodynamic Measures to Reduce the Wind-Induced Response of Buildings and Structures, *Proceedings of Structural Engineers World Congress*, San Francisco, CD-ROM:T179-6.

[25]   Maebayashi, K., Tamura, K., Shiba, K., Ogawa, Y., and Y. Inada. (Dec. 1993), Performance of a Hybrid Mass Damper System Implemented in a Tall Building, P*roceedings of International Workshop on Structural Control:* 318- 328.

[26]   Maksimovic S., Posavljak S, Maksimovic K., Nikolic- Stanojevic V., Djurkovic, V., Total fatigue life estimation of notched structural components using low cycle fatigue properties, *Journal STRAIN*,http://onlinelibrary.wiley.com.proxy.kobson.nb.rs:2048/doi/10.1111/j.1475-1305.2010.00775.x/full.

[27]   Melbourne, N.H. and T.R. Palmer. (1992), Accelerations and Comfort Criteria for Buildings Undergoing Complex Motions, *Journal of Wind Engineering and Industrial Aerodynamics,* 41-44: 105-116.

[28]   M. H. Chey, J. B. Mander, A. J. Carr, J. G. Chase, "Multi – storey semi – active tuned mass damper building system", *University of Canterbury, Mechanical engineering*, 2006,

[29]   Miyashita, K., Ohkuma, T., Tamura, Y., and M. Itoh. (1993), Wind-Induced Response of High-Rise Buildings: Effects of Corner Cuts or Openings in Square Buildings, *Journal of Wind Engineering and Industrial Aerodynamics,* 50: 319-328.

[30]   Nikolic V., Dolicanin C., Radojkovic M., Aplikation of Numerical Methods in Solvong a Phenomenon of the Theory of Thin Plates, *Scientific Technical Review*,Vol. 60, No.1., 2010. , pp.61 ... 65.

[31]   P. Horan, K. Henry, J. Kane, R. Doherty, "Investigation into tuning of a vibration absorber for a single degree of freedom system", *Bolton street, Dublin institute of technology.*

[32]   Rašković D. Theory od oscillations, *Civil engineering books*, Belgrade, 1974.

[33]   Sakamoto, M. and T. Kobori. (1993), Practical Applications of Active and Hybrid Response Control Systems, *International Workshop on Structural Control. Honolulu*, Hawaii: 52-66.

[34]   Shimada, K., and K. Hibi. (1995), Estimation of Wind Loads for a Super-Tall Building (SSH), *The Structural Design of Tall Buildings*, John Wiley & Sons, Ltd., 4:47-60.

[35]   Stamenkovic D., Maksimovic K., Nikolic-Stanojevic V., Maksimovic S., Stupar S., Vasovic I., Fatigue Life Estimation of Notched Structural Components, *Strojniški vestnik - Journal of Mechanical Engineerin*g 56(2010)12, 846-852, UDC 629.7:620.178.3, http://www.sv-jme.eu/current-volume/sv-jme-56-12-2010/.

[36]   Symans, M.D. and M.C. Constantiou. (1996), Experimental Study of Seismic Response of Structures with Semi- Active Damping Control Systems, *Proceedings of Structures Congress X.IV*, Chicago, April 15-18.

[37]   Tamura, Y., Kohsaka, R., Nakamura, O., Miyashita, K., and V. Modi. (1996), Wind-Induced Responses of an Airport Tower- Efficiency of Tuned Liquid Damper, *Journal of Wind Engineering and Industrial Aerodynamics*, 65: 121- 131.

[38]   Vujičić V., Theory of oscillations, *Contemporanely administration, Belgrade*, 67.

NUMERICAL INVESTIGATION OF LAMINAR FLOW IN SQUARE CURVED DUCT WITH 90° BEND

A. Ćoćić[1], I. Guranov[2], M. Lečić[3]

[1,2,3] Faculty of Mechanical Engineering, The University of Belgrade,
Kraljice Marije 16, 11120 Belgrade 35
e-mail: acocic@mas.bg.ac.rs, i.guranov@gmail.com, mlecic@mas.bg.ac.rs

Abstract. Numerical solution of incompressible laminar flow in square curved duct with 90° bend is performed in order to better understand the flow phenomena present in this type of flow. Simulation of flow was done in OpenFOAM, an open-source CFD software. Essentially, OpenFOAM is large C++ library which can be used to create application for solution of various problems in continuum mechanics. Besides object-oriented approach, the main advantage of OpenFOAM is that it is extendable, i.e. users can add their own applications and utilities. The solution for the flow investigated in this paper is for Reynolds number Re = 790. We used experimental results from literature as a validation tool for our simulation. The results of simulation showed very good agreement with experimental results. They also showed that centrifugal force convects the quickly moving fluid particles towards the outer wall. As a result, the axial velocity has peaks in curved region, and secondary flow with various number of vortices is also present. Development of flow in vertical straight section after the bend is also analyzed, where presence of swirl is detected.

1. Introduction

Fluid flow in curved ducts are practically inevitable thing in most devices and systems in mechanical engineering. We could only mentioned a few of them: turbomachines, ducts for air ventilation, heat exchangers, aircraft intakes, etc. Their practical importance motivated considerable research effort in the past decades, and it's still a motive today. In curved ducts, centrifugal and viscous (Tollmien-Schlichting) instabilities may exist and interact strongly [1]. The resulting nonlinear interaction between these two type of instabilities may cause the flow to evolve to exhibit turbulence. Advancing of knowledge about this three-dimensional curved flow is, thus, of fundamental importance. Nowadays, a large computer power, even on ordinary PC, enables efficient numerical simulations of flow in various engineering devices or systems. Results of simulations help us to better understand the flow phenomena by predicting flow structure and values of significant flow quantities.

We can say that main flow characterics in curved channels or pipes is formation of so called secondary flow. This was first pointed out by Eustice, [2] in his experimental work with flow in curved pipes. Main reason for formation of secondary flow is presence of centrifugal force and it has great influence on primary flow development. Also, centrifugal force causes that velocity is skewed towards the outer wall. This experimentally observed phenomenon was analytically confirmed by Dean, [3]. Presence of secondary flow increases dissipation of fluid mechanical energy, which implies a larger pressure drop. Also, wall shear stress distribution along the wall is not uniform, in contrast with straight channel or pipe.

Advance of PIV experimental equipment and techniques in past years enables visualization of these secondary flows. Jarrahi et al., [4] studied process of mixing by secondary flow in a developing laminar pulsating flow through a circular curved pipe. They noticed different secondary flow patterns during an oscillation period due to competition among the centrifugal, inertial, and viscous forces.

Besides experimental and analytical studies of these kind of flows, numerous numerical investigations are performed. Some relevant papers in that spirit are Patankar et al., [5], Humphrey, [6], Soh & Berger, [7], Tsai [8]. In papers by Soh [9] and Bara [10] studies of flow development in curved ducts with square cross-sections have been addressed on the determination of critical Dean number, above which the formation and disintegration of secondary flow can lead to multiple vortex pair solutions.

In this paper, we made a contribution to numerical studies of flow in curved duct. An open-source CFD software named OpenFOAM is used. OpenFOAM is essentially a large collection of C++ libraries which can be used to create application for solution of various problems in continuum mechanics. There are numerous advantages of open source software over commercial ones. First one is, of course, the fact that code is open; it is extendable and user can create their own applications and utilities, in contrast to "black-box" principle of commercial codes. Secondly, open-source principle implies formation of community in which people can freely communicate, cooperate and help each other in solving particular problems. They are not limited by software licenses, inability to adopt the software to their needs, etc. On the other hand, most open-source software have a lack of documentation, but on global scale every user of software give a small contribution to development of software and documentation.

The fact that OpenFOAM is written in C++ has big advantage over CFD codes written in procedural programming languages like FORTRAN and C. Object oriented approach in programming involves abstraction, inheritance and polymorphism. That enables implementation of complicated mathematical and physical models in code to be similar to high-level mathematical expressions, [11].

2. Problem description and governing equations

In this paper we simulated the flow which was studied experimentally by Humphrey, [6]. The sketch of duct is shown in Fig. 1. The flow configuration is a $90°$ bend of mean radius $92\,\mathrm{mm}$ attached to the end of the $1.8\,\mathrm{m}$ long squared channel with cross-section of $40 \times 40\,\mathrm{mm}$. Experiments in [6] were done by LDA technique and the measurements of all velocity field are available at three cross-sections before the bend, and also in three cross sections in the bend itself. These experimental results is a validation tool for our simulation. On the Fig. 1 characteristic coordinate systems are shown. Angle θ is measured along the bend, and coordinate $x^* = 0$ corresponds to the cross-section with $\theta = 0°$. When we say $x^* = -2.5$ we are thinking on cross-section at the distance $L = 2.5 \cdot 40 = 100\,\mathrm{mm}$ before bend.

Reynolds number in experiment, based on bulk velocity $V = 1.98 \cdot 10^{-2}\,\mathrm{m/s}$ and hydraulic diameter $D_H = 40\,\mathrm{mm}$ was Re = 790. The Dean number of the flow was De = Re$(\frac{1}{2}d/R_c) = 368$, where $R_c = 0.5(R_i + R_o)$ is the mean radius of curvature.
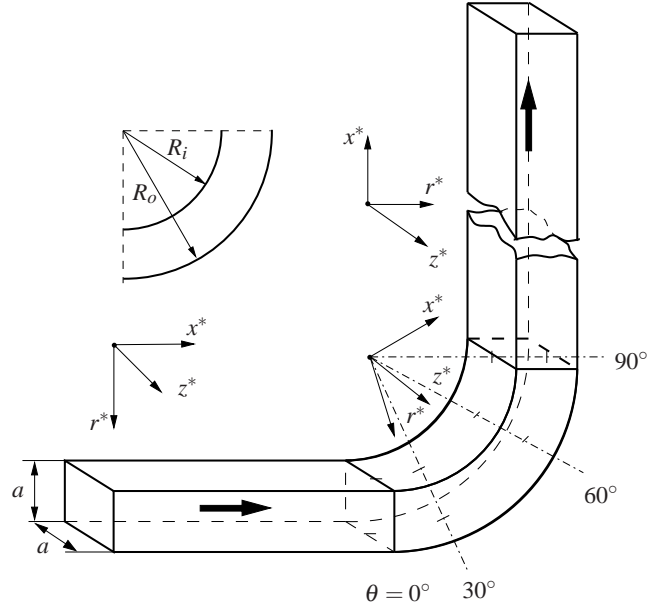
Geometry: $a = 40\,\text{mm}$, $R_i = 72\,\text{mm}$, $R_o = 112\,\text{mm}$

Non-dimensional coordinates: $z^* = \dfrac{z}{a/2}$, $\quad r^* = \dfrac{r - R_i}{R_o - R_o}$, $\quad x^* = \frac{x}{a}$

Figure 1. Sketch of computational domain, dimensions and non-dimensional coordinates.

2.1. Governing equations

The flow in channel and bend is incompressible, laminar and steady and it is described with continuity and momentum equations, which are, under that conditions

$$\nabla \cdot \vec{U} = 0 \tag{1}$$

$$\vec{U} \cdot \nabla \vec{U} = -\frac{1}{\rho} \nabla P + \nu \nabla^2 \vec{U}, \tag{2}$$

where P is generalized pressure. Form of continuity equation (1) for incompressible fluid enables that convection term in momentum equation can be written in following form: $\nabla \cdot \vec{U}\vec{U}$, where $\vec{U}\vec{U}$ is second-order tensor, whose component is $u_i u_j$. Constant density of fluid enables that we define kinematic pressure $p^* = P/\rho$. Now the momentum equation have the form

$$\nabla \cdot \vec{U}\vec{U} = -\nabla p^* + \nabla \cdot (\nu \nabla \vec{U}) \tag{3}$$

This form of momentum equation is called *strong conservation* form, which is suitable for discretisation by finite-volume method.

We need to add the following boundary condition to the equations in order to solve them for particular problem. For chosen coordinate system we can define components u_r, u_θ and u_z of vector $\vec{U}$. Now the boundary condition are:

$$x_H = -10 \ (\text{inlet plane}) : \ u = \text{fully developed duct flow}, \ v = w = 0,$$

1277

$$
\begin{aligned}
\text{walls} \qquad\qquad\qquad &: u = v = w = 0 \qquad\qquad\qquad\qquad (4)\\
x_H = 10 \ (\text{exit plane}) \quad &: \partial_\theta u_\theta = \partial_\theta u_r = \partial_\theta u_z = 0
\end{aligned}
$$

for velocity field, and

$$
\begin{aligned}
x_H = -10 \ (\text{inlet plane}) &: \partial_\theta p^* = 0\\
\text{walls} \qquad\qquad\qquad\ &: \partial_n p^* = 0 \qquad\qquad\qquad (5)\\
x_H = 10 \ (\text{exit plane}) \quad &: p^* = p_0^*
\end{aligned}
$$

for pressure field. Index n in wall boundary condition for pressure designates a direction perpendicular to wall and p_0^* is specified, constant value of kinematic pressure in exit plane. With this boundary conditions it is possible to solve the system of equations (1)-(2), using numerical methods. It is done is next section.

3. Set-up of the problem and solution procedure in OpenFOAM

OpenFOAM, as mentioned before, is first and foremost a C++ library. It is divided into a set of precompiled libraries that are dynamically linked during compilation of the solvers and utilities. Libraries such as those for physical models are supplied as source code so that users may conveniently add their own models to the libraries, [12], [13].

At the top-level of OpenFOAM code are the solvers, each designed to solve a specific problem in computational continuum mechanics. Each solver is based on finite-volume method of discretisation, which consists of three steps:

- *spatial discretisation* where solution domain is defined by a set of points that fill and bound a region of space when connected - generation of numerical mesh. In that space points, face, cells and connection between them is defined.

- *equation discretisation* where system of algebraic equation is defined in terms of discrete quantities defined at specific locations in the domain. Starting equation is partial differential equation that characterize the problem.

- *temporal discretisation* where time is divided into a finite number of time intervals (steps) - for unsteady problems

Geometry in this problem is rather simple, and OpenFOAM application `blockMesh` is used for mesh generation. This geometry also implies that mesh is orthogonal, so we don't need to introduce some non-orthogonal correctors in discretised equations. The mesh is shown in Fig. 2.

In our problem we have laminar, stationary and steady flow of incompressible fluid, and the solver designed for that type of flow is `simpleFoam`. Object-orientated approach enables the representation of the equations in code in their natural language. So, the momentum equation in `simpleFoam` solver for laminar flow is represented as

```
fvm::div(phi, U) - fvm::laplacian(nu, U) == - fvc::grad(p)
```

The syntax of the equation is straight-forward and clear; `fvm`, FiniteVolumeMethod designates implicit method of discretization of equation terms, while `fvc`, FiniteVolumeCalculus designates explicit method.

1278
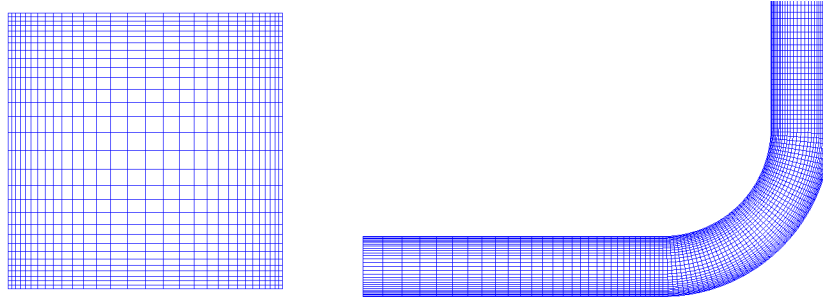
Figure 2. Numerical mesh for the problem.

Finite volume discretisation of each term is formulated by first integrating the term over a cell volume V. Most spatial derivative terms are then converted to integrals over the cell surface S bounding the volume using Gauss-Ostrogradski theorem

$$\int_v \nabla \star \phi \, dV = \oint_s \vec{n} \star \phi \, dA, \tag{6}$$

where ϕ represents any tensor field and the star notation $\star$ represents any tensor product, i.e. inner, outer and cross and the respective derivatives: divergence $\nabla \cdot \phi$, gradient $\nabla \phi$ and $\nabla \times \phi$. Volume and surface integrals are then linearized by some differencing scheme. Result of discretisation is set of algebraic equations for each cell and it can be expressed in matrix form as

$$[A]\{x\} = \{b\} \tag{7}$$

where $[A]$ is a square matrix, $\{x\}$ is the column vector of dependent variable and $\{b\}$ is the so-called "source vector", [13].

For velocity, we prescribed fully developed profile at inlet from previous simulation for straight channel, non-slip conditions at the walls and zero gradient at the outlet. For pressure, we prescribed zero gradient at inlet and walls, and fixed value $p^* = 0 \, \text{m}^2/\text{s}^2$ (gage pressure) at the outlet. Outlet was placed long enough after the bend so that we have developed, unidirectional flow at the outlet. We used upwind differencing scheme for convective therm, and central differencing scheme for gradient and laplacian therm in equation (3). For solution of Navier-Stokes equation (3) characteristic thing is that there is no independent equation for pressure, whose gradients contribute to each of three momentum equations, [14]. These difficulties are overcomed by use of numerical procedure called SIMPLE algorithm, [15], which is implemented in OpenFOAM. Preconditioned conjugate gradient methods are used for iterative solutions for system of linear equations.

Three different meshes were used. First mesh had 36000 cells, second 72000 cells and third had 200000 cells. In order to achieve faster convergence results from first mesh were prescribed to mesh with greater density by use of `mapFields` application, and after that results from mesh with 72000 cells were prescribed to the mesh with 200000 cells. At the end, simulation on mesh with 300000 cells gave the same results as the simulation on mesh with 200000 cells, and solution independence of mesh resolution is obtained. We used non-uniform mesh, by increasing the grading near the wall, in order to capture small vortices which are formed in the corners of the inner and the end walls.

4. Numerical results

From the simulation, we can see that flow is symmetric over the r, θ plane, which is expected, and it's also confirmed by experiments. It can be seen the movement of the fluid away from the inner radius wall towards the outer radius wall in bend. This movement progresses throughout the bend and it's accompanied by secondary motion directed towards the side walls and along the outer-radius wall and towards the symmetry plane along the inner-radius.
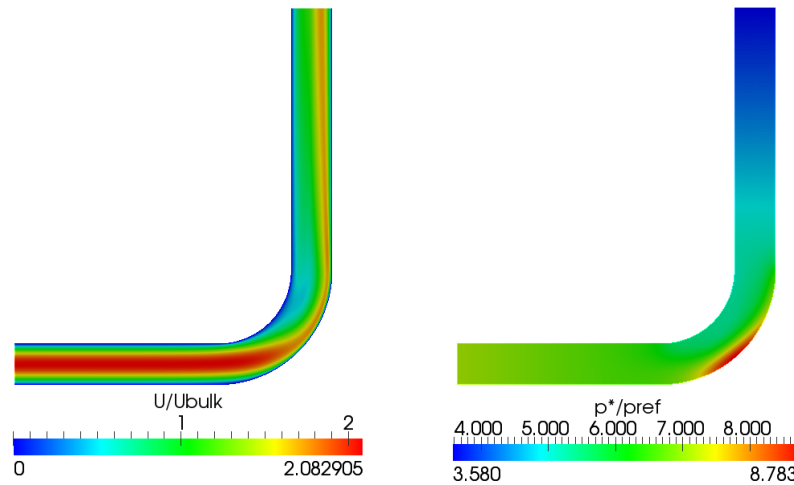
Figure 3. Velocity and pressure magnitude in middle plane of the channel - $z^* = 0$.

(a) (b) (c) (d) (e)
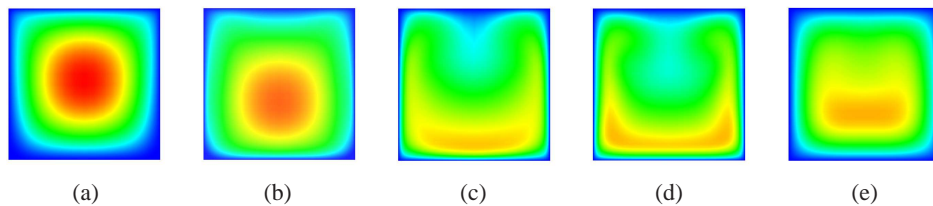
Figure 4. Contours of velocity magnitude in various cross-sections: (a) $\theta = 0°$; (b) $\theta = 30°$; (c) $\theta = 60°$; (d) $\theta = 90°$; (e) $x^* = 12.5$ after cross-section with $\theta = 90°$

Also, upstream of the curved duct, the flow is accelerated in regions near the inner-radius wall due to the favorable longitudinal pressure gradient. Conversely, the decelerated flow is observed in regions near the outer-radius wall because of the developed adverse pressure gradient downstream of $\theta = 0°$.

The comparison between experimental results in [6] and results of numerical simulations for axial velocity in (in direction of curvilinear coordinate x^*) is shown in Fig. 5. Results of simulation have very good agreement with experimental results, and all trends are well captured. We may argue that at cross-section of the bend for $\theta = 60°$ that agreement is not good. Also, with comparing measured results of velocity for constant r^* along the coordinate z^* similar trend is visible for cross-section around $\theta = 60°$. Some explanation for that remains

unclear. One of possible explanations can be that error of measurement results in that section are too high.

$\theta = 0°$

$\theta = 30°$

$\theta = 60°$

$\theta = 90°$

$$r* = (r - R_i)/(R_o - R_i)$$
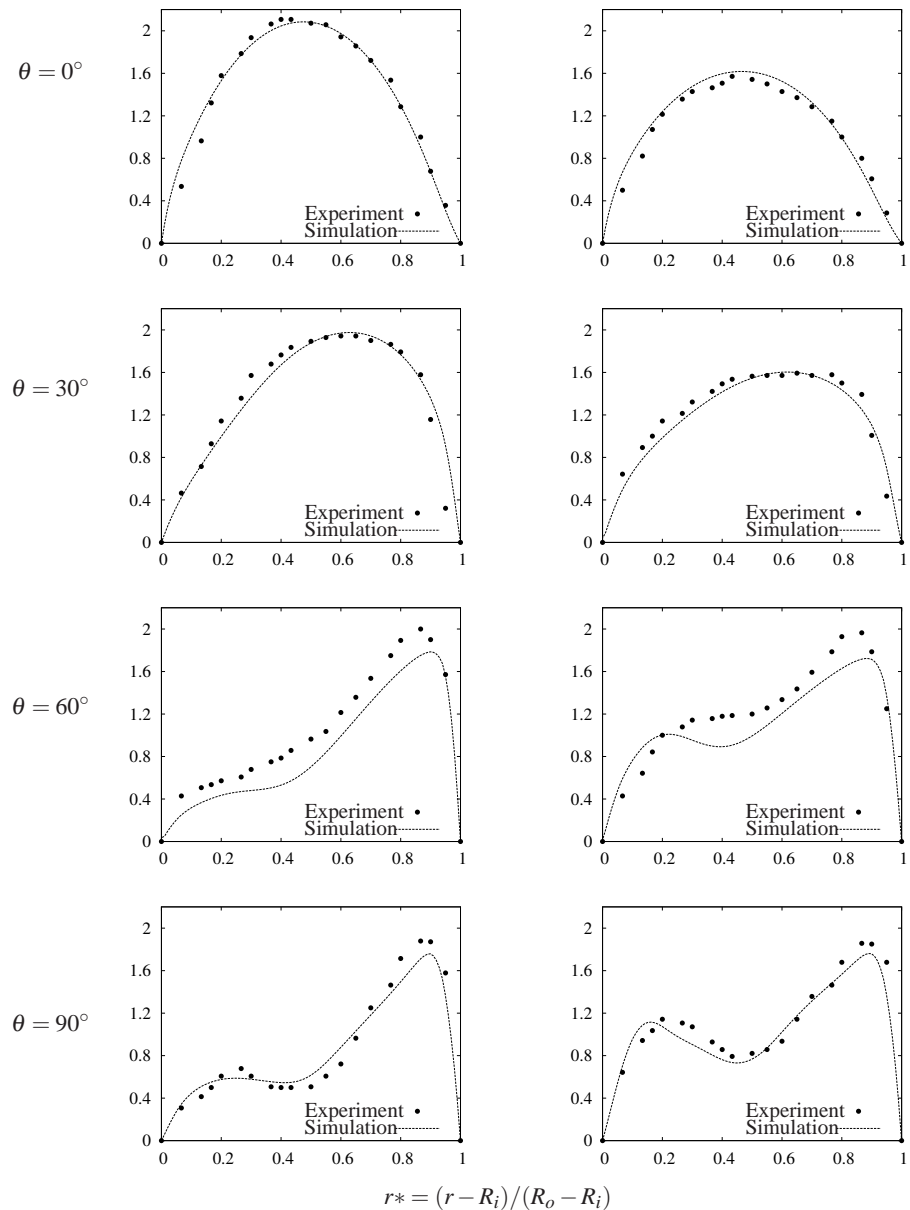
Figure 5. Comparison between measured and computed velocity profiles. Ordinate corresponds to non-dimensional velocity U/V; left column $z^* = 0.5$, right column $z^* = 0$.

From Fig. 5 the shifting of axial velocity peak towards the outer wall is also clearly visible. This is happening because of centrifugal effect. This degree of velocity skewness

increases with the increasing turning angle of the flow and such a skewed axial velocity can persist very far downstream. Our simulation showed that distance needed to obtain fully developed profile after the bend is $L \approx 50 D_H$.
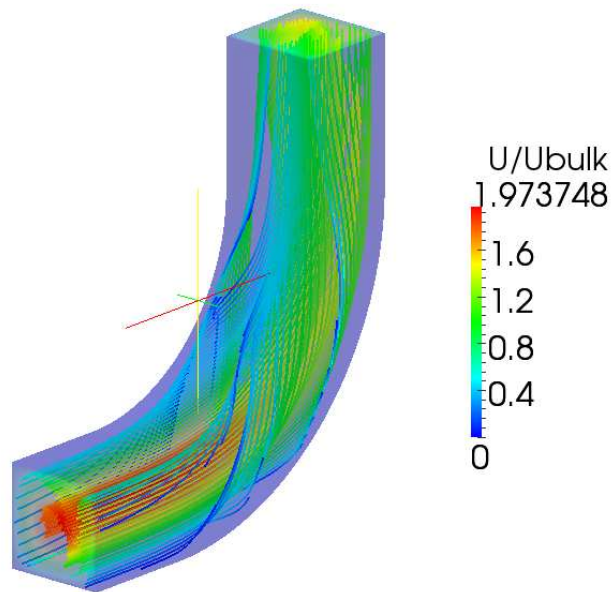
Figure 6. Some streamlines in the bend. It it visible that fluid particles are exhibited to swirling motion.

It is also very interesting to show the streamlines in such flow. Figure 6 shows some streamlines in 3D in the bend, and the presence of swirling motion is clearly visible. That swirling flow, like skewness of velocity profile, is maintained far downstream.

5. Concluding remarks

In this paper we made a numerical simulation of laminar flow of incompressible fluid in a curved duct with 90° bend in OpenFOAM. OpenFOAM is open-source CFD software, written in C++, and it's main advantage is that users can create their own applications and utilities. Results of numerical simulation show very good agreement with experimental results given in [6], which was used as validation tool for numerical results. They also give us a deeper insight in complex flow structure which is formed in bend. Also, effect of centrifugal force on flow structure is also spreading after the bend itself. We came to the conclusion that it takes $L \approx 50 D_H$ after to bend to have fully developed velocity profile.

References

[1] Bennett J., Hall P., Smith F.T. (1991) The strong nonlinear interaction of Tollmien-Schlichting waves and Taylor-Görtler vortices in curved channel flow, *J. Fluid Mech.*, Vol. 223, pp. 475-495

[2] Eustice J. (1911) Experiments on stream-line motion in curved pipes, *Proc. R. Soc. Lond. Ser. A*, Vol. 85, pp. 119-131

[3] Dean W.R. (1928), The stream-line motion of fluid in a curved pipe, *Philos. Mag.*, Vol. 30, pp. 673-693

[4] Jarrahi M., Castelain C., Peerhossaini H. (2010) Secondary flow patterns and mixing in laminar pulsating flow through a curved pipe, *Experiments in Fluids*, Online first, published: 27 November 2010, DOI: 10.1007/s00348-010-1012-z

[5] Patankar S.V., Pratap V.S., Spalding D.B. (1974) Prediction of laminar flow and heat transfer in helically coiled pipes, *J. Fluid Mech.*, Vol. 62, 1974, pp. 539-551

[6] Humhprey J.A.C, Taylor A.M.K, Whitelaw J.H. (1977), Laminar flow in a square duct of strong curvature, *Journal of Fluid Mechanics*, Vol. 83, pp. 509-527.

[7] Soh W.Y., Berger S.A. (1984) Laminar entrance flow in a curved pipe, *J. Fluid Mech.*, Vol. 148,

[8] Tsai S.F., Sheu T.W.H. (2007), Numerical exploration of flow topology and vortex stability in a curved duct, *International Journal for Numerical Methods in Engineering*, Volume 71, Issue 5, pp. 505-629

[9] Soh W.Y.(1988) Developing fluid flow in a curved duct of square cross-section and its fully developed dual solutions, *J. Fluid Mech.*, Vol. 188, pp. 337-361

[10] Bara B., Nandakumar K., Masliyah J.H. (1992), An experimental and numerical study of the Dean problem: flow development towards two-dimensional multiple solutions, *J. Fluid Mech.*, Vol. 244, pp. 339-376

[11] Weller, H.G.; Tabor G.; Jasak, H. and Fureby, C. (1998) A Tensorial Approach to CFD using Object Orientated Techniques, *Computers in Physics*, Vol. 12 No. 6, pp 620 - 631

[12] OpenFOAM User Guide, 2010, http://www.openfoam.com/docs/

[13] OpenFOAM Programming Guide, 2010, http://www.openfoam.com/docs/

[14] Ferziger J.H., Perić (2002) Computational Methods for Fluid Dynamics, 3rd Edition, *Springer*, 2002

[15] Patankar S.V. and Spalding D. B. (1972) A Calculation Procedure for Heat, Mass and Momentum Transfer in 3-Dimensional Parabolic Flows, *Int. J. Heat Mass Transfer*, Vol. 15, pp. 1787-1806.

ON THE BEHAVIOUR OF FORCED OSCILLATORS WITH A NON-NEGATIVE REAL-POWER RESTORING FORCE AND VAN DER POL DAMPING

Z. Rakaric[1], I. Kovacic[2]

[1] Department of Mechanics, Faculty of Technical Sciences, University of Novi Sad, 21000 Novi Sad, Serbia
e-mail: zvonko@uns.ac.rs
[2] Department of Mechanics, Faculty of Technical Sciences, University of Novi Sad, 21000 Novi Sad, Serbia
e-mail: ivanakov@uns.ac.rs

Abstract. Harmonically excited oscillators with a purely non-linear non-negative real-power restoring force and van der Pol damping are considered in this paper. The case of entrainment of frequency is analyzed. It corresponds to the behaviour when the free vibration frequency, which can be found from the energy conservation low of the related conservative unforced oscillators, falls in synchronism with the excitation frequency. The solution for motion is assumed in the form of a Jacobi cn elliptic function and a new elliptic averaging method is developed. Frequency response curves of the harmonic entrainment are determined. The validity and accuracy of the analytically obtained results are confirmed numerically.

1. Introduction

In this paper harmonically excited generalized van der Pol oscillators are considered, governed by the following non-dimensional equation of motion

$$\frac{d^2\xi}{d\tau^2} + \varepsilon f\left(\xi, \frac{d\xi}{d\tau}\right) + \text{sgn}(\xi)|\xi|^\alpha = F\cos\Omega\tau,$$

$$f\left(\xi, \frac{d\xi}{d\tau}\right) = \left(\xi^2 - 1\right)\frac{d\xi}{d\tau}, \tag{1a,b}$$

where ξ is the non-dimensional displacement; τ is non-dimensional time; ε is a small constant, i.e. $\varepsilon \ll 1$; F and Ω are the magnitude and frequency of harmonic excitation, respectively, with the former being of order ε ($F = \varepsilon \overline{F}$); α is the power of the restoring force that can be any non-negative real number.

The non-linear damping force defined by Eq. (1b) corresponds to van der Pol damping, which dissipates energy for large displacements and supplies energy to the system for small displacements. As such, it gives rise to limit cycle oscillations of free oscillators modelled by Eq. (1a,b) with $F=0$. When these systems are periodically excited, one can expect that the steady-state forced response might include both the unforced limit cycle oscillations as well as a response at the excitation frequency. However, if the magnitude of the excitation force is chosen appropriately and the frequency of the unforced limit cycle oscillations and the excitation frequency synchronize, then the response can occur only at

the excitation frequency. This represents the *entrainment* (*quenching*) phenomenon, when the excitation is said to have *entrained* the limit cycle oscillations or the limit cycle oscillations are said to have been *quenched* [1].

The phenomenon of entrainment was originally recognized and studied in a linear oscillator, which corresponds to Eq. (1a,b) with $\alpha=1$ [1,2]. Conditions for this phenomenon to exist were determined by applying the method of multiple scales and the corresponding frequency-amplitude curves were plotted. A pure cubic oscillator governed by Eq. (1a,b) with $\alpha=3$ was also investigated from this point of view in [3], where the first-order harmonic balance method was used. The aim of this paper is to carry out quantitative analysis of the non-linear oscillators governed by Eq. (1a,b) for any non-negative real power of the restoring force α and to investigate the behaviour associated with the entrainment phenomenon, which, as far as the authors are aware, has not been examined so far. This study, thus, provides a general insight into the effect of the van der Pol damping force on the behaviour of forced oscillators with a purely non-linear power-form restoring force. This type of restoring force has recently attracted considerable attention, as it appears in different physical and engineering systems [4]. Conservative oscillators with a fractional-order restoring force have been the subject of extensive research in the last decade (see, for example, [5] as well as the references citied therein), unlike non-conservative oscillators, which have not been studied so extensively. In [4], a general method is provided to found free oscillations of purely non-linear non-conservative oscillators. To that end, elliptic functions are used and a new method of averaging developed. The limit cycle oscillations of the oscillators modelled by Eq. (1a,b) with $F=0$ are also obtained. The study given below is a natural continuation of the work presented in [4], for the case when these oscillators are harmonically excited. A new elliptic averaging method is developed, enabling one to investigate the entrainment phenomenon.

2. Novel elliptic perturbation method

2.1. Motion of conservative oscillators

According to the assumptions introduced, both the non-conservative term $f(\xi, d\xi/d\tau)$ and the harmonic force $F\cos\Omega\tau$ represent small perturbations of the conservative oscillators

$$\frac{d^2\xi}{d\tau^2} + \text{sgn}(\xi)|\xi|^\alpha = 0. \tag{2}$$

Hence, the solution of Eq. (2) needs to be determined first, which will serve as a generating solution for the motion of the forced non-conservative oscillators (1a,b).

In order to encounter for the non-linearity, i.e. the fact that the power α can take any non-negative real value, the approximate solution for motion and velocity of Eq. (2) are assumed in the form of the Jacobi elliptic functions instead of usual trigonometric functions

$$\xi(\tau) = a\,\text{cn}[\psi, m], \tag{3a}$$

$$\frac{d\xi}{d\tau} = -a\,\omega\,\text{sn}[\psi, m]\text{dn}[\psi, m], \tag{3b}$$

where a is a constant amplitude of motion, ψ is a complete phase and the parameter m is the square of the modulus [6]. The complete phase ψ is defined by

$$\psi(\tau) = \omega\tau + \varphi(\tau), \tag{4}$$

where φ and ω are the phase and the frequency of the response, respectively.

To obtain the frequency ω and the square of the modulus m, the energy integral corresponding to the oscillators (5) is considered

$$\frac{1}{2}\left(\frac{d\xi}{d\tau}\right)^2 + \frac{|\xi|^{\alpha+1}}{\alpha+1} = \frac{|a|^{\alpha+1}}{\alpha+1}, \tag{5}$$

where the initial velocity is assumed to be zero. It should be emphasized that by a proper parameterization, the value of the amplitude a can always be made equal to unity (see [4] for details), which will be used later on for simplification.

By using Eq. (5), the following expression for the period of oscillations can be derived

$$T = = 4\int_0^a \frac{d\xi}{\left|\frac{d\xi}{d\tau}\right|} = 4\sqrt{\frac{\alpha+1}{2}}\int_0^a \frac{d\xi}{\sqrt{|\overline{a}|^{\alpha+1} - |\xi|^{\alpha+1}}} = T_{ex}^{ND} a^{\frac{1-\alpha}{2}}, \tag{6}$$

with T_{ex}^{ND} being

$$T_{ex}^{ND} = 4\sqrt{\frac{\alpha+1}{2}} \frac{\sqrt{\pi}\,\Gamma[1+\frac{1}{1+\alpha}]}{\Gamma[\frac{1}{2}+\frac{1}{1+\alpha}]}, \tag{7}$$

and Γ representing the Euler Gamma function [6].

Further, the fact that the period of the Jacobi elliptic function $cn[\psi, m]$ is known is used. It is given by $T=4K(m)$, where K is the complete elliptic of the first kind [6]. Thus, equating $4K(m)$ with Eq. (6) for the amplitude equal unity, i.e. with Eq. (7), the following expression is derived

$$4K \equiv 4K[m(\alpha)] = 4\sqrt{\frac{\alpha+1}{2}} \frac{\sqrt{\pi}\,\Gamma\left[1+\frac{1}{1+\alpha}\right]}{\Gamma\left[\frac{1}{2}+\frac{1}{1+\alpha}\right]}. \tag{8}$$

This equation defines the parameter m implicitly as a function of the power α. Some of these values corresponding to different α are calculated numerically and given in Table 1. It can be seen that the values of this parameter are negative for $\alpha < 1$ and positive for $\alpha > 1$. This is in general agreement with the findings presented in [4], where the values of the parameter m are calculated from Hamilton's variational principle. However, there are some quantitative differences between the values calculated here and in [4], but the expression (8) is considered to be more simple and convenient for the subsequently derived method than the one given in [4]. It should be noted that in a special case $\alpha = 0$, i.e. when the oscillator is linear, one has $m=0$, so that the elliptic cn function turns into the trigonometric

Cosine function. For a pure cubic oscillator $\alpha = 3$, the parameter m is equal to 0.5, which agrees with some existing results from the literature [7].

The frequency of the elliptic function is $\omega = 4K/T$, which due to Eqs. (6)-(8), gives

$$\omega = a^{\frac{\alpha-1}{2}}.$$ (9)

This expression implies that there is a specific non-linear power-form relationship between the amplitude of free oscillations and the frequency of the elliptic function.

Note that the solution defined by Eqs. (3a,b) and (4) is the solution of the equation of motion (2) provided that the following equation is satisfied

$$-\omega^2 a\,\mathrm{cn}\,\mathrm{dn}^2 + \omega^2 am\,\mathrm{sn}^2\,\mathrm{cn} + a^\alpha\,\mathrm{sgn}(\mathrm{cn})|\mathrm{cn}|^\alpha = 0,$$ (10)

where the arguments of the elliptic functions are omitted for brevity.

α	m	a_1	d_1	d_6	$\overline{D}$	P
0	−0.506160	1.138383	0.651587	0.15522	0.801715	0.92144
$1/4$	−0.353627	1.1002	0.607119	0.14637	0.865627	0.907209
$1/3$	−0.307134	1.088058	0.593378	0.143634	0.884476	0.94263
$\pi/5$	−0.158067	1.04715	0.548666	0.134721	0.942677	0.965569
$4/5$	−0.081307	1.02479	0.525209	0.130038	0.971148	0.980711
1	0	1	$1/2$	0	1	1
$\pi/2$	0.1921473	0.935912	0.438686	0.11271	1.03272	1.06463
2	0.3058305	0.893363	0.401005	0.105123	1.09159	1.12228
3	0.5	0.809093	$1/3$	0.091389	1.125626	1.28507
4	0.629107	0.740723	0.285029	0.081446	1.12668	1.4849

Table 1. Values of some parameters for certain values of the power α.

2.2. Motion of forced non-conservative oscillators

Using the analogy with the generating solution given by Eq. (3a,b), a trial solution of the slightly perturbed oscillators (1a,b) can be assumed in the same form, but with the amplitude, the complete phase and the parameter m slowly varying in time, i.e.

$$\xi(\tau) = a(\tau)\mathrm{cn}[\psi(\tau), m(\tau)],$$
$$\frac{d\xi(\tau)}{d\tau} = -a(\tau)\omega\,\mathrm{sn}[\psi(\tau), m(\tau)]\,\mathrm{dn}[\psi(\tau), m(\tau)].$$ (11a,b)

This implies that the change of these parameters needs to be taken into account. However, due to the fact that the parameter m and ω are both related to the period, the variation of the solution assumed is performed with respect to m only.

Equating the period $4K(m)$ with the last expression in Eq. (6), differentiating it with respect to time, the following time variation of the parameter m can be derived

$$\frac{dm}{d\tau} = \frac{B}{a}\frac{da}{d\tau},$$ (12)

with

$$B = \frac{(1-m)(1-\alpha)mK}{E-(1-m)K},$$ (13)

where E is the complete elliptic integral of the second kind, $E=E(\theta,m)$, and θ is the elliptic amplitude function $\theta = \mathrm{am}[4K,m]$ [6].

Further, it should be noted that based on Eq. (11a), the solution for the velocity has the form given by Eq. (11b) if the following constraint is satisfied

$$\frac{da}{d\tau}\,\mathrm{cn} - a\frac{d\varphi}{d\tau}\,\mathrm{sn\ dn} + a\frac{dm}{d\tau}\frac{\partial\mathrm{cn}}{\partial m} = 0,$$ (14)

where the arguments of the elliptic functions are again omitted for brevity, but are defined in Eq. (11a,b).

Differentiating Eq. (11b) and substituting it into Eq. (1a), as well as substituting Eq. (12) into Eq. (14), one obtains

$$-\frac{da}{d\tau}\omega\left[\mathrm{sn\ dn} + B\frac{\partial}{\partial m}(\mathrm{sn\ dn})\right] - a\,\omega\frac{d\varphi}{d\tau}\mathrm{cn}\left(1-2m\,\mathrm{sn}^2\right) = -\varepsilon\,f\left(\xi,\frac{d\xi}{d\tau}\right) + F\cos\Omega\tau,$$ (15)

$$\frac{da}{d\tau}\left[\mathrm{cn} + B\frac{\partial\mathrm{cn}}{\partial m}\right] - a\frac{d\varphi}{d\tau}\mathrm{sn\ dn} = 0.$$ (16)

The variations of the elliptic functions with respect to the parameter m that appear in Eq. (15) can be expressed in the forms given in Appendix, Eqs. (A1)-(A3). Using them and solving Eqs. (15)-(16) with respect to $da/d\tau$ and $d\varphi/d\tau$, one follows

$$-\omega D\frac{da}{d\tau} = -\varepsilon\,f\left(\xi,\frac{d\xi}{d\tau}\right)\mathrm{sn\ dn} + F\cos\Omega\tau\,\mathrm{sn\ dn},$$ (17)

$$-a\,\omega D\frac{d\varphi}{d\tau} = \left[-\varepsilon\,f\left(\xi,\frac{d\xi}{d\tau}\right) + F\cos\Omega\tau\right]\left[\mathrm{cn} + B\frac{\partial\mathrm{cn}}{\partial m}\right],$$ (18)

where

$$D = \mathrm{sn}^2\,\mathrm{dn}^2 + \mathrm{cn}^2\left(1-2m\,\mathrm{sn}^2\right) + \sigma\left[-\mathrm{sn}^2\,\mathrm{cn}^2\left(1-2m\,\mathrm{sn}^2\right) + \mathrm{sn}^2\,\mathrm{dn}^2\,\mathrm{cn}^2 - \mathrm{sn}^4\,\mathrm{dn}^2\right],$$ (19)

and

$$\sigma = \frac{m(1-\alpha)K}{2[E-(1-m)K]}.$$ (20)

Further, the term on the right-hand side of Eq. (18) can be written down as

$$\left[-\varepsilon\,f\!\left(\xi,\frac{d\xi}{d\tau}\right)+F\cos\Omega\tau\right]\!\left(\mathrm{cn}+B\,\frac{\partial\mathrm{cn}}{\partial m}\right)=$$

$$-\varepsilon\,f\!\left(\xi,\frac{d\xi}{d\tau}\right)\mathrm{cn}-\varepsilon\,f\!\left(\xi,\frac{d\xi}{d\tau}\right)\sigma_1\!\left[Z\,\mathrm{sn\,dn}-m\,\mathrm{sn}^2\,\mathrm{cn}\right]+\frac{1}{2}F\left[c_1+\sigma_1(z_1-ms_1)\right]\cos\phi,\tag{21}$$

where $\sigma_1=\sigma/m$ and where the periodic Jacobi zeta function has been introduced as given in Appendix, Eq. (A4).

In order to perform an averaging procedure, the elliptic function cn, the products sn dn, Z sn and sn^2 dn are expanded into the Fourier series, and only the first terms of these expansions are retained (see Appendix, Table A1). On the basis of that, the last term in Eq. (21) can be approximated as follows

$$F\cos\Omega\tau\,\mathrm{sn\,dn}=\frac{1}{2}Fa_1\!\left[\sin\!\left(\frac{\pi}{2K}\psi-\Omega t\right)+\sin\!\left(\frac{\pi}{2K}\psi+\Omega t\right)\right].\tag{22}$$

where a_1 is defined in Appendix, Table A1.

The form of the argument of the first Sin function in Eq. (22) is the motivation for a new variable to be introduced

$$\phi=\frac{\pi}{2K}\psi-\Omega\tau,\tag{23}$$

which represents a difference between the phase of the system response and the phase of excitation.

Taking this into account and performing an averaging procedure over a period $4K$, the general equations for the amplitude and the new phase become

$$\frac{da}{d\tau}=\frac{\varepsilon}{\omega\overline{D}}\frac{1}{4K}\int_0^{4K}f\!\left(\xi,\frac{d\xi}{d\tau}\right)\mathrm{sn\,dn}\,d\psi-\frac{Fa_1 a^{\frac{1-\alpha}{2}}}{2\overline{D}}\sin\phi,\tag{24}$$

$$\frac{d\phi}{d\tau}=\frac{\pi}{2K}a^{\frac{\alpha-1}{2}}-\Omega-\frac{\pi FP}{2K\overline{D}a\!\left(\frac{\pi a^{\frac{\alpha-1}{2}}}{2K}+\Omega\right)}\cos\phi+\frac{\pi}{2K}\frac{\varepsilon}{a\omega\overline{D}}\frac{1}{4K}\int_0^{4K}f\!\left(\xi,\frac{d\xi}{d\tau}\right)\mathrm{cn}\,d\psi\,+$$

$$\frac{\pi}{2K}\frac{\varepsilon\sigma_1}{a\omega\overline{D}}\frac{1}{4K}\int_0^{4K}f\!\left(\xi,\frac{d\xi}{d\tau}\right)\!\left[Z\,\mathrm{sn\,dn}-m\,\mathrm{sn}^2\,\mathrm{cn}\right]d\psi,\tag{25}$$

where $\overline{D}$ is an averaged value of D given by Eq. (19)

$$\overline{D}=2d_1+\sigma_1(d_2+d_3+d_4),\tag{26}$$

and where d_1-d_4 stand for the non-zero averaged values of the products existing in Eq. (19), and are defined in Appendix, Table A2. Besides this, the following notation has been introduced in Eq. (25)

$$P=c_1+\sigma_1(z_1-ms_1),\tag{27}$$

where c_1, z_1 and s_1 are the first Fourier coefficients given in Appendix, Table A1.

Also, while deriving Eqs. (24) and (25), the fact that the frequency of the free oscillation modelled by the Jacobi elliptic function is close to the excitation frequency $\omega \approx \Omega$ has been used, which is due to the case of synchronization considered here. This implies that $2\omega \approx \omega + \Omega = \pi a^{\frac{\alpha-1}{2}} / 2K + \Omega$. Hence, the response of the system defined in Eq. (11a) has the form

$$\xi(\tau) = a(\tau)\mathrm{cn}\left[\frac{2K}{\pi}(\Omega\tau + \phi), m(\tau)\right], \tag{28}$$

where the amplitude a can be obtained from Eq. (24), the phase difference ϕ from Eq. (25) and the parameter m from Eq. (8).

2.3. Motion of forced oscillators with van der Pol damping

For the case of the van der Pol damping force defined by Eq. (1b), the first order differential equations (24) and (25) for the amplitude and the phase difference become

$$\frac{da}{d\tau} = \frac{\varepsilon\, a\, d_1}{\overline{D}} - \frac{\varepsilon a^3 d_6}{\overline{D}} - \frac{1}{2}\frac{F\, a_1}{\overline{D}} a^{\frac{1-\alpha}{2}} \sin\phi, \tag{29}$$

$$\frac{d\phi}{d\tau} = \frac{\pi}{2K} a^{\frac{\alpha-1}{2}} - \Omega - \frac{\pi\, FP}{2K\overline{D}a\left(\dfrac{\pi a^{\frac{\alpha-1}{2}}}{2K} + \Omega\right)}\cos\phi, \tag{30}$$

where the values of parameters a_1, d_1, d_6, $\overline{D}$ and P are given in Table 1 for certain values of the power α.

The steady-state motion occurs when $da/d\tau = 0$ and $d\phi/d\tau = 0$. It corresponds to the solutions of

$$\frac{\varepsilon\, a\, d_1}{\overline{D}} - \frac{\varepsilon a^3 d_6}{\overline{D}} = \frac{1}{2}\frac{F\, a_1}{\overline{D}} a^{\frac{1-\alpha}{2}} \sin\phi, \tag{31}$$

$$\frac{\pi}{2K} a^{\frac{\alpha-1}{2}} - \Omega = \frac{\pi\, FP}{2K\overline{D}a\left(\dfrac{\pi a^{\frac{\alpha-1}{2}}}{2K} + \Omega\right)}\cos\phi. \tag{32}$$

Squaring and adding these equations, the amplitude-frequency equation is obtained

$$\frac{4\varepsilon^2 \left(d_1 - a^2 d_6\right)^2 a^{\alpha+1}}{a_1^2} + \left(\frac{\Omega^2 a - \left(\frac{\pi}{2K}\right)^2 a^\alpha}{\frac{\pi}{2K}\frac{P}{D}}\right)^2 = F^2. \tag{33}$$

Dividing Eq. (31) with Eq. (32), the expression for the steady–state value of ϕ is derived

$$\tan\phi = \frac{\pi P\varepsilon\left(d_1 - d_6 a^2\right)a^{\frac{\alpha-1}{2}}}{\overline{D}Ka_1\left[\left(\frac{\pi}{2K}\right)^2 a^{\alpha-1} - \Omega^2\right]}. \tag{34}$$

The local stability of the steady-state response can be checked by introducing small perturbations δ and η to the steady-state values a_0 and ϕ_0 satisfying Eqs. (31) and (32), i.e. by letting $a = a_0 + \delta$ and $\phi = \phi_0 + \eta$ [2]. By keeping linear terms in δ and η in Eqs. (29) and (30), one derives

$$\frac{d\delta}{d\tau} = \left[\frac{\varepsilon d_1}{\overline{D}} - \frac{3\varepsilon d_6}{\overline{D}}a^2 + \frac{\varepsilon(\alpha-1)}{2\overline{D}}\left(d_1 - d_6 a^2\right)\right]\delta - \left[\frac{Ka_1}{\pi P}a^{\frac{3-\alpha}{2}}\left(\left(\frac{\pi}{2K}\right)^2 a^{\alpha-1} - \Omega^2\right)\right]\eta, \tag{35}$$

$$\frac{d\eta}{d\tau} = \left[\frac{\pi(\alpha-1)}{4K}a^{\frac{\alpha-3}{2}} + \frac{\left(\frac{\pi}{2K}a^{\frac{\alpha+1}{2}} + \alpha\frac{\pi}{2K}a^{\frac{\alpha+1}{2}} + 2a\Omega\right)\left(\left(\frac{\pi}{2K}\right)^2 a^{\alpha-1} - \Omega^2\right)}{2a\left(\frac{\pi}{2K}a^{\frac{\alpha}{2}} + \sqrt{a}\Omega\right)^2}\right]\delta$$
$$+ \frac{\pi P}{Ka_1}\frac{\left(\frac{\varepsilon d_1}{\overline{D}}a - \frac{\varepsilon d_6}{\overline{D}}a^3\right)}{\left(\frac{\pi}{2K}a^{\frac{\alpha-1}{2}} + \Omega\right)}a^{\frac{\alpha-3}{2}}\eta. \tag{36}$$

The stability of the steady-state response depends on the eigenvalues of the coefficient matrix on the right-side of (35) and (36). The corresponding determinant *det* and the trace *tr* are

$$det = \frac{a^{-\frac{2+\alpha}{2}}\left\{a^{2\alpha}a_1^2\overline{D}^2\alpha\pi^4 + 4a^{\alpha+1}\pi^2\left[2d_1^2(\alpha+1)P^2\varepsilon^2 - 4a^2 d_1 d_6(3+\alpha)P^2\varepsilon^2 + \right.\right.}{8a_1\overline{D}^2 P\pi K^2\left(a^{\frac{\alpha}{2}}\pi + 2\sqrt{a}\Omega K\right)}$$
$$\underline{\left. + 2a^4 d_6^2(\alpha+5)P^2\varepsilon^2 - a_1^2\overline{D}^2(1+\alpha)\Omega^2\right]K^2 + 16a^2 a_1^2\overline{D}^2\Omega^4 K^4\right\}}, \tag{37}$$

$$tr = \frac{a^{-\frac{\alpha+1}{2}}\left(-a_1 d_1 + 5a^2 a_1 d_6 - a_1 d_1\alpha + a^2 a_1 d_6\alpha - 4d_1 P + 4a^2 d_6 P\right)}{2a_1 K\left(d_1 - 5a^2 d_6 + d_1\alpha - a^2 d_6\alpha\right)}. \tag{38}$$

Depending on the sign of the determinant, trace and the expression tr^2-$4det$, qualitatively different eigenvalues can occur, which yield conclusions about the stability of steady-state solutions [1].

3. Example

In this section the use of the equations derived previously for the study of the entrainment phenomenon in the generalized van der Pol oscillator (1a,b) is illustrated. The case when the power of the restoring force is $\alpha = 4/5$ is considered. The corresponding values of the parameters a_1, d_1, d_6, $\overline{D}$ and P are given in Table 1 in a row which is highlighted for the convenience of the reader.

In Figure 1, several frequency-response curves are plotted for a fixed value of the ordering parameter $\varepsilon = 0.2$ and for different values of the magnitude of the force F. For the sake of that, the amplitude-frequency equation (33) is used. For higher values of F, such as for example F=0.3 shown in Figure 1, the frequency-response curve in continuous, with the apparent maximum. As F decreases, the left and right branch become closer to each other, as is plotted for F=0.2. There is a value of the magnitude F when they coalesce, and then separate into two parts as plotted for F=0.1: one running near the frequency axis corresponding to lower amplitudes, labelled by the points L and N, and the other one that is detached and closed, surrounding the point (a^*, Ω^*). This point, marked by a star in Figure 1, characterizes the free limit cycle oscillations. This point lies on the backbone curve $\Omega = \pi a^{\frac{\alpha-1}{2}} \big/ 2K$, the expression for which was derived by equating the frequency-amplitude relationship (9) with the frequency of the cn function in the steady-state response (28).

In order to define the parts of these frequency-response curves that are stable and, thus, attainable, the use is made of the expressions for the determinant (37) and the trace (38) [1]. If the determinant is negative, a saddle occurs, which is always unstable. This region is shaded in the Ω-a plane in Figure 1. When the determinant is positive (outside the shaded region), unstable solutions can also occur, which happens for a positive trace. Positive values of the trace are related to the part of the plane below a dotted, almost horizontal line in Figure 1, corresponding to the zero value of the trace (38). There is also one more regions of interest plotted in Figure 1: it is a tongue between the dotted lines tr^2-det=0. Inside this tongue the values of tr^2-$4det$ are negative. The region of this tongue with the shaded part excluded is associated with unstable (stable) foci below (above) the zero-trace line. Outside the tongue, a positive (negative) trace is related to unstable (stable) nodes. Consequently, steady-state solutions are stable when det>0 and tr<0 [1]. The line dividing the frequency-amplitude plane into two parts with respect to this conclusion is emphasized in Figure 1 and plotted as a thick solid line. Hence, all the parts of the frequency-response branches that correspond to unstable steady-state solutions are below this thick line and are shown as dotted or dashed lines; the parts with stable steady-state motions are above it and are plotted as solid lines. This implies that along the frequency-response curve A-B-C-D-E-H-J corresponding to F=0.2, for example, the parts A-B and H-J are associated with unstable nodes, B-C with unstable foci, C-D with saddles, D-E with stable foci and E-H with stable nodes. Therefore, only the part D-E-H is realizable. These findings are checked numerically by carrying out direct integration of the equation of motion (1a,b). Steady-state numerical results are depicted as dots, confirming very good accuracy of the analytical results.
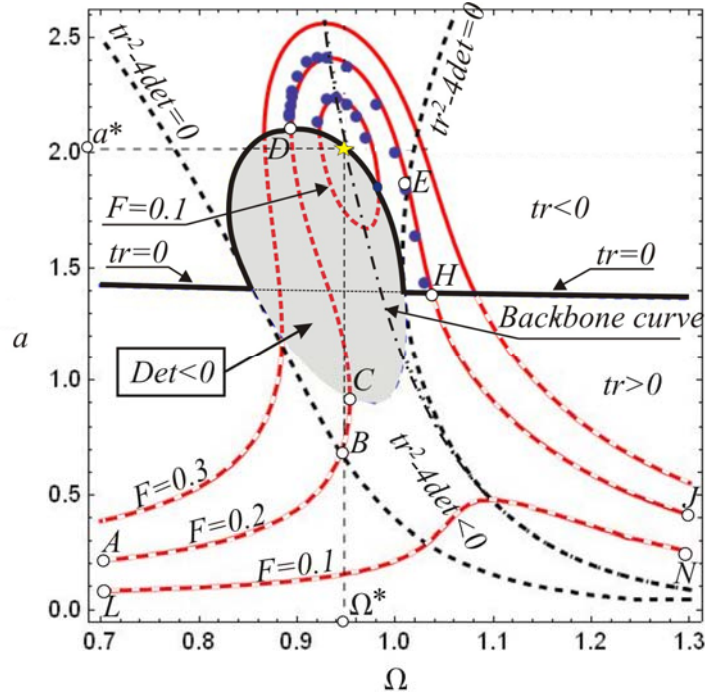
Fig 1 Frequency-response curves of the oscillator governed by Eq. (1a,b) for $\alpha = 4/5$, $\varepsilon = 0.2$ and different values of F.

It can be concluded that the entrainment phenomenon can occur in a very narrow range of the excitation frequency. For $F=0.2$, this region is between the frequencies corresponding to the points D and H. This region becomes wider if the magnitude of the force increases. Unlike in the linear systems with van der Pol damping, whose frequency-amplitude plane consists of the curves symmetric with respect to the vertical axis, in the systems with a non-negative power-form restoring force, these curves are bent to the left-hand side for the powers lower the unity (as shown in Figure 1 for $\alpha = 4/5$) and to the right-hand side for the powers higher than unity, which is not shown here, but have been verified. Thus, the corresponding behaviour is softening in the former case and hardening in the latter, shifting slightly the entrainment frequencies accordingly and bringing asymmetry into the frequency-amplitude plane.

Finally, in order to check the accuracy of the analytical approximate solution for the steady-state solution given by Eq. (28), the case $\alpha = 4/5$, $\varepsilon = 0.2$, $F = 0.2$, shown in Figure 1 is considered, but for $\Omega = 0.95$. The approximate solution obtained is

$$\xi(\tau) = 2.394\,\mathrm{cn}\big[0.98055\left(-1.915 + 0.95\tau\right)\big]. \tag{39}$$

This solution is plotted in Figure 2 together with the numerical solution of the equation of motion (1a,b) for $\xi(0)=1$ and $\dot{\xi}(0)=0$. This comparison illustrates excellent accuracy of the solution obtained.
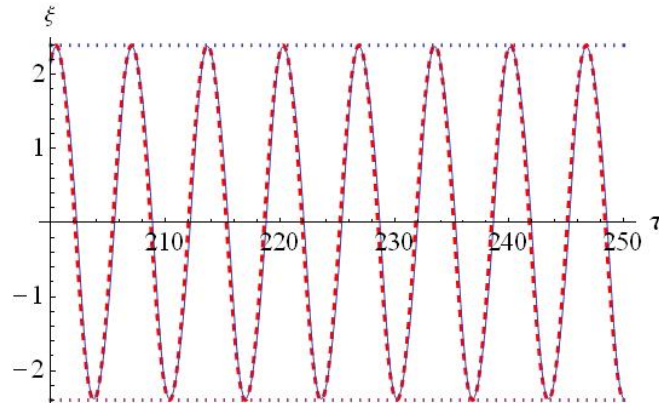
Fig 2 Comparison of the steady-state analytical solution for motion Eq. (39) (dashed line) and the corresponding numerical solution (solid line) of the equation of motion (1a,b) for $\alpha = 4/5$, $\varepsilon = 0.2$, $F = 0.2$, $\Omega = 0.95$, $\xi(0) = 1$ and $\dot{\xi}(0) = 0$; dotted line depicts the steady-state amplitude calculated from Eq. (33).

4. Conclusions

In this paper, oscillators with a non-negative real-power restoring force and van der Pol damping have been considered. The entrainment phenomenon has been investigated, when the frequency of the unforced limit cycle oscillations and the excitation frequency synchronize, so that the response occurs only at the excitation frequency. A new elliptic averaging method has been developed, which does not have any limitations regarding the value of the power of the non-linear restoring force, as this power can be any non-negative real number. The solution for motion is expressed in the form of the Jacobi cn elliptic function and has excellent accuracy with respect to the numerical solution.

Frequency-response curves for the steady-state motion have been found and the corresponding stability investigated. Parts of the frequency-response curves that are stable are determined, which correspond to the case when the excitation entrains the limit cycle oscillations. The frequency region associated with the entrainment is shifted to the lower frequencies for the powers of the restoring force lower than unity, and to the higher frequencies for the powers of the restoring force higher than unity. This region becomes larger if the magnitude of the excitation is increased.

The application of the elliptic averaging method presented is wider than the case reported for van der Pol damping, as the equations derived have a general form that includes the influence of any type of non-conservative forces. Thus, these equations can also be used to study other non-conservative forced non-linear oscillators, such as those with a polynomial damping force (dry friction, linear and quadratic viscous damping, etc).

Appendix

This Appendix contains some expressions and approximations related to the elliptic functions used in this paper.

Variations of the cn, sn and dn Jacobi elliptic functions with respect to the parameter *m* are given by:

$$\frac{\partial \mathrm{cn}[\psi,m]}{\partial m} = \frac{\mathrm{sn}[\psi,m]\mathrm{dn}[\psi,m]\{(m-1)\psi + E(\theta,m) - m\,\mathrm{sn}[\psi,m]\mathrm{cd}[\psi,m]\}}{2m(1-m)}, \quad \text{(A1)}$$

$$\frac{\partial \mathrm{sn}[\psi,m]}{\partial m} = \frac{\mathrm{cn}[\psi,m]\mathrm{dn}[\psi,m]\{(1-m)\psi - E(\theta,m) + m\,\mathrm{sn}[\psi,m]\mathrm{cd}[\psi,m]\}}{2m(1-m)}, \quad \text{(A2)}$$

$$\frac{\partial \mathrm{dn}[\psi,m]}{\partial m} = \frac{\mathrm{sn}[\psi,m]\mathrm{cn}[\psi,m]\{(m-1)\psi + E(\theta,m) - \mathrm{dn}[\psi,m]\mathrm{sc}[\psi,m]\}}{2(1-m)}. \quad \text{(A3)}$$

The Jacobi zeta function is defined by

$$Z = E(\theta,m) - \left(E(\theta,m)/K(m)\right)F_1(\theta,m), \quad \text{(A4)}$$

where $E(\theta,m)$ and $F_1(\theta,m)$ are the incomplete elliptic integral of the second and first kind, respectively, $\theta = \mathrm{am}[4K(m),m]$ is the elliptic amplitude function and $K = K(m)$ is the complete elliptic integral of the first kind.

Fourier series expansions for certain elliptic functions and their products are given in Table A1. The approximation for the cn function is given as infinite, while those for the products of some elliptic functions are given in the first approximation only. The corresponding Fourier coefficients are also tabulated.

Function	Approximation of the function	Fourier coefficient
$\mathrm{cn}[\psi,m]$	$\dfrac{2\pi}{\sqrt{m}K}\sum_{n=0}^{\infty}\dfrac{q^{n+\frac{1}{2}}}{1+q^{2n+1}}\cos\left[(2n+1)\dfrac{\pi\psi}{2K}\right]$	$q = \exp\left[-\dfrac{\pi K(1-m)}{K}\right]$
$\mathrm{sn}[\psi,m]\mathrm{dn}[\psi,m]$	$a_1\sin\left(\dfrac{\pi\psi}{2K}\right)+...$	$a_1 = \dfrac{\pi^2 q^{\frac{1}{2}}}{\sqrt{m}K^2(1+q)}$
$Z\,\mathrm{sn}[\psi,m]\mathrm{dn}[\psi,m]$	$z_1\cos\left(\dfrac{\pi}{2K}\psi\right)+...$	$z_1 = \dfrac{\pi^3\sqrt{q}\,q}{2\sqrt{m}K^3(1+q)(1-q^2)}$
$\mathrm{sn}^2[\psi,m]\mathrm{cn}[\psi,m]$	$s_1\cos\left(\dfrac{\pi}{2K}\psi\right)+...$	$s_1 = \dfrac{1}{2m}\left[-\dfrac{\pi^3\sqrt{q}}{2\sqrt{m}K^3(1+q)} + \dfrac{2\pi\sqrt{q}}{\sqrt{m}K(1+q)}\right]$

Table A1. Fourier series expansions (approximations and Fourier coefficients) for certain elliptic functions and their products.

Averaged values of the products of certain elliptic functions are presented in Table 2. These products are defined as the integrands I_i, where i=1, 2, 3 and 4, and the domain of integration corresponds to one period $4K$.

i	**Integrand** I_i	**Solution of the integral** $d_i = \dfrac{1}{4K}\int_0^{4K} I_i\, d\psi$
1	$\mathrm{sn}^2[\psi,m]\,\mathrm{dn}^2[\psi,m]$	$\dfrac{(2m-1)E(\theta,m)-4(m-1)K}{12mK}$
2	$\mathrm{sn}^2[\psi,m]\,\mathrm{cn}^2[\psi,m]\big(1-2m\,\mathrm{sn}^2[\psi,m]\big)$	$\dfrac{-\left(4m^2+m-6\right)E(\theta,m)+8\left(m^2+2m-3\right)K}{60m^2K}$
3	$\mathrm{sn}^2[\psi,m]\,\mathrm{cn}^2[\psi,m]\,\mathrm{dn}^2[\psi,m]$	$\dfrac{2[1+m(m-1)]E(\theta,m)-4[2+m(m-3)]K}{60m^2K}$
4	$\mathrm{sn}^4[\psi,m]\,\mathrm{dn}^2[\psi,m]$	$-\dfrac{[-2+m(8m-3)]E(\theta,m)+8\left[1+m-2m^2\right]K}{60m^2K}$

Table A2. Averaged values d_i (i=1, 2, 3, 4) of some integrands I_i that are the products of certain elliptic functions.

References

[1] Rand R H (2005) *Lecture Notes on Nonlinear Vibrations, version 52*
      http://audiophile.tam.cornell.edu/randdocs/nlvibe52.pdf . Accessed 13 April 2011.
[2] Nayfeh A H and Mook D T (1979) *Nonlinear Oscillations*, Wiley, NewYork.
[3] Hayashi C, Ueda Y, Akamatsu N and Itakura H (1970), On the Behavior of Self- Oscillatory Systems with
      External Force, Transactions of the Institute of Electronics and Communication Engineers of Japan, **53-A**,
      pp. 150-158.
[4] Rakaric Z and Kovacic I (2011) Approximations for Motion of the Oscillators with a Non-Negative Real-
      Power Restoring Force, *Journal of Sound and Vibration*, **330**, pp. 321-336.
[5] Mickens R E (2010) *Truly Nonlinear Oscillations: Harmonic Balance, Parametric Expansions, Iteration, and
      Averaging Methods*, World Scientific, Singapore.
[6] Gradshteyn I S and Ryzhik I M (2000) *Tables of Integrals, Series and Products*, Academic Press, New York.
[7] Yuste S B and Bejarano J D (1986) Construction of Approximate Analytical Solutions to a New Class of
      Non-Linear Oscillator Equations, *Journal of Sound and Vibration*, **110**, pp. 347-350.